

Universität
Rostock



Traditio et Innovatio



Universitätsmedizin
Rostock

Charakterisierung wirkstoffinduzierter Genexpressionsmodulationen bei SYK-, BET- und Kombinationsinhibition in Zelllinien hämatologischer B-Zell-Neoplasien

Kumulative Dissertation

zur

Erlangung des akademischen Grades

doctor rerum naturalium (Dr. rer. nat.)

der Mathematisch-Naturwissenschaftlichen Fakultät

der Universität Rostock

aus der Universitätsmedizin Rostock

Zentrum für Innere Medizin

Medizinische Klinik III – Hämatologie, Onkologie und Palliativmedizin

Direktor: Prof. Dr. Christian Junghanß

vorgelegt von

Sina Sender geb. am 26.11.1988 in Hannover

aus Rostock

Gutachter/-in:

1. Gutachter/-in:
Prof. Dr. rer. nat. habil. Ulrike Gimsa
Institut für Verhaltensphysiologie
Forschungsinstitut für Nutztierbiologie (FBN)
Universität Rostock
2. Gutachter/-in:
PD Dr. rer. nat. Hugo Murua Escobar
Zentrum für Innere Medizin, Medizinische Klinik III,
Klinik für Hämatologie, Onkologie und Palliativmedizin
Universitätsmedizin Rostock
3. Gutachter/-in:
Prof. Dr. rer. nat. Bernd Kreikemeyer
Institut für Medizinische Mikrobiologie, Virologie und Hygiene
Universitätsmedizin Rostock
4. Gutachter/-in:
Prof. Dr. med. Christian Schmidt
Klinik und Poliklinik für Innere Medizin C und Poliklinik Palliativstation
Universitätsmedizin Greifswald

Datum der Einreichung: 19. September 2022

Datum der Verteidigung: 03. Februar 2023

Für meine Familie

Originalarbeiten der kumulativen Dissertation

Die Ergebnisse der hier vorgelegten Dissertationsschrift sind in *peer-reviewed* Journalen mit *Impact Factor* Punkten publiziert worden oder unter Begutachtung.

Arbeit I:

Sender S., Sekora A., Villa Perez S., Chabanovska O., Becker A., Ngezahayo A., Junghanss C., Murua Escobar H. **Precursor B-ALL cell lines differentially respond to SYK inhibition by entospletinib** *Int. J. Mol. Sci.* 2021 Jan 8;22(2):E592. doi: 10.3390/ijms22020592.

Impact Factor 2019/20: 4.556

Arbeit II:

Sender S., Sultan AH., Palmer D., Koczan D., Sekora A., Beck J., Schuetz E., Brenig B., Fuellen G., Junghanss C., Murua Escobar H. **Evaluation of the synergistic potential of simultaneous pan- or isoform specific BET and SYK inhibition in B-cell lymphoma: an *in vitro* approach under review** in *Cancers* (*Manuscript ID: cancers-1798753*); eingereicht am 17.06.2022, 2. Revisionsrunde *under review* seit 14.09.2022

Impact Factor 2021/2022: 6.639

Arbeit III:

Kong W., **Sender S.**, Perez SV., Sekora A., Ruetgen B., Junghanss C., Nolte I., Murua Escobar H. **Pan- and isoform-specific inhibition of the bromodomain and extra-terminal proteins and evaluation of synergistic potential with entospletinib in canine lymphoma** *Anticancer Res.* 2020 Jul;40(7):3781-3792. doi: 10.21873/anticancerres.14367

Impact Factor 2019/20: 1.940

Inhalt

1. Zusammenfassung	1
2. Einleitung	2
2.1 Zielgerichtete Therapien und präzisionsonkologische Ansätze	2
2.2 Tyrosinkinase-Inhibitoren (TKIs)	3
2.3 Spleen Tyrosin Kinase (SYK)	4
2.3.1 Struktur und Funktion	4
2.3.2 SYK als therapeutisches Target in hämatologischen Neoplasien	4
2.3.3 Spezifischer SYK Inhibitor Entospletinib.....	5
2.4 Bromodomänen und extra-terminale Domänen (BET) Proteine	6
2.4.1 Struktur und Funktion	6
2.4.2 BET als therapeutisches Target in hämatologischen Neoplasien	7
2.4.3 Pan BET Inhibitor I-BET151	7
2.4.4 Isoform-spezifischer und bivalenter BET Inhibitor AZD5153.....	8
2.5 Kombinationstherapeutische Ansätze	8
2.5.1 Kombinationstherapien mit SYK oder BET Inhibition	9
2.6 Der Hund als Modellorganismus - Übertragung ins canine Modell	11
3. Zielstellung	12
4. Methoden	13
4.1 Evaluation der Substanzinduzierten Effekte <i>in vitro</i>	13
4.1.1 Verwendete Zelllinien	13
4.1.2 Substanzexpositionen	15
4.1.3 Evaluation zellbiologischer Parameter.....	15
4.1.3.1 Bestimmung der Zellproliferation und der metabolischen Aktivität.....	15
4.1.3.2 Durchflusszytometrische Bestimmung der Apoptose-Induktion	15
4.1.3.3 Durchflusszytometrische Bestimmung der Zellzyklusmodulation	15
4.1.3.4 Morphologische Charakterisierung mittels Pappenheimfärbung	15
4.1.3.5 Immunfluoreszenzfärbung zur Detektion von SYK	16
4.1.3.6 Intrazelluläre Färbung von Phosphoproteinen mittels Durchflusszytometrie	16
4.1.4 Evaluation molekularbiologischer Parameter.....	16
4.1.4.1 Proteinexpressionsbestimmung mittels Western Blot	16
4.1.4.2 RNA Isolation	16
4.1.4.3 Targeted RNA Panel Sequenzierung mittels PGM	16
4.1.4.4 Transkriptomanalysen mittels RNA Sequenzierung.....	17

4.1.4.5	Genexpressionsanalysen mittels Microarray	17
4.1.4.6	Bioinformatische Auswertung der Genexpressionsanalysen	17
4.2	Statistik, Illustration und Synergieberechnung	18
5.	Ergebnisse.....	19
5.1	Arbeit I	19
5.2	Arbeit II	22
5.3	Arbeit III	25
6.	Diskussion.....	28
6.1	SYK als potentielles therapeutisches Target in Zelllinien der Vorläufer B-ALL	28
6.2	SYK Inhibition zeigt heterogene Ergebnisse in Hinblick auf die Zellvitalität in humanen und caninen B-Zell Neoplasien.....	29
6.3	Entospletinib Exposition zeigt einen unterschiedlichen Wirkmechanismus in Vorläufer B-ALL Zelllinien.....	30
6.4	Isoform-spezifische bivalente BET Inhibition dominiert über pan-BET Inhibition in humanen und caninen B-Lymphom-Zelllinien.....	32
6.5	Kombination einer SYK und BET Inhibition als potentielle Kombinationsstrategie in B-Zell Lymphomen.....	32
6.6	Die simultane Inhibition führt zu einer kombinationsspezifischen Gensignatur in der DLBCL SU-DHL-4.....	34
7.	Ausblick.....	40
8.	Literaturverzeichnis.....	42
9.	Abkürzungsverzeichnis.....	54
10.	Abbildungsverzeichnis.....	58
11.	Tabellenverzeichnis.....	58
12.	Originalarbeiten	59
12.1	Arbeit I	59
12.2	Arbeit II	82
12.3	Arbeit III	113
13.	Lebenslauf.....	126
14.	Publikationsverzeichnis (anti-Chronologisch).....	128
14.1	Veröffentlichte Originalarbeiten	128
14.2	Veröffentlichte Originalarbeiten im Vorfeld zur Promotion	130
14.3	Vorträge auf internationalen und nationalen Fachtagungen	131

14.4	Posterbeiträge auf internationalen und nationalen Fachtagungen.....	132
15.	Eidesstattliche Erklärung.....	134
16.	Danksagung.....	135
17.	Anhang.....	137
17.1	Ergänzende Abbildung.....	137
17.2	Ergänzende Tabelle.....	138

1. Zusammenfassung

Zielgerichtete Therapien sind, neben den molekulardiagnostischen Methoden zur Aufklärung der patientenspezifischen molekularen Aberrationen, das wichtigste Instrument in der Präzisionsonkologie. Molekulare Veränderungen wie somatisch erworbene molekulare Aberrationen auf Nukleinsäureebene, Deregulationen und Signalwegsmodulationen, können mittels zielgerichteter Therapien adressiert werden. B-Zell Rezeptor assoziierte Kinasen (BAKs), einschließlich der Spleen Tyrosin Kinase (SYK), stellen aufgrund ihrer proximalen Nähe zum B-Zell Rezeptor (BZR) und des häufig aberrant regulierten BZR Signalwegs in hämatologischen Neoplasien des B-Zell Typs eine vielversprechende Zielstruktur für Tyrosinkinase-Inhibitoren dar. Neben den BAKs spielen auch epigenetische Regulatoren eine zentrale Rolle therapeutischer Interventionen, indem reversible epigenetische Veränderungen direkt adressiert werden. Durch ihre Funktionen innerhalb der Transkriptionsregulation beeinflussen sie direkt verschiedene Proto-Onko- sowie Tumorsuppressorgene und damit wichtigste biologische Prozesse der Zellregulation. Die epigenetischen „Reader“ Proteine der Bromodomänen und extraterminale Domänen (BET)-Familie sind Hauptregulatoren der Transkription und modulieren, durch die zielgerichtete Inhibition, wichtige zelluläre Prozesse.

In der hier vorliegenden Promotionsarbeit wurde daher zunächst SYK als Zielstruktur in Vorläufer B-ALL Zelllinien evaluiert. Als vergleichender Ansatz wurde weiterhin eine isoform-spezifische bivalente BET Inhibition mittels AZD5153 einer pan-BET Inhibition mittels I-BET151 in humanen und caninen B-Lymphom-Zelllinien gegenübergestellt. Die anschließende simultane SYK Inhibition mittels Entospletinib in Kombination mit AZD5153 oder I-BET151 wurde anhand zellbiologischer und molekularbiologischer Methoden in humanen und caninen B-Lymphom-Zelllinien charakterisiert.

SYK konnte in dieser Arbeit als potentielles therapeutisches Target für Subgruppen von Vorläufer B-ALL Zellen identifiziert werden. Weiterhin wurde ein unterschiedlicher molekularer Wirkmechanismus von Entospletinib in den hier getesteten Zelllinien ermittelt. Es konnte gezeigt werden, dass die anti-proliferativen Effekte des isoform-spezifischen bivalenten BET Inhibitors AZD5153 die Effekte der pan BET Inhibition in den humanen und caninen B-Lymphom-Zelllinien übersteigt. Beide BET Inhibitoren verstärkten in Kombination mit dem SYK Inhibitor Entospletinib die anti-proliferativen Effekte, z.T. synergistisch. Ein G0/G1 Zellzyklusarrest wurde ebenfalls induziert, allerdings ohne Beeinflussung der Apoptose. Weiterführende Genexpressionsanalysen der Entospletinib und AZD5153 Kombination wiesen eine kombinationsspezifische Gensignatur in der DLBCL Zelllinie SU-DHL-4 auf, die vor allem biologische Prozesse wie die DNA Replikation und Zellteilung als zentralen Wirkmechanismus identifizierte.

2. Einleitung

2.1 Zielgerichtete Therapien und präzisionsonkologische Ansätze

Basierend auf molekularen- und zellbiologischen Erkenntnissen konnten bereits in den frühen 1980er Jahren erste molekulare Mechanismen, die zu neoplastischen Veränderungen führen, identifiziert werden. Die veränderten molekularen Zielstrukturen konnten 1980 erstmals mit zielgerichteten Therapien, wie dem monoklonalen Antikörper AB89, adressiert werden. Der klinische Erfolg blieb allerdings zunächst aus. Eine wirklich effektive zielgerichtete Therapie gelang erst mit der Weiterentwicklung der Omics Technologien wie der Genomik, Transkriptomik und Proteomik (zusammengefasst im Übersichtsartikel ¹). Mit der Einführung von Hochdurchsatzsequenzierungen onkologischer Erkrankungen konnten komplexe Charakterisierungen tumorrelevanter somatischer Alterationen vorgenommen werden. Es eröffnete sich die Möglichkeit, basierend auf den molekularen Signaturen, gezielte therapeutische Ansätze über gerichtete Adressierung der Proteine zu evaluieren und in die klinische Anwendung zu überführen. Die Erkenntnis darüber, dass aberrante Onkogene und/oder Tumorsuppressorgene eine Schlüsselrolle bei Tumorentstehung, -erhalt und -progression spielen können, ermöglicht es, diese deregulierten Signalwege über zielgerichtete Therapien anzusteuern und somit das Tumorstadium zu inhibieren ². Auch epigenetische Modulationen, wie veränderte DNA-Methylierungsmuster, Chromatinzusammensetzungen und Histonmodifikationen können zu veränderten Expressionen von Proto-Onkogenen und/oder Tumorsuppressorgenen führen und damit die Tumorstadiumprogression fördern ³. Zielgerichtete therapeutische Ansätze sollen, im Vergleich zu den konventionellen onkologischen Standardtherapien Tumorstadiumresektion, Chemotherapie und Bestrahlung, die aberrant regulierten Zielstrukturen präzise auf molekularer Ebene adressieren. Beispiele solcher zielgerichteten Therapien sind Kinase- und Checkpoint Inhibitoren sowie monoklonale Antikörper.

Der erfolgreiche Einsatz des monoklonalen HER2/neu (human epidermal growth receptor 2 oder ERBB2, erb-b2 receptor tyrosine kinase 2) Antikörpers Trastuzumab und des bekannten Tyrosinkinase-Inhibitors Imatinib sind erste Beispiele gerichteter therapeutischer Ansätze. Diese über konventionelle Screening-Techniken identifizierten therapeutischen Zielstrukturen haben in Kombination mit verfügbaren Hochdurchsatzsequenzierungen die molekulare Charakterisierung und damit die Entwicklung neuer zielgerichteter Substanzen nachhaltig gefördert. Moderne diagnostisch-therapeutische Konzepte basieren auf molekularen Charakteristika und fördern über den therapeutischen Erfolg die weitere Biomarker-Forschung und deren Validierung ⁴.

2.2 Tyrosinkinase-Inhibitoren (TKIs)

Die Entwicklung von Tyrosinkinase-Inhibitoren (TKIs) spielt bei zielgerichteten Therapien eine wichtige Rolle, da Tyrosinkinasen die Initiierung und Progression von Tumoren beeinflussen können⁵. Eine Vielzahl von TKIs bindet reversibel oder irreversibel an die hoch konservierten ATP-Bindungsstellen der Kinasen und inhibiert damit deren Kinaseaktivität^{6,7}. Kinasen sind in der Lage, Phosphatgruppen von ATP auf andere Substrate zu transferieren und regulieren damit die wichtigsten zellulären Prozesse wie Proliferation, Überleben, Apoptose und Differenzierung⁷⁻⁹. Das Eingreifen in diese Prozesse ermöglicht eine gezielte Induktion von Tumorzelltod und Apoptose. Je nach Typ des Tyrosinkinase-Inhibitors findet die Bindung der Inhibitoren an die aktive Konformation (Typ I) der ATP Bindungsstelle der Kinasen, die inaktive Konformation (Typ II) oder fern von der ATP Bindungsstelle (Typ III) statt¹⁰. Unterschieden werden Nicht-Rezeptor Tyrosin Kinasen (NRTK), Rezeptor Tyrosin Kinasen (RTK), Serin/Threonin Kinase-Inhibitoren und Lipid Kinase-Inhibitoren^{7,11}.

Eine der bedeutendsten zielgerichteten Therapien ist die Hemmung der konstitutiv aktiven Tyrosinkinase (NRTK) BCR::ABL1 (früher BCR-ABL1) bei der chronischen myeloischen Leukämie (CML). Durch die Translokation von Chromosom 9 und Chromosom 22 entsteht das für die CML charakteristische, sogenannte Philadelphia Chromosom (Ph), welches zu verschiedenen Formen des Fusionsproteins BCR::ABL1 führt¹²⁻¹⁴. Die aktive Hemmung dieser Fusionsproteine über den Tyrosinkinase-Inhibitor Imatinib (Glivec®; CGP57148B; STI571) induziert die Proliferationsinhibition von leukämischen Zellen^{15,16}. Durch die signifikante Verbesserung der 10 Jahres Überlebensrate (overall survival rate) der CML Patienten von 78,8 % (Interferon alfa + Cytarabine) auf 83,3 % (Imatinib) wurde Imatinib 2001 von der Food and Drug Administration (FDA) und der European Medicines Agency (EMA) zugelassen^{17,18}. Der Einsatz von Imatinib bei Ph+ akuter lymphatischer Leukämie (ALL) führte ebenfalls zu einer Zunahme der Überlebensrate und damit 2013 zur Zulassung als Erstlinientherapie bei der ALL^{19,20}. Der BCR::ABL1 Inhibitor Dasatinib (Sprycel®) der zweiten Generation fand 2006 durch die FDA und EMA bei Ph⁺ CML und ALL die Zulassung. Die Punktmutation T315I innerhalb des ABL Gens bei der CML stellt allerdings ein Problem bzgl. der Resistenz gegenüber den Inhibitoren beider Generationen dar. Dies hatte die Entwicklung der Inhibitoren der dritten Generation zur Folge²¹. Der BCR::ABL1 Inhibitor Ponatinib (Iclusig®) wurde 2012 durch die FDA und 2013 durch die EMA freigegeben²². Neben den Fusionsproteinen wie BCR::ABL1 gehören weitere intrazelluläre Kinasen zu den NRTKs die mittels TKI adressiert werden können. Hierzu gehören bspw. die Janus Kinase (JAK), die Spleen Tyrosin Kinase (SYK) und die Bruton's Tyrosin Kinase (BTK). Durch die FDA wurden bislang der JAK1/2 Inhibitor Ruxolitinib (Jakafi®), der JAK3 Inhibitor Tofacitinib (Xeljanz®), der BTK Inhibitor Ibrutinib (Imbruvica®) und der SYK Inhibitor Fostamatinib (Tavlesse®) zugelassen^{7,23}.

2.3 Spleen Tyrosin Kinase (SYK)

2.3.1 Struktur und Funktion

SYK ist eine 72 kDa NRTK, die in hämatopoetischen Zellen stark exprimiert wird²⁴. SYK besteht aus zwei N-terminalen Tandem SH2 Src homology 2 (SH2) Domänen, die von einer Inter-SH2 Domäne (Interdomäne A) separiert werden. C-terminal besitzt SYK eine Kinase Domäne, die durch eine Linker Region von der SH2 Domäne getrennt wird (Abbildung 5, Anhang)²⁵. Die vielen Tyrosine innerhalb der Linker Region bieten Bindungsstellen für diverse Proteine, sobald diese phosphoryliert sind²⁶. Die SH2 Domänen stellen eine *immune receptor tyrosine-based activating motifs* (ITAM) Bindungs-Domäne dar. Immunrezeptoren, wie beispielsweise der B-Zell Rezeptor (BZR), besitzen auf der zytosolischen Seite der Plasmamembran Ig- α und Ig- β Proteine, die die ITAM Region darstellen und durch Rezeptorligation phosphoryliert werden²⁷⁻³⁰. Die dual phosphorylierten ITAMs (ppITAM) rekrutieren SYK durch die Bindung derer SH2 Domänen. Folglich wird SYK phosphoryliert und aktiviert und katalysiert somit die Signalweiterleitung unterschiedlicher Signalkaskaden, wie z.B. Phosphoinositid-3-Kinase/ AKT Serine/Threonine Kinase (PI3K/AKT), Mitogen-Activated Protein Kinase (ERK) und BTK/ Phospholipase C Gamma 2 (PLC γ 2)³¹⁻³³. Weiterhin ist SYK in der Lage, durch Autophosphorylierung oder Phosphorylierung durch andere Kinasen, rezeptorunabhängig, die Signalweiterleitung zu induzieren^{34,35}. Die durch SYK initiierte Signalweiterleitung führt zur Aktivierung wichtiger zellulärer Prozesse wie Zellproliferation, Differenzierung, Zytoskelett Remodellierung und Zytokinausschüttung³⁶.

SYK spielt in B-Zell Neoplasien, bedingt durch die Funktion innerhalb der B-Zell Reifung, wie dem Übergang von pro B- zu prä B-Zellen, sowie der Proliferation und dem Überleben reifer B-Zellen, eine wichtige Rolle^{24,37,38}. Beispielsweise können tonische BZR Signale zu einer konstitutiven Aktivierung von SYK führen, was SYK als Proto-Onkogen fungieren lässt und somit zur Tumorigenese von hämatologischen Neoplasien wie der chronisch lymphatischen Leukämie (CLL)³⁹, dem Diffus großzelligen B-Zell-Lymphom (DLBCL)⁴⁰, dem Mantelzelllymphom (MZL)⁴¹ und dem Follikulären Lymphom (FL)⁴² führt. Die Rolle bei der Vorläufer B-ALL ist allerdings bislang nicht vollständig geklärt. Auf der einen Seite wird von einer SYK Defizienz in der pädiatrischen B-ALL und auf der anderen Seite von einer SYK Aktivierung bei Hochrisiko Vorläufer B-ALL Patienten ausgegangen^{43,44}.

2.3.2 SYK als therapeutisches Target in hämatologischen Neoplasien

Der B-Zell Rezeptor Signalweg stellt als wichtiges regulatorisches Netzwerk in hämatopoetischen Zellen mit seinen BAKs einen möglichen Angriffspunkt zielgerichteter Therapien dar. SYK bspw. reguliert durch die proximale Nähe zum BZR und der damit verbundenen Signalweiterleitung, auch BZR unabhängig, wichtige zelluläre Prozesse, die durch eine gezielte Inhibition beeinflusst werden können. In der CLL konnte bereits gezeigt

werden, dass SYK anti-apoptotische Funktionen aufweist und das Überleben von CLL Zellen reguliert^{39,45}. Außerdem führte in murinen B-Zell Vorläufern die Deregulation von SYK zu der Entwicklung von Blasten und damit zu einer Vorläufer B-ALL. Dies resultierte in der Annahme, dass SYK auch in der Vorläufer B-ALL als Proto-Onkogen fungiert und damit als potentielles therapeutisches Target in Frage kommt⁴⁶.

Der bekannteste SYK Inhibitor Fostamatinib (R788) (TAVALISSE™) wurde 2018 von der FDA und 2020 von der EMA bei der Autoimmunerkrankung Immunthrombozytopenie (ITP) zugelassen⁴⁷. Die am häufigsten aufgetretenen Nebenwirkungen waren mild oder moderat, zumeist gut tolerierbar und kontrollierbar und umfassten Diarrhö, Hypertonie, Übelkeit, Schwindelanfälle sowie ein erhöhtes Level der Alanin-Aminotransferase und Aspartat-Aminotransferase⁴⁸. Neben den FIT1, FIT2 und FIT3 Studien, die als Grundlage für die Zulassung von Fostamatinib dienten, findet man zahlreiche weitere aktive und bereits beendete Studien zu dem SYK Inhibitor der ersten Generation⁴⁷. Die Indikationen der Studien sind vornehmlich hämatologische Erkrankungen, ITP und rheumatoide Arthritis (*ClinicalTrials.gov*: 56 Studien insgesamt; 14.09.2022). Neben der Wirkung des SYK Inhibitors Fostamatinib bei ITP konnten ebenfalls präklinische Effekte auf B-Zell Neoplasien festgestellt werden. Es konnte bereits gezeigt werden, dass die Inhibition von SYK über Fostamatinib zu einer Inhibition der SYK-abhängigen Signalweiterleitung führt, Apoptose *in vitro* induziert und die Tumorlast *in vivo* bei B-Lymphomen und der CLL verringerte⁴⁹⁻⁵¹.

2.3.3 Spezifischer SYK Inhibitor Entospletinib

Entospletinib wurde als SYK Inhibitor der zweiten Generation entwickelt, mit deutlich höherer Selektivität im Vergleich zu der Prodrug Fostamatinib bzw. R406 und weniger Nebenwirkungen. Entospletinib ist ein ATP kompetitiver, selektiver und oral verfügbarer SYK Inhibitor. Er blockiert die Kinasedomäne von SYK, indem die ATP Bindungsstelle besetzt und somit deren Kinaseaktivität gehemmt wird⁵². Die ersten prä-klinischen Studien mit Entospletinib in der CLL zeigten eine Reduktion der Zellvitalität in sensitiven CLL Patienten Zellen und synergistische Effekte in Kombination mit dem PI3K Inhibitor Idelalisib. Synergistische Effekte konnten ebenfalls bei CLL Patienten Zellen beobachtet werden, die zuvor resistent gegenüber beiden Monotherapien waren⁵³. Allerdings ist die Nutzung von Idelalisib in der Klinik seit August 2016 durch einen Rote-Hand-Brief stark eingeschränkt⁵⁴. Weiterhin konnte eine SYK Inhibition durch Entospletinib Apoptose induzieren und die schützende Mikroumgebung in co-kultivierten CLL Zellen *in vitro* stören⁵⁵. *In vivo* konnte beim Ösophaguskarzinom ebenfalls eine Inhibition des Tumorwachstums durch Entospletinib festgestellt werden⁵⁶. Aktuellere präklinische Studien aus dem Jahr 2021 zeigen auch, dass Entospletinib die Chemosensitivität in Lungenkrebszellen bei „multidrug“ Resistenz wiederherstellt⁵⁷. Außerdem zeigte sich eine durch *RAS Proto-Oncogene (RAS)* und *Protein*

Tyrosine Phosphatase Non-Receptor Type 11 (PTPN11) Mutationen induzierte Resistenz gegenüber der SYK Inhibition mittels Entospletinib in der AML, die in Kombination mit einem MEK (Mitogen-Activated Protein Kinase Kinase) Inhibitor verhindert werden kann ⁵⁸.

In einer klinischen Phase I Studie zur Prüfung der Sicherheit und Verträglichkeit sowie pharmakokinetischer- und pharmakodynamischer Analysen konnte gezeigt werden, dass Entospletinib sowohl in Einzel- als auch in Mehrfachdosen bei gesunden Probanden verträglich war und eine bessere Effizienz im Vergleich zu Fostamatinib bzw. R406 zeigte ⁵⁹. Die beobachteten Nebenwirkungen waren meist mild bis moderat, ohne das Auftreten von Grad 4 Nebenwirkungen. Am häufigsten aufgetreten sind Kopfschmerzen, Rhinorrhö und Schmerzen im Mund Rachen Raum ⁵⁹. In einer multizentrischen Phase II Studie aus Nordamerika (NCT01799889) konnte weiterhin gezeigt werden, dass 61 % der rezidivierenden oder refraktären CLL Patienten auf die Therapie mit Entospletinib mit klinisch akzeptabler Toxizität ansprachen ⁶⁰. Eine weitere Phase II Studie (NCT01799889) demonstrierte, dass Entospletinib eine Option nach nicht-erfolgreicher BZR Inhibition (BTK oder PI3K δ Inhibition) bei CLL Patienten darstellt ⁶¹. Bei Patienten mit vorangeschrittenem und rezidiviertem DLBCL konnte in einer Phase II Studie nur eine eingeschränkte Aktivität von Entospletinib nachgewiesen werden, wobei kein Patient eine komplette oder partielle Remission zeigte ⁶². Aktuell findet man bei *ClinicalTrials.gov* 15 Studien zu Entospletinib, überwiegend für hämatologische Neoplasien (14.09.2022). Die meisten Studien sind bereits mit Ergebnissen abgeschlossen, zwei befinden sich zurzeit noch in der Rekrutierungsphase und eine ist aktiv und rekrutiert nicht mehr.

2.4 Bromodomänen und extra-terminale Domänen (BET) Proteine

2.4.1 Struktur und Funktion

Die Proteine aus der Bromodomänen und extra-terminale Domänen (BET)-Familie, insbesondere das Bromodomänen-enthaltene Protein 2 (BRD2), BRD3, BRD4 und das Bromodomänen Testikel-spezifische Protein (BRDT) spielen eine wichtige Rolle bei der Erkennung von Histonen und der Transkriptionsregulation. BET Proteine fungieren als epigenetische „Reader“ Proteine, indem sie durch ihre N-terminalen Bromodomänen (BD) acetyliertes Lysin an Histonen erkennen, dieses binden und anschließend Komponenten der Transkriptionsregulationskomplexe rekrutieren ^{63–65}. Die Schlüsselmediatoren der Transkriptionselongation BRD2 und BRD4 spielen eine zentrale Rolle in der Initiierung und der Aufrechterhaltung der Transkription. Während BRD2 mit der RNA Polymerase II (Pol II) und E2F Transkriptionsfaktoren vor allem Promotoren unterschiedlicher Zellzyklusregulationsgene aktiviert, fungiert BRD4 als Ser2 Kinase, phosphoryliert die Pol II und initiiert somit die Transkription. Außerdem rekrutiert BRD4 den positiven Transkriptions-Elongations-Faktor-Komplex (P-TEFb), bindet diesen über ihre BDs an acetyliertes Chromatin und startet somit

den Elongationsprozess. Hinsichtlich dessen, besitzen die BET Proteine wichtige Funktionen bei der Transkriptionsinitiierung, der Genexpressionsregulation und der Zellzyklusprogression⁶⁶⁻⁶⁸.

2.4.2 BET als therapeutisches Target in hämatologischen Neoplasien

Durch die Funktion der BET Proteine als Transkriptionsinitiatoren kontrollieren sie wichtige Prozesse innerhalb des Genregulationsprozesses. In unterschiedlichen Tumorentitäten stellen deregulierte Histonmodifikationen wie Lysinacetylierung oder -methylierung, die die Genregulation kontrollieren, einen prognostischen Marker dar^{65,69}. „Gain-of-Function“ (GoF) Translokationen und Überexpressionen von BET Proteinen können die Genregulation verändern und so zu einer aberranten Onkogenexpression führen⁷⁰⁻⁷². Die Regulation wichtiger biologischer Prozesse durch ihre Funktion als Transkriptionsregulatoren machen die BET Proteine interessant für eine gezielte Inhibition. Die ersten BET Inhibitoren JQ1 und I-BET762 (GSK525762A) wurden 2010 beschrieben^{73,74}. Der BRD4 Inhibitor JQ1 konnte erfolgreich ein BRD Fusionsonkoprotein vom Chromatin freisetzen, welches beim Nuclear-protein-in-testis (NUT)-Mittellinienkarzinom durch die „GoF“ Translokation t(15;19)(q14, p13.1) (*BRD4-NUT*-Fusionsgen) entsteht und dadurch zu Proliferation und einem Differenzierungsstopp führt^{73,75,76}. JQ1 ist in der Lage, an die acetylierten Lysin-Bindungsdomänen der BET Proteine kompetitiv zu binden und somit Apoptose zu induzieren und die Zellproliferation zu hemmen⁷³. Durch die Herunterregulierung von Proto-Onkogenen wie bspw. *MYC Proto-Oncogene*, *BHLH Transcription Factor (MYC)* führte die BET Inhibition auch bei hämatologischen Neoplasien ohne BRD4 Aberrationen zu Anti-Tumor-Aktivität^{70,71,77-79}. Auch konnten bereits bei der akuten myeloischen Leukämie (AML) anti-leukämische Effekte, Apoptose-Induktion und *MYC* Herunterregulation durch eine BET Inhibition gezeigt werden⁸⁰⁻⁸². Basierend auf diesen Ergebnissen folgten einige klinische Studien in soliden und hämatologischen Neoplasien, bislang (14.09.2022) allerdings ohne Zulassung durch die FDA oder EMA^{83,84}.

2.4.3 Pan BET Inhibitor I-BET151

Bei I-BET151 (GSK1210151A) handelt es sich um einen pan-BET Inhibitor der selektiv BRD2, BRD3, BRD4 und indirekt BRD9 inhibiert. Er wurde 2011 als optimierte Variante mit verbesserter Wirksamkeit, Selektivität, Pharmakokinetik und Halbwertszeit im Vergleich zur Vorgängersubstanz I-BET762 entwickelt. I-BET151 bindet die acetylierte Lysin-Erkennungssequenz BD1 der BRD Proteine und setzt sie vom Chromatin frei⁷⁷. I-BET151 zeigte bei leukämischen Zelllinien mit unterschiedlichen onkogenen Treibermutationen vor allem eine hohe Effizienz bei *KMT2A*-rearrangierten Leukämien. Außerdem konnten Apoptose und ein Zellzyklusarrest in diesen Zellen durch die BET Inhibition induziert werden. Genexpressionsanalysen in diesen Zelllinien zeigten vor allem die Herunterregulierung von

KMT2A Zielgenen wie *BCL2 Apoptosis Regulator (BCL-2)*, *Cyclin Dependent Kinase 6 (CDK6)* und *MYC*⁷⁷. Die BET Inhibition durch I-BET151 zeigte weiterhin eine Anti-Tumor-Aktivität in unterschiedlichsten Tumorentitäten, darunter hämatologische Neoplasien wie AML, ALL, Non-Hodgkin-Lymphome (NHL) und in soliden Tumoren wie Mammakarzinom, Gliom, Melanom, Ovarialkarzinom u.m.⁸⁵. Klinische Studien mit I-BET151 laufen derzeit nicht (14.09.2022).

2.4.4 Isoform-spezifischer und bivalenter BET Inhibitor AZD5153

Bei AZD5153 hingegen handelt es sich um einen isoform-spezifischen, selektiven, oral verfügbaren BRD4 Inhibitor. AZD5153 ist ein bivalenter BET Inhibitor, d.h. ein Molekül ist in der Lage, beide BDs des BRD4 Proteins simultan zu binden. Im Vergleich dazu binden JQ1, I-BET762 und I-BET151 monovalent an die BET Proteine (ein Molekül pro BD). Die simultane Ligation beider BDs durch AZD5153 führt zu einer effizienteren Freisetzung des BRD4 vom Chromatin bei geringeren Konzentrationen. Die Testung von 60 hämatologische Zelllinien auf ihre Sensitivität gegenüber AZD5153, zeigte stark anti-proliferative Effekte bei allen getesteten Zelllinien. Unabhängig von der Sensitivität gegenüber AZD5153 wurde *MYC* in unterschiedlichen hämatologischen Zelllinien effizient herunterreguliert. Auch hierbei zeigte sich eine stärkere Herunterregulation durch AZD5153 im Vergleich zur Vorgängersubstanz I-BET762. *In vivo* zeigte AZD5153 ebenfalls Anti-Tumor-Aktivität in hämatologischen Xenograft Modellen⁸⁶. Neuste Untersuchungen aus dem Jahr 2022 zeigen, dass AZD5153 auch beim hepatozellulärem Karzinom (HCC) *in vitro* und *in vivo* anti-proliferative Effekte und genexpressionsmodulatorische Effekte aufweist⁸⁷. Aktuell laufen vier klinische Studien mit AZD5153, von diesen sind zwei bereits abgeschlossen, eine in der Rekrutierungsphase und eine rekrutiert zurzeit noch nicht (14.09.2022).

2.5 Kombinationstherapeutische Ansätze

Weinstein postulierte bereits 2002, dass die Inhibition von aktivierten Onkogenen oder inaktivierten Tumorsuppressorgenen zur Wachstumsinhibition von Tumorzellen führt, aufgrund ihrer stärkeren Abhängigkeit diesen gegenüber im Vergleich zu nicht-neoplastischen Zellen. Weiterhin verdeutlicht er, dass es die Kombinationsansätze sein werden, die für eine effektive Krebstherapie benötigt werden, da es durch Einzelsubstanzen zu Substanzvermittelten Mutationen kommen kann⁸⁸. Neben den konventionellen therapeutischen Interventionen wie Resektion, Bestrahlung und Chemotherapie, ermöglichen Kombinationsansätze mit Chemotherapeutika und TKIs eine noch gezieltere Therapie basierend auf den individuellen molekularen Signaturen der Patienten. Entscheidende Vorteile von kombinationstherapeutischen Ansätzen sind neben der Verringerung von Nebenwirkungen durch reduzierte Dosierungen, auch die Verringerung von „Drug Escape“ Mechanismen und die Vermeidung von Resistenzbildungen⁸⁹. Durch den erfolgreichen

Einsatz von Kombinationsansätzen bei unterschiedlichsten Entitäten, wurden bereits viele Kombinationen durch die FDA und EMA zugelassen. Die wohl bekannteste Kombinationstherapie ist die Kombinationschemotherapie CHOP welche bei hochmalignen Lymphomen wie der DLBCL angewandt wird. Die Kombinationstherapie besteht aus den Wirkstoffen Cyclophosphamid (C), Doxorubicin (Hydroxydaunorubicin (H)), Vincristin (Onkovin® (O)) und Prednisolon (P). Die Hinzunahme des monoklonalen CD20-Antikörpers Rituximab ergänzte die Kombinationschemotherapie als Immunchemotherapie „R-CHOP“ und wurde von der FDA als Erstlinientherapie bei der DLBCL im Jahr 2006 zugelassen. Die Hinzunahme von Rituximab konnte die 2 Jahres Überlebensrate (overall survival rate) der DLBCL Patienten von 57 % auf 70 % und die Vollständige Remission (CR) von 63 % auf 76 % erhöhen ⁹⁰. Auch TKIs werden als Kombinationsansätze intensiv präklinisch und klinisch evaluiert. So wurde beispielsweise der BTK Inhibitor Acalabrutinib bei Patienten mit CLL als Monotherapie oder in Kombination mit dem monoklonalen CD20-Antikörper Obinutuzumab von der FDA und der EMA zugelassen ⁹¹. Ebenfalls der FLT3 Inhibitor bei der FLT3-mutierten AML in Kombination mit Chemotherapie ⁹². Ein im Jahr 2014 durch die FDA zugelassener Kombinationsansatz zur Vermeidung der Resistenzbildung, ist die Verwendung des B-Raf Proto-Oncogene, Serine/Threonine Kinase (B-Raf) Inhibitors Dabrafenib mit dem MEK Inhibitor Trametinib beim mutierten V600E/K und metastasierten Melanom ^{93,94}.

2.5.1 Kombinationstherapien mit SYK oder BET Inhibition

Präklinisch werden verschiedene Kombinationsansätze *in vitro* und *in vivo* untersucht. Darunter Kombinationsansätze mit SYK oder BET Inhibition. Der erste Kombinationsansatz von Entospletinib mit dem PI3K δ Inhibitor Idelalisib zeigte in Kombination deutlich synergistische Effekte bei der CLL ⁵³. Die entsprechende Phase II Studie bei CLL und NHL wurde allerdings aufgrund starker Nebenwirkungen abgebrochen ⁹⁵. Eine neuere Studie (AALL0631) aus dem Jahr 2021 bei der kindlichen ALL zeigt, dass die Kombination aus Entospletinib und Vincristine (VCR) bei *RAS*-wildtyp *KMT2A*-rearrangierten ALL Patienten Proben *in vivo* die Proliferation im Vergleich zur Monotherapie effizient inhibierte ⁹⁶. Die *RAS* vermittelte Resistenz gegenüber einer SYK Inhibition bei der AML konnte 2019 in einer weiteren Studie, durch die Kombination mit dem MEK Inhibitor PD0325901, ausgehebelt werden, sowohl bei AML Zelllinien *in vitro* als auch bei patientenabgeleiteten Xenografts *in vivo* ⁵⁸. Auch ist Entospletinib in der Lage, die Sensitivität gegenüber dem BCL-2 Inhibitor Venetoclax in CLL Patienten Zellen wiederherzustellen ⁹⁷.

Die Kombinationen mit Entospletinib werden auch klinisch erfolgreich getestet. Dabei zeigte sich beispielsweise in Phase I Studien (2019 und 2021) eine gute Verträglichkeit von Entospletinib und dem BTK Inhibitor Tirabrutinib in der CLL (NCT01799889) ⁶¹ und DLBCL (NCT02457598) ⁹⁸. Auch die Kombination aus Entospletinib und Chemotherapie zeigte eine

gute Verträglichkeit in einer international-multizentrischen Phase Ib/II Studie von 2020 bei der AML mit *HOXA9/MEIS1* Überexpression (NCT02343939) ⁹⁹. In einer Phase I/II Dosisescalationsstudie von 2021 bei CLL und NHL wurde die Kombination aus Entospletinib mit dem CD20-Antikörper Obinutuzumab getestet. Auch hier zeigte sich eine gute Verträglichkeit und Wirksamkeit (NCT03010358) ¹⁰⁰. Eben diese Kombination zeigte in der CLL eine Herunterregulation von Myeloid Cell Leukemia Sequence 1 (BCL2-Related) (MCL1) und Programmed Cell Death 1 (PD-1). Zweiteres führt zu der Annahme, dass diese Kombination eine immunmodulatorische Funktion hat und teilweise die T-Zell Immunität wiederherstellt ¹⁰¹.

Auch Kombinationen mit BET Inhibitoren werden präklinisch intensiv untersucht (Übersichtsarbeit von Doroshov, Eder & LoRusso, 2017 ⁶⁸) und zeigen allesamt weitestgehend synergistische Effekte. Der isoform spezifische BET Inhibitor AZD5153 demonstriert beispielsweise eine verbesserte Wirksamkeit des PARP Inhibitors BMN673 bei Kolonkarzinomzelllinien ¹⁰². Die Kombination von AZD5153 mit dem Cyclin-abhängigen Kinase Inhibitor (CDK1, 2, 5, und 9) Dinaciclib führte *in vivo* zu einem verringertem Tumolvolumen im Neuroblastom PDX Modell ¹⁰³. Außerdem war AZD5153 in der Lage, die Sensibilität gegenüber dem CDK4/6 Inhibitor Palbociclib im Organoid- und Xenograft Modell wiederherzustellen und durch Zellzyklusarrest und Apoptose-Induktion synergistisch zu agieren ¹⁰⁴. Ebenfalls konnte die Kombination aus AZD5153 und dem WEE1 G2 Checkpoint Kinase (WEE1) Inhibitor AZD1775 die Zellproliferation synergistisch senken und das Tumorstadium *in vivo* beim nicht-kleinzelligen Bronchialkarzinom verringern ¹⁰⁵. Der pan BET Inhibitor I-BET151 in Kombination mit dem Zytostatikum Temozolomid induziert *in vitro* und *in vivo* synergistische Effekte in Glioblastomzelllinien ¹⁰⁶. Außerdem konnten beim metastasierendem Melanom in Kombination mit dem MCL-1 Inhibitor S63845 synergistische Effekte *in vitro*, in 3D Sphäroiden und *in vivo* nachgewiesen werden ¹⁰⁷. In BET Inhibitor (BETi) resistenten Leukämie Zellen konnte *in vitro* und *in vivo* die Kombination aus I-BET151 und dem CDK7 Inhibitor THZ1 das Tumorstadium verringern ¹⁰⁸.

Kombinationsansätze, auch mit TKIs, scheinen aufgrund der Vielzahl erfolgreicher präklinischer und klinischer Daten eine sinnvolle Alternative zu den konventionellen therapeutischen Interventionen zu bieten. Die intensive Testung neuer Kombinationen stellt dabei einen wichtigen Ansatz zur Evaluierung der Wirksamkeit, Verträglichkeit und Toxizität bzgl. neuer kombinationsspezifischer Nebenwirkungen dar. Die Untersuchungen zur Aufklärung der zugrundeliegenden molekularen Mechanismen sind dabei von entscheidender Bedeutung. Modellorganismen stellen dabei die Brücke in der translationalen Forschung dar, diese Fragen zu beantworten.

2.6 Der Hund als Modellorganismus - Übertragung ins canine Modell

Modellorganismen und Tiermodelle sind in der biomedizinischen und translationalen Forschung zur Evaluierung und Validierung von *in vitro* generierten Daten wichtig. Insbesondere für die präklinische Substanztestung sind Modellsysteme unabdingbar. Während Zellkulturen ein schnelles, robustes und reproduzierbares Testsystem darstellen, fehlt den Zellen, bedingt durch das Wachstum in 2D Monolayer-Kulturen, die Komplexität der Tumormikroumgebung und die daraus resultierende Interaktionen zu nicht-malignen Zellen, Stroma und Immunzellen ¹⁰⁹. Konventionelle *in vivo* Maus Modelle überwinden partiell diese Problematik. Die experimentelle Verifikation im *in vivo* Mausmodell ist allerdings limitiert durch die artifiziellen Eigenschaften, die das Mausmodell mit sich bringt. Dies sind vor allem die Problematik der fehlenden Übertragbarkeit, Inzucht und damit fehlende genetische Heterogenität, Unterschiede im Immunsystem und Immundefizienz ¹¹⁰⁻¹¹². Auch die Entstehung von Tumoren erfolgt zumeist artifiziell, durch die Xenotransplantation von humanen Tumorzellen in immunsupprimierte Mäuse oder genetisch veränderte Mausmodelle ¹¹³.

Das canine Modell kann einen Teilaspekt dieser Limitationen überwinden. Durch die Ähnlichkeit morphologischer, biologischer und molekularer Signaturen, Behandlungsprotokolle und Ansprechbarkeit stellt das canine DLBCL Modell ein ausgezeichnetes Pendant zum Menschen dar. Eine ähnliche Tumorpräsentation und die Anwesenheit eines funktionstüchtigen Immunsystems machen dieses alternative Auszuchtmodell so interessant ¹¹⁴. Durch die Übertragbarkeit und den direkten Transfer können beide Spezies von diesem komparativen, onkologischen Ansatz profitieren. In enger Abstimmung mit Veterinärmedizinern können Forschungsergebnisse, mit verringertem Aufwand, in die veterinärmedizinische Patientenversorgung einfließen. Durch die langjährige Kooperation mit der Stiftung Tierärztliche Hochschule Hannover (Prof. Dr.med.vet. Ingo Nolte) sind Heilversuche im Hund mit DLBCL möglich. Trotz CHOP Protokoll ist es durch die fehlende Möglichkeit, Rituximab aufgrund der zu geringen Affinität zum caninen CD20 in diese Kombination mit aufzunehmen, und dem Relaps nach ca. 12 Monaten, notwendig, neue Therapiestrategien auch im Hund zu evaluieren ^{115,116}. Die Möglichkeit, vielversprechende *in vitro* generierte humane und canine Daten direkt auf den Hund übertragen zu können, stellt einen richtungsweisenden Ansatz als Zwischenschritt zur klinischen Testung und Studie dar.

3. Zielstellung

Zielgerichtete Therapien mittels „small molecules“ wie den TKIs konnten sich im Laufe der letzten Jahre durch ihren erfolgreichen Einsatz, auch bei hämatologischen Neoplasien, als mono- und kombinationstherapeutische Ansätze etablieren. Die gezielte Inhibition aberrant regulierter Zielstrukturen und der daraus resultierend veränderten Signaltransduktion erlaubt ein spezifisches und begrenztes Eingreifen in den Organismus, einhergehend mit der Eindämmung des Tumorwachstums oder dem Induzieren des Tumorzelltodes. Bei hämatologischen Neoplasien können unter anderem B-Zell Rezeptor assoziierte Kinasen (BAKs) oder epigenetische Regulatoren von Mutationen oder einer aberranten Regulation betroffen sein.

Ziel der vorliegenden Promotionsarbeit war die Evaluation der wirkstoffinduzierten Effekte durch die Inhibition von SYK und BET Proteinen, sowie deren simultane Inhibition in humanen und caninen Zelllinien hämatologischer Neoplasien. Die zell- und molekularbiologische Charakterisierung erfolgte in einem *in vitro* Ansatz hämatologischer Zelllinien des B-Zell Typs. Hierzu gehören unter anderem Zelllinien der B-ALL sowie des DLBCL und des Burkitt-Lymphoms (BL).

Folgende Zielstellungen wurden im Rahmen dieser Arbeit verfolgt, bearbeitet und erfolgreich publiziert, um die Funktion von SYK und die Kombinationsinhibition in hämatologischen Neoplasien zu evaluieren:

1. Charakterisierung und Evaluation von SYK als Zielstruktur in humanen Zelllinien der Vorläufer B-ALL unterschiedlichen Subtyps (pro B-ALL und prä B-ALL) **(Arbeit I)**
2. Evaluierung der zell- und molekularbiologischen Effekte nach SYK Inhibition mit Entospletinib in humanen B-ALL Zelllinien **(Arbeit I)**
3. Vergleichender Ansatz von pan-BET und isoform-spezifischer BET Inhibition in humanen B-Lymphom-Zelllinien **(Arbeit II)** und der caninen DLBCL Zelllinie CLBL-1 **(Arbeit III)**
4. Evaluierung der zellbiologischen Effekte der simultanen Inhibition von BET und SYK in humanen B-Lymphom-Zelllinien **(Arbeit II)** und der caninen DLBCL Zelllinie CLBL-1 **(Arbeit III)**
5. Charakterisierung der kombinationsinduzierten Genexpressionsmodulation durch simultane SYK und BET Inhibition in der humanen DLBCL Zelllinie SU-DHL-4 **(Arbeit II)**

4. Methoden

Der detaillierte methodische Ablauf kann den angehängten Originalpublikationen sowie den zitierten Literaturstellen entnommen werden. Die für die Arbeit wichtigsten Methoden sind im Folgenden in Kürze zusammengefasst. Eine Übersichtsdarstellung der Expositionsexperimente aller drei Arbeiten kann der Abbildung 1 entnommen werden.

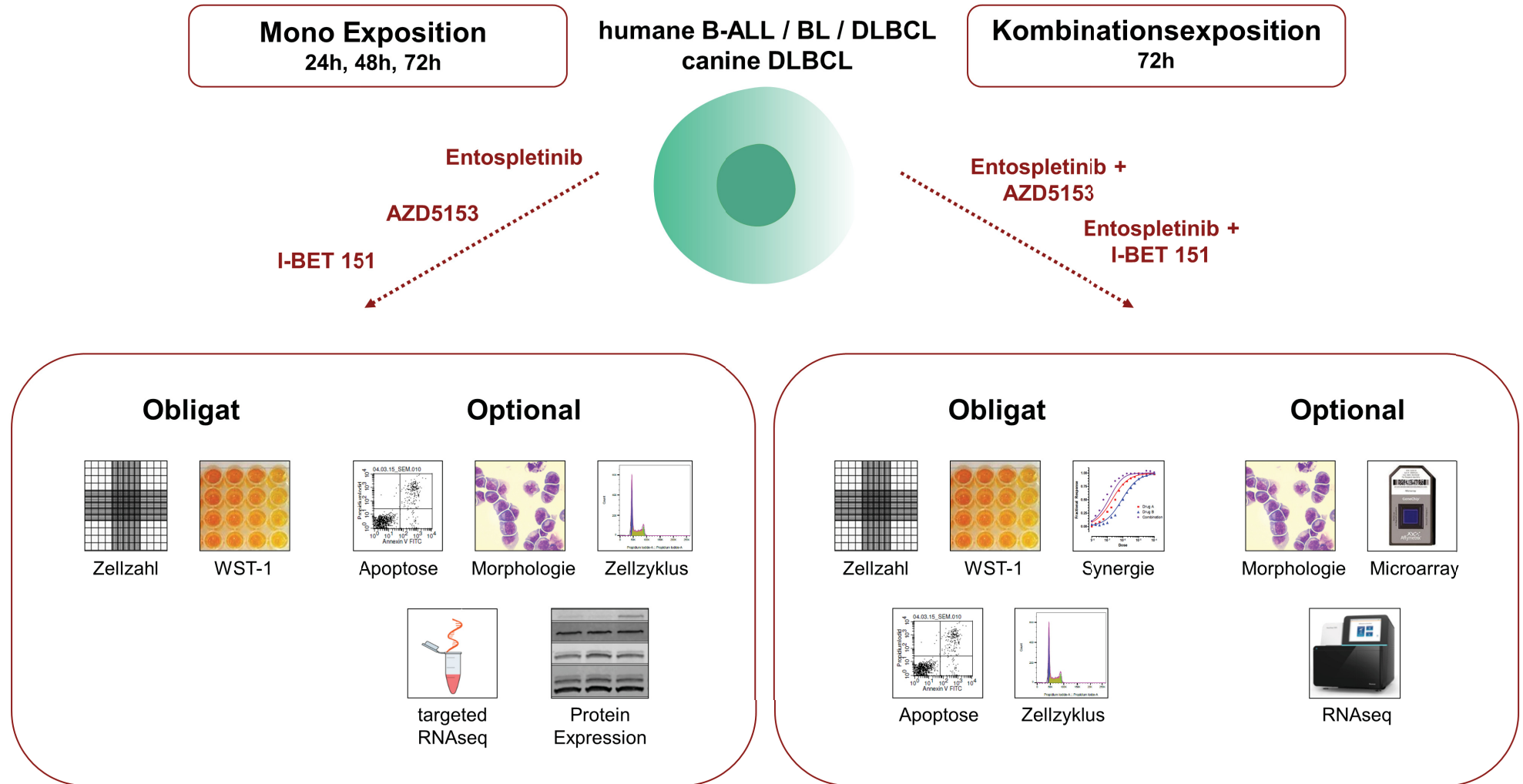
4.1 Evaluation der Substanzinduzierten Effekte *in vitro*

4.1.1 Verwendete Zelllinien

In der hier vorliegenden Arbeit wurden humane und canine hämatologische Zelllinien des B-Zell Typs verwendet. Für die Arbeit I wurden drei humane Zelllinien der B-ALL untersucht, darunter die prä B-ALL NALM-6, pro B-ALL SEM und pro B-ALL RS4;11. Das größte Unterscheidungsmerkmal dieser Zelllinien ist der Vorläufer B-Zell Rezeptor auf der Zelloberfläche der prä B-ALL NALM-6 (prä-BZR⁺), welcher auf den pro B-ALL Zelllinien (prä-BZR⁻) nicht vorliegt. Außerdem tragen SEM und RS4;11 die *KMT2A::AFF1* (früher: *MLL-AF4*) Translokation t(4;11). Weiterhin wurden für Arbeit II vier humane B-Zell Lymphom-Zelllinien verwendet. Dabei handelt es sich um zwei BL Zelllinien (DG-75 und RAJI), sowie zwei DLBCL Zelllinien (SU-DHL-4 und U-2946). In Arbeit III wurde vergleichend zu Arbeit II die canine DLBCL Zelllinie CLBL-1 verwendet (Tabelle 1). Detaillierte Informationen zu den Zelllinien sind dem Anhang zu entnehmen (Tabelle 2). Die Kultivierung der Zelllinien erfolgte gemäß der vom Leibniz-Institut DSMZ - Deutsche Sammlung von Mikroorganismen und Zellkulturen vorgegebenen Kultivierungsinformationen bei 37 °C und 5 % CO₂.

Tabelle 1: Verwendete humane und canine hämatologische Zelllinien Es wurden Zelllinien von drei unterschiedlichen hämatologischen Neoplasien verwendet. Jeweils drei humane Zelllinien der B-ALL, zwei humane Zelllinien des BL, zwei humane Zelllinien des DLBCL und eine canine Zelllinie des DLBCLs. Eine detaillierte Auflistung inklusive der Zelllinien Charakteristika befindet sich im Anhang (**Tabelle 2**). GCB: Germinal Center B-Cell-like; ABC: Activated B-Cell-like

Entität	Zelllinie	Spezies	Subtyp
B-Zell akute lymphatische Leukämie	NALM-6	Homo sapiens	prä B-ALL
	SEM	Homo sapiens	pro B-ALL
	RS4;11	Homo sapiens	pro B-ALL
Burkitt Lymphom	DG-75	Homo sapiens	
	RAJI	Homo sapiens	
Diffus großzelliges B-Zell-Lymphom	SU-DHL-4	Homo sapiens	GCB
	U-2946	Homo sapiens	ABC
	CLBL-1	canis lupus familiaris	ABC



Obligat: Analysen sind bei allen Mono- und Kombinationsapplikationen erfolgt
Optional: Analysen sind bei einem Teil der Mono- und Kombinationsapplikationen erfolgt

Abbildung 1: Übersichtsdarstellung der Expositionsexperimente aus Arbeit I – III Schematische Darstellung der Einzelsubstanzapplikationen oder Kombinationsexpositionen der drei Inhibitoren Entospletinib, AZD5153 und I-BET151 auf humane B-ALL, BL oder DLBCL Zelllinien oder auf die canine DLBCL Zelllinie CLBL1. Obligat gekennzeichnete Methoden wurden an allen Zelllinien durchgeführt. Optional gekennzeichnete Methoden wurden an einem Teil der Zelllinien durchgeführt.

4.1.2 Substanzexpositionen

Für alle Expositionsexperimente wurden die Zelllinien mit einer Dichte von $0,33 \times 10^6$ Zellen/ ml in Zellkulturplatten eingesät. Die Zelllinien wurden mit den Einzelsubstanzen Entospletinib (0,001 μM – 20 μM), AZD5153 (0,001 μM – 10 μM), I-BET151 (0,001 μM – 10 μM) für 24 h – 72 h inkubiert, wohingegen Kombinationsexperimente mit IC_{20} angenäherten Werten bei einer Inkubation von 72 h erfolgten. Dimethylsulfoxid (DMSO) fungierte bei allen Experimenten als Kontrollsubstanz. Alle Experimente wurden in mindestens drei biologischen Replikaten angefertigt.

4.1.3 Evaluation zellbiologischer Parameter

Nach jeweiliger Substanzexposition (Einzelsubstanz- und Kombinationsexposition) erfolgte die Bestimmung zellbiologischer Parameter (siehe Abbildung 1).

4.1.3.1 Bestimmung der Zellproliferation und der metabolischen Aktivität

Die Zellproliferationsbestimmung erfolgte über eine Trypanblau-Färbung mit anschließender Zellzählung.

Die Evaluation der metabolischen Aktivität erfolgte über das Tetrazoliumsalz WST-1 (TaKaRa Bio Inc., Kusatsu, Japan), welches in metabolisch aktiven Zellen zu Formazan umgewandelt wird und anschließend eine spektrophotometrische Messung erlaubt ¹¹⁷. Die Messungen erfolgten in technischen Triplikaten nach 2 und 3 Stunden WST-1-Inkubation.

4.1.3.2 Durchflusszytometrische Bestimmung der Apoptose-Induktion

Die Apoptose-Induktion wurde durchflusszytometrisch (FACSVerse™ und FACSSuite Software (Version 4.0.2) Becton, Dickinson and Company (BD)) mittels Annexin V-FITC/ Propidiumiodid (PI) Doppelfärbung bestimmt. Annexin V bindet Phosphatidylserine die während der Apoptose an die Außenseite der Zellmembran verlagert werden. Das für lebende und frühapoptotische Zellen membranundurchlässige PI gelangt in die spätapoptotischen und nekrotischen Zellen und lagert sich dort in die DNA ein.

4.1.3.3 Durchflusszytometrische Bestimmung der Zellzyklusmodulation

Für die Zellzyklusanalysen wurde ebenfalls der DNA-interkalierende Farbstoff PI verwendet, um den DNA Gehalt der Zellen nach Exposition zu bestimmen. Die Messung erfolgte am FACSVerse™ und die Auswertung mittels der Software FlowJo (BD).

4.1.3.4 Morphologische Charakterisierung mittels Pappenheimfärbung

Eine morphologische Charakterisierung der Zellen nach Exposition erfolgte mittels Färbung nach Pappenheim (May-Grünwald/ Giemsa). Die anschließende mikroskopische Auswertung erfolgte am EVOS® XL Core Imaging System (AMG, Washington, DC, USA).

4.1.3.5 Immunfluoreszenzfärbung zur Detektion von SYK

Mittels Immunfluoreszenzfärbungen wurde die zelluläre SYK Expression charakterisiert. Hierfür wurden Zellen zunächst mit einem primären SYK Antikörper (sc-1240, Santa Cruz Biotechnology, Santa Cruz, TX, USA) und anschließend mit sekundärem Fluorochrom-markiertem Antikörper (goat Anti-mouse IgG Alexa Fluor Plus 488, Thermo Fisher Scientific, MA, USA) inkubiert. Die Zellkerne wurden DAPI gefärbt (ROTI®Mount FluorCare DAPI, Carl Roth, Karlsruhe, Germany). Die Fluoreszenzaufnahmen erfolgten am Nikon Eclipse TE2000-E Konfokalen Laser Scanning Mikroskop mittels EZ-C1 Software (Nikon, Düsseldorf, Germany, Version 3.80). Die Verarbeitung der Bilder erfolgte mit der ImageJ/Fiji Software (Version 1.49b / Java 1.6.0_24).

4.1.3.6 Intrazelluläre Färbung von Phosphoproteinen mittels Durchflusszytometrie

Die Durchflusszytometrische Bestimmung intrazellulärer Proteine und Phosphoproteine erfolgte ebenfalls am FACSVerse™. Die fixierten und permeabilisierten Zellen wurden mit bereits konjugierten Antikörpern (SYK-FITC und pSYK (Y348)-PE) inkubiert und die mittlere Fluoreszenzintensität (MFI) anschließend durchflusszytometrisch bestimmt.

4.1.4 Evaluation molekularbiologischer Parameter

Neben der Bestimmung zellbiologischer Parameter, erfolgten ebenfalls molekularbiologische Analysen.

4.1.4.1 Proteinexpressionsbestimmung mittels Western Blot

Die Bestimmung der Proteinexpression erfolgte über Western Blot Analysen. Die exponierten Zellen wurden mit RIPA Puffer und Ultraschall lysiert und anschließend über den Bradford Protein Assay (Bio-Rad, München, Germany) quantifiziert. Die denaturierten Proteine wurden mittels Criterion TGX Precast Gels (Bio-Rad) gelelektrophoretisch aufgetrennt und mittels Trans-Blot® Turbo™ Transfer System (Bio-Rad) auf eine Polyvinylidenfluorid (PVDF) Membran übertragen. Nach einer einstündigen Inkubation in Odyssey Blocking-Puffer (LI-COR, Nebraska, USA), erfolgte die Inkubation mit dem primären Antikörper und anschließend dem sekundären fluoreszenzgekoppelten Antikörper. Die Detektion der Proteine erfolgte am LI-COR Odyssey® CLx Imaging System und die Auswertung anschließend mittels Image Studio Lite Software (LI-COR).

4.1.4.2 RNA Isolation

Alle RNA Isolationen erfolgten mittels miRNeasy Mini Kit (QIAGEN, Venlo, Niederlande) gemäß Herstellerangaben¹¹⁸.

4.1.4.3 Targeted RNA Panel Sequenzierung mittels PGM

Genexpressionsanalysen wurden mittels AmpliSeq RNA targeted sequencing am Ion Personal Genome Machine™ (PGM™) System (Ion Torrent™) (Thermo Fisher Scientific, Waltham,

Massachusetts, USA) und einem eigens designtem RNA Primer Panel durchgeführt. Die RNA Library Präparation erfolgte gemäß Herstellerangaben (Ion AmpliSeq™ Library Kit 2.0 - USER GUIDE - MAN0006735). Dabei wird die RNA quantifiziert, in cDNA umgeschrieben, die cDNA amplifiziert, die Amplikons teilverdaut, an Adapter ligiert und aufgereinigt. Nach erfolgreicher Library Herstellung werden die Proben mittels Ion Library TaqMan Quantification Kit (Thermo Fisher Scientific) quantifiziert und es folgt eine klonale Amplifizierung, die Isolierung template-positiver Partikel und schließlich der Sequenzierlauf am PGM. Die Auswertung der Daten erfolgte mittels Transcriptome Analysis Console (TAC) Software (Thermo Fisher Scientific, Waltham, MA, USA, Version 4.0.0.25).

4.1.4.4 Transkriptomanalysen mittels RNA Sequenzierung

Gesamt-Transkriptomanalysen erfolgten über RNA Sequenzierung in Kooperation mit der Firma Chronix Biomedical GmbH. Für die Herstellung der Sequenzierlibraries wurde 1 µg Gesamt-RNA mit einer RNA integrity number (RIN) > 8 verwendet. Es erfolgte die Anreicherung der Poly-A RNA mittels NEBNext Poly (A) mRNA Magnetic Isolation Module (New England Bioabs, Ipswich, USA) und die Adapterligation mittels NEBNext Ultra RNA preparation Kit (New England Biolabs). Der Sequenzierlauf erfolgte auf einem Illumina NextSeq500 (Illumina, San Diego, USA) mit ca. 30×10^6 Reads pro Probe.

4.1.4.5 Genexpressionsanalysen mittels Microarray

Die Genexpressionsanalysen mittels Microarray erfolgten in Kooperation mit Dr.rer.nat. Dirk Koczan aus dem Institut für Immunologie der Universitätsmedizin Rostock. Die RNA Qualität wurde mittels Bioanalyzer 2100 (Agilent, Santa Clara, CA, USA) bestimmt und RNA mit einer RIN > 9.4 verwendet. 200 µg Gesamt RNA wurden für die Synthese der Erststrang cDNA genutzt. Anschließend erfolgte die Zweitstrang cRNA Synthese. Die Aufreinigung der cRNA erfolgte über eine magnetische Bead-basierte Methode. Weiterhin wurden 15 µg cRNA für den zweiten Zyklus der „sense“ Strang Einzelstrang-cDNA Synthese verwendet, gefolgt von der RNase H Hydrolyse, Aufreinigung und Quantifizierung. 5.5 µg Einzelstrang cDNA wurde fragmentiert und anschließend mittels Bioanalyzer kontrolliert, gefolgt von der Biotin-End-Markierung. Die Hybridisierung erfolgte dann im GeneChip Hybridisierungssofen 645 (Affymetrix, Santa Clara, CA, USA) bei 45°C über Nacht, gefolgt von einem Waschschrift und der Färbung in der Affymetrix Fluidics station 450. Schließlich wurden die Microarrays im GeneChip Scanner 3000 7G (Affymetrix) bei einer Auflösung von 0.7 Mikron gescannt.

4.1.4.6 Bioinformatische Auswertung der Genexpressionsanalysen

Die bioinformatische Auswertung der Genexpressionsanalysen mittels RNA Sequenzierung und Microarray Analysen erfolgten in enger Kooperation mit Dr. Daniel Palmer und Prof. Dr.rer.nat. Georg Füllen aus dem Institut für Biostatistik und Informatik in Medizin und Altersforschung (IBIMA).

4.2 Statistik, Illustration und Synergieberechnung

Die statistischen Analysen und grafischen Darstellungen erfolgten mit der GraphPad Prism Software (San Diego, CA, USA, Version 8.0.2). In den Abbildungen sind jeweils der Mittelwert und die Standardabweichung ($\pm SD$) dargestellt. Die Normalverteilung der Daten wurde mittels Shapiro-Wilk Test überprüft. Statistische Signifikanzen der normalverteilten Daten wurden mittels one-way ANOVA (Dunnett's multiple comparison Test oder Tukey's Test als Post-hoc-Analyse) oder t -Test und die nicht-normalverteilten Daten mittels Kruskal-Wallis Test berechnet. Statistische Signifikanzen wurden mit $*p < 0.05$, $**p < 0.01$, $***p < 0.001$ ($n \geq 3$) dargestellt.

Die mathematische Berechnung der synergistischen Effekte erfolgte nach dem Bliss-Independence Modell ($EA+EB - EA \cdot EB$), wobei ein berechneter Erwartungswert aus den Effekten der Kombination mit dem experimentellen Wert verglichen wird ¹¹⁹.

5. Ergebnisse

Die wesentlichen Ergebnisse werden im folgenden Ergebnisteil, thematisch geordnet nach der jeweiligen Originalarbeit, zusammengefasst. Ebenfalls wird der Eigenanteil der zur Dissertation eingereichten Publikationen stichpunktartig dargestellt.

Neben den im Text zur Verfügung gestellten Illustrationen sind weitere Abbildungen sowie detaillierte Ergebnisdarstellungen den jeweiligen Originalarbeiten (Abschnitt 12) zu entnehmen.

5.1 Arbeit I

Precursor B-ALL cell lines differentially respond to SYK inhibition by entospletinib

Sender S., Sekora A., Villa Perez S., Chabanovska O., Becker A., Ngezahayo A., Junghanss C., Murua Escobar H.

Int. J. Mol. Sci. 2021 Jan 8;22(2):E592. doi: 10.3390/ijms22020592.
Impact Factor 2019/20: 4.556

Eigenanteil an der Originalarbeit:

- Grundlegende Beteiligung an der Studienplanung
- Durchführung aller *in vitro* Arbeiten: Western Blots, Immunfluoreszenzfärbungen, intrazelluläre Färbung und Durchflusszytometrie, Nukleinsäureisolierungen, RNA Panel Design mittels Ion AmpliSeq Designer, RNA Panel Sequenzierung, Zellvitalitätsbestimmungen (Proliferation und metabolische Aktivität), Apoptose/Nekrose Messungen mittels Durchflusszytometrie, morphologische Untersuchungen nach Pappenheim, Beteiligung an den Zellzyklusbestimmungen
- Datenauswertung, Analyse, Interpretation und grafische Darstellungen aller hier gezeigten Ergebnisse
- Vollständige initiale Verfassung des Manuskripts
- Bearbeitung der Revision des Manuskripts nach Begutachtung der Co-Autoren und während des *peer-review* Verfahrens

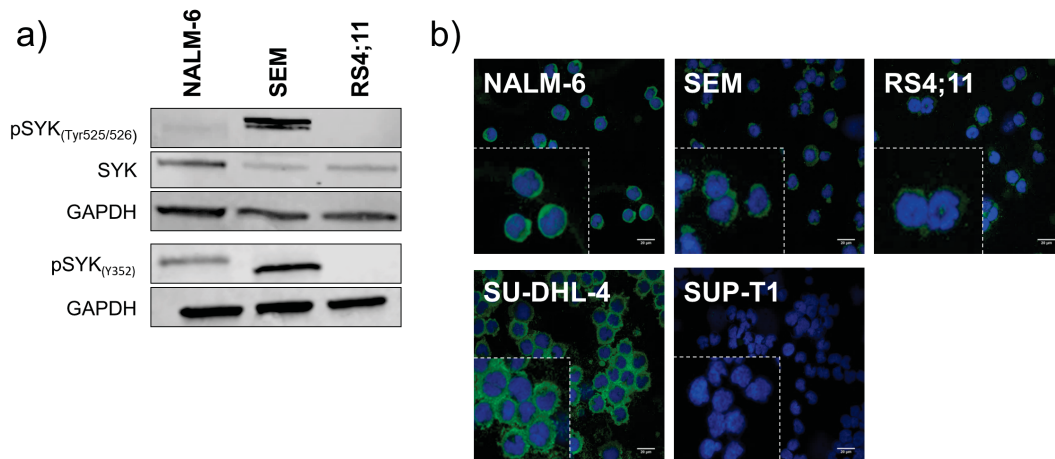
Die hier vorgelegte Arbeit I untersucht die Charakterisierung von SYK als potentiell therapeutisches Target in Vorläufer B-ALL Zelllinien in einem zellbasierten *in vitro* Ansatz.

Zunächst wurden drei Vorläufer B-ALL Zelllinien (prä B-ALL Zelllinie NALM-6 und pro B-ALL Zelllinien SEM und RS4;11) auf die Expression von SYK hin untersucht, indem die basale Proteinexpression mittels Western Blot, Immunfluoreszenz und intrazellulärer Durchflusszytometrie bestimmt wurde. NALM-6 zeigte dabei die stärkste SYK Expression, unabhängig von der zu testenden Methode. Die Zelllinien SU-DHL-4 (DLBCL) und SUP-T1 (T-Zell Lymphom) fungierten dabei als Positiv-, bzw. Negativkontrolle. Die aktive, phosphorylierte Form von SYK (pSYK) wurde über unterschiedliche Phosphorylierungsstellen ebenfalls über Western Blot und intrazelluläre Färbung ermittelt, wobei SEM die stärkste pSYK Expression zeigte (Arbeit I, Abbildung 1).

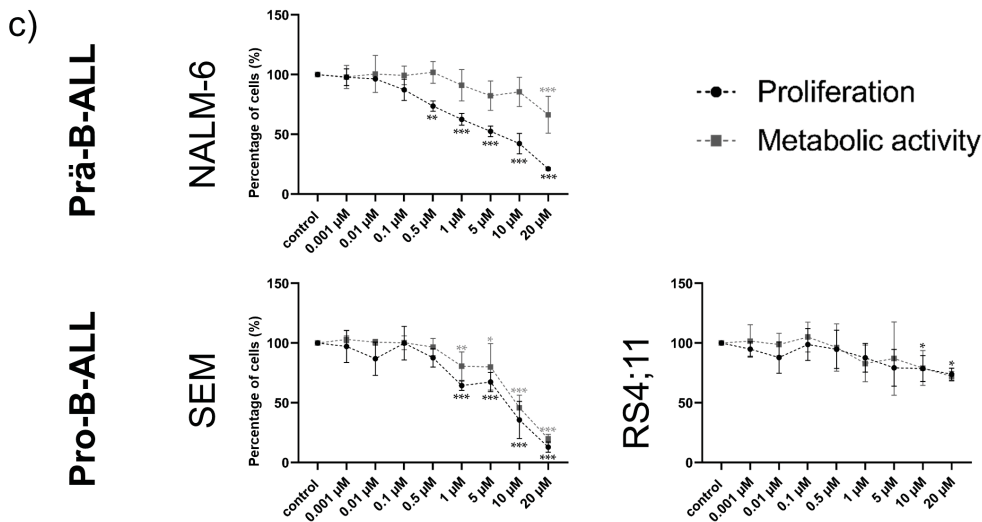
Die Inhibition und Sensitivität der Zelllinien gegenüber dem SYK Inhibitor Entospletinib wurde über die Bestimmung der Zellproliferation und der metabolischen Aktivität (24 h, 48 h, 72 h) analysiert. Es zeigte sich eine zeit- und konzentrationsabhängige Abnahme der Zellvitalität in der prä B-ALL NALM-6 und der pro B-ALL SEM. Die pro B-ALL RS4;11 war weitestgehend resistent gegenüber der Entospletinib Applikation (Arbeit I, Abbildung 3). Durchflusszytometrisch wurde die durch Entospletinib bedingte Apoptose-Induktion bestimmt und zeigte eine deutliche Zunahme von früh- und spätapoptotischen/ nekrotischen Zellen in den hohen Entospletinib Konzentrationen in den Zelllinien NALM-6 und SEM. Morphologisch zeigten sich hier ebenfalls Veränderungen, die auf eine Apoptose-Induktion und Stress der Zellen hindeuten (Arbeit I, Abbildung 4). Zellzyklusmodulationen konnten durch die Entospletinib Exposition in den Zelllinien nicht nachgewiesen werden (Arbeit I, Abbildung 5).

Über eine RNA Panel Sequenzierung und eines eigens designten Primerpanels (inkl. 179 Gene) wurde die Genexpression von im B-Zell Rezeptor- und PI3K Signalweg enthaltenen Genen bestimmt. Hierbei zeigte sich eine signifikante Genmodulation der Signalwege nach Entospletinib Exposition vorrangig in NALM-6 Zellen, wobei *PTPN6* und *BCL-6*, als am stärksten modulierte Gene und potentielle Hauptmodulatoren identifiziert werden konnten (Arbeit I, Abbildung 6). Die Expression von downstream Proteinen (Arbeit I, Abbildungen 7,8 und 9) zeigte eine Abnahme von pSHP-1 und BCL-6 in NALM-6 Zellen. Eine signifikante Abnahme der pSYK Expression an zwei Phosphorylierungsstellen konnte bei SEM beobachtet werden. Damit einhergehend konnte auch eine Abnahme von p53 festgestellt werden. Bis auf die Verminderung des pERK1/2 Levels konnten bei RS4;11 keine weiteren, signifikanten Modulationen durch Entospletinib nachgewiesen werden. p53 und BCL-6 wurden als Hauptmodulatoren bei SEM bzw. NALM-6 identifiziert (**Abbildung 2**).

Charakterisierung von SYK



Inhibition von SYK



Molekulare Untersuchung nach SYK Inhibition

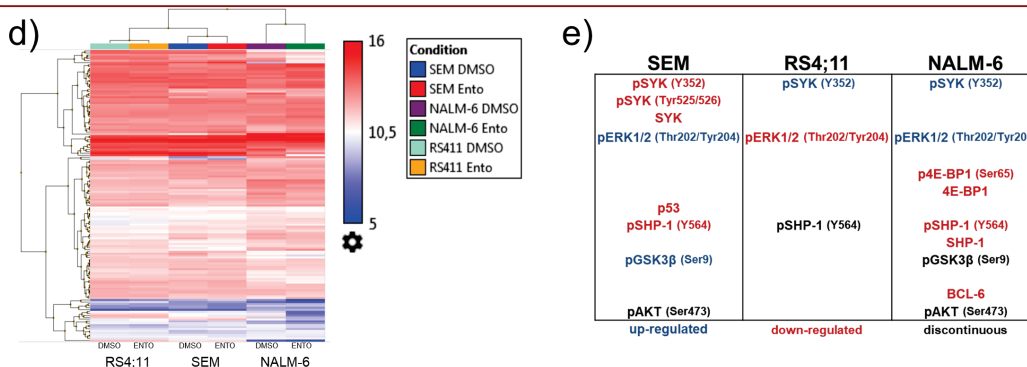


Abbildung 2: Einfluss der Entospletinib Exposition auf Zelllinien der B-ALL *in vitro*. a) Basale Bestimmung von SYK und pSYK in B-ALL Zelllinien mittels Western Blot. b) Basale Bestimmung der SYK Proteinexpression über Immunfluoreszenzfärbung. Überlagerungsdarstellung von Alexa Fluor Plus 488 grün-markiertem SYK und blau (DAPI) gefärbtem Nukleus mittels konfokaler Laserscanning Mikroskopie. c) Zellviabilität nach Entospletinib Exposition. Zeit- und konzentrationsabhängige Reduktion der Zellproliferation und metabolischen Aktivität in NALM-6, SEM und RS4;11 nach 72 h Exposition. Daten sind dargestellt als Mittelwerte \pm Standardabweichung. Statistische Signifikanz wurde mittels one-way ANOVA und anschließendem Dunnett's Test berechnet, dargestellt als * $p < 0.033$, ** $p < 0.002$, *** $p < 0.001$ im Vergleich zur DMSO Kontrolle ($n \geq 3$). d) Entospletinib-induzierte Genexpressionsänderungen, dargestellt als Hierarchische Clusteranalyse, jeweils für 1 μ M exponierte Zellen und deren DMSO Kontrolle nach 72 h Exposition. e) Entospletinib-induzierte down-stream Proteinmodulationen, zusammengefasste Darstellung der Western Blot Ergebnisse.

5.2 Arbeit II

Evaluation of the synergistic potential of simultaneous pan- or isoform specific BET and SYK inhibition in B-cell lymphoma: an *in vitro* approach

Sender S., Sultan A H., Palmer D., Koczan D., Sekora A., Beck J., Schuetz E., Brenig B., Fuellen G., Junghanss C., Murua Escobar H.

Cancers. Manuskript ID: cancers-1798753; Manuskript eingereicht am 17.06.2022, 2. Revisionsrunde *under review* seit 14.09.2022
Impact Factor 2021/22: 6.639

Erbrachter Eigenanteil an der Originalarbeit:

- Grundlegende Beteiligung an der Studienplanung
- Maßgebliche Beteiligung an der Durchführung von *in vitro* Arbeiten: Zellvitalitätsbestimmungen (Proliferation und metabolische Aktivität), morphologische Untersuchungen nach Pappenheim, Zellzyklusanalysen
- Datenauswertung, Analyse, Interpretation und grafische Darstellungen aller *in vitro* Ergebnisse
- Enge Zusammenarbeit mit der Bioinformatik und Ideenaustausch für Analysen und Ergebnisdarstellung
- Vollständige Datenauswertung und Interpretation der Transkriptom- und Microarrayanalysen
- Vollständige initiale Verfassung des Manuskripts
- Bearbeitung der Revision des Manuskripts nach Begutachtung der Co-Autoren und nach peer-review Verfahren

Die Arbeit II stellt zum einen eine vergleichende *in vitro* Analyse des pan BET Inhibitors I-BET151 und des Isoform-spezifischen, bivalent fungierenden BET Inhibitors AZD5153 in Zelllinien der B-Zell Lymphome dar. Weiterhin sollten beide BET Inhibitoren auf potenziell synergistische Effekte mit einer simultanen SYK Inhibition durch Entospletinib hin untersucht, sowie der zugrundeliegende molekulare Mechanismus analysiert werden.

Zunächst wurde die Zellvitalität von je zwei Zelllinien des BL (DG-75 und RAJI) und des DLBCL (SU-DHL-4 und U-2946) nach 24 h, 48 h und 72 h Einzelsubstanzexposition bestimmt. Es zeigte sich bereits in geringen Dosen eine deutliche zeit- und konzentrationsabhängige, signifikante Abnahme der Zellvitalität (Arbeit II, Abbildung 1). AZD5153 konnte im Vergleich zu I-BET151 die Zellviabilität in geringeren Dosen signifikant reduzieren und ergab demnach geringere IC50 Werte (Arbeit II, Abbildung S1). Die Zellvitalität von Entospletinib exponierten Zellen hingegen konnte nur bei der DLBCL Zelllinie SU-DHL-4 signifikant reduziert werden (Arbeit II, Abbildung S2).

Die simultane Inhibition von BET (AZD5153: 0,01 μ M; I-BET151: 0,1 μ M) und SYK (Entospletinib: 1 μ M) führte zu einer verstärkten Abnahme der Proliferation in allen getesteten B-Lymphom-Zelllinien (Arbeit II, Abbildung 2a, b). Vor allem in der DLBCL SU-DHL-4 konnte die zusätzliche SYK Inhibition die anti-proliferativen Effekte verstärken. Mittels Bliss Berechnung zeigte sich ein moderat synergistisches Potenzial, welches von den Effekten der Einzelsubstanzexposition abhängig war (Arbeit II, Abbildung 2c). Weiterhin konnten beide Kombinationen z.T. einen G0/G1 Zellzyklusarrest auslösen. (Arbeit II, Abbildung 4a, b; S3). Eine signifikante Apoptose-Induktion konnte hingegen bei keiner Zelllinie gezeigt werden (Arbeit II, Abbildungen 4c, d).

Um den molekularen Wirkmechanismus der Kombination (Entospletinib + AZD5153) zu identifizieren, wurden Genexpressionsanalysen durchgeführt. Die Analysen erfolgten an SU-DHL-4 über Transkriptomanalysen (RNASeq). Die Kombination aus Entospletinib und AZD5153 induzierte eine entschieden stärkere Genmodulation im Vergleich zu den beiden Einzelsubstanzen. Außerdem induzierte die Kombination eine für die Kombination spezifische Gensignatur. So ergab sich vor allem eine Modulation der Gene *ADGRA2*, *MYB*, *TNFRSF11A*, *S100A10*, *PLEKHH3*, *DHRS2* und *FOXP1-AS1* (Arbeit II, Abbildungen 5, 6, S7, S8, Ergänzende Tabelle S1, S4). Weiterhin wurden durch Gene Ontology (GO) Enrichment Analysen GO Termini identifiziert, die mehrheitlich exklusiv für die entsprechenden Bedingungen waren. Auch hier induzierte die Kombination eine kombinationsspezifische Modulation im Vergleich zu den Einzelsubstanzen, wobei vor allem die biologischen Prozesse der DNA Replikation und Zellteilung von der Kombinationsexposition betroffen waren (Arbeit II, Abbildungen 7, 8, S13 -S15, S5-S7) (**Abbildung 3**).

Genexpressionsmodulation nach Kombinationsexposition

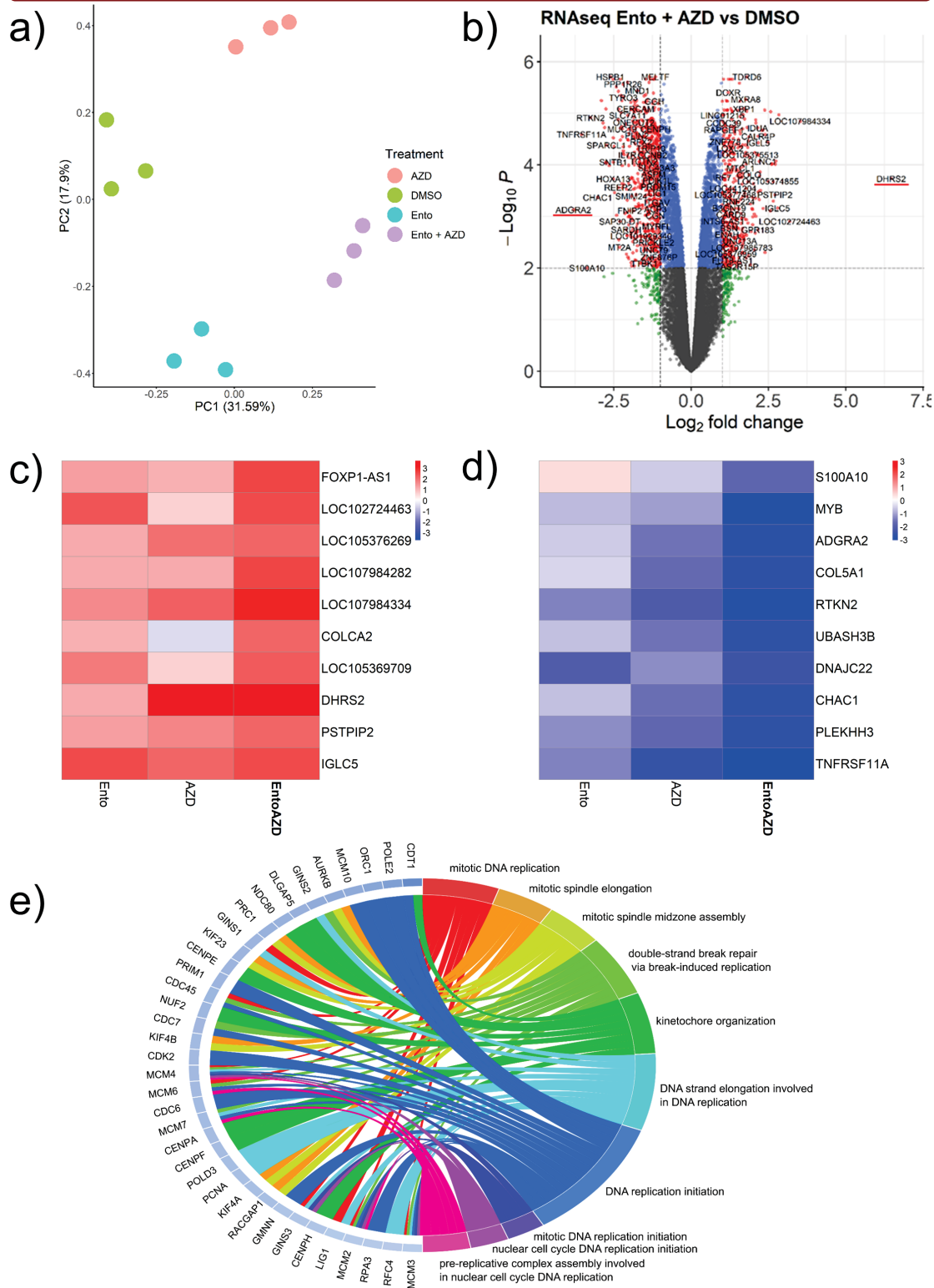


Abbildung 3: Genexpressionsmodulation in der DLBCL Zelllinie SU-DHL-4 nach Entospletinib und AZD5153 Kombinationsexposition a) Hauptkomponentenanalyse (PCA – Principal Component Analysis) der exponierten DLBCL Zelllinie SU-DHL-4. Die dargestellte Varianz zwischen den einzelnen Proben zeigt eine deutliche Clusterbildung zwischen den Kontroll-, Einzelsubstanz- und Kombinationsexponierten SU-DHL-4 Zellen. b) Differenziell deregulierte Gene (DEGs; $p < 0.05$, \log Fold Change (FC) > 2) dargestellt als Volcano Plot der Entospletinib + AZD5153 Kombination im Vergleich zur DMSO Kontrolle. Rot unterstrichen sind die am stärksten deregulierten Gene. c) Heatmap der Top10 hochregulierten Gene nach Kombinationsapplikation. d) Heatmap der Top10 herunterregulierten Gene nach Kombinationsapplikation. Farbskala $|\log FC|$ e) Chord Plot der Top10 Gene Ontology (GO) terms (signifikant herunterreguliert) verbunden zu den jeweils differentiell exprimierten Genen.

5.3 Arbeit III

Pan- and isoform-specific inhibition of the bromodomain and extra-terminal proteins and evaluation of synergistic potential with entospletinib in canine lymphoma

Kong W., **Sender S.**, Perez SV., Sekora A., Ruetgen B., Junghanss C., Nolte I., Murua Escobar H.

Anticancer Res. 2020 Jul;40(7):3781-3792.

Impact Factor 2019: 1.940

Erbrachter Eigenanteil an der Originalarbeit:

- Maßgebliche Studienplanung, angelehnt an Arbeit II als vergleichender Ansatz im caninen *in vitro* Modell
- Wesentliche Betreuung der durchgeführten *in vitro* Experimente
- Betreuung und Mitwirkung an der Datenauswertung, Analyse und Interpretation
- Maßgebliches Korrektorat des angefertigten Manuskripts

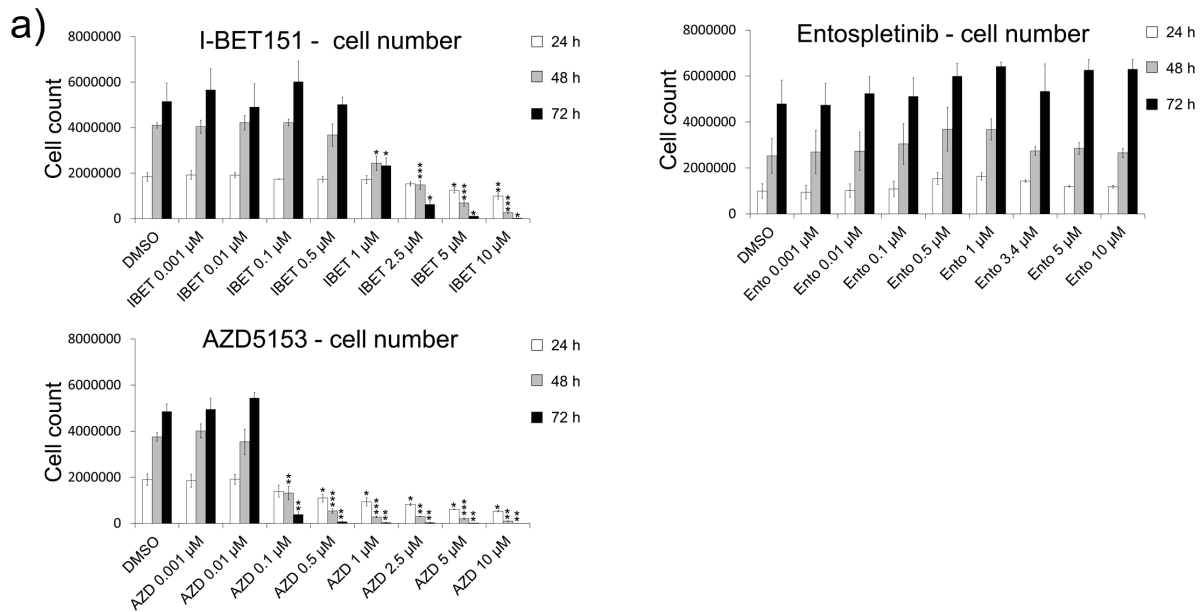
Die Arbeit III erfolgte parallel zu Arbeit II und sollte als vergleichender Ansatz für das canine Modell dienen. Ziel der Arbeit III war es, die vergleichende Analyse eines pan- und eines Isoform-spezifischen BET Inhibitors in einem caninen *in vitro* Modell zu evaluieren sowie weiterhin potenzielle synergistische Effekte zu identifizieren, wenn diese mit dem SYK Inhibitor Entospletinib kombiniert werden.

Angelehnt an Arbeit II, wurden der pan BET Inhibitor I-BET151 und der isoform-spezifische bivalente BET Inhibitor AZD5153 in einem vergleichenden Ansatz in der caninen DLBCL Zelllinie CLBL-1 *in vitro* untersucht. Beide Inhibitoren wurden zunächst als Einzelsubstanzapplikation in aufsteigenden Konzentrationen in der caninen DLBCL Zelllinie CLBL-1 getestet. Eine Evaluation der Zellvitalität zeigte nach 24 h, 48 h und 72 h Substanzexposition eine signifikante Reduktion der Zellproliferation sowie der metabolischen Aktivität, bereits bei geringer Dosisapplikation. Wie auch in Arbeit II zeigten sich für AZD5153 geringere IC₅₀ Werten als für I-BET151 (Arbeit III, Abbildung 1). Die Messung der induzierten Früh- und Spätapoptose/ Nekrose mittels Durchflusszytometrie nach Einzelsubstanzapplikation zeigte eine signifikante, konzentrationsabhängige und leicht zeitabhängige Apoptose-Induktion in den CLBL-1 Zellen (Arbeit III, Abbildung 2). Die Einzelsubstanzapplikation des SYK-Inhibitors Entospletinib zeigte keine signifikanten Effekte auf die Zellvitalität, sodass von einer Resistenz gegenüber Entospletinib ausgegangen werden kann (Arbeit III, Abbildung 1).

Die anschließende Kombinationsexposition von I-BET151 (0,75 µM) und Entospletinib (1 µM) auf CLBL-1 Zellen verstärkte die anti-proliferierenden und anti-apoptotischen Effekte moderat nach 72 h. Mittels Bliss Berechnung konnte ein leicht synergistischer Effekt identifiziert werden (Arbeit III, Abbildung 3). Die Kombinationsapplikation von AZD5153 (0,05 µM) und Entospletinib (1 µM) konnte keine weitere Effektsteigerung im Vergleich zur Einzelsubstanzapplikation mit AZD5153 induzieren. Die geringen bzw. negativen Bliss Werte bestätigten dies (Arbeit III, Abbildung 4) (**Abbildung 4**).

Ergänzend wurden morphologische Veränderungen nach Einzelsubstanzexposition und Kombinationsexposition evaluiert. Die Einzelsubstanzen induzierten nur leichte morphologische Veränderungen wie nukleäre Vakuolisierung und Membranbläschen. Für beide Kombinationsansätze konnten stärkere morphologische Veränderungen wie der komplette Zerfall der Plasmamembran, zelluläre Fragmentierung, Membranbläschen und die Entstehung von Apoptosekörperchen festgestellt werden (Arbeit III, Abbildung 5 und 6).

Einzelsubstanzexposition



Kombinationsexposition

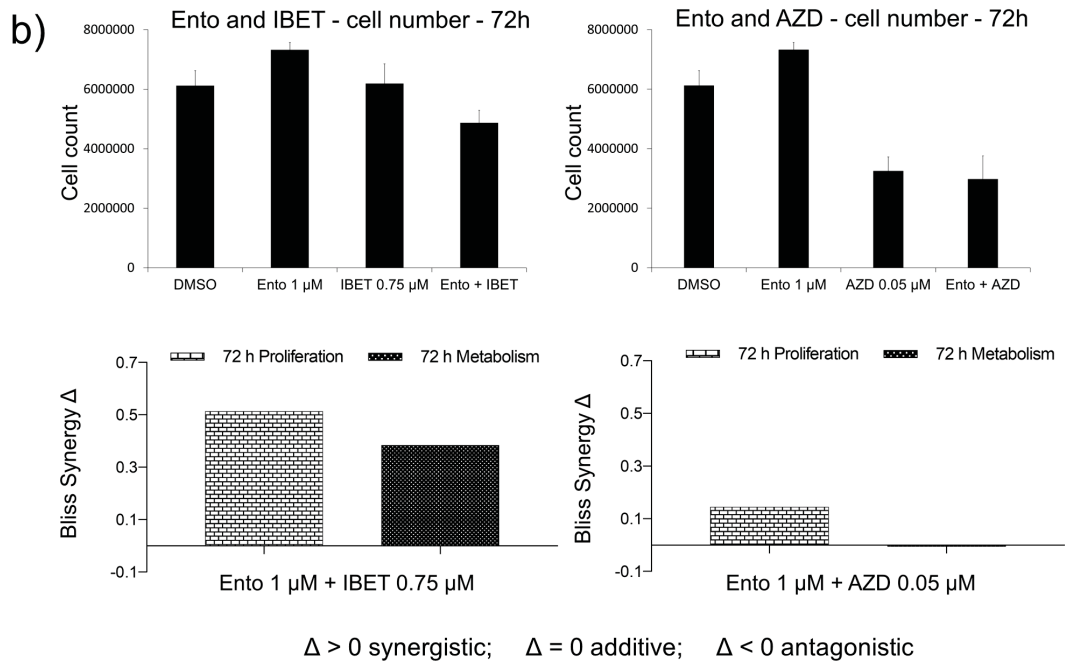


Abbildung 4: Evaluation der Zellviabilität nach einzelner oder simultaner BET und SYK Inhibition in der caninen DLBCL Zelllinie CLBL-1. a) Zellviabilität nach pan-BET Inhibition (I-BET151, 0,001 - 10 μ M) und isoform-spezifischer BET Inhibition (AZD5153, 0,001 - 10 μ M) nach 24 h, 48 h und 72 h Exposition. Zeit- und konzentrationsabhängige Reduktion der Zellproliferation, stärkerer Effekt identifiziert durch AZD5153. Entospletinib (0,001 - 10 μ M) Exposition zeigt keinen Einfluss auf die Zellproliferation von CLBL-1. **b)** Einfluss der simultanen Inhibition von BET und SYK in CLBL-1 und Berechnung des synergistischen Effekts mittels Bliss Independence Model. Werte von $\Delta = 0$, > 0 und < 0 definieren eine additive, synergistische oder antagonistische Interaktion. Abbildungen sind dargestellt als Mittelwert (\pm SD) dreier unabhängiger Experimente. Signifikante Änderungen sind dargestellt als * $p < 0.05$, ** $p < 0.01$, *** $p < 0.001$, berechnet mittels student's t -Test im Vergleich zur DMSO Kontrolle.

6. Diskussion

Zielgerichtete Therapien und kombinationstherapeutische Ansätze mittels TKIs stellen durch ihren erfolgreichen Einsatz bei B-Zell Neoplasien bereits jetzt eine Behandlungsoption, neben den konventionellen Therapieprotokollen dar. TKIs und Kombinationstherapien wurden z.T. bereits durch die FDA und EMA zugelassen und in den Leitlinien integriert^{17–20,90–94}. Bei älteren Patienten mit AML konnte der BCL-2 Inhibitor Venetoclax in Kombination mit Azacitidin die Erstlinientherapie sogar bereits ablösen^{120,121}. Aufgrund komplexer und patientenindividueller Gensignaturen ist die präklinische Evaluierung neuer Kombinationen dringend erforderlich. Das Ziel neuer Kombinationen ist unter anderem, Nebenwirkungen, „Drug Escape“ Mechanismen und Substanz-vermittelte Resistenzmutationen zu vermeiden. In präklinischen Studien konnten so durch Kombinationen beispielsweise Resistenzen umgangen oder die Sensitivität verbessert oder wiederhergestellt werden^{96,97,102,104,108}. Dies ist möglich, weil Patienten, basierend auf ihren genetischen Signaturen, mittels Hochdurchsatzsequenzierung effizient stratifizierbar sind. Die sich daraus ergebenden stratifizierten Untergruppen können dann, spezifisch und personalisiert, mittels zielgerichteter Therapien und spezifischen Inhibitoren behandelt werden.

In der hier vorliegenden Arbeit konnte SYK als potentiell therapeutisches Target in Vorläufer B-ALL Zelllinien identifiziert werden. Die Ergebnisse dieser Arbeit tragen dazu bei, SYK als potentielle Zielstruktur bei Subgruppen der Vorläufer B-ALL zu nutzen und weiterhin als Option für Kombinationstherapien zu verstehen. Mit der Evaluierung der kombinationsspezifischen Effekte von Entospletinib und AZD5153 in B-Lymphom-Zelllinien, sowie der Identifizierung des zugrundeliegenden Wirkmechanismus' in der DLBCL Zelllinie SU-DHL-4, wurden grundlegende Voraussetzung für weiterführende funktionelle Untersuchungen dieser Kombination geschaffen.

6.1 SYK als potentiell therapeutisches Target in Zelllinien der Vorläufer B-ALL

SYK als potentielle Zielstruktur in pro- oder prä B-ALL Vorläuferzellen wird bislang kontrovers diskutiert. Während in der pädiatrischen B-ALL von einer SYK Defizienz ausgegangen wird, liegt eine SYK Aktivierung in Hochrisiko Vorläufer B-ALL und in *ETV6::RUNX1* B-ALL vor und gilt daher als potentielle Zielstruktur^{43,44,122}. Die Untersuchung der SYK Expression und Aktivierung (pSYK) zeigte sowohl im Western Blot und der Immunfluoreszenzfärbung, als auch bei der intrazellulären durchflusszytometrischen Analyse eine deutliche Aktivierung von SYK in der pro B-ALL Zelllinie SEM. In anderen Studien zeigte sich bereits eine mehrheitlich starke pSYK Expression bei der *KMT2A* rearrangierten B-ALL im Kleinkind- und Kindsalter⁹⁶. Dies ist vergleichbar mit der starken pSYK Expression bei SEM, bei der es sich ebenfalls um eine

juvenile pro B-ALL handelt, die Träger der *KMT2A::AFF1* Fusion ist. Post-translationale Modifikationen von Proteinen, wie deren Phosphorylierung, spielen eine entscheidende Rolle bei der Tumorprogression. Somatische Mutationen oder aberrante Regulationen können zur Fehlregulation der Phosphorylierungsprozesse führen und damit zu einer verstärkten oder verminderten Aktivierung der entsprechenden Proteine beitragen¹²³. Keine der drei hier getesteten Zelllinien ist Träger einer somatischen SYK Mutation¹²⁴. SYK ist im Allgemeinen sehr selten von genetischen Aberrationen betroffen^{125,126}. Der fehlende prä-BZR in SEM und RS4;11 deutet eher auf eine prä-BZR-unabhängige SYK Aktivierung hin. Die unterschiedlich starke Phosphorylierung von SYK könnte also mit der Aktivierung über andere ITAM-enhaltene Rezeptoren, andere Kinasen oder Autophosphorylierung zusammenhängen.

6.2 SYK Inhibition zeigt heterogene Ergebnisse in Hinblick auf die Zellvitalität in humanen und caninen B-Zell Neoplasien

Die Exposition von Entospletinib auf die pro B-ALL Zelllinie SEM und die prä B-ALL Zelllinie NALM-6 induzierte eine starke Reduktion der Zellproliferation und der metabolischen Aktivität. Weiterhin konnten pro-apoptische Effekte bei SEM und etwas geringer bei NALM-6 in den höchsten Konzentrationen nachgewiesen werden. Dies wurde bei morphologischen Untersuchungen mittels Pappenheimfärbung ebenfalls bestätigt. Zellzyklusmodulationen hingegen gab es unter den getesteten Bedingungen in allen drei Zelllinien nicht. Im Vergleich zu anderen Studien, in denen Entospletinib bei der CLL getestet wurde, konnten stärkere anti-proliferative und pro-apoptische Effekte nachgewiesen werden^{53,55}. Auch beim DLBCL konnte der SYK Inhibitor R406 Apoptose in sensitiven DLBCL Zelllinien induzieren⁴⁰. Ein Grund dafür könnte sein, dass diese beiden B-Zell Neoplasien stärker von einem funktionsfähigem B-Zell Rezeptor abhängig sind als die B-ALL. Außerdem kann die Inhibition mittels B-Zell Rezeptor assoziierter Kinasen (BAKs) wie BTK und SYK in CLL Zellen den „cross-talk“ mit der Mikroumgebung und die BZR Signalweiterleitung stören. Dies ist bedingt durch die starke Abhängigkeit der CLL Zellen gegenüber ihrer Mikroumgebung, dem Zell-„Homing“, der Chemokin- und Zytokin Interaktionen und der Aktivierung der BZR Signalweiterleitung^{127,128}. SYK besitzt weiterhin zellzyklusregulatorische Funktionen in Hinsicht auf die G2 Checkpoint Regulation. Die Inhibition von SYK beim DLBCL führt entsprechend zu einem Arrest innerhalb des G1/S Übergangs, wohingegen die hier getesteten humanen B-ALL Zelllinien unter den getesteten Bedingungen keine Zellzyklusmodulation zeigten¹²⁹.

Die weniger starke Abhängigkeit der Vorläufer B-ALL Zellen gegenüber der Mikroumgebung, könnte ein Grund für die geringere Entospletinib Sensitivität im Vergleich zu anderen B-Zell Neoplasien sein. Die unterschiedliche Responsivität gegenüber Entospletinib scheint allerdings unabhängig vom Vorhandensein des prä-BZR und der SYK Aktivierung zu sein und

eher von ihren genetischen und molekularen Charakteristika abzuhängen. Dies könnte auch ursächlich für das unterschiedliche Ansprechverhalten der beiden pro B-ALLs SEM und RS4;11 sein.

Dahingegen zeigte sich bei der Entospletinib Exposition auf humane und canine B-Lymphom-Zelllinien ein eher moderates Ansprechen. Entospletinib induzierte zeit- und dosis-abhängig signifikante anti-proliferative und metabolismus-reduzierende Effekte bei der DLBCL Zelllinie SU-DHL-4. Die DLBCL Zelllinie U-2946 zeigte ebenfalls eine Tendenz zur Abnahme dieser beiden Parameter, diese war allerdings unstat und blieb insignifikant. Die beiden humanen BL- und die canine DLBCL Zelllinie hingegen schienen resistent gegenüber der Entospletinib Exposition zu sein. Eine Apoptose-Induktion konnte bislang nur in hohen Konzentrationen (10 µM) bei der humanen DLBCL Zelllinie SU-DHL-4 nachgewiesen werden (Daten nicht gezeigt, n=2).

Wie bereits für die AML gezeigt werden konnte, steht eine Entospletinib Resistenz im Zusammenhang mit der Aktivierung des RAS/MAPK/ERK Signalwegs ⁵⁸. Auch in der pro B-ALL Zelllinie RS4;11 konnte eine hohe pERK1/2 Expression gezeigt werden, was auf eine erhöhte Aktivität des Signalwegs hindeutet. Trotz der Abnahme von pERK1/2 durch die Exposition wurde die Zellvitalität nicht beeinflusst. In einer anderen Studie konnten wir zeigen, dass in der caninen DLBCL Zelllinie CLBL-1 pERK1/2 ebenfalls hoch exprimiert vorliegt und somit für die Entospletinib Resistenz verantwortlich sein könnte ¹³⁰. Die Untersuchung von pERK1/2 bei den humanen BL Zelllinien DG-75 und RAJI ergab ebenfalls (Daten nicht gezeigt) eine erhöhte Aktivierung. Die humanen DLBCL Zelllinien hingegen zeigten eine geringere pERK1/2 Expression, was die bessere Responsivität erklären könnte.

6.3 Entospletinib Exposition zeigt einen unterschiedlichen Wirkmechanismus in Vorläufer B-ALL Zelllinien

Um die molekularen Wirkmechanismen einer Entospletinib Exposition in allen drei humanen B-ALL Zelllinien zu identifizieren und zu charakterisieren, wurden proteinbiochemische Analysen und Genexpressionsanalysen durchgeführt. Alle drei Zelllinien zeigten deutliche Signalwegmodulierungen nach der Entospletinib Exposition mittels Western Blot. Bei der pro B-ALL Zelllinie SEM zeigte sich die stärkste Modulation in der Reduktion von pSYK_{Tyr525/526} und p53 und in der Steigerung der pERK1/2 Expression. Die starke Reduktion der p53 Expression könnte in Zusammenhang mit der Funktion von SYK als p53 (*TP53* Gen) Modulator stehen, Seneszenz zu regulieren ^{131,132}. p53 fungiert als Tumorsuppressor und induziert Apoptose, Zellzyklusarrest und Seneszenz, wenn es hoch exprimiert vorliegt ¹³³. In vielen Tumorentitäten liegt *TP53* mutiert vor, was einen Funktionsverlust (Loss-of-Function – LoF) oder Funktionsgewinn (Gain-of-Function – GoF) hervorrufen kann ¹³⁴. Auch die pro B-ALL Zelllinie SEM ist Träger der *TP53* p.R248Q Mutation (c. 743G>A; COSM10662; rs11540652)

und könnte somit die hohe basale p53 Expression erklären ¹²⁴. Diese Mutation konnte durch das Hämatologische Speziallabor der Universitätsmedizin Rostock über Hochdurchsatzsequenzierung der Zelllinie SEM mit einer Allelfrequenz von 55,4 % identifiziert werden. Einige *TP53* Hotspot Mutationen (R157H, R282W, R248Q und R249) können durch DNA Destabilisierung zu ungefalteten p53 Proteinen und damit zu Funktionsverlust des p53 wildtyps (wt) führen ¹³⁵. Die Mutation R248Q bspw. kann durch Proteinfehlfaltungen mutierte p53 Aggregate bilden, die wt p53 Proteine inaktivieren und zu Funktionsverlust führen oder mit anderen Tumorsuppressoren (p63, p73) co-Aggregate bilden, die zu Funktionsgewinn führen. Sowohl Funktionsverlust als auch Funktionsgewinn des p53 kann die Tumorprogression erhöhen ^{136,137}. Dahingegen könnte die Reduktion der Expression von p53 und die Steigerung der Expression von pERK1/2, pAKT und pGSK3 β (Glycogen Synthase Kinase 3 Beta) einen Anhaltspunkt für einen „Drug Escape“ Mechanismus gegenüber der Entospletinib Exposition darstellen ¹³⁸. So konnte in der AML, wie bereits erwähnt, ein aktivierter RAS/MAPK/ERK Signalweg mit einer Resistenzbildung in Verbindung gebracht werden ^{58,139}.

Der zugrundeliegende Mechanismus von Entospletinib scheint bei der prä B-ALL Zelllinie NALM-6 im Vergleich zu SEM ein anderer zu sein. Entospletinib reduzierte die Proteinexpression und Phosphorylierung der Phosphatase SHP-1 (Gen: *PTPN6*) sowie die Expression des Transkriptionsfaktors BCL-6. Ebenfalls zeigte sich eine Reduktion der Expression von *PTPN6* und *BCL-6* auf mRNA Ebene. SHP-1 ist ein Negativregulator von SYK und somit in der Lage, die Signalweiterleitung ausgehend vom BZR herabzusetzen ^{140,141}. Die reduzierte Expression von *BCL-6* ist eine direkte Folge der pSYK Reduktion. Geng *et al.* konnte bereits zeigen, dass die *BCL-6* Expression in prä-BZR⁺ ALL von SYK abhängig ist und dadurch direkt von der prä-BZR Signalweiterleitung abhängt ¹⁴². Die hohe Expression von BCL-6 (auf RNA und Proteinebene) in der pro B-ALL Zelllinie RS4;11 hingegen, könnte ein Anhaltspunkt dafür sein, dass unabhängig von der prä-BZR Signalweiterleitung, die hohe BCL-6 Expression die Zelle vor Apoptose schützt. In *KMT2A* rearrangierten B-ALL Zellen konnte die hohe BCL-6 Expression mit einer schlechten Prognose in Verbindung gebracht werden, da BCL-6 die Expression des Apoptoseregulators BCL2 Like 11 (BIM) negativ reguliert und somit die Apoptose unterbindet ¹⁴³. Die BCL-6-BIM Interaktion könnte demnach die unterschiedlichen Wirkmechanismen von Entospletinib in den drei hier getesteten Zelllinien erklären. Wohingegen die hohe BCL-6 Expression die Resistenz gegenüber der Entospletinib Exposition in RS4;11 begründen könnte.

6.4 Isoform-spezifische bivalente BET Inhibition dominiert über pan-BET Inhibition in humanen und caninen B-Lymphom-Zelllinien

Die vergleichende Analyse der BET Inhibition mittels pan BET Inhibitor I-BET151 und Isoform-spezifischem bivalenten Inhibitor AZD5153 zeigte in beiden humanen BL Zelllinien, den beiden humanen DLBCL Zelllinien und der caninen DLBCL Zelllinie eine stärkere Inhibition der Proliferation und der metabolischen Aktivität durch AZD5153. Die verbesserte Wirksamkeit des isoform-spezifischen BET Inhibitors AZD5153 wurde bereits damit begründet, dass AZD5153 in der Lage ist, beide BRD4 Bromodomänen simultan zu binden, was folglich zu einer effizienteren und anhaltenden Dislokation des BRD4 vom Chromatin führt^{86,144}. Die IC_{50} Werte von I-BET151 zwischen der humanen DLBCL Zelllinie SU-DHL-4 und der caninen DLBCL Zelllinie CLBL-1 sind sowohl für I-BET151 (SU-DHL-4: $IC_{50} = 0,8030 \mu\text{M}$; CLBL-1 $IC_{50} = 0,870 \mu\text{M}$) als auch AZD5153 (SU-DHL-4: $IC_{50} = 0,1087 \mu\text{M}$; CLBL-1: ($IC_{50} = 0,054 \mu\text{M}$) vergleichbar.

6.5 Kombination einer SYK und BET Inhibition als potentielle Kombinationsstrategie in B-Zell Lymphomen

Die Kombination einer simultanen SYK und BET Inhibition zeigte, unabhängig vom eingesetzten BET Inhibitor, eine signifikant gesteigerte Effizienz bezüglich der Proliferationsinhibition. Vor allem in den humanen Zelllinien DG-75, SU-DHL-4 und U-2946 konnte die Proliferation signifikant gegenüber der Kontrolle reduziert werden. Eine signifikante Abnahme gegenüber der Einzelsubstanz Entospletinib zeigte sich bei den BL Zelllinien DG-75 und RAJI und der DLBCL U-2946. Bei der DLBCL Zelllinie SU-DHL-4 konnte eine signifikante Reduktion der Proliferation der Kombinationen im Vergleich zu dem jeweiligen BET Inhibitor nachgewiesen werden. Die metabolische Aktivität wurde alleinig in SU-DHL-4 Zellen durch die Kombination im Vergleich zu den BET Einzelsubstanzen signifikant reduziert. Mittels Bliss Berechnung konnten in den drei Zelllinien DG-75, RAJI und U-2946 synergistische Effekte identifiziert werden. Aufgrund der bereits starken anti-proliferativen Effekte der Entospletinib Einzelsubstanzapplikation, war dies in SU-DHL-4 mittels Bliss nicht möglich.

In der caninen DLBCL hingegen konnte zwar eine verstärkte Reduktion der Proliferation und metabolischen Aktivität durch die Entospletinib und I-BET151 Kombination verzeichnet werden, allerdings nicht signifikant gegenüber den Einzelsubstanzen. Die Entospletinib und AZD5153 Kombination zeigte keinerlei verstärkende Aktivität gegenüber AZD5153, möglicherweise bedingt durch die bereits hohe Effizienz der Einzelsubstanz. Die Bliss Werte bestätigen dies. In anderen Studien konnte allerdings gezeigt werden, dass die Kombination von BET Inhibitoren mit B-Zell assoziierten Kinasen, unter anderem Entospletinib in Zelllinien der CLL, oder PI3K Inhibitoren in B-Lymphom-Zelllinien, zu synergistischen Effekten führt^{145,146}. Im caninen DLBCL Modell ist die Datenlage bzgl. der Einzelsubstanz- oder

Kombinationsinhibition von SYK und BET begrenzt. Es konnte allerdings gezeigt werden, dass die BET Inhibition mittels OTX015 ebenfalls zu einer Reduktion der Zellproliferation in der caninen DLBCL Zelllinie CLBL-1 führt ¹⁴⁷.

Weiterführende zellbiologische Untersuchungen zeigten, dass unter den hier getesteten Bedingungen in den humanen B-Lymphom-Zelllinien keine Apoptose induziert werden konnte. Die morphologischen Veränderungen waren ebenfalls nur moderat und konnten somit keine Apoptose-Induktion nachweisen. Bei der caninen DLBCL Zelllinie hingegen konnte signifikant Frühapoptose durch AZD5153 alleine und beide Kombinationen im Vergleich zur Kontrolle induziert werden. Allerdings erfolgte keine Steigerung der Apoptose durch die Kombination im Vergleich zu den Einzelsubstanzen. Auch die morphologischen Veränderungen waren im Vergleich zu den humanen Zelllinien deutlicher. Weiterhin wurde in den humanen B-Lymphom-Zelllinien eine signifikante G0/G1 Zellzyklus Blockade identifiziert, die teilweise bereits durch AZD5153 ausgelöst werden konnte. I-BET151 als Einzelsubstanz erzielte keine signifikante Zellzyklusmodulation. Eine Effektsteigerung beider Kombinationen verglichen zu den BET Einzelsubstanzen konnte nur bei der DLBCL U-2946 festgestellt werden, allerdings nicht signifikant gegenüber den Einzelsubstanzen. Ein G0/G1 Zellzyklusarrest konnte ebenfalls bereits durch die Vorgängersubstanz JQ1 in DLBCL Zelllinien gezeigt werden ¹⁴⁸. Auch in der BL Zelllinie RAJI wurde durch JQ1 ein G0/G1 Arrest ausgelöst ⁷¹. Dies konnte in der vorliegenden Arbeit in RAJI nicht nachgewiesen werden. Allerdings konnte für AZD5153 bereits gezeigt werden, eine G1/S Zellzyklusblockade in einer Double-Hit Lymphom (DHL; *MYC* und *BCL-2* betroffen) DLBCL Zelllinie auszulösen, ohne dabei Apoptose zu induzieren ¹⁴⁴. Diese Beobachtung deckt sich mit den unseren. In weiterführenden Arbeiten konnte in der caninen DLBCL Zelllinie CLBL-1 ebenfalls ein G0/G1 Zellzyklus Arrest, sowohl durch beide BET-inhibierenden Einzelsubstanzen als auch durch die Kombinationen, identifiziert werden (Daten nicht gezeigt, n≥3).

Die signifikanten Effekte auf die Proliferation ohne Apoptose-Induktion können weitreichende Ursachen haben. Es konnte bereits gezeigt werden, dass AZD5153 *MYC* effektiv und konzentrationsabhängig herunterreguliert und damit auch wichtige Regulatoren der BZR Signalweiterleitung ^{86,144,146}. Die signifikante Herunterregulation des anti-apoptotischen Proteins *BCL-2* blieb bei der DLBCL DHL als der auch double expressing lymphoma durch AZD5153 in einer Studie von Takimoto-Shimomura *et al.* allerdings aus ¹⁴⁴. Die in unserer Studie getesteten B-Lymphom-Zelllinien weisen unterschiedliche Eigenschaften bzgl. *MYC* und *BCL-2* auf. Während die DLBCL SU-DHL-4 eine Triple-Hit Lymphom- (THL) (*BCL-2*, *BCL-6* und *MYC* Rearrangement) Zelllinie ist ^{149,150}, tragen die DLBCL U-2946 ¹⁵¹ und die BL Zelllinien RAJI ^{152,153} und DG-75 ^{153,154} die Translokation t(8;14) und besitzen ein *MYC-IGH* Fusionsgen. Die BL Zelllinie DG-75 besitzt außerdem die *BAX* frameshift Deletion p.M38fs.

Der Verlust des Apoptose Mediators BAX konnte kürzlich mit einer Venetoclax Resistenz bei Patienten mit Richter's Syndrom in Verbindung gebracht werden ¹⁵⁵. Dies könnte ebenfalls mit der Resistenz gegenüber Entospletinib zusammenhängen. Die canine DLBCL Zelllinie CLBL-1 hingegen zeigt eine Überexpression von *MYC* und *BCL-2* im Vergleich zu nicht-neoplastischen Lymphknoten ¹⁵⁶. Nur in der caninen Zelllinie konnte eine leichte Apoptose-Induktion verzeichnet werden. Die Apoptose-Induktion scheint also unabhängig von *BCL-2* zu sein. In einer Arbeit von 2019 induzierte ebenfalls erst eine zusätzliche *BCL-2* Inhibition mittels AZD4320 Apoptose in DLBCL Zelllinien ¹⁴⁴. Die Kombination mit Entospletinib in den hier getesteten B-Lymphom-Zelllinien konnte allerdings keine weitere Verstärkung der Apoptose-Induktion induzieren. Anders als bei den in Arbeit I untersuchten B-ALL Zelllinien war Entospletinib hier bereits in der Lage, als Einzelsubstanz in den hohen Konzentrationen Apoptose zu induzieren ¹¹⁷. In weiterführenden Arbeiten konnten beide Kombinationen in SEM die Apoptose-Induktion verstärken (Daten nicht gezeigt, N≥3). Auch in der CLL konnten Entospletinib und R406 Apoptose auslösen. Die Apoptosemessungen erfolgten hier allerdings bereits nach 24 Stunden ⁵⁵. Chen *et al.* zeigte bereits, dass R406 in der Lage ist, Apoptose in der DLBCL zu induzieren, allerdings erfolgten die Analysen hier 96 Stunden nach der Exposition ⁴⁰. Wieso die Kombination aus AZD5153 oder I-BET151 mit Entospletinib nicht in der Lage war, Apoptose nach 72 h auszulösen, bleibt zu klären. Eine Vermutung sind die unterschiedlichen Expositions- und Messbedingungen (Zeit und Konzentration). Allerdings zeigen die bei der SU-DHL-4 gemessenen Apoptosedaten auch eine hohe Standardabweichung, die die Signifikanz ebenfalls beeinträchtigt haben könnten. Denn sowohl die Entospletinib Einzelsubstanzapplikation, als auch die beiden Kombinationen zeigen einen gewissen Trend in Richtung Apoptose-Induktion.

6.6 Die simultane Inhibition führt zu einer kombinationsspezifischen Gensignatur in der DLBCL SU-DHL-4

Neben den veränderten zellbiologischen Parametern moduliert die Entospletinib und AZD5153 Kombination ebenfalls die Genexpression in der DLBCL Zelllinie SU-DHL-4. Mittels Transkriptomanalysen konnte in der Entospletinib + AZD5153 Kombination eine deutlich gesteigerte Anzahl differentiell exprimierter Gene (DEGs) im Vergleich zu den Monosubstanzen und eine gesteigerte Spanne der Expressionshöhe (logFC) festgestellt werden. Auch die Einzelsubstanzen Entospletinib und AZD5153 waren bereits in der Lage, die Genexpression nach der Exposition zu modulieren, allerdings deutlich geringer. Weiterhin zeigte die Kombination eine hohe Anzahl exklusiv differentiell exprimierter Gene und weist demnach eine kombinationsspezifische Gensignatur nach Inhibition auf.

Genexpressionsmodulation durch die Entospletinib Einzelsubstanzapplikation

Das durch Entospletinib am stärksten hochregulierte Gen ist die unbekanntes *long intergenic non-coding RNA* (lincRNA) *LINC01781*. lincRNAs spielen eine wichtige Rolle bei der Regulierung zellulärer Prozesse wie beispielsweise der Genexpressionsregulation, der Chromatinremodellierung und RNA Stabilisierung (zusammengefasst in den Übersichtsartikeln ^{157,158}). Inwieweit die *LINC01781* eine Rolle bei der durch Entospletinib induzierten Genexpressionsmodulation spielt, kann in dieser Arbeit nicht vollständig geklärt werden. Allerdings kann davon ausgegangen werden, dass *LINC01781* durch die Rolle als lincRNA bei der Genexpressionsregulation wie bspw. der Transkriptionsregulation involviert ist und damit die Genexpression anderer Gene beeinflusst. Ein weiteres stark hochreguliertes Gen ist die *Activation-induced cytidine deaminase (AICDA)* und essentiell für die somatischen Hypermutationen und den Klassenwechsel der Immunoglobulin (Ig) Gene in normalen B-Zellen ¹⁵⁹. Es konnte bereits gezeigt werden, dass eine hohe *AICDA* Expression mit einem schweren Verlauf bei der DLBCL in Zusammenhang steht. Die hohe *AICDA* Expression führte sowohl zu einer vermehrten inter-Tumor und intra-Tumor Heterogenität der Cytosinmethylierung als auch zu Hypomethylierung ¹⁶⁰. Die starke Hochregulation von *AICDA* könnte ein Zeichen für Resistenz- oder „Drug Escape“ Mechanismen sein, die durch die Entospletinib Applikation in SU-DHL-4 Zellen ausgelöst werden.

Dahingegen ist *SLC8A1 (Sodium/Calcium Exchanger 1)* das am stärksten herunterregulierte Gen nach der Entospletinib Exposition. Der $\text{Na}^+/\text{Ca}^{2+}$ Austauscher *SLC8A1 (NCX1)* spielt eine wichtige Rolle bei der Calcium Homöostase ¹⁶¹. Eine veränderte Calcium Signalweiterleitung ist mit der Tumorentstehung, -Progression und -Metastasierung assoziiert ¹⁶². Entsprechend scheint NCX1 in einigen Tumorentitäten überexprimiert vorzuliegen ^{161,163,164}. Folglich konnte gezeigt werden, dass die Inhibition von NCX1 zu einer Apoptose-Induktion und einem Zellzyklusarrest in der Prostatakarzinomzelllinie PC3 führt und den PI3K und Jun N-terminal kinase (JNK) Signalweg moduliert ¹⁶¹. Beim Peniskarzinom wurde *SLC8A1* ebenfalls mit Apoptose und Proliferation, durch eine veränderte Calcium Konzentration, in Verbindung gebracht ¹⁶⁵. Es konnte weiterhin gezeigt werden, dass eine SYK Aktivierung zu einer Ca^{2+} Ausschüttung führt ¹⁶⁶. Daher kann davon ausgegangen werden, dass Entospletinib ebenfalls die Calcium Signalweiterleitung und damit *SLC8A1* beeinflusst. Da in der vorliegenden Arbeit in der Entospletinib + AZD5153 Kombination ebenfalls eine signifikante Herunterregulation von *SLC8A1* identifiziert wurde, auch im Vergleich zur AZD5153 Einzelsubstanzapplikation, kann vermutet werden, dass *SLC8A1* einen wichtigen Regulator des Wirkmechanismus' der Entospletinib- und Kombinationsexposition darstellt. Ein weiteres Calcium assoziiertes Gen ist *S100A4 (S100 Calcium Binding Protein A4)* und konnte durch Entospletinib ebenfalls herunterreguliert werden. Das Protein spielt eine entscheidende Rolle in der Ca^{2+}

Homöostase, der Proliferation, der Apoptose und dem Zellzyklus. Es konnte bereits gezeigt werden, dass *S100A4* in soliden Tumoren und der AML überexprimiert vorliegt und bei der AML für Wachstum und Überleben notwendig ist^{167,168}. Die Kombination verstärkte deutlich die Herunterregulation von *S100A4*. Ebenso induzierte die Kombination eine signifikante Herunterregulation des *S100 Calcium Binding Protein A10 (S100A10)*.

Genexpressionsmodulation durch die AZD5153 Einzelsubstanzapplikation

Die AZD5153 Einzelsubstanzexposition induzierte eine signifikante Hochregulation des Gens der Dehydrogenase/Reductase 2 (*DHRS2*). Die Funktion von *DHRS2* ist bislang nicht vollständig geklärt und wird heterogen diskutiert. Zum einen konnte bereits gezeigt werden, dass *DHRS2* als Tumorsuppressor fungiert^{169,170}. Beim Ösophaguskarzinom konnte die Überexpression zu einem verringerten Tumolvolumen führen und ein Knockdown das Tumolvolumen hingegen erhöhen¹⁷⁰. Die Inhibition von Histon-Deacetylasen (HDAC) führte ebenfalls zu einer Hochregulation von *DHRS2* und wird daher mit der Sensitivität diesen gegenüber in Verbindung gebracht¹⁷¹. Allerdings konnte eine hohe Expression von *DHRS2* auch bei resistenten Leberkrebszellen beobachtet werden. Die Anwendung des BET Inhibitors Hjp-6-171 erhöhte hier die Expression von *DHRS2* sowohl in sensitiven, als auch in resistenten Zellen, was eher auf einen „Drug Escape“- oder Resistenzmechanismus schließen lässt¹⁷².

Der Transkriptionsrepressor *GFI1B (Growth Factor Independent 1B Transcriptional Repressor)* wurde in der DLBCL SU-DHL-4 durch AZD5153 am stärksten herunterreguliert. Wie im Übersichtsartikel von Beauchemin und Möröy bereits evaluiert, rekrutiert *GFI1B* Chromatinmodifikatoren an die Zielgene und besitzt demnach eine ähnliche Funktion wie *BRD4*¹⁷³. Eine direkte Interaktion zwischen *GFI1B* und *BRD4* ist allerdings nicht bekannt. Weiterhin induzierte AZD5153 die Herunterregulation von *Ras Association Domain Family Member 6 (RASSF6)*. Es ist bekannt, dass das pro-apoptotische Gen *RASSF6* bei geringer Expression mit Substanzresistenzen und verringerter Apoptoserate assoziiert ist und vice versa die Hochregulation die Proliferation inhibiert¹⁷⁴⁻¹⁷⁷. Die Entospletinib + AZD5153 Kombination neutralisierte diesen Effekt, indem *RASSF6* nicht mehr signifikant moduliert worden ist.

Kombinationsspezifische Gensignatur durch die Entospletinib und AZD5153 Kombination

Die Entospletinib und AZD5153 Kombination war nicht nur in der Lage, die Genexpressionsänderung deutlich zu verstärken, sie führte auch zu einer kombinationsspezifischen Gensignatur in SU-DHL-4 Zellen. Die Genexpressionsanalyse der Kombination zeigte vor allem, dass der BET Inhibitor AZD5153 einen entscheidenden Anteil

an der starken Genmodulation trägt. Die zusätzliche Inhibition von SYK führte entsprechend zu der kombinationsspezifischen Genexpressionsmodulation in SU-DHL-4 Zellen.

Das Gen *DHRS2* wird durch die Kombination am stärksten hochreguliert. Wie oben bereits beschrieben, erfolgte eine starke Hochregulation bereits durch AZD5153. Die simultane Applikation mit Entospletinib verstärkte die Expressionssteigerung. Ob dieser Effekt den protektiven Mechanismus eines Tumorsuppressors unterstützt und damit vor weiterer Tumorprogression schützt oder es sich um einen „Drug Escape“- oder Resistenzmechanismus handelt, bleibt allerdings zu klären.

Das Gen *Adhesion G Protein-Coupled Receptor A2 (ADGRA2)* konnte als das am stärksten herunterregulierte Gen nach der simultanen Exposition von Entospletinib und AZD5153 identifiziert werden. *ADGRA2* ist auch bekannt als *Tumor Endothelial Marker 5 (TEM5)* oder *G-Protein Coupled Receptor 124 (GPR124)* und spielt vorrangig bei soliden Tumoren eine Rolle. Durch die hohe Expression von TEM5 beim kolorektalen Karzinom wird angenommen, dass der Rezeptor mit einem schlechten Gesamtüberleben in Zusammenhang steht und als Progressions- und Biomarker dienen kann¹⁷⁸. Beim Glioblastom führte generell eine Veränderung der GPR124 Expression zur Reduktion der Zellproliferation. Folglich wird vermutet, dass GPR124 sowohl anti- als auch pro-proliferative Signale weiterleitet¹⁷⁹. Die Funktion von *ADGRA2* in Lymphomen ist bislang unbekannt. Mittels der Datenbank „depmap portal“ konnte für die DLBCL Zelllinie SU-DHL-4 eine missense Mutation identifiziert werden, die zu einem Aminosäureaustausch (p.A765T) führt. Allerdings ist diese Mutation laut COSMIC Datenbank unbekannt.

Das Gen *TNF receptor superfamily member 11a (TNFRSF11A)*, auch bekannt als RANK, ist ebenfalls signifikant durch die Kombination herunterreguliert worden. *TNFRSF11A* spielt bei diversen biologischen Prozessen wie Apoptose, Zellüberleben und Differenzierung eine Rolle. Dies erfolgt durch die Aktivierung diverser Signalwege wie der des *Nuclear factor κB (NF-κB)*, JNK, p38, ERK und PI3K^{180,181}. Eine aberrante *TNFRSF11A* Expression konnte bereits mit einigen Tumorentitäten in Verbindung gebracht werden. So zeigte sich beispielsweise eine Überexpression von *TNFRSF11A* beim Mammakarzinom, Prostatakarzinom mit hohem Metastasierungspotenzial und beim Gliom^{182–185}. Es konnte ferner gezeigt werden, dass eine aberrante Expression von *TNFRSF11A* auch bei Leukämien eine Rolle spielen kann. In CLL Zellen konnte eine höhere *TNFRSF11A* Expression im Vergleich zu peripheren CD19⁺ B-Zellen aus Kontrollmäusen nachgewiesen werden. Eine anschließende Behandlung mit einem anti-RANKL (*microenvironmental RANK ligand*) Antikörper konnte die leukämische Last signifikant reduzieren. Das deutet darauf hin, dass die RANKL-RANK Achse zum einen eine Rolle bei der CLL spielt und zum anderen die supportive Mikroumgebung der CLL Zellen unterstützt, da diese durch den anti-RANKL Antikörper gestört werden kann¹⁸⁶. Auch beim

DLBCL spielt *TNFRSF11A* eine wichtige Rolle, indem es den Signalweg des NF- κ B positiv reguliert und dieser häufig vor allem bei ABC-DLBCL und zum Teil bei GCB-DLBCL konstitutiv aktiviert ist. Gene des NF- κ B Signalwegs können häufig mutiert vorliegen. Dies betrifft ebenfalls *TNFRSF11A*, allerdings seltener¹⁸⁷. Da *TNFRSF11A* nicht nur durch die Kombination, sondern bereits durch beide Einzelsubstanzen signifikant herunter reguliert worden ist, handelt es sich hier nicht um einen kombinationsspezifischen, sondern einen global induzierten Effekt. Allerdings konnte die Kombination den Effekt noch einmal deutlich verstärken.

Weiterhin zeigte sich, wie bereits oben beschrieben, eine kombinationsspezifische Herunterregulation des Gens *S100A10*. Eine aberrante *S100A10* Expression konnte bereits mit der Tumorentwicklung, Invasion und einer schlechten Prognose in Zusammenhang gebracht werden. Durch die aberrante Expression von *S100A10* in verschiedensten Tumorzellen kann es als Biomarker fungieren^{188–191}. Weiterhin konnte bereits eine anti-apoptotische Funktion in Tumorzellen beobachtet werden, bedingt durch die Störung der pro-apoptotischen Funktion des Proteins *Bcl-2-associated death protein* (BAD) (zusammengefasst im Übersichtsartikel¹⁸⁸).

Die aberrante Expression des Transkriptionsregulators *MYB Proto-Oncogene, Transcription Factor* (*MYB*) wurde bereits häufig bei Leukämien mit Translokationen, Lymphomen und soliden Tumoren beobachtet^{192,193}. In der DLBCL Zelllinie SU-DHL-4 konnte ebenfalls eine Hochregulation von *MYB* nachgewiesen werden¹⁹⁴. Die Kombination war in der Lage, *MYB* signifikant herunterzuregulieren. In soliden Tumoren konnte eine Herunterregulation sowohl die Proliferation als auch die Invasion inhibieren^{195,196}.

Die Entospletinib und AZD5153 Kombination führt zu kombinationsspezifischen Gene Ontology terms

Um das Verständnis um den kombinationsspezifischen Wirkmechanismus von Entospletinib und AZD5153 in der DLBCL SU-DHL-4 zu präzisieren, wurden Gene Ontology (GO) Enrichment Analysen durchgeführt und später zu GO „Clusters“ zusammengefasst.

Auch hier wurden kombinationsspezifische, biologische Prozesse identifiziert, die alleinig durch die Entospletinib + AZD5153 Kombination moduliert worden sind. Es zeigte sich vor allem, dass biologische Prozesse wie die DNA Replikation und Zellteilung von der Kombination beeinflusst werden. Während eine Vielzahl an GO Terms signifikant herunterreguliert worden sind, konnten keine als signifikant hochreguliert identifiziert werden. Die Betrachtung der Top10 GO Terms (herunterreguliert) identifizierte auch die entsprechend zugehörigen differentiell exprimierten Gene. Wie die Zuordnung zu den entsprechenden GO Terms bereits verrät, spielen die meisten Gene eine Rolle bei der DNA Replikation oder der Zellteilung. So

konnten unterschiedliche Genfamilien identifiziert werden, die im DNA Replikationsprozess eine Rolle spielen. Hier zeigten sich Gene aus den *mini chromosome maintenance (MCM)*, Centromer (*CEN*), *cell division cycle (CDC)*, *Kinesin Family (KIF)* und *GINS complex subunit (GINS)* Familien als besonders häufig differentiell exprimiert und entsprechend den GO Terms zugeordnet.

MCM Gene wurden häufig zu unterschiedlichen GO Terms der Top10 Herunterregulierten zugeordnet. Diese DNA Helikasen entwinden die DNA Doppelstränge und regulieren und initiieren somit den DNA Replikationsprozess¹⁹⁷. Auch bei der Tumorentwicklung können diese Enzyme involviert sein. Bei unterschiedlichen Tumorentitäten, wie bspw. Leukämien und Lymphomen, liegt *MCM3* überexprimiert vor¹⁹⁸. Beim DLBCL konnte *MCM2* durch die erhöhte Expression sogar als negativer prognostischer Marker identifiziert werden¹⁹⁹. Gene der *GINS* Familie wie *GINS1* und *GINS2* sind ebenfalls bei der Initiation des DNA Replikationsprozesses involviert. Die vermehrte Hochregulation dieser Gene bei unterschiedlichen Tumorentitäten macht diese zu potentiellen prognostischen Markern^{200,201}. Einige Gene der *CDC* Familie wurden ebenfalls vermehrt identifiziert. *CDC7* beispielsweise konnte bereits in einigen Tumoren als hoch exprimiert und damit als Biomarker eingestuft werden^{202–204}. Die Inhibition von *CDC7* bspw. durch den Inhibitor BMS-863233 wird demnach bereits sowohl prä-klinisch als auch klinisch untersucht (zusammengefasst im Übersichtsartikel²⁰⁴). Bislang gibt es nur eine abgeschlossene klinische Studie mit Ergebnissen. Diese zeigt ein akzeptables Sicherheitsprofil und Anti-Tumor-Aktivität (NCT02699749)²⁰⁵. Die meisten klinischen Studien wurden allerdings terminiert (clinicaltrials.gov, 17.08.2022). Weiterhin konnten sowohl *CDC7* als auch *MCM2* beim DLBCL als prognostischer Marker identifiziert werden²⁰⁶. Das Gen *CDC45* war durch die Kombination ebenfalls signifikant herunterreguliert und in den Top10 GO Terms präsent. *CDC45* ist Teil des CMG (*CDC45/MCM2-7/GINS*) Komplexes, welcher für die DNA Replikationsinitiierung zuständig ist^{207,208}. Komponenten des CMG Komplexes wurden bereits häufig als überexprimiert in unterschiedlichen Tumorentitäten identifiziert und demnach als prognostischer Marker und Ziel therapeutischer Intervention in Betracht gezogen²⁰⁹. Die Modulierung der Gene des CMG Komplexes durch die Entospletinib und AZD5153 Kombination lässt vermuten, dass dieser Komplex eine entscheidende Rolle bei den durch die Kombination induzierten Effekten besitzt.

Die Ergebnisse der funktionellen GO Enrichment Analysen verdeutlichen demnach ein Eingreifen vornehmlich in die DNA Replikationsprozesse in der DLBCL Zelllinie SU-DHL-4. Weiterhin spielen die meisten der identifizierten Gene eine Rolle bei der Tumorprogression, sind häufig von einer tumorspezifischen aberranten Expression betroffen und können daher als Bio- oder Prognosemarker dienen. Auch die Visualisierung und Kondensierung der GO Terms zu sogenannten GO Clusters unterstreicht die Annahme, dass vorrangig Prozesse

herunterreguliert werden, die mit DNA Replikationsprozessen und Zellteilung durch die Entospletinib + AZD5153 Kombination in SU-DHL-4 Zellen in Zusammenhang stehen.

Die signifikante Herunterregulation der Gene des CMG Komplexes und die Funktion der herunterregulierten GO Terms indiziert, dass die Kombination vor allem DNA Replikationsprozesse in der DLBCL Zelllinie SU-DHL-4 stört. Die Herunterregulation von DNA Replikation- und Zellzyklus betreffenden Prozessen kann durch die evaluierten Zellzyklusdaten untermauert werden. Die Funktion der BET Proteine als Transkriptionsregulatoren wird durch AZD5153 entsprechend inhibiert und macht sich bei der Herunterregulation von DNA Replikationsprozessen bemerkbar. Man kann also davon ausgehen, dass sowohl die anti-proliferativen Effekte als auch die Genexpressionsmodulation vorrangig durch AZD5153 induziert wird und Entospletinib diese Effekte verstärkt, moduliert und entsprechend kombinationsspezifisch macht.

7. Ausblick

Präklinische Studien im Hinblick auf Kombinationstestungen und der entsprechenden Evaluierung des Wirkmechanismus', stellen eine zentrale Rolle für den erfolgreichen Einsatz neuer Kombinationen dar. Sowohl Resistenzvermeidung als auch die Verringerung des Nebenwirkungsregimes sollten hier von zentraler Bedeutung für den klinischen Einsatz sein. Die Möglichkeit, Patienten nach ihren spezifischen Gensignaturen zu stratifizieren, macht es möglich, Patienten-individuelle und angepasste therapeutische Ansätze und Kombinationsregimes zu evaluieren und intelligent einzusetzen.

Die Ergebnisse der vorliegenden Promotionsarbeit und der inkludierten Veröffentlichungen stellen zum einen die Basis für die Aufklärung des Wirkmechanismus' von Entospletinib in Zelllinien der Vorläufer B-ALL dar. Des Weiteren schaffen sie die Grundlage für die Aufklärung des Wirkmechanismus der Entospletinib und AZD5153 Kombination in humanen und caninen B-Lymphom-Zelllinien.

Die Charakterisierung von SYK und die anti-proliferativen Effekte durch Entospletinib in der pro- und prä B-ALL dienen nun als Ausgangspunkt weiterer Untersuchungen in Hinblick auf bspw. Kombinationstestungen mit anderen B-Zell Rezeptor assoziierten Kinasen, dem isoform-spezifischen BET Inhibitor AZD5153 oder anderen Schlüsselregulatoren.

Die ferner gezeigten synergistischen Effekte durch die simultane SYK und BET Inhibition in den humanen B-Lymphom-Zelllinien und die Identifizierung des Wirkmechanismus' von Entospletinib und AZD5153 in der DLBCL Zelllinie SU-DHL-4 stellt die Grundlage für die weitere Evaluation dieser Kombination dar. Zum einen könnte die Sensitivität gegenüber der Kombination bei den weniger sensitiven B-Lymphom-Zelllinien verbessert werden, indem

sequentielle oder Mehrfachgaben der Inhibitoren eingesetzt werden, vergleichend zu der simultanen Applikation. Die Einführung eines dritten Inhibitors, um Apoptose zu induzieren, ist ebenfalls möglich. Außerdem könnte Entospletinib durch einen anderen B-Zell assoziierten Kinase Inhibitor ausgetauscht werden, um die weniger starken anti-proliferativen Effekte in den B-Lymphom-Zelllinien zu erhöhen und eine gezielte Apoptose-Induktion auszulösen.

Die induzierten Genexpressionsmodulationen durch die Einzelsubstanzen und die Substanzkombination können ebenfalls als Grundlage dafür dienen, „Drug Escape“ Mechanismen und substanz-vermittelte Resistenzen, durch den weiteren Einsatz entsprechender Inhibitoren, zu umgehen. Weiterhin sind Proteom- und Phosphoproteomanalysen denkbar, um eine genauere Darstellung der Proteinexpressionsmodulation zu erhalten. Die Integration des Proteoms könnte über Multi-Omics-Daten weiteren Aufschluss über den zugrundeliegenden Mechanismus geben. Die mittels RNA Sequenzierung und Proteom identifizierten Prädiktoren könnten anschließend über funktionelle Analysen verifiziert werden.

Die hier vorliegende Promotionsarbeit fokussiert sich auf einen *in vitro* basierten Ansatz in einem stabilen Zellkulturmodell. Die Ausweitung auf 3D *in vitro* Ansätze, Primärmaterial und *in vivo* Modelle würde die Funktion und die zugrundeliegenden Mechanismen der hier evaluierten Substanzen und Substanzkombinationen zum einen validieren und zum anderen spezifischer charakterisieren. Vor allem die Ausweitung auf *in vivo* Modelle würde zeigen, welche Effekte und Nebenwirkungen der Kombination in einem Organismus, ggf. mit funktionsfähigen Immunsystem zu erwarten sind und die Übertragbarkeit in die Klinik erleichtern. Nach erfolgreicher Evaluation und Optimierung der hier vorgestellten Kombination aus Entospletinib und AZD5153 wäre es denkbar, den therapeutischen Ansatz auf den Hund zu übertragen und als Alternative zum CHOP Protokoll oder als Zweitlinientherapie zu nutzen.

8. Literaturverzeichnis

1. Falzone, L., Salomone, S. & Libra, M. Evolution of cancer pharmacological treatments at the turn of the third millennium. *Front. Pharmacol.* **9**, (2018).
2. Pagliarini, R., Shao, W. & Sellers, W. R. Oncogene addiction: pathways of therapeutic response, resistance, and road maps toward a cure. *EMBO Rep.* **16**, 280–296 (2015).
3. Ilango, S., Paital, B., Jayachandran, P., Padma, P. R. & Nirmaladevi, R. Epigenetic alterations in cancer. *Front. Biosci. (Landmark Ed.)* **25**, 1058–1109 (2020).
4. Doroshow, D. B. & Doroshow, J. H. Genomics and the history of precision oncology. *Surg. Oncol. Clin. N. Am.* **29**, 35–49 (2020).
5. Huang, L., Jiang, S. & Shi, Y. Tyrosine kinase inhibitors for solid tumors in the past 20 years (2001–2020). *J. Hematol. Oncol.* **2020** *131* **13**, 1–23 (2020).
6. Tong, M. & Seeliger, M. A. Targeting conformational plasticity of protein kinases. *ACS Chem. Biol.* **10**, 190–200 (2015).
7. Wu, P., Nielsen, T. E. & Clausen, M. H. FDA-approved small-molecule kinase inhibitors. *Trends Pharmacol. Sci.* **36**, 422–439 (2015).
8. Johnson, L. N. & Lewis, R. J. Structural basis for control by phosphorylation. *Chem. Rev.* **101**, 2209–2242 (2001).
9. Adams, J. A. Kinetic and catalytic mechanisms of protein kinases. *Chem. Rev.* **101**, 2271–2290 (2001).
10. Chahrouh, O., Cairns, D. & Omran, Z. Small molecule kinase inhibitors as anti-cancer therapeutics. *Mini-Reviews Med. Chem.* **12**, 399–411 (2012).
11. Hubbard, S. R. & Till, J. H. Protein tyrosine kinase structure and function. *Annu Rev Biochem.* **69**, 373–398 (2000).
12. Nowell, P. C. & Hungerford, D. A. Chromosome studies on normal and leukemic human leukocytes. *J. Natl. Cancer Inst.* **25**, 85–109 (1960).
13. Rowley, J. D. A new consistent chromosomal abnormality in chronic myelogenous leukaemia identified by quinacrine fluorescence and giemsa staining. *Nature* **243**, 290–293 (1973).
14. Ben-Neriah, Y., Daley, G. Q., Mes-Masson, A. M., Witte, O. N. & Baltimore, D. The chronic myelogenous leukemia-specific P210 protein is the product of the bcr/abl hybrid gene. *Science* **233**, 212–214 (1986).
15. Carroll, M. *et al.* CGP 57148, a tyrosine kinase inhibitor, inhibits the growth of cells expressing BCR-ABL, TEL-ABL, and TEL-PDGFR fusion proteins. *Blood* **90**, 4947–4952 (1997).
16. Deininger, M. W. N., Goldman, J. M., Lydon, N. & Melo, J. V. The tyrosine kinase inhibitor CGP57148B selectively inhibits the growth of BCR-ABL–positive cells. *Blood* **90**, 3691–3698 (1997).
17. Druker, B. J. *et al.* Efficacy and safety of a specific inhibitor of the BCR-ABL tyrosine kinase in chronic myeloid leukemia. *N. Engl. J. Med.* **344**, 1031–1037 (2001).

18. Hochhaus, A. *et al.* Long-term outcomes of Imatinib treatment for chronic myeloid leukemia. *N. Engl. J. Med.* **376**, 917–927 (2017).
19. Bernt, K. M. & Hunger, S. P. Current concepts in pediatric Philadelphia chromosome-positive acute lymphoblastic leukemia. *Front. Oncol.* **4**, (2014).
20. Iqbal, N. & Iqbal, N. Imatinib: A breakthrough of targeted therapy in cancer. *Chemother. Res. Pract.* **2014**, 1–9 (2014).
21. Javidi-Sharifi, N. & Hobbs, G. Future directions in chronic phase CML treatment. *Curr. Hematol. Malig. Rep.* **16**, 500–508 (2021).
22. Brivio, E. *et al.* Targeted inhibitors and antibody immunotherapies: Novel therapies for paediatric leukaemia and lymphoma. *Eur. J. Cancer* **164**, 1–17 (2022).
23. Mullard, A. FDA approves first-in-class SYK inhibitor. *Nat. Rev. Drug Discov.* **17**, 385 (2018).
24. Turner, M. *et al.* Perinatal lethality and blocked B-cell development in mice lacking the tyrosine kinase Syk. *Nature* **378**, 298–302 (1995).
25. Sada, K., Takano, T., Yanagi, S. & Yamamura, H. Structure and function of Syk protein-tyrosine kinase. *J. Biochem.* **130**, 177–186 (2001).
26. Furlong, M. T. *et al.* Identification of the major sites of autophosphorylation of the murine protein-tyrosine kinase Syk. *Biochim. Biophys. Acta* **1355**, 177–190 (1997).
27. Grädler, U. *et al.* Structural and biophysical characterization of the Syk activation switch. *J. Mol. Biol.* **425**, 309–333 (2013).
28. Turner, M., Schweighoffer, E., Colucci, F., Di Santo, J. P. & Tybulewicz, V. L. Tyrosine kinase SYK: essential functions for immunoreceptor signalling. *Immunol. Today* **21**, 148–154 (2000).
29. Hombach, J., Lottspeich, F. & Reth, M. Identification of the genes encoding the IgM-alpha and Ig-beta components of the IgM antigen receptor complex by amino-terminal sequencing. *Eur. J. Immunol.* **20**, 2795–2799 (1990).
30. Reth, M. Antigen receptors on B lymphocytes. *Annu Rev Immunol.* **10**, 97–121 (1992).
31. Moon, K. D. *et al.* Molecular basis for a direct interaction between the Syk protein-tyrosine kinase and Phosphoinositide 3-Kinase. *J. Biol. Chem.* **280**, 1543–1551 (2005).
32. Yasuda, T. *et al.* Erk kinases link pre-B cell receptor signaling to transcriptional events required for early B cell expansion. *Immunity* **28**, 499–508 (2008).
33. Baba, Y. *et al.* BLNK mediates Syk-dependent Btk activation. *Proc. Natl. Acad. Sci.* **98**, 2582–2586 (2001).
34. Mansueto, M. S. *et al.* A reevaluation of the spleen tyrosine kinase (SYK) activation mechanism. *J. Biol. Chem.* **294**, 7658–7668 (2019).
35. Zhang, J., Billingsley, M. L., Kincaid, R. L. & Siraganian, R. P. Phosphorylation of Syk activation loop tyrosines is essential for Syk function. An in vivo study using a specific anti-Syk activation loop phosphotyrosine antibody. *J. Biol. Chem.* **275**, 35442–35447 (2000).
36. Mócsai, A., Ruland, J. & Tybulewicz, V. L. J. The SYK tyrosine kinase: a crucial player in diverse biological functions. *Nat. Rev. Immunol.* **10**, 387–402 (2010).

37. Cheng, A. M. *et al.* Syk tyrosine kinase required for mouse viability and B-cell development. *Nature* **378**, 303–306 (1995).
38. Cornall, R. J., Cheng, A. M., Pawson, T. & Goodnow, C. C. Role of Syk in B-cell development and antigen-receptor signaling. *Proc. Natl. Acad. Sci. U. S. A.* **97**, 1713–8 (2000).
39. Buchner, M. *et al.* Spleen tyrosine kinase is overexpressed and represents a potential therapeutic target in chronic lymphocytic leukemia. *Cancer Res.* **69**, 5424–5432 (2009).
40. Chen, L. *et al.* SYK-dependent tonic B-cell receptor signaling is a rational treatment target in diffuse large B-cell lymphoma. *Blood* **111**, 2230–2237 (2008).
41. Rinaldi, A. *et al.* Genomic and expression profiling identifies the B-cell associated tyrosine kinase Syk as a possible therapeutic target in mantle cell lymphoma. *Br. J. Haematol.* **132**, 303–316 (2006).
42. Irish, J. M., Czerwinski, D. K., Nolan, G. P. & Levy, R. Altered B-cell receptor signaling kinetics distinguish human follicular lymphoma B cells from tumor-infiltrating nonmalignant B cells. *Blood* **108**, 3135–42 (2006).
43. Goodman, P. A., Wood, C. M., Vassilev, A., Mao, C. & Uckun, F. M. Spleen tyrosine kinase (Syk) deficiency in childhood pro-B cell acute lymphoblastic leukemia. *Oncogene* **20**, 3969–3978 (2001).
44. Perova, T. *et al.* Therapeutic potential of spleen tyrosine kinase inhibition for treating high-risk precursor B cell acute lymphoblastic leukemia. *Sci. Transl. Med.* **6**, 236ra62 (2014).
45. Baudot, A. D. *et al.* The tyrosine kinase Syk regulates the survival of chronic lymphocytic leukemia B cells through PKCdelta and proteasome-dependent regulation of Mcl-1 expression. *Oncogene* **28**, 3261–3273 (2009).
46. Wossning, T. *et al.* Deregulated Syk inhibits differentiation and induces growth factor-independent proliferation of pre-B cells. *J. Exp. Med.* **203**, 2829–2840 (2006).
47. Markham, A. Fostamatinib: First global approval. *Drugs* **78**, 959–963 (2018).
48. Paik, J. Fostamatinib: A review in chronic immune thrombocytopenia. *Drugs* **81**, 935–943 (2021).
49. Braselmann, S. *et al.* R406, an orally available spleen tyrosine kinase inhibitor blocks Fc receptor signaling and reduces immune complex-mediated inflammation. *J. Pharmacol. Exp. Ther.* **319**, 998–1008 (2006).
50. Young, R. M. *et al.* Mouse models of non-Hodgkin lymphoma reveal Syk as an important therapeutic target. *Blood* **113**, 2508 (2009).
51. Suljagic, M. *et al.* The Syk inhibitor fostamatinib disodium (R788) inhibits tumor growth in the Eμ- TCL1 transgenic mouse model of CLL by blocking antigen-dependent B-cell receptor signaling. *Blood* **116**, 4894–905 (2010).
52. Currie, K. S. *et al.* Discovery of GS-9973, a selective and orally efficacious inhibitor of spleen tyrosine kinase. *J. Med. Chem.* **57**, 3856–3873 (2014).
53. Burke, R. T. *et al.* A potential therapeutic strategy for chronic lymphocytic leukemia by combining idelalisib and GS-9973, a novel spleen tyrosine kinase (Syk) inhibitor. *Oncotarget* **5**, 908–915 (2014).
54. Nowotsch, C., Pletcher, B., Hr, R. W. & Hrn, M. Rote-Hand-Brief zu Zydelig® (Idelalisib):

- Aktualisierte Empfehlungen nach Abschluss der Überprüfung der Sicherheitsdaten. (2016).
55. Paiva, C. *et al.* SYK inhibition thwarts the BAFF - B-cell receptor crosstalk and thereby antagonizes Mcl-1 in chronic lymphocytic leukemia. *Haematologica* **102**, 1890–1900 (2017).
 56. Barbhuiya, M. A. *et al.* Identification of spleen tyrosine kinase as a potential therapeutic target for esophageal squamous cell carcinoma using reverse phase protein arrays. *Oncotarget* **9**, 18422–18434 (2018).
 57. Narayanan, S. *et al.* The spleen tyrosine kinase inhibitor, Entospletinib (GS-9973) restores chemosensitivity in lung Cancer cells by modulating ABCG2-mediated multidrug resistance. *Int. J. Biol. Sci.* **17**, 2652 (2021).
 58. Cremer, A. *et al.* Resistance mechanisms to SYK inhibition in acute myeloid leukemia. *Cancer Discov.* **10**, 214–231 (2020).
 59. Ramanathan, S. *et al.* Pharmacokinetics, pharmacodynamics, and safety of Entospletinib, a novel pSYK inhibitor, following single and multiple oral dosing in healthy volunteers. *Clin. Drug Investig.* **37**, 195–205 (2017).
 60. Sharman, J. *et al.* An open-label phase 2 trial of entospletinib (GS-9973), a selective spleen tyrosine kinase inhibitor, in chronic lymphocytic leukemia. *Blood* **125**, 2336–43 (2015).
 61. Awan, F. T. *et al.* Entospletinib monotherapy in patients with relapsed or refractory chronic lymphocytic leukemia previously treated with B-cell receptor inhibitors: results of a phase 2 study. <https://doi.org/10.1080/10428194.2018.1562180> **60**, 1972–1977 (2019).
 62. Burke, J. M. *et al.* An open-label, phase II trial of Entospletinib (GS-9973), a selective spleen tyrosine kinase inhibitor, in diffuse large B-cell lymphoma. *Clin. Lymphoma Myeloma Leuk.* **18**, e327–e331 (2018).
 63. Dhalluin, C. *et al.* Structure and ligand of a histone acetyltransferase bromodomain. *Nature* **399**, 491–496 (1999).
 64. Filippakopoulos, P. *et al.* Histone recognition and large-scale structural analysis of the human bromodomain family. *Cell* **149**, 214–231 (2012).
 65. Pervaiz, M., Mishra, P. & Günther, S. Bromodomain drug discovery – the past, the present, and the future. *Chem. Rec.* **18**, 1808–1817 (2018).
 66. Maruyama, T. *et al.* A mammalian bromodomain protein, Brd4, interacts with replication factor C and inhibits progression to S phase. *Mol. Cell. Biol.* **22**, 6509 (2002).
 67. Muller, S., Filippakopoulos, P. & Knapp, S. Bromodomains as therapeutic targets. *Expert Rev. Mol. Med.* **13**, (2011).
 68. Doroshow, D. B., Eder, J. P. & LoRusso, P. M. BET inhibitors: a novel epigenetic approach. *Ann. Oncol.* **28**, 1776–1787 (2017).
 69. Mosashvilli, D. *et al.* Global histone acetylation levels: prognostic relevance in patients with renal cell carcinoma. *Cancer Sci.* **101**, 2664–2669 (2010).
 70. Delmore, J. E. *et al.* BET bromodomain inhibition as a therapeutic strategy to target c-Myc. *Cell* **146**, 904–17 (2011).
 71. Mertz, J. A. *et al.* Targeting MYC dependence in cancer by inhibiting BET

- bromodomains. *Proc. Natl. Acad. Sci. U. S. A.* **108**, 16669–16674 (2011).
72. Pfister, S. X. & Ashworth, A. Marked for death: targeting epigenetic changes in cancer. *Nat. Rev. Drug Discov.* **16**, 241–263 (2017).
73. Filippakopoulos, P. *et al.* Selective inhibition of BET bromodomains. *Nature* **468**, 1067–1073 (2010).
74. Nicodeme, E. *et al.* Suppression of inflammation by a synthetic histone mimic. *Nature* **468**, 1119–1123 (2010).
75. French, C. A. The importance of diagnosing NUT midline carcinoma. *Head Neck Pathol.* **7**, 11–16 (2013).
76. French, C. A. *et al.* BRD–NUT oncoproteins: a family of closely related nuclear proteins that block epithelial differentiation and maintain the growth of carcinoma cells. *Oncogene* **27**, 2237–2242 (2007).
77. Dawson, M. A. *et al.* Inhibition of BET recruitment to chromatin as an effective treatment for MLL-fusion leukaemia. *Nature* **478**, 529–533 (2011).
78. Zuber, J. *et al.* RNAi screen identifies Brd4 as a therapeutic target in acute myeloid leukaemia. *Nature* **478**, 524–528 (2011).
79. Bernasconi, E. *et al.* Preclinical evaluation of the BET bromodomain inhibitor BAY 1238097 for the treatment of lymphoma. *Br. J. Haematol.* **178**, 936–948 (2017).
80. Coudé, M. M. *et al.* BET inhibitor OTX015 targets BRD2 and BRD4 and decreases c-MYC in acute leukemia cells. *Oncotarget* **6**, 17698–17712 (2015).
81. Dawson, M. A. *et al.* Recurrent mutations, including NPM1c, activate a BRD4-dependent core transcriptional program in acute myeloid leukemia. *Leukemia* **28**, 311–320 (2014).
82. Djamai, H. *et al.* Biological effects of BET inhibition by OTX015 (MK-8628) and JQ1 in NPM1-mutated (NPM1c) acute myeloid leukemia (AML). *Biomedicines* **9**, (2021).
83. Spriano, F., Stathis, A. & Bertoni, F. Targeting BET bromodomain proteins in cancer: The example of lymphomas. *Pharmacol Ther.* **215**, 107631 (2020).
84. Alqahtani, A. *et al.* Bromodomain and extra-terminal motif inhibitors: A review of preclinical and clinical advances in cancer therapy. *Futur. Sci OA.* **5**, (2019).
85. Lai, J., Liu, Z., Zhao, Y., Ma, C. & Huang, H. Anticancer effects of I-BET151, an inhibitor of bromodomain and extra-terminal domain proteins. *Front. Oncol.* **11**, 716830 (2021).
86. Rhyasen, G. W. *et al.* AZD5153: A novel bivalent BET bromodomain inhibitor highly active against hematologic malignancies. *Mol. Cancer Ther.* **15**, 2563–2574 (2016).
87. Lin, C.-H. *et al.* AZD5153, a bivalent BRD4 inhibitor, suppresses hepatocarcinogenesis by altering BRD4 chromosomal landscape and modulating the transcriptome of HCC cells. *Front. Cell Dev. Biol.* **10**, 661 (2022).
88. Weinstein, I. B. Cancer: Addiction to oncogenes - The Achilles heal of cancer. *Science* vol. 297 63–64 (2002).
89. Nastiuk, K. L. & Krolewski, J. J. Opportunities and challenges in combination gene cancer therapy. *Adv. Drug Deliv. Rev.* **98**, 35–40 (2016).
90. Coiffier, B. *et al.* CHOP chemotherapy plus Rituximab compared with CHOP alone in

- elderly patients with diffuse large-B-Cell lymphoma. *N. Engl. J. Med.* **346**, 235–242 (2002).
91. Kim, M. S. & Prasad, V. US Food and Drug Administration approvals for Bruton tyrosine kinase inhibitors in patients with chronic lymphocytic leukemia: Potential inefficiencies in trial design and evidence generation. *Cancer* **126**, 4270–4272 (2020).
 92. Stone, R. M. *et al.* Midostaurin plus chemotherapy for acute myeloid leukemia with a FLT3 mutation. *N. Engl. J. Med.* **377**, 454–464 (2017).
 93. Flaherty, K. T. *et al.* Combined BRAF and MEK inhibition in melanoma with BRAF V600 mutations. *N. Engl. J. Med.* **367**, 1694–1703 (2012).
 94. Long, G. V. *et al.* Combined BRAF and MEK inhibition versus BRAF inhibition alone in melanoma. *N. Engl. J. Med.* **371**, 1877–1888 (2014).
 95. Barr, P. M. *et al.* Phase 2 study of idelalisib and entospletinib: pneumonitis limits combination therapy in relapsed refractory CLL and NHL. *Blood* **127**, 2411–2415 (2016).
 96. Loftus, J. P. *et al.* Combinatorial efficacy of entospletinib and chemotherapy in patient-derived xenograft models of infant acute lymphoblastic leukemia. *Haematologica* **106**, 1067–1078 (2021).
 97. Elías, E. E. *et al.* Autologous T-cell activation fosters ABT-199 resistance in chronic lymphocytic leukemia: rationale for a combined therapy with SYK inhibitors and anti-CD20 monoclonal antibodies. *Haematologica* **103**, e458–e461 (2018).
 98. Morschhauser, F. *et al.* Phase 1b study of tirabrutinib in combination with idelalisib or entospletinib in previously treated B-cell lymphoma. *Leukemia* **35**, 2108 (2021).
 99. Walker, A. R. *et al.* Entospletinib in combination with induction chemotherapy in previously untreated acute myeloid leukemia: Response and predictive significance of HOXA9 and MEIS1 expression. *Clin. Cancer Res.* **26**, 5852–5859 (2020).
 100. Kittai, A. S. *et al.* Entospletinib and obinutuzumab in patients with relapsed/refractory chronic lymphocytic leukemia and B-cell malignancies. *Haematologica* **106**, 2022–2025 (2021).
 101. Lam, V. *et al.* Proapoptotic and immunomodulatory effects of SYK inhibitor entospletinib in combination with obinutuzumab in patients with chronic lymphocytic leukaemia. *Br. J. Clin. Pharmacol.* **88**, 836–841 (2022).
 102. Zhang, P. *et al.* BRD4 inhibitor AZD5153 suppresses the proliferation of colorectal cancer cells and sensitizes the anticancer effect of PARP inhibitor. *Int. J. Biol. Sci.* **15**, 1942–1954 (2019).
 103. Wood, L. *et al.* Combining inhibitors of Brd4 and cyclin-dependent kinase can decrease tumor growth in neuroblastoma with MYCN amplification. *J. Pediatr. Surg.* **56**, 1199–1202 (2021).
 104. Liu, C. *et al.* AZD5153 reverses palbociclib resistance in ovarian cancer by inhibiting cell cycle-related proteins and the MAPK/PI3K-AKT pathway. *Cancer Lett.* **528**, 31–44 (2022).
 105. Takashima, Y. *et al.* Bromodomain and extraterminal domain inhibition synergizes with WEE1-inhibitor AZD1775 effect by impairing nonhomologous end joining and enhancing DNA damage in nonsmall cell lung cancer. *Int. J. Cancer* **146**, 1114–1124 (2020).
 106. Yao, Z., Yang, S., Zhao, H., Yang, H. & Jiang, X. BET inhibitor I-BET151 sensitizes

- GBM cells to temozolomide via PUMA induction. *Cancer Gene Ther.* **27**, 226–234 (2020).
107. Tseng, H. Y. *et al.* Co-targeting bromodomain and extra-terminal proteins and MCL1 induces synergistic cell death in melanoma. *Int. J. cancer* **147**, 2176–2189 (2020).
108. Guo, L. *et al.* A combination strategy targeting enhancer plasticity exerts synergistic lethality against BETi-resistant leukemia cells. *Nat. Commun.* **11**, (2020).
109. Hoarau-Véchet, J., Rafii, A., Touboul, C. & Pasquier, J. Halfway between 2D and animal models: Are 3D cultures the ideal tool to study cancer-microenvironment interactions? *Int. J. Mol. Sci.* **19**, (2018).
110. Korneev, K. V. Mouse models of sepsis and septic shock. *Mol. Biol.* **2019** *535* **53**, 704–717 (2019).
111. Beura, L. K. *et al.* Normalizing the environment recapitulates adult human immune traits in laboratory mice. *Nature* **532**, 512–516 (2016).
112. Masopust, D., Sivula, C. P. & Jameson, S. C. Of mice, dirty mice, and men: Using mice to understand human immunology. *J. Immunol.* **199**, 383–388 (2017).
113. Zitvogel, L., Pitt, J. M., Daillère, R., Smyth, M. J. & Kroemer, G. Mouse models in oncoimmunology. *Nat. Rev. Cancer* **2016** *1612* **16**, 759–773 (2016).
114. Ito, D., Frantz, A. M. & Modiano, J. F. Canine lymphoma as a comparative model for human non-Hodgkin lymphoma: recent progress and applications. *Vet. Immunol. Immunopathol.* **159**, 192–201 (2014).
115. Wolf-Ringwall, A. *et al.* Prospective evaluation of flow cytometric characteristics, histopathologic diagnosis and clinical outcome in dogs with naïve B-cell lymphoma treated with a 19-week CHOP protocol. *Vet. Comp. Oncol.* **18**, 342–352 (2020).
116. Impellizeri, J. A., Howell, K., McKeever, K. P. & Crow, S. E. The role of rituximab in the treatment of canine lymphoma: an ex vivo evaluation. *Vet. J.* **171**, 556–558 (2006).
117. Sender, S. *et al.* Precursor B-ALL cell lines differentially respond to syk inhibition by entospletinib. *Int. J. Mol. Sci.* **22**, 1–22 (2021).
118. miRNeasy Mini Handbook - QIAGEN. <https://www.qiagen.com/us/resources/resourcedetail?id=da6c8d17-58c4-411c-a334-bc1754876db3&lang=en>.
119. Fouquier, J. & Guedj, M. Analysis of drug combinations: current methodological landscape. *Pharmacol. Res. Perspect.* **3**, e00149 (2015).
120. Cömert, M. *et al.* Venetoclax Azacitidine combination therapy in first-line treatment of acute myeloid leukemia patients: A single center experience. *Hematol. Transfus. Cell Ther.* **43**, S33–S34 (2021).
121. DiNardo, C. D. *et al.* Venetoclax combined with decitabine or azacitidine in treatment-naïve, elderly patients with acute myeloid leukemia. *Blood* **133**, 7–17 (2019).
122. Serafin, V. *et al.* SYK targeting represents a potential therapeutic option for relapsed resistant pediatric ETV6-RUNX1 B-acute lymphoblastic leukemia patients. *Int. J. Mol. Sci.* **20**, (2019).
123. Reimand, J. & Bader, G. D. Systematic analysis of somatic mutations in phosphorylation signaling predicts novel cancer drivers. *Mol. Syst. Biol.* **9**, 637 (2013).

124. DepMap, Broad (2022): DepMap 22Q2 Public. figshare. Dataset. https://figshare.com/articles/dataset/DepMap_22Q2_Public/19700056/2.
125. Cerami, E. *et al.* The cBio cancer genomics portal: an open platform for exploring multidimensional cancer genomics data. *Cancer Discov.* **2**, 401–404 (2012).
126. Gao, J. *et al.* Integrative analysis of complex cancer genomics and clinical profiles using the cBioPortal. *Sci. Signal.* **6**, (2013).
127. Herishanu, Y. *et al.* The lymph node microenvironment promotes B-cell receptor signaling, NF- κ B activation, and tumor proliferation in chronic lymphocytic leukemia. *Blood* **117**, 563–574 (2011).
128. Ponader, S. *et al.* The Bruton tyrosine kinase inhibitor PCI-32765 thwarts chronic lymphocytic leukemia cell survival and tissue homing in vitro and in vivo. *Blood* **119**, 1182–1189 (2012).
129. Cheng, S. *et al.* SYK inhibition and response prediction in diffuse large B-cell lymphoma. *Blood* **118**, 6342–6352 (2011).
130. Kong, W. *et al.* BTK and PI3K inhibitors reveal synergistic inhibitory anti-tumoral effects in canine diffuse large B-cell lymphoma cells. *Int. J. Mol. Sci.* **22**, (2021).
131. Althubiti, M. Spleen tyrosine kinase inhibition modulates p53 activity. **10**, 1179066017731564 (2017).
132. Bailet, O. *et al.* Spleen tyrosine kinase functions as a tumor suppressor in melanoma cells by inducing senescence-like growth arrest. *Cancer Res.* **69**, 2748–2756 (2009).
133. Vousden, K. H. & Lane, D. P. p53 in health and disease. *Nat Rev Mol Cell Biol.* vol. 8 275–283 (2007).
134. Kandoth, C. *et al.* Mutational landscape and significance across 12 major cancer types. *Nature* **502**, 333–339 (2013).
135. Ang, H. C., Joerger, A. C., Mayer, S. & Fersht, A. R. Effects of common cancer mutations on stability and DNA binding of full-length p53 compared with isolated core domains. *J. Biol. Chem.* **281**, 21934–21941 (2006).
136. Silva, J. L., Gallo, C. V. D. M., Costa, D. C. F. & Rangel, L. P. Prion-like aggregation of mutant p53 in cancer. *Trends Biochem Sci.* vol. 39 260–267 (2014).
137. Xu, J. *et al.* Gain of function of mutant p53 by coaggregation with multiple tumor suppressors. *Nat. Chem. Biol.* **7**, 285–295 (2011).
138. McCubrey, J. A. *et al.* Roles of the RAF/MEK/ERK and PI3K/PTEN/AKT pathways in malignant transformation and drug resistance. *Adv. Enzyme Regul.* **46**, 249–279 (2006).
139. Cremer, A. *et al.* Resistance mechanisms to SYK inhibition in AML. *Blood* **132**, 2638–2638 (2018).
140. Dustin, L. B. *et al.* Expression of dominant-negative src-homology domain 2-containing protein tyrosine phosphatase-1 results in increased Syk tyrosine kinase activity and B cell activation. *J. Immunol.* **162**, 2717–24 (1999).
141. Müschen, M. Autoimmunity checkpoints as therapeutic targets in B cell malignancies. *Nat. Rev. Cancer* (2018) doi:10.1038/nrc.2017.111.
142. Geng, H. *et al.* Self-enforcing feedback activation between BCL6 and pre-B cell receptor signaling defines a distinct subtype of acute lymphoblastic leukemia. *Cancer Cell* **27**,

- 409–425 (2015).
143. Hurtz, C. *et al.* Rationale for targeting BCL6 in MLL-rearranged acute lymphoblastic leukemia. **33**, 1265–1279 (2019).
 144. Takimoto-Shimomura, T. *et al.* Dual targeting of bromodomain-containing 4 by AZD5153 and BCL2 by AZD4320 against B-cell lymphomas concomitantly overexpressing c-MYC and BCL2. *Invest. New Drugs* **37**, 210–222 (2019).
 145. Kim, E. *et al.* The BET inhibitor GS-5829 targets chronic lymphocytic leukemia cells and their supportive microenvironment. *Leukemia* **34**, 1588–1598 (2020).
 146. Derenzini, E. *et al.* BET inhibition-induced GSK3 β feedback enhances lymphoma vulnerability to PI3K inhibitors. *Cell Rep.* **24**, 2155–2166 (2018).
 147. Aresu, L. *et al.* New molecular and therapeutic insights into canine diffuse large B-cell lymphoma elucidates the role of the dog as a model for human disease. *Haematologica* **104**, e256–e259 (2019).
 148. Chapuy, B. *et al.* Discovery and characterization of super-enhancer-associated dependencies in diffuse large B cell lymphoma. *Cancer Cell* **24**, 777–790 (2013).
 149. Drexler, H. G., Eberth, S., Nagel, S. & MacLeod, R. A. F. Malignant hematopoietic cell lines: in vitro models for double-hit B-cell lymphomas. *Leuk. Lymphoma* **57**, 1015–1020 (2016).
 150. Hecht, B. K. M. C., Epstein, A. L., Berger, C. S., Kaplan, H. S. & Hecht, F. Histiocytic lymphoma cell lines: immunologic and cytogenetic studies. *Cancer Genet. Cytogenet.* **14**, 205–218 (1985).
 151. Quentmeier, H. *et al.* Diffuse large B cell lymphoma cell line U-2946: Model for MCL1 inhibitor testing. *PLoS One* **11**, (2016).
 152. Karpova, M. B. *et al.* Raji revisited: cytogenetics of the original Burkitt's lymphoma cell line. *Leukemia* **19**, 159–161 (2005).
 153. Gabay, C., Ben-Bassat, H., Schlesinger, M. & Laskov, R. Somatic mutations and intraclonal variations in the rearranged V κ genes of B-non-Hodgkin's lymphoma cell lines. *Eur. J. Haematol.* **63**, 180–191 (1999).
 154. Ben-bassats, H. *et al.* Establishment in continuous culture of a new type of lymphocyte from a 'Burkitt like' malignant lymphoma (line D.G.-75). *Int. J. cancer* **19**, 27–33 (1977).
 155. Thomalla, D. *et al.* Deregulation and epigenetic modification of BCL2-family genes cause resistance to venetoclax in hematologic malignancies. *Blood* (2022).
 156. Taher, L. *et al.* Comparative high-resolution transcriptome sequencing of lymphoma cell lines and de novo lymphomas reveals cell-line-specific pathway dysregulation. *Sci. Rep.* **8**, (2018).
 157. Panzeri, I., Rossetti, G., Abrignani, S. & Pagani, M. Long intergenic noncoding RNAs: Novel drivers of human lymphocyte differentiation. *Front. Immunol.* **6**, 175 (2015).
 158. Ransohoff, J. D., Wei, Y. & Khavari, P. A. The functions and unique features of long intergenic non-coding RNA. *Nat. Rev. Mol. Cell Biol.* **19**, 143–157 (2018).
 159. Casellas, R. *et al.* Mutations, kataegis and translocations in B cells: Understanding AID promiscuous activity. *Nat Rev Immunol.* vol. 16 164–176 (2016).
 160. Teater, M. *et al.* AICDA drives epigenetic heterogeneity and accelerates germinal

- center-derived lymphomagenesis. *Nat. Commun.* **9**, 1–10 (2018).
161. Long, Z. *et al.* The reverse-mode NCX1 activity inhibitor KB-R7943 promotes prostate cancer cell death by activating the JNK pathway and blocking autophagic flux. *Oncotarget* **7**, 42059–42070 (2016).
162. Chovancova, B. *et al.* Calcium signaling affects migration and proliferation differently in individual cancer cells due to nifedipine treatment. *Biochem. Pharmacol.* **171**, 113695 (2020).
163. Kim, Y. T., Jo, S. S., Park, Y. J., Lee, M. Z. & Suh, C. K. Distinct cellular calcium metabolism in radiation-sensitive RKO human colorectal cancer cells. *Korean J. Physiol. Pharmacol.* **18**, 509–516 (2014).
164. Dong, H. *et al.* Molecular mechanisms underlying Ca²⁺-mediated motility of human pancreatic duct cells. *Am. J. Physiol. - Cell Physiol.* **299**, (2010).
165. Muñoz, J. J. *et al.* Down-regulation of SLC8A1 as a putative apoptosis evasion mechanism by modulation of calcium levels in penile carcinoma. *J. Urol.* **194**, 245–251 (2015).
166. Siaw, W. N., Di Capite, J., Singaravelu, K. & Parekh, A. B. Sustained activation of the tyrosine kinase syk by antigen in mast cells requires local Ca²⁺ influx through Ca²⁺ release-activated Ca²⁺ channels. *J. Biol. Chem.* **283**, 31348–31355 (2008).
167. Alanazi, B. *et al.* Integrated nuclear proteomics and transcriptomics identifies S100A4 as a therapeutic target in acute myeloid leukemia. *Leukemia* **34**, 427–440 (2020).
168. Bai, H., Qian, J. L. & Han, B. H. S100A4 is an independent prognostic factor for patients with lung cancer: A meta-analysis. *Genet. Test. Mol. Biomarkers* **18**, 371–374 (2014).
169. Ekmekci, S. S. *et al.* LEF1 induces DHRS2 gene expression in human acute leukemia Jurkat T-cells. *Turkish J. Hematol.* **37**, 226 (2020).
170. Zhou, Y. *et al.* DHRS2 inhibits cell growth and motility in esophageal squamous cell carcinoma. *Oncogene* **37**, 1086 (2018).
171. Han, Y. *et al.* Decreased DHRS2 expression is associated with HDACi resistance and poor prognosis in ovarian cancer. *Epigenetics* **15**, 122 (2020).
172. Liu, Y. *et al.* Multi-omics characterization of WNT pathway reactivation to ameliorate BET inhibitor resistance in liver cancer cells. *Genomics* **113**, 1057–1069 (2021).
173. Beauchemin, H. & Möröy, T. Multifaceted Actions of GF11 and GF11B in Hematopoietic Stem Cell Self-Renewal and Lineage Commitment. *Front Genet.* **11**, 591099 (2020).
174. Liang, Y. Y. *et al.* Downregulation of Ras association domain family member 6 (RASSF6) underlies the treatment resistance of highly metastatic nasopharyngeal carcinoma cells. *PLoS One* **9**, (2014).
175. Zhu, N. *et al.* Overexpression of RAS-association domain family 6 (RASSF6) inhibits proliferation and tumorigenesis in hepatocellular carcinoma cells. *Oncol. Res.* **25**, 1001–1008 (2017).
176. Chen, E. *et al.* Decreased level of RASSF6 in sporadic colorectal cancer and its anti-tumor effects both in vitro and in vivo. *Oncotarget* **7**, 19813–19823 (2016).
177. Guo, W. *et al.* Decreased expression and frequent promoter hypermethylation of RASSF2 and RASSF6 correlate with malignant progression and poor prognosis of gastric cardia adenocarcinoma. *Mol. Carcinog.* **55**, 1655–1666 (2016).

178. Pietrzyk, Ł. & Wdowiak, P. Serum TEM5 and TEM7 concentrations correlate with clinicopathologic features and poor prognosis of colorectal cancer patients. *Adv. Med. Sci.* **64**, 402–408 (2019).
179. Cherry, A. E. *et al.* GPR124 regulates microtubule assembly, mitotic progression, and glioblastoma cell proliferation. *Glia* **67**, 1558 (2019).
180. Dempsey, P. W., Doyle, S. E., He, J. Q. & Cheng, G. The signaling adaptors and pathways activated by TNF superfamily. *Cytokine Growth Factor Rev.* **14**, 193–209 (2003).
181. González-Suárez, E. & Sanz-Moreno, A. RANK as a therapeutic target in cancer. *FEBS J.* **283**, 2018–2033 (2016).
182. Bonifaci, N. *et al.* Evidence for a link between TNFRSF11A and risk of breast cancer. *Breast Cancer Res. Treat.* **129**, 947–954 (2011).
183. Chen, G. *et al.* Expression of RANKL/RANK/OPG in primary and metastatic human prostate cancer as markers of disease stage and functional regulation. *Cancer* **107**, 289–298 (2006).
184. Jin, M. *et al.* Feedback activation of NF-KB signaling leads to adaptive resistance to EZH2 inhibitors in prostate cancer cells. *Cancer Cell Int.* **21**, 1–10 (2021).
185. von dem Knesebeck, A. *et al.* RANK (TNFRSF11A) is epigenetically inactivated and induces apoptosis in gliomas. *Neoplasia* **14**, 526 (2012).
186. Alankus, B. *et al.* Pathological RANK signaling in B cells drives autoimmunity and chronic lymphocytic leukemia. *J. Exp. Med.* **218**, (2021).
187. Compagno, M. *et al.* Mutations of multiple genes cause deregulation of NF-kappaB in diffuse large B-cell lymphoma. *Nature* **459**, 717–721 (2009).
188. Tanty, N. A. *et al.* The prognostic value of S100A10 expression in cancer. *Oncol. Lett.* **17**, 1417–1424 (2019).
189. Huang, D. *et al.* Annexin A2-S100A10 heterotetramer is upregulated by PML/RAR α fusion protein and promotes plasminogen-dependent fibrinolysis and matrix invasion in acute promyelocytic leukemia. *Front. Med.* **11**, 410–422 (2017).
190. Li, Y. *et al.* S100A10 accelerates aerobic glycolysis and malignant growth by activating mTOR-signaling pathway in gastric cancer. *Front. Cell Dev. Biol.* **8**, 1430 (2020).
191. Arai, K., Iwasaki, T., Sonoda, A. & Endo, A. Membranous overexpression of S100A10 is associated with a high-grade cellular status of breast carcinoma. *Med. Mol. Morphol.* **53**, 104–114 (2020).
192. Pattabiraman, D. R. & Gonda, T. J. Role and potential for therapeutic targeting of MYB in leukemia. *Leukemia* **27**, 269–277 (2013).
193. Ramsay, R. G. & Gonda, T. J. MYB function in normal and cancer cells. *Nat Rev Cancer.* **8**, 523–534 (2008).
194. Robetorye, R. S. *et al.* Microarray analysis of B-cell lymphoma cell lines with the t(14;18). *J. Mol. Diagnostics* **4**, 123–136 (2002).
195. Zhang, B. *et al.* Hsa-miR-495 acts as a tumor suppressor gene in glioma via the negative regulation of MYB. *Mol. Med. Rep.* **14**, 977–982 (2016).
196. Yu, L. *et al.* MicroRNA-424 is down-regulated in hepatocellular carcinoma and

- suppresses cell migration and invasion through c-Myb. *PLoS One* **9**, (2014).
197. Bochman, M. L. & Schwacha, A. The mcm complex: Unwinding the mechanism of a replicative helicase. *Microbiol. Mol. Biol. Rev.* **73**, 652 (2009).
 198. Ha, S. A. *et al.* Cancer-associated expression of minichromosome maintenance 3 gene in several human cancers and its involvement in tumorigenesis. *Clin. Cancer Res.* **10**, 8386–8395 (2004).
 199. Obermann, E. C. *et al.* Expression of minichromosome maintenance protein 2 as a marker for proliferation and prognosis in diffuse large B-cell lymphoma: a tissue microarray and clinico-pathological analysis. *BMC Cancer* **5**, 162 (2005).
 200. Ouyang, F. *et al.* GINS2 is a novel prognostic biomarker and promotes tumor progression in early-stage cervical cancer. *Oncol. Rep.* **37**, 2652–2662 (2017).
 201. Ahmad, M. *et al.* Up-regulation of GINS1 highlighted a good diagnostic and prognostic potential of survival in three different subtypes of human cancer. *Braz. J. Biol.* **84**, (2021).
 202. Wang, Q. & Zheng, W. Upregulation of CDC7 associated with cervical cancer incidence and development. *Biomed Res. Int.* **2021**, (2021).
 203. Cheng, A. N. *et al.* Increased Cdc7 expression is a marker of oral squamous cell carcinoma and overexpression of Cdc7 contributes to the resistance to DNA-damaging agents. *Cancer Lett.* **337**, 218–225 (2013).
 204. Liu, R. & Huang, Y. CDC7 as a novel biomarker and druggable target in cancer. *Clin Transl Oncol.* **10**, 1856–1864 (2022).
 205. Shimizu, T. *et al.* First-in-human phase 1 study of TAK-931, an oral cell division cycle 7 (CDC7) inhibitor, in patients (pts) with advanced solid tumors. *J Clin Oncol.* **36**, 2506–2506 (2018).
 206. Hou, Y. *et al.* Expression of Cdc7 and mcm2 as a marker for proliferation and prognosis in diffuse large B cell lymphoma. *Chinese J. Oncol.* **33**, 911–915 (2011).
 207. Ilves, I., Petojevic, T., Pesavento, J. J. & Botchan, M. R. Activation of the MCM2-7 helicase by association with Cdc45 and GINS proteins. *Mol. Cell* **37**, 247–258 (2010).
 208. Takaya, J., Kusunoki, S. & Ishimi, Y. Protein interaction and cellular localization of human CDC45. *J. Biochem.* **153**, 381–388 (2013).
 209. Seo, Y. S. & Kang, Y. H. The human replicative helicase, the CMG complex, as a target for anti-cancer therapy. *Front. Mol. Biosci.* **5**, 26 (2018).

9. Abkürzungsverzeichnis

ABL1	ABL Proto-Oncogene 1, Non-Receptor Tyrosine Kinase
ADGRA2	Adhesion G Protein-Coupled Receptor A2
AICDA	Activation-induced cytidine deaminase
AKT	AKT Serine/Threonine Kinase
ALL	Akute lymphatische Leukämie
AML	Akute myeloische Leukämie
AZD	AZD5153
BAKs	B-Zell Rezeptor assoziierte Kinasen
B-ALL	B-Zell akute lymphatische Leukämie
BCL-2	BCL2 Apoptosis Regulator
BCR	BCR Activator Of RhoGEF And GTPase
BCR::ABL1	Fusionsgen, das durch Translokation der Chromosomen 9 und 22 entsteht, Es kodiert das konstitutiv aktivierte BCR::ABL1 Fusionsprotein
BD	Bromodomäne
BET	Bromodomänen und extra-terminale Domänen Proteine
BETi	BET Inhibitor
BIM	BCL2 Like 11
BL	Burkitt Lymphom
BRD2-4,9	Bromodomänen-enthaltene Proteine 2-4,9
BRDT	Bromodomänen Testikel-spezifisches Protein
BTK	Bruton's Tyrosin Kinase
BZR	B-Zell Rezeptor
Ca ²⁺	Calcium
CDC	Cell division cycle
CDK	Cyclin Dependent Kinase
CEN	Centromer
CLL	Chronisch lymphatische Leukämie
CMG	CDC45/MCM2-7/GINS Komplex
CML	Chronische myeloische Leukämie

CR	Vollständige Remission, complete remission
DEG	Differentiell exprimierte Gene
DHL	Double-Hit Lymphom
DHRS2	Dehydrogenase/Reductase 2
DLBCL	Diffus großzelliges B-Zell-Lymphom
DMSO	Dimethylsulfoxid
EMA	European Medicines Agency
Ento	Entospletinib
ERK	Mitogen-Activated Protein Kinase
FDA	Food and Drug Administration
FIT	Fostamatinib for Immune Thrombocytopenia
FL	Folikuläres Lymphom
FLT3	Fms Related Receptor Tyrosine Kinase 3
GFI1B	Growth Factor Independent 1B Transcriptional Repressor
GINS	GINS complex subunit
GO	Gene Ontology
GoF	Gain-of-Function
pGSK3 β	Glycogen Synthase Kinase 3 Beta
HCC	Hepatozelluläres Karzinom
HER2	human epidermal growth receptor 2
HOXA9	Homeobox A9
I-BET	I-BET151
IC50	Mittlere Inhibitorische Konzentration
Ig	Immunoglobulin
Ig- α	Immunoglobulin alpha - B-cell antigen receptor complex-associated protein alpha chain
Ig- β	Immunoglobulin beta - B-cell antigen receptor complex-associated protein beta chain
ITAM	immune receptor tyrosine-based activating motifs
ITD	Interne Tandemduplikation
ITP	Immunthrombozytopenie
JAK	Janus Kinase

JNK	c-Jun-N-terminale Kinasen
KIF	Kinesin Family
LoF	Loss-of-Function
lincRNA	long intergenic non-coding RNA
logFC	log fold change
MCL1	MCL1 Apoptosis Regulator, BCL2 Family Member
MCM	Mini chromosome maintenance
MEIS1	Meis Homeobox 1
MEK	Mitogen-Activated Protein Kinase Kinase
MFI	Mittlere Fluoreszenzintensität
MLL	mixed lineage leukemia
MM	Multiples Myelom
mTOR	Mechanistic Target Of Rapamycin Kinase
MYB	MYB Proto-Oncogene, Transcription Factor
MYC	MYC Proto-Oncogene, BHLH Transcription Factor
MZL	Mantelzelllymphom
Na ⁺	Natrium
NF-κB	Nuclear factor κB
NHL	Non-Hodgkin-Lymphom
NRTK	Nicht-Rezeptor Tyrosin Kinasen
NUT	Nuclear-protein-in-testis
PARP	Poly(ADP-Ribose) Polymerase
PD-1	Programmed Cell Death 1
Ph	Philadelphia Chromosom
PI3K	Phosphatidylinositol-4,5-Bisphosphate 3-Kinase
PI3Kδ	Phosphatidylinositol-4,5-Bisphosphate 3-Kinase Catalytic Subunit Delta
PLCγ2	Phospholipase C Gamma 2
Pol II	RNA Polymerase II
P-TEFb	positiver Transkriptions-Elongations-Faktor-Komplex
PTPN11	Protein Tyrosine Phosphatase Non-Receptor Type 11
PVDF	Polyvinylidenfluorid

RAS	Familie der RAS Proto-Onkogene, GTPase
RASSF6	Ras Association Domain Family Member 6
RIN	RNA integrity number
RTK	Rezeptor Tyrosin Kinasen
S100A4	S100 Calcium Binding Protein A4
Ser2	Serin 2
SH2	Src homology 2
SLC8A1	Sodium/Calcium Exchanger 1
STAT	Signal Transducers and Activators of Transcription
SYK	Spleen Tyrosin Kinase
t(4;11)	Translokation der Chromosomen 4 und 11
TAC	Transcriptome Analysis Console
TKI	Tyrosinkinase-Inhibitor
TNFRSF11A	TNF receptor superfamily member 11a
TP53	Tumor Protein P53
VEGF	Vascular Endothelial Growth Factor
WEE1	WEE1 G2 Checkpoint Kinase
wt	Wildtyp
Y	Aminosäure Tyrosin

10. Abbildungsverzeichnis

Abbildung 1: Übersichtsdarstellung der Expositionsexperimente aus Arbeit I – III	14
Abbildung 2: Einfluss der Entospletinib Exposition auf Zelllinien der B-ALL <i>in vitro</i>	21
Abbildung 3: Genexpressionsmodulation in der DLBCL Zelllinie SU-DHL-4 nach Entospletinib und AZD5153 Kombinationsexposition.....	24
Abbildung 4: Evaluation der Zellvitalität nach einzelner oder simultaner BET und SYK Inhibition in der caninen DLBCL Zelllinie CLBL-1.	27
Abbildung 5: Spleen Tyrosin Kinase Struktur.....	137

11. Tabellenverzeichnis

Tabelle 1: Verwendete humane und canine hämatologische Zelllinien	13
Tabelle 2: Detaillierte Auflistung der verwendeten Zelllinien inkl. Charakteristika.....	138

12. Originalarbeiten

12.1 Arbeit I

Precursor B-ALL cell lines differentially respond to SYK inhibition by entospletinib

Sender S., Sekora A., Villa Perez S., Chabanovska O., Becker A., Ngezahayo A., Junghanss C., Murua Escobar H.

Int. J. Mol. Sci. 2021 Jan 8;22(2):E592. doi: 10.3390/ijms22020592.
Impact Factor 2019/20: 4.556



Article

Precursor B-ALL Cell Lines Differentially Respond to SYK Inhibition by Entospletinib

Sina Sender ¹, Anett Sekora ¹, Simon Villa Perez ¹, Oleksandra Chabanovska ¹, Annegret Becker ², Anaclet Ngezahayo ², Christian Junghanss ¹ and Hugo Murua Escobar ^{1,*}

¹ Division of Medicine, Department of Hematology, Oncology and Palliative Medicine, University of Rostock, 18057 Rostock, Germany; sina.sender@med.uni-rostock.de (S.S.); Anett.Sekora@med.uni-rostock.de (A.S.); dsibsimonvilla@gmail.com (S.V.P.); oleksandra.chabanovska@uni-rostock.de (O.C.); Christian.Junghanss@med.uni-rostock.de (C.J.)

² Department of Cell Physiology and Biophysics, Institute of Cell Biology and Biophysics, Leibniz University Hannover, 30419 Hannover, Germany; becker@cell.uni-hannover.de (A.B.); ngezahayo@cell.uni-hannover.de (A.N.)

* Correspondence: hugo.murua.escobar@med.uni-rostock.de; Tel.: +49-381494-7639; Fax: +49-494-7422

Abstract: Background: Impaired B-cell receptor (BCR) function has been associated with the progress of several B-cell malignancies. The spleen tyrosine kinase (SYK) represents a potential therapeutic target in a subset of B-cell neoplasias. In precursor B-acute lymphoblastic leukemia (B-ALL), the pathogenic role and therapeutic potential of SYK is still controversially discussed. We evaluate the application of the SYK inhibitor entospletinib (Ento) in pre- and pro-B-ALL cell lines, characterizing the biologic and molecular effects. Methods: SYK expression was characterized in pre-B-ALL (NALM-6) and pro-B-ALL cell lines (SEM and RS4;11). The cell lines were exposed to different Ento concentrations and the cell biological response analyzed by proliferation, metabolic activity, apoptosis induction, cell-cycle distribution and morphology. BCR pathway gene expression and protein modulations were further characterized. Results: Ento significantly induced anti-proliferative and pro-apoptotic effects in NALM-6 and SEM, while barely affecting RS4;11. Targeted RNAseq revealed pronounced gene expression modulation only in NALM-6, while Western Blot analyses demonstrated that vital downstream effector proteins, such as pAKT, pERK, pGSK3 β , p53 and BCL-6, were affected by Ento exposure in the inhibitor-sensitive cell lines. Conclusion: Different acting modes of Ento, independent of pre-BCR dependency, were characterized, unexpected in SEM. Accordingly, SYK classifies as a potential target structure in a subset of pro-B-ALLs.

Keywords: entospletinib; Ento; GS-9973; B-ALL; acute lymphoblastic leukemia; expression analysis; SYK; BCR; pathway-specific inhibitors



Citation: Sender, S.; Sekora, A.; Villa Perez, S.; Chabanovska, O.; Becker, A.; Ngezahayo, A.; Junghanss, C.; Murua Escobar, H. Precursor B-ALL Cell Lines Differentially Respond to SYK Inhibition by Entospletinib. *Int. J. Mol. Sci.* **2021**, *22*, 592. <https://doi.org/10.3390/ijms22020592>

Received: 10 December 2020

Accepted: 7 January 2021

Published: 8 January 2021

Publisher's Note: MDPI stays neutral with regard to jurisdictional claims in published maps and institutional affiliations.



Copyright: © 2021 by the authors. Licensee MDPI, Basel, Switzerland. This article is an open access article distributed under the terms and conditions of the Creative Commons Attribution (CC BY) license (<https://creativecommons.org/licenses/by/4.0/>).

1. Introduction

B-cell receptor (BCR) signaling, as an essential regulating network, provides the main signals for survival and proliferation in hematopoietic cells [1]. In B-lymphoid malignancies, BCR signaling can be impaired by activating mutations, deletions or hyperactivated tonic BCR signaling. Impaired function of the BCR can therefore lead to B-cell malignant pathogenesis as chronic lymphocytic leukemia (CLL) or lymphoma [2]. Based on this, the BCR signaling cascade with its involved genes can serve as target genes for targeted therapies in B-cell neoplasias as CLL and B-cell lymphomas. A potential target structure is represented by SYK, the spleen tyrosine kinase. SYK, as a 72 kDa, non-receptor tyrosine kinase proximal to the BCR, is one major checkpoint for B-cell maturation and required for pro-B- (cytoplasmic I μ ⁻/surface I μ ^{M-}) to pre-B-cell (cytoplasmic I μ ⁺/surface I μ ^{M-}) transition [3–6]. During immunoreceptor engagement, the cytoplasmic tails of the BCR auxiliary transmembrane proteins Ig- α and Ig- β , which constitute the immunoreceptor tyrosine-based activation motifs (ITAMs), are phosphorylated [7]. As a result, SYK is

recruited to the ITAMs, becomes phosphorylated, and thus activated [2]. Now, SYK directly phosphorylates BLNK and transmits signals to several signaling pathway cascades downstream of the BCR, including PI3K/AKT, ERK and BTK/PLC γ 2 [8–12]. Moreover, SYK fulfills certain functions independent of BCR signaling, e.g., signal transduction from tumor necrosis factor (TNF) superfamily receptors, integrins and cytokines [2]. Activation of these pathways leads to proliferation, differentiation, cytoskeletal remodeling, cytokine release and survival [2]. In several hematological malignancies, such as CLL [13], diffuse large B-cell lymphoma (DLBCL) [14], mantle cell lymphoma (MCL) [15] and follicular lymphoma (FL) [16], SYK acts as a proto-oncogene and is thus involved in tumorigenesis. Here, tonic BCR signaling leads to constitutively activated SYK [17].

Indeed, Goodman et al. reported a SYK deficiency in pediatric precursor pro-B-ALL [18], whereas Perova et al. demonstrated in pediatric and adult B-ALL samples a pre-BCR independent SYK activation in high-risk precursor B-ALL patients and with that an apoptosis induction by specific SYK inhibition [19].

Based on pre-clinical evaluation, several SYK inhibitors are developed and under clinical investigation, e.g., fostamatinib disodium (R788) [20], entospletinib (GS-9973) [21] and cerdulatinib (PRT062070) [22]. In 2018, FDA approval of fostamatinib disodium ensued as Tavalisse for patients with chronic immune thrombocytopenia with prior unsuccessful treatment [23]. A second-generation compound, entospletinib (GS-9973), as one of the most selective SYK inhibitors, was developed as a consequence of the prodrug fostamatinib, which showed dose-limiting adverse events in patients with relapsed or refractory B-cell lymphoid malignancies, probably based on poor kinase selectivity and off-target effects [20]. Entospletinib is an ATP competitive kinase inhibitor and disrupts the kinase activity of SYK. Additionally, entospletinib exhibits an excellent selectivity profile with high efficacy for SYK inhibition and presumably lower dose-limiting adverse effects [24]. Especially, the combination of PI3K δ inhibitor idelalisib and entospletinib showed to disrupt the BCR and chemokine signaling in CLL pre-clinically [25]. A Phase 2 study with CLL patients also showed lymph node reduction and partial response with acceptable tolerability by entospletinib (Ento) administration [21].

The observed effects based on SYK inhibition in precursor B-ALL *in vitro* are mostly defined by BCR or pre-BCR dependency. Köhrer et al. likewise showed an anti-tumorigenic potential of SYK inhibition by PRT318 in pre-B-ALL cell lines (BCR⁺), whereas pro-B-ALL cell lines were not affected (BCR⁻) [4].

Due to the controversially discussed SYK function, especially in precursor B-ALL, the characterization of SYK as a potential target structure is an essential need. Here, we provide an *in vitro*-based study, which aimed to illustrate the application of entospletinib as a specific SYK inhibitor on pre- and pro-B-acute lymphoblastic leukemia cell lines, in order to further demonstrate a possible application in a subset of precursor B-ALL and, moreover, to elucidate the underlying diverging acting modes.

2. Results

2.1. Pro-B-ALL Cell Line SEM is Characterized by High SYK and pSYK Expression

SYK expression was evaluated by Western blot analyses, immunofluorescence staining and intracellular flow cytometry. Pre-B-ALL cell line NALM-6 (pre-BCR⁺) revealed the highest amount of total SYK during Western blot analyses (Figure 1a). Pro-B-ALL cell lines SEM and RS4;11 (pre-BCR⁻) showed less total SYK expression. Total SYK expression was also visualized by immunofluorescence staining in all cell lines and the strongest signal was confirmed in the pre-B-ALL cell line NALM-6 within all tested B-ALL cell lines (Figure 1b). The positive-control B-cell lymphoma cell line SU-DHL-4 revealed a high SYK expression, while the negative-control T-cell lymphoma cell line SUP-T1 was SYK-negative (Figure 1b).

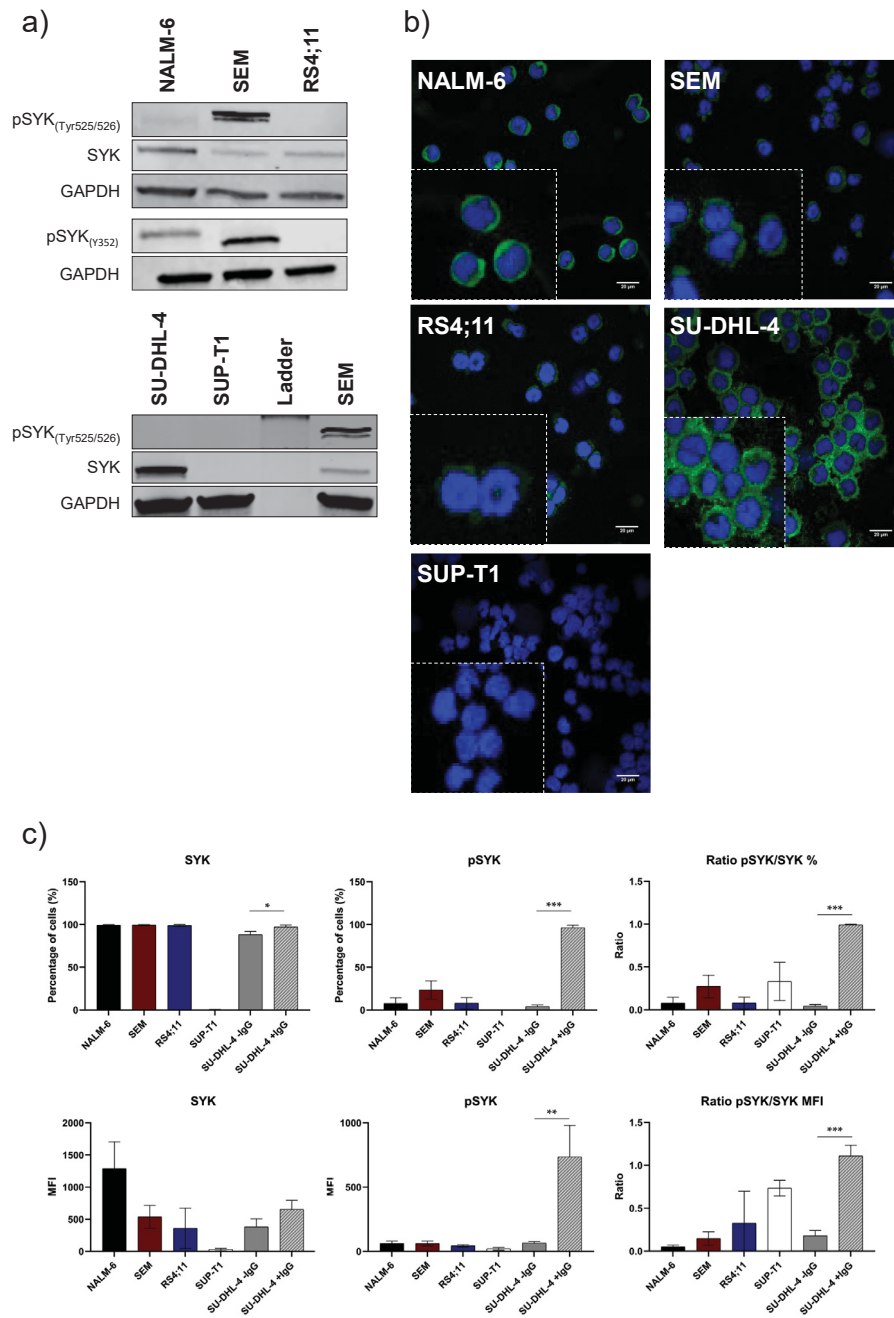


Figure 1. Basal characterization of SYK and pSYK expression in B-ALL cell lines. Characterization of basal SYK protein expression in B-ALL cell lines. Highest SYK expression was observed in pre-B-ALL NALM-6, while pro-B-ALL SEM showed the highest pSYK expression. (a) SYK and pSYK expression of two phosphorylation sites (Tyr525/526 and Y352) under non-stimulating conditions in the B-ALL cell lines and the DLBCL cell line SU-DHL-4 as well as the T-cell lymphoma cell line SUP-T1 (positive and negative control, respectively). (b) Immunofluorescent staining of SYK in the B-ALL cell lines and control cell lines (composite image of the Alexa Fluor Plus 488 green-labeled SYK and blue DAPI-stained nucleus) by confocal microscopy. (c) Intracellular staining of SYK-FITC and pSYK(Y348)-PE by flow cytometry in unstimulated B-ALL cells showing SYK and pSYK expression based on percentage (%) and mean fluorescent intensity (MFI) (SUP-T1 cell line as the negative control and IgG-stimulated SU-DHL-4 as the positive control). The mean fluorescence intensity (MFI) of all cell lines is expressed in arbitrary units (AU). Data are presented as the mean ± SD. Statistical significance was calculated by *t*-test and displayed as * $p < 0.033$, ** $p < 0.002$, *** $p < 0.001$ ($n \geq 3$).

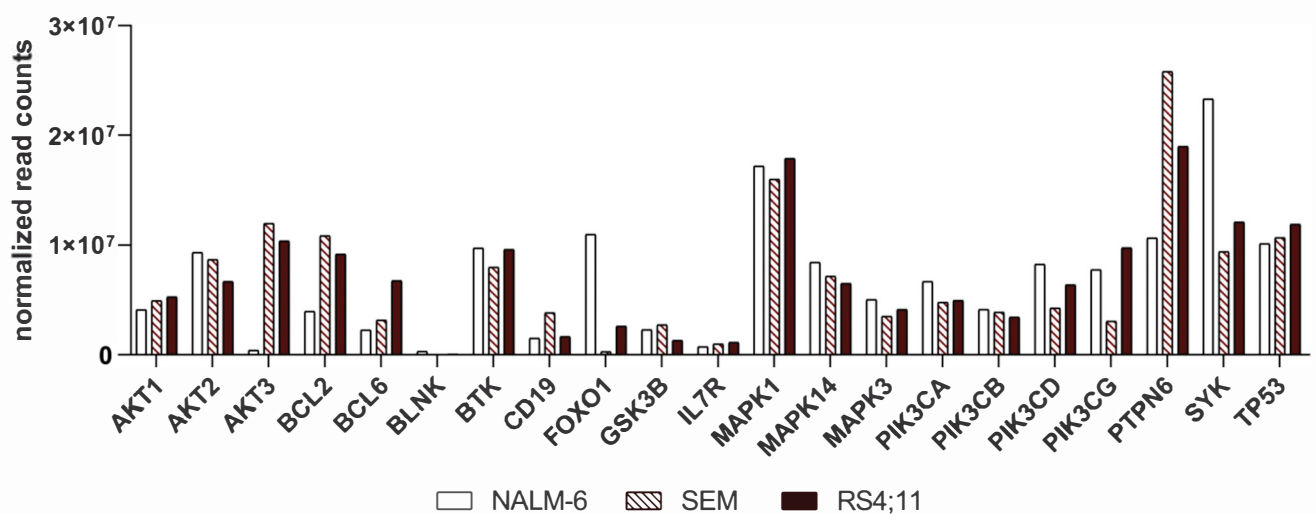
Furthermore, intracellular flow cytometry demonstrated almost entirely SYK-positive cells for all tested cells except for the negative control SUP-T1. Comparison of the mean

fluorescence intensities (MFIs) revealed significant differences between the B-ALL cell lines showing highest MFI values for NALM-6.

In contrast to the total form of SYK, the amount of the activated and phosphorylated SYK form (phospho SYK; pSYK) varied within the analyzed cell lines using Western blot detection (Figure 1a). Two different SYK phosphorylation sites were analyzed for pSYK characterization via Western blot. Thereby, the auto-phosphorylation site Tyr525/526 and activation site Y352 (Interdomain Linker Region [26]) revealed an unexpected high amount of activated SYK in the pro-B-ALL cell line SEM and less in NALM-6 and RS4;11 (Figure 1a). Flow cytometric detection of pSYK, using an alternative antibody detecting phosphorylation site Y348, revealed low pSYK levels for all cell lines except for the IgG-stimulated, positive-control cell line SU-DHL-4 (Figure 1c). Percentagewise, again the pro-B-ALL cell line SEM revealed the highest pSYK level within the unstimulated B-ALL cell lines.

2.2. Basal Expression Analysis of Key B-Cell Receptor Genes in the B-Acute Lymphoblastic Cell Lines NALM-6, SEM and RS4;11

To evaluate the basal RNA expression level of SYK as well as key regulators in the B-cell-receptor pathway, we performed targeted RNAseq with 179 genes involved in the BCR, PI3K/AKT pathway signaling and more. The highest SYK expression was detected in pre-B-ALL NALM-6 with two-fold higher expression compared to both the pro-B-ALL cell lines (the normalized read counts of a subset of vital kinases and proteins of these pathways are shown in Figure 2 and Supplementary Table S1, and the read counts and normalized read counts in Supplementary Tables S2 and S3).



AKT1 and *AKT2* showed similar expression in all three cell lines, while *AKT3* is highly expressed in both the pro-B-ALL cell lines and only slightly expressed in the pre-B-ALL cell line NALM-6. The *BCL-2* and *BCL-6* expression differs between the cell lines, whereas *BCL-6* is highest expressed in RS4;11. Furthermore, *BTK* was found present in all three cell lines at a similar kind of intensity. The PI3K subunits *PI3K α* and *PI3K β* are likely moderately expressed in all three cell lines, whereas the *PI3K δ* , *PI3K γ* and *PI3KR1* subunits vary between the cell lines. *PI3K δ* is highest expressed in NALM-6; the merest *PI3K γ* expression is revealed in SEM and the *PI3KR1* subunit is significantly highly expressed in NALM-6. *TP53* and *ERK* expression is nearly equal in all cell lines. All MAP kinases are represented in all cell lines in a similar intensity. However, *PTPN6* revealed the highest expression in the pro-B-ALL cell line SEM.

2.3. Ento Sensitivity Is Independent of the Pre-BCR Status

Ento exposure on pre-B-ALL NALM-6 (pre-BCR⁺) showed a concentration and slightly time-dependent decrease in cell proliferation, most affected at 72 h (Figure 3a). The metabolic activity was only moderately affected by Ento and re-increases with a longer incubation time. Interestingly, Ento exposure showed anti-proliferative effects also on the pro-B-ALL cell line SEM (pre-BCR⁻) (Figure 3b). Significant effects were observed starting with 5 μM for 24 h and 1 μM Ento for 48 h and 72 h exposure. The metabolic activity was similarly affected, slightly ascending with incubation time. In contrast, the pro-B-ALL RS4;11 (pre-BCR⁻) showed only a moderate reduction in proliferation at the highest concentration 10 μM and 20 μM applied for 48 h and 72 h (Figure 3c). The IC50 calculation based on 72 h proliferation is shown in Figure S1 (Supplementary File B), where the IC50 of RS4;11 was not reached.

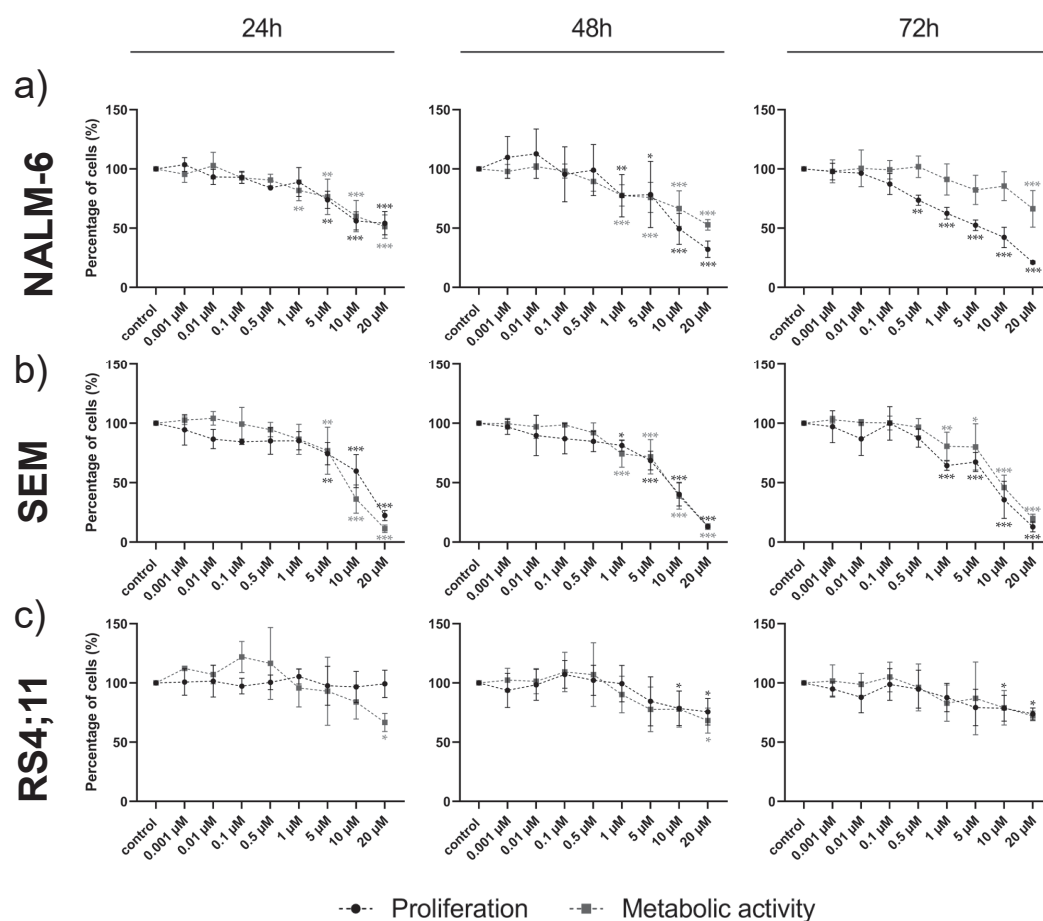


Figure 3. Cell viability after entospletinib exposure in B-ALL cell lines. Time- and concentration-dependent reduction in cell proliferation and metabolic activity in the pre-B-ALL cell line NALM-6 and pro-B-ALL cell lines SEM and RS4;11 by entospletinib. Cell proliferation and metabolic activity for entospletinib serially diluted at different concentrations (0.001 μM –20 μM) for 24 h, 48 h and 72 h (a) NALM-6, (b) SEM and (c) RS4;11. Data are presented as the mean \pm SD. Statistical significance was calculated by one-way ANOVA followed by Dunnett’s multiple comparison test as a post-hoc analysis and displayed as * $p < 0.033$, ** $p < 0.002$, *** $p < 0.001$ versus the control group ($n \geq 3$).

2.4. Pro-Apoptotic Effects Are Provoked by High Entospletinib Concentrations, Independent of Pre-BCR Dependency

High Ento concentrations induced significant early and late apoptosis/necrosis in the pre-B-ALL NALM-6 cell line during all tested time points (Figure 4a). However, in

the pro-B-ALL cell line SEM, high Ento concentrations induced significant early and late apoptosis/necrosis to a higher extent even compared to pre-B-ALL NALM-6. During the early time point (24 h), Ento mainly provokes late apoptosis, while the early apoptosis rate increased during the later time points (48 h and 72 h) (Figure 4b). In contrast, pro-B-ALL RS4;11 was almost resistant to apoptosis induction by Ento (Figure 4c). Exemplarily, apoptosis measurements of the SEM cells are given in Figure S2 (Supplementary File B).

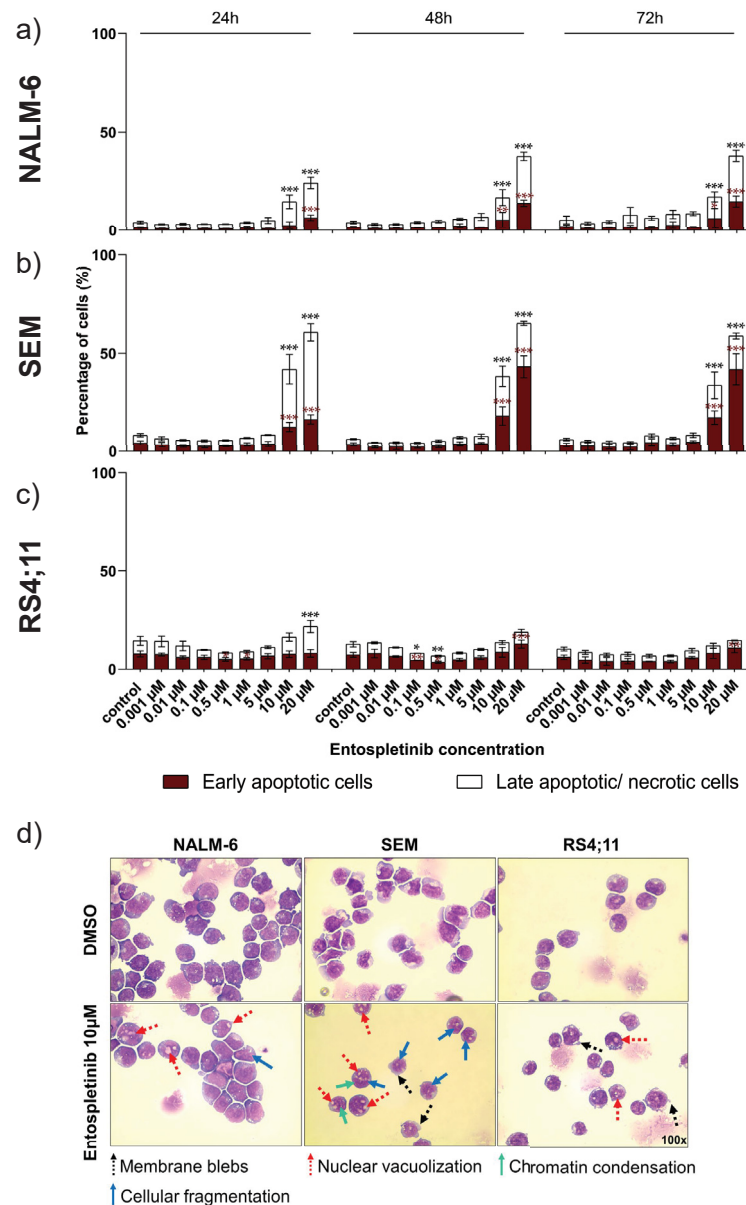


Figure 4. Apoptosis induction in B-ALL after entospletinib (Ento) exposure. Concentration-dependent apoptosis induction by entospletinib in pre-B-ALL NALM-6 and pro-B-ALL SEM. B-ALL cells were exposed to serially diluted entospletinib concentrations (0,001 µM–20 µM). Apoptosis induction was determined by Annexin V/PI staining for an exposure time of 24 h, 48 h and 72 h. (a) NALM-6 cells, (b) SEM and (c) RS4;11, respectively. (d) Representative light microscopy images (×100) of entospletinib-exposed B-ALL cells after 72 h. Cytospins were stained with May-Gruenwald Giemsa stain (Pappenheim method) after 24 h, 48 h and 72 h entospletinib exposure at different concentrations (1 µM, 5 µM and 10 µM). Data are presented as the mean ± SD. Statistical significance was calculated by one-way ANOVA followed by Dunnett’s test as a post-hoc analysis and displayed as * $p < 0.033$, ** $p < 0.002$, *** $p < 0.001$ versus the control group ($n \geq 3$). Black asterisks indicate significance of late apoptotic/necrotic cells and red asterisks indicate significance of early apoptotic cells.

2.5. Morphological Characterization Indicates Pro-Apoptotic Effects in Pre- and Pro-B-ALL Cell Lines In Vitro

The representative images of the Ento-exposed B-ALL cells (Figure 4d) indicate morphological changes in the sensitive B-ALL cell lines and moderate changes in the non-responsive cell line RS4;11 cells after Ento exposure. In NALM-6, cellular fragmentation and nuclear vacuolization can be determined. The light microscopy images of SEM indicate membrane blebs, nuclear vacuolization, cellular fragmentation and slight chromatin condensation after 72 h Ento exposure. The observed morphological changes indicate stress and apoptosis induction in both the sensitive B-ALL cell lines. In RS4;11, mainly membrane blebs and nuclear vacuolization were observed. Representative images of all the tested concentrations (1 μ M, 5 μ M and 10 μ M) and all time points (24 h, 48 h and 72 h) further confirmed morphological changes in all B-ALL cell lines and indicates apoptosis induction (Supplementary Figure S3).

2.6. Entospletinib Does Not Induce Cell-Cycle Arrest in B-ALL Cell Lines

Cell-cycle distribution was investigated in the pre-B-ALL cell line NALM-6 and pro-B-ALL cell lines SEM and RS4;11 after Entospletinib exposure. Both concentrations of Ento (low concentration 1 μ M or high concentration 10 μ M) were not able to induce changes in cell-cycle distribution after 72 h incubation in the tested B-ALL cell lines (Figure 5a–c). Exemplarily, the cell-cycle distribution of the Ento-exposed SEM cells is shown in Figure 5d.

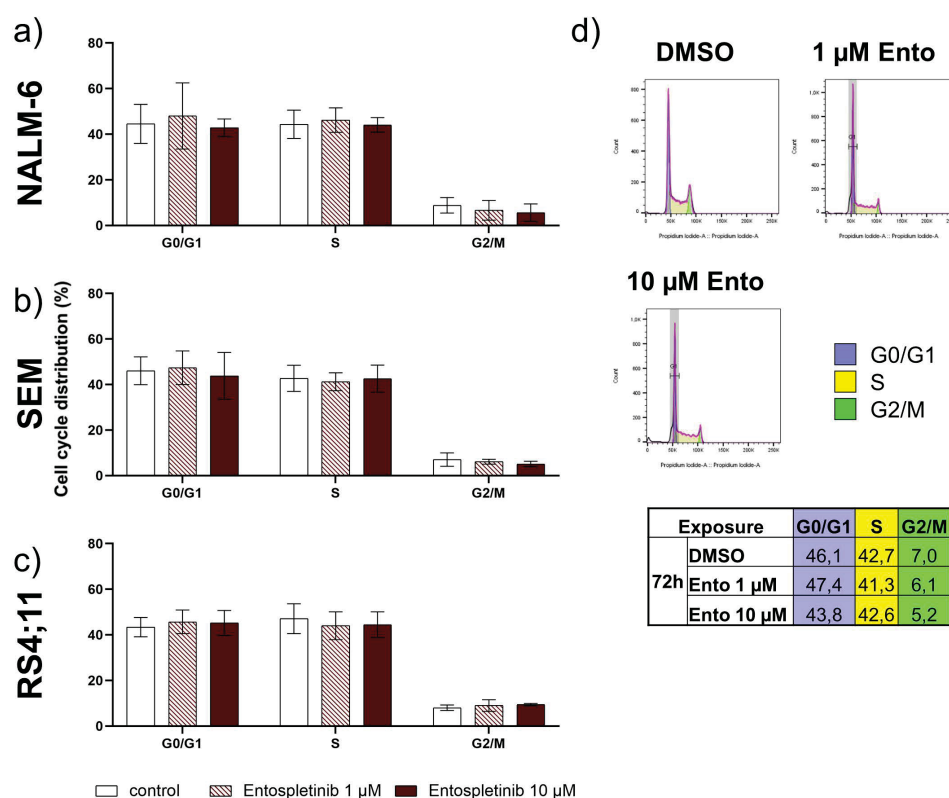


Figure 5. Flow cytometric cell-cycle analysis of the B-ALL cells after entospletinib exposure. B-ALL cell lines NALM-6, SEM and RS4;11 were exposed to 1 μ M or 10 μ M entospletinib for 72 h. (a) Mean cell-cycle distribution of NALM-6, (b) SEM and (c) RS4;11. (d) Representative histograms of the cell-cycle distribution of the SEM cells exposed to entospletinib or the vehicle, calculated by FlowJo Software, and the mean calculation of the cell-cycle phases. Data are presented as the mean \pm SD. Statistical significance was calculated by one-way ANOVA followed by Dunnett's test as a post-hoc ($n \geq 3$).

2.7. Entospletinib Downregulates Gene Expression of *PTPN6* and *BCL-6* in Pre-B-ALL NALM-6

Principle component analysis (PCA) indicates clear clustering of the appropriate cell line samples (Figure 6a). NALM-6 sample distribution exhibits a clear variance between the Ento-exposed and control cells, while the SEM and RS4;11 samples do not differ from each other. Using filter criteria of $\text{Avg}(\log_2) \geq 5$, fold change ≥ 2 or ≤ 2 within Transcriptome Analysis Console (TAC) software, we identified 1.13% relevantly up- and 10.73% downregulated genes in the pre-B-ALL cell line NALM-6. We found 2 up- and 19 downregulated genes within the BCR/PI3K/AKT pathway following Ento exposure (Figure 6c). *PTPN6* is the most downregulated gene in Ento-exposed NALM-6 cells compared to the DMSO control (fold change: -10.99), followed by *BCL-6* (fold change: -9.62). Furthermore, we detected the downregulation of *LAT2*, *IL7R*, *DAPP1*, *CD22* and more. Ento administration only upregulated a minor set of some BCR genes like *AKT3* and *RPS6KB1* in NALM-6. However, the pro-B-ALL SEM showed only 1.13% up- and 1.13% downregulated genes (Figure 6a,b,d,e). *CD79B* (fold change: 2.41) and *FOXO1* (fold change: 2.04) were upregulated, whereas *VEGFA* (fold change: -2.01) and *SPRY2* (fold change: -2.01) were downregulated after Ento exposure. In contrast, in the pro-B-ALL RS4;11, no relevant gene expression changes could be identified after Ento mono exposure during RNA panel sequencing. All read counts and normalized read counts are shown in Supplementary Tables S4–S9.

2.8. Downstream Protein Characterization Unveiled *p53* and *BCL-6* as Key Targets by Entospletinib Exposure

In the pre-B-ALL cell line NALM-6 no phosphorylation of $\text{SYK}_{\text{Tyr}525/526}$ was detected, while $\text{SYK}_{\text{Y}352}$ slightly increased during the tested time points (Figure 7c). Total SYK was not affected. pERK and total ERK expression remained mostly unaffected. A slight concentration-dependent decrease in p4E-BP1 was observed in NALM-6, whereas p53 was not detectable. pSHP-1 and total SHP-1 were only detectable starting from 48 h (Supplementary File B, Figure S4). Both decreased with increasing Ento concentrations. Further, pGSK3 β considerably increased after 1 μM Ento exposure, but not in the higher concentrations. Total GSK3 β remained unaffected. Interestingly, *BCL-6* was detected in the DMSO control and decreased after Ento exposure, independently of the concentration. Further, a strong pAKT level was detected after 1 μM Ento exposure, which then declined with higher concentrations again. The appropriate total AKT expression was consistent. Complete Western blot analyses for 24 h, 48 h and 72 h Ento exposure on NALM-6 cells are shown in Supplementary File B (Figure S4).

Phosphorylated SYK decreased concentration dependent in the pro-B-ALL cell line SEM, validated for both phosphorylation residues Tyr525/526 and Y352 (Figure 8 and Supplementary File B, Figure S5). Application of 10 μM Ento almost completely inhibited the pSYK expression, while total SYK remained unaffected. Interestingly, pERK expression increased by Ento exposure in SEM, while total ERK remained unaffected. Strikingly, the tumor suppressor p53 vigorously decreased concentration dependently in SEM. Furthermore, the phosphorylated SHP-1 decreased only during the first 24 h and pGSK3 β increased independently of concentration and time. Total GSK3 β was not influenced. Furthermore, *BCL-6* protein expression has not been detected in SEM during the tested time points. Another interesting modification has been observed in the amount of phosphorylation of AKT residue Ser473. In SEM cells, pAKT was increased in all samples after Ento exposure compared to the DMSO control. Distinct changes were observed after long-term incubation (72 h), whereby 1 μM Ento exposure induced distinct modification merely after 24 h and 48 h. Total AKT expression remained unaffected during all time points. Complete Western blot analyses for 24 h, 48 h and 72 h Ento exposure on SEM cells are shown in Supplementary File B (Figure S5).

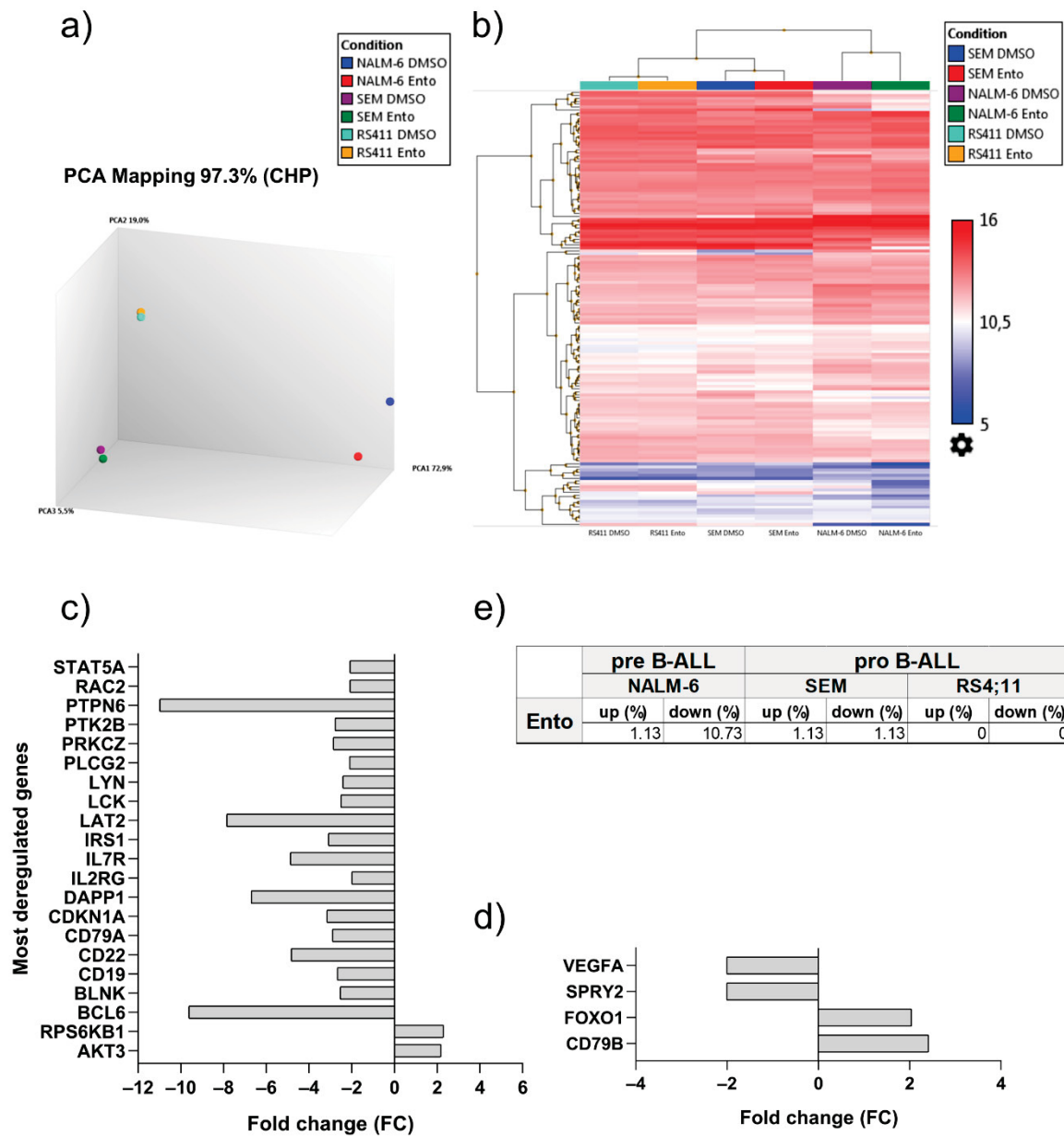


Figure 6. Entospletinib-induced gene expression changes in the B-ALL cell lines. Entospletinib-induced gene expression changes within the BCR and PI3K/AKT pathway predominantly in pre-B-ALL NALM-6 and slightly in pro-B-ALL SEM. (a) Principle component analysis of the control and 1 μM Ento-exposed B-ALL cell lines revealed distinct clustering of the appropriate cell line samples and variance in the NALM-6 cells after Ento exposure. (b) Hierarchical clustering of all the relevant regulated genes demonstrates the gene expression changes in the B-ALL cell lines. (c) Fold changes of the significantly deregulated genes in NALM-6 and (d) SEM. (e) Percentage-wise deregulation after 1 μM Ento exposure.

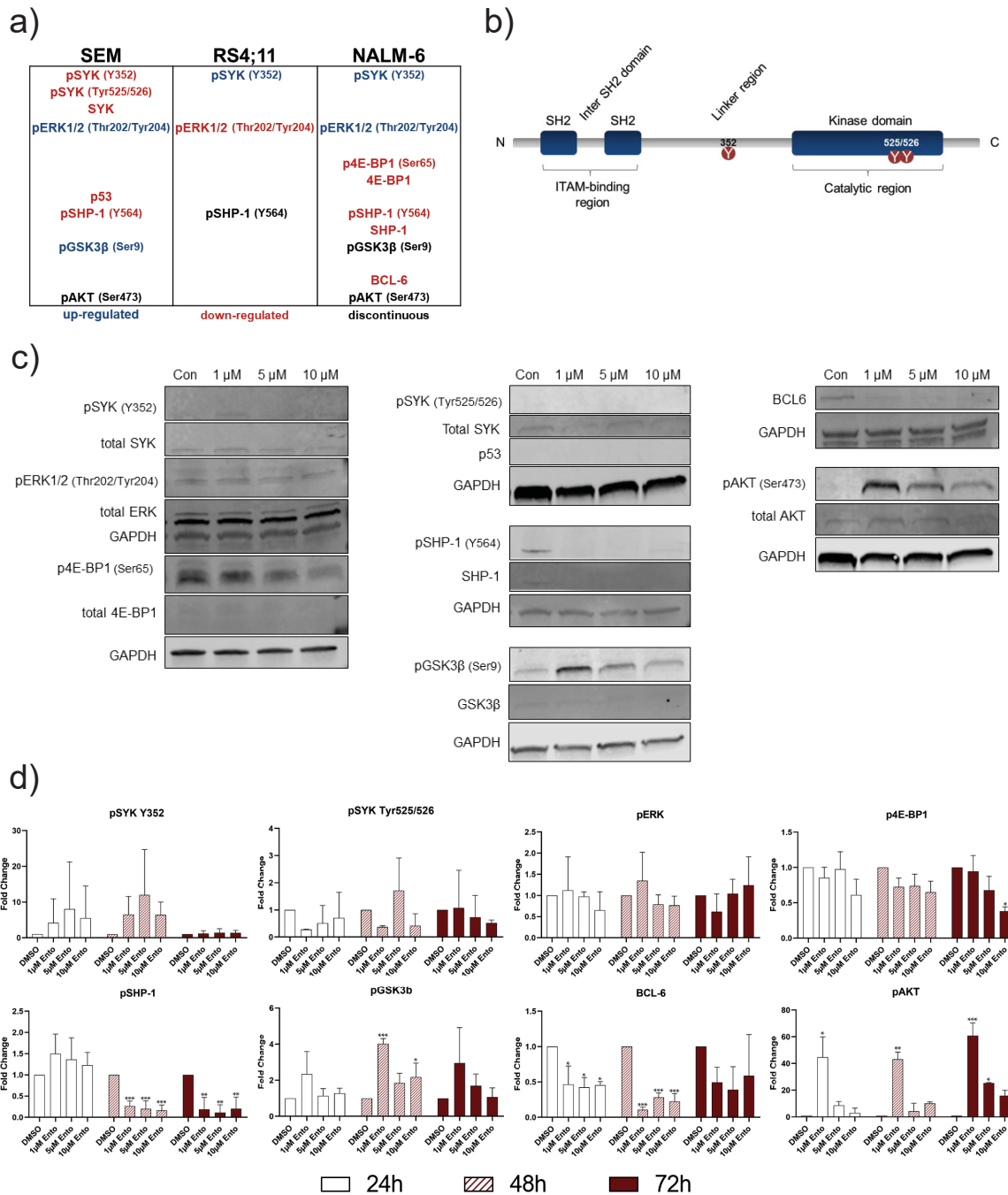


Figure 7. Entospletinib-induced distinct downstream protein modifications in pre-B-ALL NALM-6. Western Blot analyses revealed distinct changes in the SYK downstream proteins in pre-B-ALL NALM-6. (a) Condensed conclusion of protein modifications in all tested B-ALL cell lines. (b) Schematic illustration of the SYK protein structure, showing the amino acids used to examine the phosphorylation status. (c) Representative Western blot images of NALM-6 cells after 72 h entospletinib exposure. (d) Western blot quantification of key proteins after 24 h, 48 h and 72 h exposure (≥ 3 independent Western blots). Data are presented as the mean \pm SD. Statistical significance was calculated by one-way ANOVA followed by Dunnett’s test as a post-hoc analysis and displayed as * $p < 0.033$, ** $p < 0.002$, *** $p < 0.001$ versus the control group ($n \geq 3$).

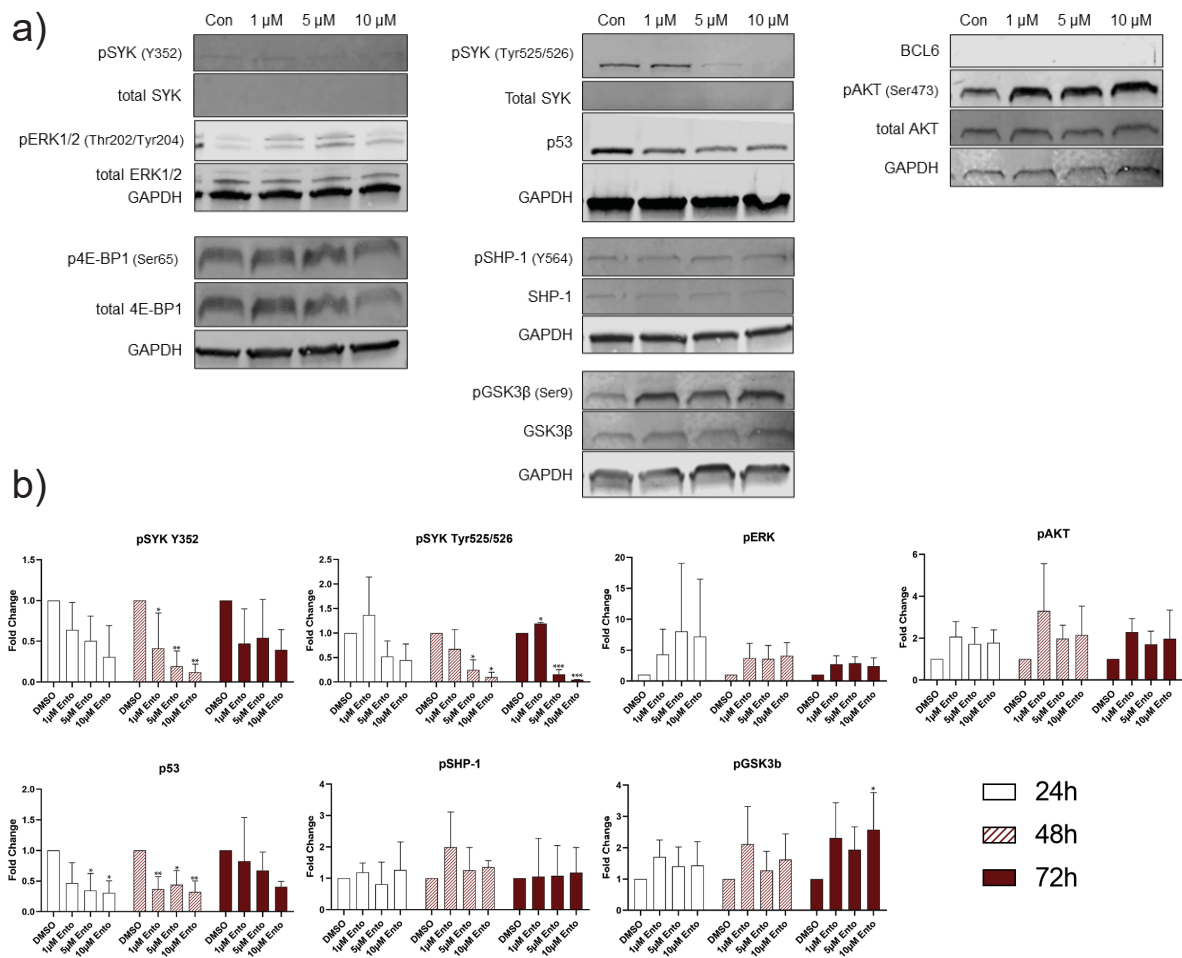


Figure 8. Entospletinib-induced distinct downstream protein modifications in pro-B-ALL SEM. (a) Representative Western blot images of SEM cells after 72 h exposure. (b) Western blot quantification of key proteins (≥ 3 independent Western blots for 24 h, 48 h and 72 h time points). Data are presented as the mean \pm SD. Statistical significance was calculated by one-way ANOVA followed by Dunnett's test as a post-hoc analysis and displayed as * $p < 0.033$, ** $p < 0.002$, *** $p < 0.001$ versus the control group ($n \geq 3$).

In the second pro-B-ALL cell line RS4;11, an increase of SYK_{Y352} level was detected during the tested time points while total SYK remained unaffected (Figure 9 and Supplementary File B, Figure S6). pERK expression was distinctly reduced after Ento exposure during all tested time points, while total ERK was not affected. Further, no p53 expression was detected during the tested conditions. pSHP-1 results were discontinuous and showed an increase only after 1 μ M Ento exposure during 72 h incubation, while total SHP-1 was not affected. Moreover, high level of BCL-6 was detected in all samples and time points without any alteration. No obvious expression changes were observed in pGSK3 β and total GSK3 β , pAKT and total AKT during the tested conditions. Complete western blot analyses for 24 h, 48 h and 72 h Ento exposure on RS4;11 cells are shown in Supplementary File B (Figure S6).

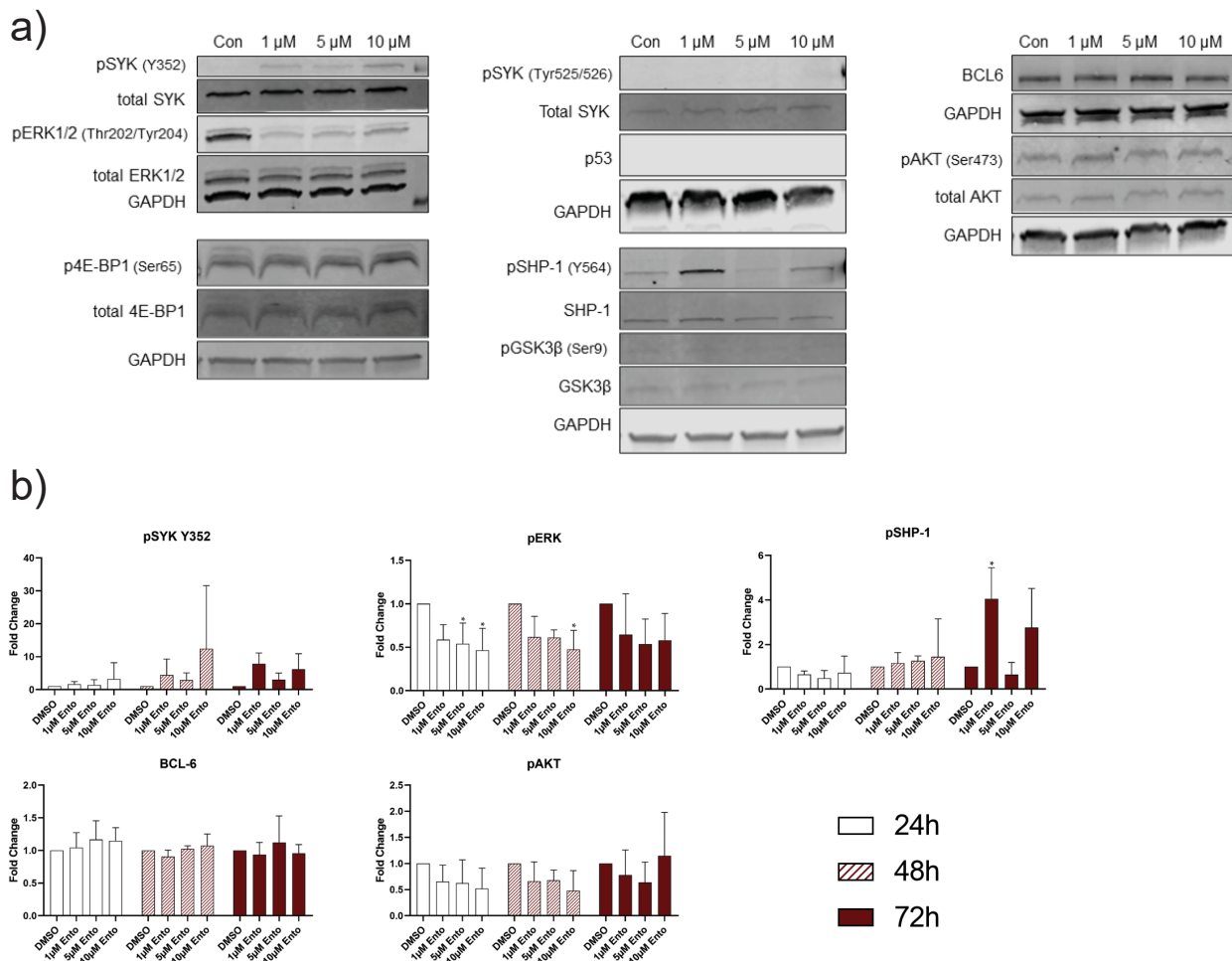


Figure 9. Entospletinib induced moderate downstream protein modifications in pro-B-ALL RS4;11. Entospletinib induces moderate protein expression changes in pro-B-ALL RS4;11. (a) Representative Western Blot images of RS4;11 cells after Ento exposure (b) Western Blot quantification of key proteins (≥ 3 independent Western Blots for 24 h, 48 h and 72 h time points). Data are presented as the mean \pm SD. Statistical significance was calculated by One-way ANOVA followed by Dunnett's test as post hoc ($n \geq 3$).

Moreover, Western blot densitometric analyses of the NALM-6 exposed cells confirmed significant changes in BCL-6, pSHP-1, pGSK3 β and pAKT expression (Figure 7d). Further distinct changes were observed in SYK_{Y352} and p4E-BP1 expression. Pro-B-ALL SEM Western blot quantification also verified the most vigorous and significant alteration of SYK_{Tyr525/526}, SYK_{Y352} and p53. Further modifications were observed in pERK, pGSK3 β and pAKT expression. Exemplarily, the densitometric analysis of the mostly affected proteins are shown in Figure 8b. The quantification of Ento-exposed pro-B-ALL cell line RS4;11 revealed distinct modifications in SYK_{Y352} and pERK expression (Figure 9b).

3. Discussion

Targeting B-cell receptor associated kinases, such as SYK, represents a major therapeutic tool in the treatment of B-cell malignancies such as CLL and DLBCL. In progenitor and precursor B-ALL, the function and druggability of SYK is still controversially discussed. Here, we identified a diverse acting mode of entospletinib, which not only relies on pre-BCR dependency. Anti-proliferative and pro-apoptotic effects were observed in both pre-B-ALL (NALM-6) and pro-B-ALL (SEM) cell lines, while a second pro-B-ALL (RS4;11) remained resistant, independently of the applied Ento concentration. Currently, BCR dependency is considered as a response marker to SYK inhibition. Here, pre-BCR⁺ and pre-BCR⁻ ALL cells can be distinguished by kinase inhibitor sensitivity, where only

pre-BCR⁺ ALL cells selectively respond to SYK inhibition [27]. However, in this study we describe an exception for pro-B-ALL cells, showing a comparable sensitivity to SYK inhibition as do the pre-B-ALL cells, with comparable Ento IC50 values. Further, the observed pro-apoptotic effects were slightly more pronounced in the pro-B-ALL cells (SEM) compared to the pre-B-ALL cells (NALM-6). In contrast, apoptosis induction was not observed in the second pro-B-ALL cell line RS4;11. Compared to other studies testing Ento in CLL in vitro, the anti-proliferative as well as pro-apoptotic effects were slightly higher compared to our tested B-ALL cell lines [25,28]. CLL cells depends on their microenvironment, cell homing, chemokine/cytokine interactions and activation of B-cell receptor signaling [29]. Disrupting BCR signaling by BCR-associated kinase inhibition, e.g., BTK or SYK, lead to cross-talk blockage within the microenvironment and thus of BCR signaling [30], which makes SYK inhibition in CLL highly effective. In accordance to that, strong apoptosis induction in sensitive DLBCL cell lines by SYK inhibitor R406 was also shown and reasoned by intact BCR signaling [14]. Presumably, CLL and DLBCL depend more on functional BCR signaling compared to precursor B-ALL and progenitor B-ALL in any case, due to the lacking BCR or pre-BCR. Depending on whether a pre-BCR is present or not, it can be assumed that the acting mode of SYK inhibition and the followed signal transduction will differ from each other. Cell-cycle distribution of pre-B-ALL cells (NALM-6) and pro-B-ALL cells (SEM and RS4;11) were not affected by Ento treatment. This is in contrast to the findings in DLBCL cell lines to SYK inhibition by PRT318. In this study, SYK inhibition induced cell-cycle arrest by blocking G1/S transition in a part of the sensitive DLBCL cell lines [31]. Moreover, SYK itself is known to be a master regulator of anti-apoptotic signaling in B-lineage leukemias and lymphomas with cell-cycle regulatory function by G2 checkpoint regulation. SYK occurs to be essential for cell-cycle control due to CDC25C phosphatase inactivation by phosphorylation of S216 residues and further maintaining CDK1 inactive. This prevents CDK1 entry into mitosis and encourages SYK as an important regulator during the cell-cycle process [32]. In B-ALL cell lines, cell-cycle distribution does not seem to be influenced by SYK inhibition.

We further investigated the Ento-induced effects on BCR and PI3K/AKT downstream signaling by Western blot analyses. Here, we focused on the pivotal kinases. All tested cell lines exhibit different pathway modulation after Ento exposure. Whereas RS4;11 protein expression was only moderately modified by Ento treatment, SEM and NALM-6 were markedly affected. The most conspicuous alterations in the pro-B-ALL cell line SEM was the reduction of pSYK_{Tyr525/526} and p53 and the increase of pERK1/2. It is already known, that SYK is able to modulate p53 activity [33,34]. p53 (*TP53* gene) normally bears a tumor-suppressor function, where a high p53 induces apoptosis, cell-cycle arrest and senescence [35]. In cancers, *TP53* is frequently mutated [36], resulting in loss-of-function (LoF), dominant-negative (DN) or gain-of-function (GoF) effects. *TP53* hot-spot mutants, as R157H, R282W, R248Q and R249, can destabilize the DNA-binding domain, which can lead to partially unfolded p53 proteins and therefore loss of the p53 wild type (wt) function [37]. The substitution in R248Q also causes structural alteration in the respective DNA contact sites [38,39]. Further, R248Q, have been shown to build aggregates caused by protein misfolding [38,39]. Aggregated p53 mutants inactivate p53 and leads to LoF effects. Moreover, aggregated p53 forms can also co-aggregate with other tumor suppressors, such as p63 or p73. This interaction with new DNA-binding sites can explain the GoF effects that, in turn, increases cancer progression [38].

The pro-B-ALL cell line SEM carries the *TP53* p.R248Q mutation [40] (COSM10662), which could explain the high p53 expression of the stabilized p53 mutant. Ento was able to reduce p53 in the pro-B-ALL cell line SEM as a consequence of the pSYK decrease.

In pre-B-ALL NALM-6, especially 1 μM Ento induced obvious changes within BCR and PI3K/AKT signaling. Here, we found pAKT and pGSK3β upregulated by Ento exposure. Moreover, in DLBCL cell lines, SYK inhibition by R406 reduced the downstream signaling of the BCR by pAKT, pGSK3β and pERK reduction [41]. In contrast, Ento exposure on pro-B-ALL SEM increased the pERK1/2 level concentration independently. Previously, it

was demonstrated that Raf/MEK/ERK activation can induce drug resistance. Moreover, a decrease in p53 was associated with drug resistance [42]. The pAKT and pGSK3 β levels were also increased in SEM after Ento exposure. These distinct modifications in SEM seem to indicate a drug-escape mechanism caused by entospletinib exposure. In acute myeloid leukemia (AML), an activated RAS/MAPK/ERK pathway also was observed after Ento exposure and linked to resistance to Ento [43,44].

The reduction in PTPN6 and pSHP-1 in NALM-6 in response to SYK inhibition presumably occurs due to a negative feedback loop based on a decreased pSYK level. PTPN6, also known as SHP-1, is a downstream protein tyrosine phosphatase of SYK that negatively regulates SYK and attenuates BCR signaling [45,46]. Whereas SYK is important for B-cell development, SHP-1 is a negative regulator of B lymphocyte activation [47] and counteracts the phosphorylation of SYK [48].

However, Western blot analyses revealed a downregulation of BCL-6 and pSHP-1 in NALM-6 after Ento exposure. This observation was also confirmed by RNA panel sequencing, where *BCL-6* and *PTPN6* were likewise mostly downregulated. It was already shown that BCL-6 directly depends on pre-BCR signaling, where SYK inhibition reduced BCL-6 in the *TCF3-PBX1* ALL cell line and patient-derived *TCF3-PBX1* ALL cells [27]. Further, Geng et al. demonstrated a SYK-dependent BCL-6 expression in pre-BCR⁺ ALL cells and with that a poor outcome for high BCL-6 expression levels in pre-BCR⁺ ALL [27]. It was concluded that BCL-6 expression depends on tonic pre-BCR signaling due to BCL-6 repression by SYK and SRC inhibition [27]. However, we found BCL-6 highly expressed in the pro-B-ALL cell line RS4;11, at the RNA and protein level, where Ento exposure did not affect the BCL-6 expression nor cell viability. This could suggest that, independent of pre-BCR signaling, high BCL-6 expression prevents the cell from apoptosis induction due to the BCL-6–BIM axis. This mechanism was already proved in a recent study, where BCL-6 function was elucidated in *MLL*-rearranged B-ALL. Initially, it was shown that especially *MLL*-rearranged B-ALL showed an upregulated BCL-6 expression, which is also related to a poor prognosis. Moreover, it was shown that BCL-6 is able to bind the BCL2L11 locus (BIM) and consequently regulates BIM expression. The deletion of *BCL-6* induced an increased BIM level [49]. Altogether, a high BCL-6 expression keeps pro-apoptotic BIM under control, which in turn prevents apoptosis induction in *MLL*-rearranged B-ALL. Low BIM expression or BIM loss correlates with a pro-survival behavior and was already observed in many cancers as a survival strategy [50,51]. For that reason, the low BCL-6 expression in *MLL*-rearranged sensitive SEM cells, high BCL-6 expression in *MLL*-rearranged resistant RS4;11 and the reduction of BCL-6 expression in NALM-6 could be explained by the BCL-6–BIM axis and with that the sensitivity to Ento exposure. Concerning this, a new study from Toscan et al. revealed a strategy to overcome glucocorticoid resistance in ALL due to recovering the BIM function [52].

Altogether, our present study demonstrates anti-proliferative, metabolism modulating and pro-apoptotic effects in pre- and pro-B-ALL cell lines in vitro, independent of pre-BCR presence. We further unveiled that the *TP53* variant in pro-B-ALL SEM and the BCL-6–BIM axis can probably explain the entospletinib sensitivity and therefor provides a rationale for Ento application also in a subset of pro-B-ALL.

4. Materials and Methods

4.1. Cell Lines and Reagents

Human B-ALL pre-B-ALL cell line NALM-6 (pre-BCR⁺), pro-B-ALL cell lines SEM and RS4;11 (pre-BCR⁻), B lymphoma cell line SU-DHL-4 and T lymphoma cell line SUP-T1 were purchased from the German Collection of Microorganisms and Cell Cultures (DSMZ, Braunschweig, Germany). The cells were cultured as recommended by the manufacturer at 37 °C and 5% CO₂ in media supplemented with 10 % heat-inactivated FCS (Biochrom, Berlin, Germany) and 100 μ g/mL penicillin and streptomycin (Biochrom, Berlin, Germany). Mycoplasma contamination was regularly tested.

Entospletinib (GS-9973) was purchased from Selleck Chemicals (Absource Diagnostics GmbH, München, Germany, catalog no. S7523). A 10 mM Stock solution was prepared according to the manufacturer's instructions and stored at $-80\text{ }^{\circ}\text{C}$.

4.2. Drug Exposure Experiments

B-ALL cell lines (3.3×10^5 cells/mL) were treated with serial end-concentrations (0.001–10 μM) of entospletinib. Cells were cultured in the appropriate medium containing 0.1% (*v/v*) DMSO as the solvent of the drug or dose ranges of entospletinib as single substance for 24 h, 48 h and 72 h. Following, the effect on cell proliferation (trypan blue staining), metabolism (WST-1 assay), apoptosis/necrosis (annexin V/PI staining), cell morphology and protein expression were determined. All experiments were performed at least in three biological replicates.

4.3. Cell Proliferation

Pro-B-ALL cells SEM and RS4;11 as well as pre-B-ALL cell line NALM-6 were seeded at a density of 5×10^5 cells in 1.5 mL in 24-well plates as duplets (Greiner Bio-One GmbH, Frickenhausen, Germany). The B-ALL cell lines were exposed to the entospletinib or 0.1% (*v/v*) DMSO as control. The cells were harvested 24 h, 48 h and 72 h after drug incubation and washed with PBS (Biochrom, Berlin, Germany), (10 min, 180 g, $4\text{ }^{\circ}\text{C}$). The number of viable cells was determined by cell count with a hemocytometer after trypan blue staining (Sigma-Aldrich Chemie GmbH, Steinheim, Germany).

4.4. WST-1 Proliferation Assay

Cells were seeded at a density of 5×10^4 cells/well in 96-well plates with 150 μL cell culture medium containing DMSO as the control or entospletinib, in triplicate. Evaluation of the metabolic activity was analyzed via tetrazolium compound WST-1 (TaKaRa Bio Inc., Kusatsu, Japan, catalog no. MK400) according to the manufacturer's protocol. Briefly, after an appropriate incubation time, the cells were incubated with 15 μL WST-1 premix WST-1 for up to 3 h. The absorbance at 450 nm and a reference wavelength at 750 nm were determined using the GloMax- Multi Microplate Multimode Reader (Promega, Madison, WI, USA). The absorbance of only culture medium containing the WST-1 reagent was used as the background control.

4.5. Apoptosis Assay

Early and late apoptosis was analyzed by annexin V FITC (BD Biosciences, Heidelberg, Germany, catalog no. 556419) and propidium iodide (PI) (Sigma Aldrich, St. Louis, MO, USA, catalog no. P4864-10ML) staining according to the manufacturer's protocol. Drug-exposed and control cells were harvest from 24-well plates and washed twice with cold PBS (10 min, 180 g, $4\text{ }^{\circ}\text{C}$). The cell pellets were resuspended in a 100 μL annexin binding buffer (BD Biosciences, Heidelberg, Germany, catalog no. 556454) and stained with 5 μL annexin V FITC for 15 min at room temperature in the dark. Cell suspensions were adjusted to a final volume of 500 μL with the annexin binding buffer and stained with PI (20 $\mu\text{g}/\text{mL}$) immediately before measurement. Unstained and single stained control cells were included in each experiment. Measurements were performed using FACS VerseTM (BD Biosciences, Heidelberg, Germany) and BD FACSuite Software (Version 4.0.2, BD Biosciences, Heidelberg, Germany).

4.6. Cell-Cycle Analysis

The DNA intercalating dye propidium iodide (PI) was used for cell-cycle analysis to quantify the DNA content. Cells were treated with 1 μM and 10 μM entospletinib or DMSO as the vehicle. After 48 h and 72 h at $37\text{ }^{\circ}\text{C}$ entospletinib exposure, cells were harvested. After centrifugation at $180 \times g$ for 10 min at $4\text{ }^{\circ}\text{C}$ the cells were washed twice with PBS, followed by fixing the cells with 70 % ice cold ethanol and a freezing cycle at $-20\text{ }^{\circ}\text{C}$ (≥ 24 h). Subsequently, the fixation solution was removed by centrifugation

at $180\times g$ for 10 min at $4\text{ }^{\circ}\text{C}$. The fixed cells were then washed twice with PBS. After centrifugation the cell pellet was then resuspended in $500\text{ }\mu\text{L}$ ribonuclease A (1 mg/mL) (Carl Roth, Karlsruhe, Germany, catalog no. 7156.2). RNase treatment ensued 45 min at $37\text{ }^{\circ}\text{C}$. After a centrifugation step at $180\times g$ for 10 min at $4\text{ }^{\circ}\text{C}$, the cells were washed again with PBS for two times. PBS was removed by a centrifugation, the pellet was resuspended in $400\text{ }\mu\text{L}$ PI Solution ($50\text{ }\mu\text{g/mL}$) (Sigma-Aldrich Chemie GmbH, Steinheim, Germany, catalog no. P4864-10ML) and analyzed by flow cytometry (FACS VerseTM, BD Biosciences, Heidelberg, Germany) and BD FACSuite Software (Version 4.0.2, BD Biosciences, Heidelberg, Germany).

4.7. Immunofluorescence Staining

Coated cytoslides (Tharmac, Waldsolms, Germany, catalog no. JC311-100) were prepared with 5×10^4 cells per slide (750 rpm, 10 min) in a Cytospin 3 centrifuge (Shandon, Frankfurt/Main, Germany). Slides were fixed in ice-cold methanol for 10 min. Afterward, the cells were permeabilized, blocked and stained with SYK antibody (1:400 diluted in 1% BSA) (sc-1240, Santa Cruz Biotechnology, Santa Cruz, TX, USA). Slides were washed and stained with secondary goat Anti-mouse IgG Alexa Fluor Plus 488 (1:1000 diluted in 1% BSA) (Thermo Fisher Scientific, MA, USA). The antibodies used are listed in Supplementary File C, Table S3. Finally, the cells were mounted, and the cell nuclei stained with Roti-Mount FluorCare DAPI (Carl Roth, Karlsruhe, Germany, catalog no. HP20.1). Fluorescence images were captured using a Nikon Eclipse TE2000-E confocal laser scanning microscope (Alexa Fluor 488 for SYK and FluorCare DAPI for nucleic staining (Carl Roth, Karlsruhe, Germany)), with a $60\times$ water-immersion objective and the EZ-C1 software program (Nikon, Düsseldorf, Germany, Version 3.80). Fluorescence images were processed with the ImageJ/Fiji software (Version 1.49b / Java 1.6.0_24 (64bit) [53,54].

4.8. Pappenheim Staining

Coated cytoslides (Tharmac, Waldsolms, Germany, catalog no. JC311-100) were prepared with 5×10^4 cells per slide (750 rpm, 10 min) in a Cytospin 3 centrifuge (Shandon, Frankfurt/Main, Germany). The slides were stained for 6 min with May-Grünwald working solution (Merck, Darmstadt, Germany, catalog no. 101424), rinsed with microscopy buffer according to WEISE (pH7.2) (Merck, Darmstadt, Germany, catalog no. 109468), stained for 20 min in a Giemsa working solution (Merck, Darmstadt, Germany, catalog no. 109204) and rinsed thoroughly with the microscopy buffer again. The slides were air dried at room temperature before analysis. To evaluate the morphological changes of the cells, the slides were analyzed by EVOS[®] XL Core Imaging System (AMG, Washington, DC, USA).

4.9. Protein Extraction and Western Blot Analyses

Treated cells were lysed using RIPA buffer ($10\times$ RIPA Buffer; $100\times$ Protease/Phosphatase Inhibitor Cocktail (Cell Signaling Technology, Danvers, MA, USA, catalog no. #9806; catalog no. #5872)) and ultrasound. Protein concentrations were determined by Bradford Protein Assay (Bio-Rad, München, Germany). For each sample, $30\text{ }\mu\text{g}$ protein were separated on Criterion TGX Precast Gels (Bio-Rad, München, Germany, catalog no. 5671123). They were blotted onto a PVDF membrane (Trans-Blot Turbo Transfer Pack $0.2\text{ }\mu\text{M}$ PVDF, Bio-Rad, catalog no. 1704157) using Trans-Blot[®] TurboTM Transfer System (Bio-Rad, 2.5 A, 25 V, 10 min). After blockage in 1:3 diluted Odyssey Blocking Buffer (LI-COR, Nebraska, USA, catalog no. 927-50000) for one hour, the membranes were incubated with the primary antibody overnight at $4\text{ }^{\circ}\text{C}$. The antibodies used are listed in Supplementary File C, Tables S1 and S2. The membranes were then washed in PBS-T and incubated with the secondary antibody for one hour. After a washing step in PBS-T the detection was performed with a LI-COR Odyssey Imaging System and Image Studio Lite software (LI-COR, Lincoln, NE, USA).

4.10. Intracellular Phospho-Specific Flow Cytometry and Stimulation

The detection of the intracellular targets pSYK and SYK was carried out by intracellular flow cytometry (FACS Verse™, BD Biosciences, Heidelberg, Germany). The SUP-T1 T-cell lymphoma cell line acted as the negative control due to lacking SYK expression. The IgG-stimulated B-lymphoma cell line SU-DHL-4 acted as the positive control. AffiniPure F(ab')₂ Fragment Goat Anti-Human IgG, F(ab')₂ fragment specific was used for stimulation and purchased from Dianova (Jackson ImmunoResearch, West Grove, PA, USA, catalog no. #109-006-097). Here, SU-DHL-4 was seeded in 24-well plates (10⁶ cells/mL) and stimulated for 15 min with 5 µg/mL IgG at 37 °C and 5 % CO₂ [9]. Cells were harvested directly from cell culture flasks and washed twice with 2 mL PBS. Cells were fixed with 4% formaldehyde (16%, methanol-free, Ultra-Pure EM Grade, Polysciences, Warrington, PA, USA, catalog no. 18814-10) to a final concentration of 4 % for 15 min at room temperature. Subsequently, cells were washed with an excess of PBS and resuspended in an appropriate amount of PBS. For permeabilizing the cells, ice-cold methanol was gently added to a final concentration of 90%. The cells were then incubated for 30 min on ice. Staining was started by washing the cells with an excess of PBS (300 µL, 10 min, 4 °C). Cells were resuspended in incubation buffer (0.5% BSA in PBS) containing the antibody to a total volume of 100 µL. The conjugated antibodies used are listed in Supplementary File C, Table S4. Cells were then incubated for 60 min in the dark at room temperature. Thereafter, stained cells were washed twice with PBS, resuspended in 300 µL PBS and were analyzed by flow cytometry (FACS Verse™, BD Biosciences, Heidelberg, Germany). For all experiments, the unstimulated, autofluorescence and isotype controls were analyzed simultaneously. All experiments were performed at least in three biological replicates.

4.11. RNA Extraction and Isolation

Treated cells or control cells were grown in 6-well plates for up to 72 h, harvested and washed three times with cold PBS by centrifugation steps at 180× g for 8 min. Cell pellets were resuspended in QIAzol Lysis Reagent (QIAGEN, Venlo, Netherlands, catalog no. 79306) and RNA Isolation was performed with miRNeasy Mini Kit (QIAGEN, Venlo, Netherlands, catalog no. 217004) according to the manufacturer's instructions. In brief, after lysis, the aqueous phase that contains the total RNA of the lysed cells were extracted and purified by a silica membrane of RNeasy Mini spin columns. The remaining DNA was digested by RNase-free DNase (QIAGEN, Venlo, Netherlands, catalog no. 79256) and the contaminants were washed away. Total RNA was eluted by nuclease-free water and RNA concentration measured on a Nanodrop Spectrophotometer ND1000 (PEQLAB Biotechnologie GmbH, Erlangen, Germany, Version 3.7.1).

4.12. Targeted RNA Sequencing and Data Analysis

Expression analyses were performed with AmpliSeq RNA targeted sequencing on the Ion Personal Genome Machine™ (PGM™) System (Ion Torrent™) (Thermo Fisher Scientific, Waltham, Massachusetts, USA). For targeted RNA sequencing, an in-house custom panel was designed with the Ion AmpliSeq Designer (Thermo Fisher Scientific), containing 179 genes mainly involved in B-cell-receptor and PI3K/AKT pathway signaling and more. Ion AmpliSeq RNA Libraries were prepared according to the manufacturer's protocol (MAN0006735). In brief, RNA was quantified with the Qubit RNA HS Assay Kit (Thermo Fisher Scientific, Waltham, MA, USA, catalog no. Q32852) on the Qubit 2.0 Fluorometer (Life Technologies, Carlsbad, CA, USA) and transcribed into cDNA using SuperScript VILO cDNA Synthesis Kit (Thermo Fisher Scientific, catalog no. 11754-050). cDNA targets were amplified, amplicons partially digested, ligated to the adapters and purified with the Ion AmpliSeq™ Library Kit 2.0 (Thermo Fisher Scientific, Waltham, MA, USA, catalog no. 4475345). All steps were performed in the ProFlex PCR System (Thermo Fisher Scientific, Waltham, MA, USA). The final library was quantified by the Ion Library TaqMan Quantification Kit (Thermo Fisher Scientific, Waltham, MA, USA, catalog no. 4468802) with the ViiA 7 Real-Time PCR System (Thermo Fisher Scientific, Waltham, MA,

USA). Thereafter, template preparation was carried out with the Ion PGM Hi-Q View OT2 Kit—200 in the Ion One Touch 2 Instrument (Thermo Fisher Scientific, Waltham, MA, USA, catalog no. A29900) and enrichment of template-positive Ion Sphere Particles (ISPs) with the Ion OneTouch ES (Thermo Fisher Scientific, Waltham, MA, USA, catalog no. 4478525). Finally, the sequencing run was performed with the PGM System. The evaluations of the data sets were performed using Transcriptome Analysis Console (TAC) Software (Thermo Fisher Scientific, Waltham, MA, USA, Version 4.0.0.25). The following filter criteria were set to identify relevantly regulated genes: Avg (log2) > 5, fold change > 2 or < −2.

4.13. Statistics and Reproducibility

Statistical data are presented as the mean ± standard deviation (SD) from at least three biologically independent samples using GraphPad Prism Software (San Diego, CA, USA, Version 8.0.2). Statistical differences between multiple comparisons were analyzed using one-way ANOVA followed by Dunnett's multiple comparison test as a post-hoc analysis. Differences were considered statistically significant for * $p < 0.05$, ** $p < 0.001$, *** $p < 0.0001$.

5. Conclusions

In this study, we provided evidence for a potential anti-leukemic effect of entospletinib in pre- and pro-B-ALL cell lines in vitro, independent of their pre-BCR status. Opposed to the expectation, the pro-B-ALL cell line SEM showed a good Ento response, such as anti-proliferative, metabolism and pro-apoptotic effects. We identified a diverse acting mode of Ento, independent of pre-BCR dependency, based on gene and protein modulation after Ento exposure. Here, the *TP53* variant in pro-B-ALL SEM and the BCL-6–BIM axis are probably Ento key targets and can explain the Ento sensitivity, therefor providing a rationale for Ento application also in a subset of pro-B-ALL.

Supplementary Materials: The following are available online at <https://www.mdpi.com/1422-0067/22/2/592/s1> and includes Supplementary File A (Tables), Supplementary File B (Figures) and Supplementary File C (methods).

Author Contributions: Conceptualization, S.S. and H.M.E.; investigation, S.S., A.S., S.V.P., O.C. and A.B.; methodology, S.S.; resources, A.N., C.J. and H.M.E.; supervision, A.N., C.J. and H.M.E.; validation, S.S.; visualization, S.S.; writing—original draft, S.S.; writing—review and editing, H.M.E. All authors have read and agreed to the published version of the manuscript.

Funding: This research received no external funding.

Data Availability Statement: Data is contained within the article or Supplementary Materials.

Acknowledgments: We would like to thank Michael Müller and Wendy Bergmann (Department of Core Facility for Cell Sorting and Cell Analysis, Rostock University Medical Center, Germany) for the possibility of Flow Cytometry device usage and technical support.

Conflicts of Interest: The authors declare no conflict of interest.

Abbreviations

4E-BP1	Eukaryotic Translation Initiation Factor 4E
AKT	Protein Kinase B
ALL	Acute lymphoblastic leukemia
AML	Acute myeloid leukemia
ATP	Adenosine triphosphate
Avg	Average
B-ALL	B-acute lymphoblastic leukemia
BCL-2	BCL2 Apoptosis Regulator
BCL-6	BCL6 Transcription Repressor
BCR	B-cell receptor
BCR-	B-cell receptor negative
BCR+	B-cell receptor positive

BIM	Bcl-2-like protein 11
BLNK	B Cell Linker
BTK	Bruton Tyrosine Kinase
CD22	B-Lymphocyte Cell Adhesion Molecule
CD79B	B-Cell Antigen Receptor Complex-Associated Protein Beta Chain
CDC25C	Cell Division Cycle 25C
CDK1	Cyclin Dependent Kinase 1
CLL	Chronic lymphocytic leukemia
DAPP1	Dual Adaptor Of Phosphotyrosine And 3-Phosphoinositides 1
DLBCL	Diffuse large B-cell lymphoma
DN	Dominant negative
Ento	Entospletinib
ERK	Extracellular signal-regulated kinases
FDA	Food and Drug Administration
FL	Follicular lymphoma
FOXO1	Forkhead Box O1
GoF	Gain-of-function
GS-9973	Entospletinib, SYK inhibitor
GSK3 β	Glycogen Synthase Kinase 3 Beta
IC50	Half maximal inhibitory concentration
Ig μ	Immunoglobulin heavy chains
IgG	Immunoglobulin G
IgM	Immunoglobulin M
Ig- α	Immunoglobulin (Ig) α cytoplasmic domain
Ig- β	Immunoglobulin (Ig) β cytoplasmic domain
IL7R	Interleukin 7 Receptor
ITAMs	Immunoreceptor tyrosine-based activation motifs
LAT2	Linker For Activation Of T Cells Family Member 2
LoF	Loss-of-function
MAP	Mitogen-activated protein
MCL	Mantle cell lymphoma
MEK	Mitogen-activated protein kinase kinase
MFI	Mean fluorescence intensity
MLL	Mixed lineage leukemia
p	Phospho
p53	Tumor Protein P53
p63	Tumor protein P63
p73	Tumor protein P73
PCA	Principle component analysis
PI3K	Phosphoinositide 3-kinase
PRT318	SYK Inhibitor
PTPN6	Protein Tyrosine Phosphatase Non-Receptor Type 6
R406	SYK Inhibitor
Raf	RAF proto-oncogene serine/threonine-protein kinase
RAS	Rat sarcoma
RPS6KB1	Ribosomal Protein S6 Kinase B1
S	Serine
Ser	Serine
SHP-1	Protein Tyrosine Phosphatase Non-Receptor Type 6
SPRY2	Sprouty RTK Signaling Antagonist 2
SYK	Spleen tyrosine kinase
TAC	Transcriptome Analysis Console
TCF3-PBX1	Fusion gene Transcription Factor 3 and PBX Homeobox 1
TNF	Tumor necrosis factor
TP53	Tumor Protein P53
Tyr	Tyrosin
VEGFA	Vascular Endothelial Growth Factor A
wt	Wild type
Y	Tyrosin

References

1. Kenkre, V.P.; Kahl, B.S. The Future of B-Cell Lymphoma Therapy: The B-Cell Receptor and its Downstream Pathways. *Curr. Hematol. Malig. Rep.* **2012**, *7*, 216–220. [[CrossRef](#)] [[PubMed](#)]
2. Mócsai, A.; Ruland, J.; Tybulewicz, V.L.J. The SYK tyrosine kinase: A crucial player in diverse biological functions. *Nat. Rev. Immunol.* **2010**, *10*, 387–402. [[CrossRef](#)] [[PubMed](#)]
3. Turner, M.; Mee, P.J.; Costello, P.S.; Williams, O.; Price, A.A.; Duddy, L.P.; Furlong, M.T.; Geahlen, R.L.; Tybulewicz, V.L. Perinatal lethality and blocked B-cell development in mice lacking the tyrosine kinase Syk. *Nature* **1995**, *378*, 298–302. [[CrossRef](#)] [[PubMed](#)]
4. Köhrer, S.; Havranek, O.; Seyfried, F.; Hurtz, C.; Coffey, G.P.; Kim, E.; Hacken, E.T.; Jäger, U.; Vanura, K.; O'Brien, S.; et al. Pre-BCR signaling in precursor B-cell acute lymphoblastic leukemia regulates PI3K/AKT, FOXO1 and MYC, and can be targeted by SYK inhibition. *Leukemia* **2016**, *30*, 1246–1254. [[CrossRef](#)] [[PubMed](#)]
5. Cornall, R.J.; Cheng, A.M.; Pawson, T.; Goodnow, C.C. Role of Syk in B-cell development and antigen-receptor signaling. *Proc. Natl. Acad. Sci. USA* **2000**, *97*, 1713–1718. [[CrossRef](#)]
6. Cheng, A.M.; Rowley, B.; Pao, W.; Hayday, A.; Bolen, J.B.; Pawson, T. Syk tyrosine kinase required for mouse viability and B-cell development. *Nature* **1995**, *378*, 303–306. [[CrossRef](#)]
7. Reth, M. Antigen receptor tail clue. *Nature* **1989**, *338*, 383–384. [[CrossRef](#)]
8. Kurosaki, T. Molecular dissection of B cell antigen receptor signaling (review). *Int. J. Mol. Med.* **1998**, *1*, 515–527. [[CrossRef](#)]
9. Toapanta, F.R.; Bernal, P.J.; Sztein, M.B. Diverse phosphorylation patterns of B cell receptor-associated signaling in naïve and memory human B cells revealed by phosphoflow, a powerful technique to study signaling at the single cell level. *Front. Cell. Infect. Microbiol.* **2012**, *2*, 128. [[CrossRef](#)]
10. Baba, Y.; Hashimoto, S.; Matsushita, M.; Watanabe, D.; Kishimoto, T.; Kurosaki, T.; Tsukada, S. BLNK mediates Syk-dependent Btk activation. *Proc. Natl. Acad. Sci. USA* **2001**, *98*, 2582–2586. [[CrossRef](#)]
11. Yasuda, T.; Sanjo, H.; Pagès, G.; Kawano, Y.; Karasuyama, H.; Pouyssegur, J.; Ogata, M.; Kurosaki, T. Erk Kinases Link Pre-B Cell Receptor Signaling to Transcriptional Events Required for Early B Cell Expansion. *Immunity* **2008**, *28*, 499–508. [[CrossRef](#)] [[PubMed](#)]
12. Herzog, S.; Hug, E.; Meixlsperger, S.; Paik, J.; DePinho, R.A.; Reth, M.; Jumaa, H. SLP-65 regulates immunoglobulin light chain gene recombination through the PI(3)K-PKB-Foxo pathway. *Nat. Immunol.* **2008**, *9*, 623–631. [[CrossRef](#)] [[PubMed](#)]
13. Buchner, M.; Fuchs, S.; Prinz, G.; Pfeifer, D.; Bartholomé, K.; Burger, M.; Chevalier, N.; Vallat, L.; Timmer, J.; Gribben, J.G.; et al. Spleen Tyrosine Kinase Is Overexpressed and Represents a Potential Therapeutic Target in Chronic Lymphocytic Leukemia. *Cancer Res.* **2009**, *69*, 5424–5432. [[CrossRef](#)] [[PubMed](#)]
14. Chen, L.; Monti, S.; Juszczynski, P.; Daley, J.; Chen, W.; Witzig, T.E.; Habermann, T.M.; Kutok, J.L.; Shipp, M.A. SYK-dependent tonic B-cell receptor signaling is a rational treatment target in diffuse large B-cell lymphoma. *Blood* **2008**, *111*, 2230–2237. [[CrossRef](#)] [[PubMed](#)]
15. Rinaldi, A.; Kwee, I.; Taborelli, M.; Largo, C.; Uccella, S.; Martin, V.; Poretti, G.; Gaidano, G.; Calabrese, G.; Martinelli, G.; et al. Genomic and expression profiling identifies the B-cell associated tyrosine kinase Syk as a possible therapeutic target in mantle cell lymphoma. *Br. J. Haematol.* **2006**, *132*, 303–316. [[CrossRef](#)]
16. Irish, J.M.; Czerwinski, D.K.; Nolan, G.P.; Levy, R. Altered B-cell receptor signaling kinetics distinguish human follicular lymphoma B cells from tumor-infiltrating nonmalignant B cells. *Blood* **2006**, *108*, 3135–3142. [[CrossRef](#)]
17. Gururajan, M.; Jennings, C.D.; Bondada, S. Cutting Edge: Constitutive B Cell Receptor Signaling Is Critical for Basal Growth of B Lymphoma. *J. Immunol.* **2006**, *176*, 5715–5719. [[CrossRef](#)]
18. Goodman, P.A.; Wood, C.M.; Vassilev, A.; Mao, C.; Uckun, F.M. Spleen tyrosine kinase (Syk) deficiency in childhood pro-B cell acute lymphoblastic leukemia. *Oncogene* **2001**, *20*, 3969–3978. [[CrossRef](#)]
19. Perova, T.; Grandal, I.; Nutter, L.M.J.; Papp, E.; Matei, I.R.; Beyene, J.; Kowalski, P.E.; Hitzler, J.K.; Minden, M.D.; Guidos, C.J. Therapeutic potential of spleen tyrosine kinase inhibition for treating high-risk precursor B cell acute lymphoblastic leukemia. *Sci. Transl. Med.* **2014**, *6*, 236ra62. [[CrossRef](#)]
20. Friedberg, J.W.; Sharman, J.; Sweetenham, J.; Johnston, P.B.; Vose, J.M.; Lacasce, A.; Schaefer-Cutillo, J.; de Vos, S.; Sinha, R.; Leonard, J.P.; et al. Inhibition of Syk with fostamatinib disodium has significant clinical activity in non-Hodgkin lymphoma and chronic lymphocytic leukemia. *Blood* **2010**, *115*, 2578–2585. [[CrossRef](#)]
21. Sharman, J.; Hawkins, M.; Kolibaba, K.; Boxer, M.; Klein, L.; Wu, M.; Hu, J.; Abella, S.; Yasenchak, C. An open-label phase 2 trial of entospletinib (GS-9973), a selective spleen tyrosine kinase inhibitor, in chronic lymphocytic leukemia. *Blood* **2015**, *125*, 2336–2343. [[CrossRef](#)] [[PubMed](#)]
22. Horwitz, S.M.; Feldman, T.A.; Hess, B.T.; Khodadoust, M.S.; Kim, Y.H.; Munoz, J.; Patel, M.R.; Phillips, T.J.; Smith, S.D.; Smith, S.M.; et al. A Phase 2 Study of the Dual SYK/JAK Inhibitor Cerdulatinib Demonstrates Good Tolerability and Clinical Response in Relapsed/Refractory Peripheral T-Cell Lymphoma and Cutaneous T-Cell Lymphoma. *Blood* **2019**, *134* (Suppl. 1), 466. [[CrossRef](#)]
23. Mullard, A. FDA approves first-in-class SYK inhibitor. *Nat. Rev. Drug Discov.* **2018**, *17*, 385. [[CrossRef](#)] [[PubMed](#)]
24. Currie, K.S.; Kropf, J.E.; Lee, T.; Blomgren, P.; Xu, J.; Zhao, Z.; Gallion, S.; Whitney, J.A.; Maclin, D.; Lansdon, E.B.; et al. Discovery of GS-9973, a Selective and Orally Efficacious Inhibitor of Spleen Tyrosine Kinase. *J. Med. Chem.* **2014**, *57*, 3856–3873. [[CrossRef](#)] [[PubMed](#)]

25. Burke, R.T.; Meadows, S.; Loriaux, M.M.; Currie, K.S.; Mitchell, S.A.; Maciejewski, P.; Clarke, A.S.; Dipaolo, J.A.; Druker, B.J.; Lannutti, B.J.; et al. A potential therapeutic strategy for chronic lymphocytic leukemia by combining idelalisib and GS-9973, a novel spleen tyrosine kinase (Syk) inhibitor. *Oncotarget* **2014**, *5*, 908–915. [CrossRef] [PubMed]
26. Grädler, U.; Schwarz, D.; Dresing, V.; Musil, D.; Bomke, J.; Frech, M.; Greiner, H.; Jäkel, S.; Rysiok, T.; Müller-Pompalla, D.; et al. Structural and Biophysical Characterization of the Syk Activation Switch. *J. Mol. Biol.* **2013**, *425*, 309–333. [CrossRef] [PubMed]
27. Geng, H.; Hurtz, C.; Lenz, K.B.; Chen, Z.; Baumjohann, D.; Thompson, S.; Goloviznina, N.A.; Chen, W.; Huan, J.; LaTocha, D.; et al. Self-enforcing feedback activation between BCL6 and pre-B cell receptor signaling defines a distinct subtype of acute lymphoblastic leukemia. *Cancer Cell* **2015**, *27*, 409–425. [CrossRef]
28. Paiva, C.; Rowland, T.A.; Sreekantham, B.; Godbersen, C.; Best, S.R.; Kaur, P.; Loriaux, M.M.; Spurgeon, S.E.F.; Danilova, O.V.; Danilov, A.V. SYK inhibition thwarts the BAFF-B-cell receptor crosstalk and thereby antagonizes Mcl-1 in chronic lymphocytic leukemia. *Haematologica* **2017**, *102*, 1890–1900. [CrossRef]
29. Herishanu, Y.; Pérez-Galán, P.; Liu, D.; Biancotto, A.; Pittaluga, S.; Vire, B.; Gibellini, F.; Njuguna, N.; Lee, E.; Stennett, L.; et al. The lymph node microenvironment promotes B-cell receptor signaling, NF- κ B activation, and tumor proliferation in chronic lymphocytic leukemia. *Blood* **2011**, *117*, 563–574. [CrossRef]
30. Ponader, S.; Chen, S.-S.; Buggy, J.J.; Balakrishnan, K.; Gandhi, V.; Wierda, W.G.; Keating, M.J.; O'Brien, S.; Chiorazzi, N.; Burger, J.A. The Bruton tyrosine kinase inhibitor PCI-32765 thwarts chronic lymphocytic leukemia cell survival and tissue homing in vitro and in vivo. *Blood* **2012**, *119*, 1182–1189. [CrossRef]
31. Cheng, S.; Coffey, G.P.; Zhang, X.H.; Shaknovich, R.; Song, Z.; Lu, P.; Pandey, A.; Melnick, A.M.; Sinha, U.; Wang, Y.L. SYK inhibition and response prediction in diffuse large B-cell lymphoma. *Blood* **2011**, *118*, 6342–6352. [CrossRef] [PubMed]
32. Uckun, F.M.; Ma, H.; Ozer, Z.; Goodman, P.; Zhang, J.; Qazi, S. A previously unknown unique challenge for inhibitors of SYK ATP-binding site: Role of SYK as a cell cycle checkpoint regulator. *EBioMedicine* **2014**, *1*, 16–28. [CrossRef] [PubMed]
33. Althubiti, M. Spleen Tyrosine Kinase Inhibition Modulates p53 Activity. *J. Cell Death* **2017**, *10*, 1179066017731564. [CrossRef] [PubMed]
34. Bauet, O.; Fenouille, N.; Abbe, P.; Robert, G.; Rocchi, S.; Gonthier, N.; Denoyelle, C.; Ticchioni, M.; Ortonne, J.; Ballotti, R.; et al. Spleen tyrosine kinase functions as a tumor suppressor in melanoma cells by inducing senescence-like growth arrest. *Cancer Res.* **2009**, *69*, 748–756.
35. Vousden, K.H.; Lane, D.P. p53 in health and disease. *Nat. Rev. Mol. Cell Biol.* **2007**, *8*, 275–283. [CrossRef]
36. Kandoth, C.; McLellan, M.D.; Vandin, F.; Ye, K.; Niu, B.; Lu, C.; Xie, M.; Zhang, Q.; McMichael, J.F.; Wyczalkowski, M.A.; et al. Mutational landscape and significance across 12 major cancer types. *Nature* **2013**, *502*, 333–339. [CrossRef]
37. Ang, H.C.; Joerger, A.C.; Mayer, S.; Fersht, A.R. Effects of Common Cancer Mutations on Stability and DNA Binding of Full-length p53 Compared with Isolated Core Domains. *J. Biol. Chem.* **2006**, *281*, 21934–21941. [CrossRef]
38. Silva, J.L.; Gallo, C.V.D.M.; Costa, D.C.; Rangel, L.P. Prion-like aggregation of mutant p53 in cancer. *Trends Biochem. Sci.* **2014**, *39*, 260–267. [CrossRef]
39. Xu, J.; Reumers, J.; Couceiro, J.R.; De Smet, F.; Gallardo, R.; Rudyak, S.; Cornelis, A.; Rozenski, J.; Zwolinska, A.; Marine, J.-C.; et al. Gain of function of mutant p53 by coaggregation with multiple tumor suppressors. *Nat. Chem. Biol.* **2011**, *7*, 285–295. [CrossRef]
40. Cancer Cell Line Encyclopedia (CCLE). Available online: <http://www.broadinstitute.org/ccle> (accessed on 12 July 2019).
41. Sasi, B.K.; Martines, C.; Xerxa, E.; Porro, F.; Kalkan, H.; Fazio, R.; Turkalj, S.; Bojnik, E.; Pyszynska, B.; Stachura, J.; et al. Inhibition of SYK or BTK augments venetoclax sensitivity in SHP1-negative/BCL-2-positive diffuse large B-cell lymphoma. *Leukemia* **2019**, *33*, 2416–2428. [CrossRef]
42. McCubrey, J.A.; Steelman, L.S.; Abrams, S.L.; Lee, J.T.; Chang, F.; Bertrand, F.E.; Navolanic, P.M.; Terrian, D.M.; Franklin, R.A.; D'Assoro, A.B.; et al. Roles of the RAF/MEK/ERK and PI3K/PTEN/AKT pathways in malignant transformation and drug resistance. *Adv. Enzym. Regul.* **2006**, *46*, 249–279. [CrossRef] [PubMed]
43. Cremer, A.; Ellegast, J.M.; Pikman, Y.; Alexe, G.; Ross, L.; Goodale, A.; Piccioni, F.; Frank, E.S.; Oellerich, T.; Stegmaier, K. Resistance Mechanisms to SYK Inhibition in AML. *Blood* **2018**, *132*, 2638. [CrossRef]
44. Cremer, A.; Ellegast, J.M.; Alexe, G.; Frank, E.S.; Ross, L.; Chu, S.H.; Pikman, Y.; Robichaud, A.; Goodale, A.; Haupl, B.; et al. Resistance Mechanisms to SYK Inhibition in Acute Myeloid Leukemia. *Cancer Discov.* **2019**, *10*, 214–231. [CrossRef] [PubMed]
45. Dustin, L.B.; Plas, D.R.; Wong, J.; Hu, Y.T.; Soto, C.; Chan, A.C.; Thomas, M.L. Expression of dominant-negative src-homology domain 2-containing protein tyrosine phosphatase-1 results in increased Syk tyrosine kinase activity and B cell activation. *J. Immunol.* **1999**, *162*, 2717–2724. [PubMed]
46. Müschen, M. Autoimmunity checkpoints as therapeutic targets in B cell malignancies. *Nat. Rev. Cancer* **2018**, *132*, 1587. [CrossRef] [PubMed]
47. Neel, B.G. Role of phosphatases in lymphocyte activation. *Curr. Opin. Immunol.* **1997**, *9*, 405–420. [CrossRef]
48. Alsadeq, A.; Hobeika, E.; Medgyesi, D.; Kläsener, K.; Reth, M. The Role of the Syk/Shp-1 Kinase-Phosphatase Equilibrium in B Cell Development and Signaling. *J. Immunol.* **2014**, *193*, 268–276. [CrossRef]
49. Hurtz, C.; Chan, L.N.; Geng, H.; Ballabio, E.; Xiao, G.; Deb, G.; Khoury, H.; Chen, C.-W.; Armstrong, S.A.; Chen, J.; et al. Rationale for targeting BCL6 in MLL-rearranged acute lymphoblastic leukemia. *Genes Dev.* **2019**, *33*, 1265–1279. [CrossRef]
50. Sakakibara-Konishi, J.; Oizumi, S.; Kikuchi, J.; Kikuchi, E.; Mizugaki, H.; Kinoshita, I.; Dosaka-Akita, H.; Nishimura, M. Expression of Bim, Noxa, and Puma in non-small cell lung cancer. *BMC Cancer* **2012**, *12*, 286. [CrossRef]

51. Faber, A.C.; Corcoran, R.B.; Ebi, H.; Sequist, L.V.; Waltman, B.A.; Chung, E.; Incio, J.; Digumarthy, S.R.; Pollack, S.F.; Song, Y.; et al. BIM Expression in Treatment-Naïve Cancers Predicts Responsiveness to Kinase Inhibitors. *Cancer Discov.* **2011**, *1*, 352–365. [[CrossRef](#)]
52. Toscan, C.E.; Jing, D.; Mayoh, C.; Lock, R.B. Reversal of glucocorticoid resistance in paediatric acute lymphoblastic leukaemia is dependent on restoring BIM expression. *Br. J. Cancer* **2020**, *122*, 1769–1781. [[CrossRef](#)] [[PubMed](#)]
53. Schindelin, J.; Arganda-Carreras, I.; Frise, E.; Kaynig, V.; Longair, M.; Pietzsch, T.; Preibisch, S.; Rueden, C.; Saalfeld, S.; Schmid, B.; et al. Fiji: An open-source platform for biological-image analysis. *Nat. Methods* **2012**, *9*, 676–682. [[CrossRef](#)] [[PubMed](#)]
54. Schneider, C.A.; Rasband, W.S.; Eliceiri, K.W. NIH Image to ImageJ: 25 years of image analysis. *Nat. Methods* **2012**, *9*, 671–675. [[CrossRef](#)] [[PubMed](#)]

12.2 Arbeit II

Evaluation of the synergistic potential of simultaneous pan- or isoform specific BET and SYK inhibition in B-cell lymphoma: an *in vitro* approach

Sender S., Sultan A H., Palmer D., Koczan D., Sekora A., Beck J., Schuetz E., Brenig B., Fuellen G., Junghanss C., Murua Escobar H.

Cancers. Manuskript ID: cancers-1798753; Manuskript eingereicht am 17.06.2022, 2. Revisionsrunde *under review* seit 14.09.2022
Impact Factor 2021/22: 6.639

Article

Evaluation of the synergistic potential of simultaneous pan- or isoform specific BET and SYK inhibition in B-cell lymphoma: an *in vitro* approach

Sina Sender ¹, Ahmad Wael Sultan ¹, Daniel Palmer ², Dirk Koczan ³, Anett Sekora ¹, Julia Beck ⁴, Ekkehard Schuetz ⁴, Leila Taher ⁵, Bertram Brenig ⁶, Georg Fuellen ², Christian Junghanss ¹ and Hugo Murua Escobar ^{2,*}

¹ Hematology, Oncology, Palliative Medicine, Department of Medicine, Clinic III, Rostock University Medical Center, 18057 Rostock, Germany; sina.sender@med.uni-rostock.de; wael.sultan@web.de; anett.sekora@med.uni-rostock.de; Christian.junghanss@med.uni-rostock.de

² Rostock University Medical Center, Institute for Biostatistics and Informatics in Medicine and Ageing Research, 18057 Rostock, Germany; daniel.palmer@uni-rostock.de; Georg.Fuellen@med.uni-rostock.de

³ Institute for Immunology, Core Facility Genomics, Rostock University Medical Center, 18057 Rostock, Germany; dirk.koczan@med.uni-rostock.de

⁴ Chronix Biomedical GmbH, 37079 Goettingen, Germany; jbeck@chronixbiomedical.de; esc@chronixbiomedical.de

⁵ Institute of Biomedical Informatics, Graz University of Technology, Stremayrgasse 16/I, 8010, Graz, Austria; leila.taher@tugraz.at

⁶ Institute of Veterinary Medicine, University of Goettingen, 37077 Goettingen, Germany; bbrenig@gwdg.de

* Correspondence: hugo.murua.escobar@med.uni-rostock.de; Tel: +49381494-7639, Fax: +49494-7422

Simple Summary: B-cell lymphomas represent the majority of non-Hodgkin lymphomas and are the most common lymphoid malignancies in the western world. Genetic alterations or epigenetic modulations can lead to tumor initiation and tumor progression. Aside from standard care, targeted, individualized therapies can be highly effective. Here, we evaluated the impact of simultaneous specific inhibition of two key regulators involved in B lymphoid tumor progression. Spleen tyrosine kinase (SYK) is a B-cell receptor associated kinase acting as a proto-oncogene in B-cell malignancies, while Bromodomain and extra-terminal domain (BET) proteins are epigenetic reader proteins involved in histone recognition and transcription regulation. The simultaneous inhibition of SYK and BET showed enhanced anti-proliferative effects, as well as inducing a distinct combination-specific gene expression profile, suggesting SYK and BET inhibition as a promising combination in the treatment of B-cell lymphoma.

Abstract:

Background: Both bromodomain and extra-terminal domain (BET) proteins and spleen tyrosine kinase (SYK) represent promising targets in Diffuse large B-cell (DLBCL) and Burkitt's lymphoma (BL). We evaluated the anti-lymphoma activity of the isoform specific bivalent BET inhibitor AZD5153 (AZD) and the pan-BET inhibitor I-BET151 (I-BET) as single agents and in combination with SYK inhibitor Entospletinib (Ento) *in vitro*.

Methods: The effect of the single agents on cell proliferation and metabolic activity was evaluated in two DLBCL and two BL cell lines. Proliferation, metabolic activity, apoptosis, cell cycle and morphology were further investigated after a combined treatment of AZD or I-BET and Ento. RNAseq profiling of combined AZD+Ento treatment was performed in SU-DHL-4 cells.

Citation: Lastname, F.; Lastname, F.; Lastname, F. Title. *Cancers* **2022**, *14*, x. <https://doi.org/10.3390/xxxxx>

Academic Editor: Firstname Lastname

Received: date

Accepted: date

Published: date

Publisher's Note: MDPI stays neutral with regard to jurisdictional claims in published maps and institutional affiliations.



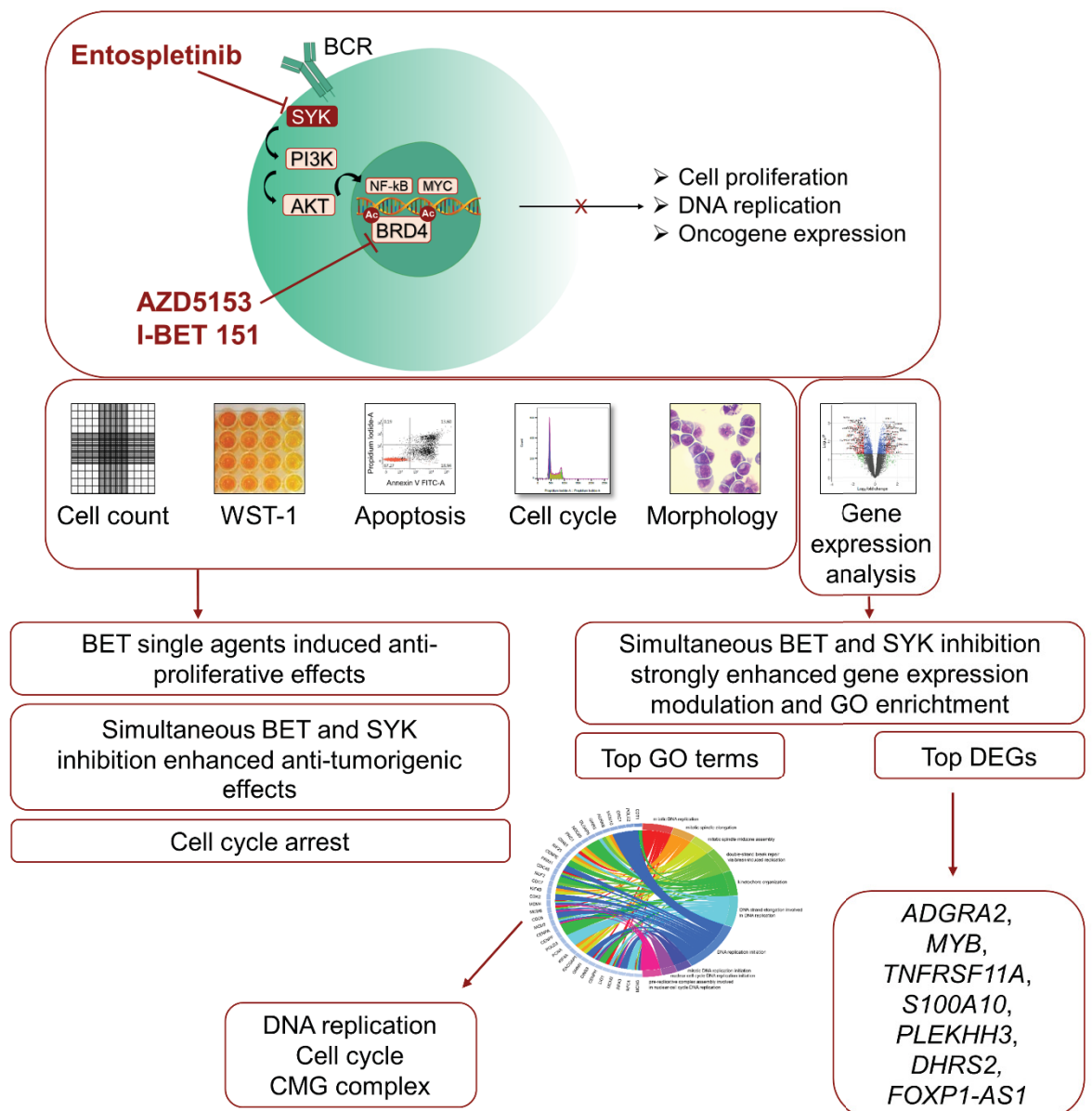
Copyright: © 2022 by the authors. Submitted for possible open access publication under the terms and conditions of the Creative Commons Attribution (CC BY) license (<https://creativecommons.org/licenses/by/4.0/>).

Results: Both BET inhibitors reduced cell proliferation and metabolic activity in a dose and time dependent manner. Combined BET and SYK inhibition enhanced the anti-proliferative effect and induced a G0/G1 cell cycle arrest. SU-DHL-4 demonstrated a pronounced modulation of gene expression by AZD, which was markedly increased by additional SYK inhibition. Functional enrichment analyses identified combination-specific GO terms related to DNA replication and cell division. Genes such as *ADGRA2*, *MYB*, *TNFRSF11A*, *S100A10*, *PLEKHH3*, *DHRS2* and *FOXP1-AS1* were identified as possible key regulators.

Conclusion: Simultaneous inhibition of BET and SYK enhanced the anti-proliferative effects, and induced a combination-specific gene expression signature.

Keywords: BET, I-BET151, AZD5153, Entospletinib, SYK, gene expression, drug combination, lymphoma, DLBCL, BL

Graphical abstract:



1. Introduction

Targeted therapies by small molecule inhibitors and their combinations have been shown to efficiently affect tumor growth and survival in hematological neoplasias. B-cell receptor associated kinases (BAKs) like spleen tyrosine kinase (SYK), as well as the Bromodomain (BRD)-containing proteins such as the bromodomain and extra-terminal domain (BET) proteins play a critical role in signaling pathway transduction. The specific inhibition of BET and SYK represents a promising tool in hematological neoplasias.

BET co-activators represent a group of epigenetic readers involved in histone recognition and transcription regulation [1], [2]. BET proteins consist of a hydrophobic pocket within an acetylated lysine binding site (Ac-K), which can be competitively blocked by BET inhibitors thus preventing their binding to Ac-K chromatin [2]–[4]. Induction of BET inhibitors has been shown to trigger a depletion of BRD4 from promoters and enhancers in DLBCL [5]. Decreased BRD4 has consequently been shown to suppress a number of oncogenes such as c-MYC, BCL-6 and BCL-2 in DLBCL and other hematological malignancies, suggesting BET inhibition may be a valid therapeutic option to consider [5]–[9].

Early BET inhibitors JQ1 and I-BET762 (GSK525762A) were designed to target the BRD4-NUT (nuclear protein in testis) fusion protein in aggressive NUT midline carcinoma. The specific binding of these inhibitors to BRD4, induces the displacement of BRD4 fusion from chromatin and leads to tumor regression *in vivo* [10], [11]. Following this, the targeting of wild-type BRD4 in hematological malignancies has likewise been shown to result in anti-tumor activity due to proto-oncogene down-regulation [6]–[9], [12].

Based on the promising results of targeting BET proteins in hematological and solid tumors, several BET inhibitors have been developed and are under clinical investigation, although currently without FDA approval (reviewed in [13], [14]).

Most prominent BET inhibitors are pan-BET inhibitors, with specificity to more than one representative BET family protein. Representative pan-BET inhibitors are I-BET151 (GSK1210151A) [6], ABBV-075 [15], I-BET-762 (GSK525762) [11] and OTX015 (MK 8628) [16]. The isoform-specific inhibitors in particular, such as the monovalent inhibitors JQ1 [10] and CPI-0610 [17] or the bivalent inhibitors such as AZD5153 or ABBV-744 [18], [19], demonstrate specific BET inhibition. To further improve the anti-tumor potential of BET inhibitors, various combinations with immune modulators [20], epigenetic drugs [12], [21], DNA damage repair inhibitors [22] or antibodies [23] are under pre-clinical and clinical investigation and have revealed pre-clinical efficacy in lymphoma. In particular, targeting the B-cell receptor (BCR) signaling cascade enables a promising approach for B-cell neoplasias due to their dependency on BCR survival signals [24]. Various small molecules engaging BCR or its downstream signaling, such as BTK [12], [23], [25], [26], CDK [25], PI3K [23], [27], BCL-2 [28] or SYK inhibitors [26], have shown synergistic activity with BET inhibition in lymphomas. Thus, combinations with BCR associated kinases (BAKs) offer high potential for synergistic efficacy. The combination of BET inhibitors with the specific spleen tyrosine kinase (SYK) inhibitor Entospletinib (Ento) appears promising, as SYK is a direct downstream kinase of the BCR and responsible for several cellular processes such as proliferation, differentiation, cytoskeletal remodeling, cytokine release and survival [29].

Here, we aimed to compare the anti-tumorigenic effect of a simultaneous SYK inhibition by Entospletinib with pan-BET inhibition by I-BET151 (I-BET) or isoform specific bivalent BET inhibition by AZD5153 (AZD) in a DLBCL and Burkitt's lymphoma *in vitro* approach. We investigated the synergistic potential of additional specific SYK inhibition and the resulting specific gene expression modulation patterns in both B-lymphoma subtypes. Inhibitor-based transcriptome modulation was evaluated by RNA sequencing and supported by microarray analyses.

We uncovered additional anti-tumorigenic effects in B-lymphoma cell lines induced by simultaneous SYK and BET inhibition, which was investigated by analyzing proliferation,

metabolic activity, apoptosis and cell cycle analyses. Cellular processes such as DNA replication and cell cycle were identified as key modulating pathways by high-throughput RNA sequencing.

2. Materials and Methods

2.1. Human cell lines, reagents and inhibitor exposure

Human Burkitt's lymphoma (BL) cell lines DG-75 and RAJI and Diffuse large B-cell lymphoma (DLBCL) cell lines SU-DHL-4 (GCB) and U-2946 (ABC) were purchased from the German Collection of Microorganisms and Cell Cultures (DSMZ, Braunschweig, Germany), cultured as recommended by the manufacturer in RPMI 1640 media (Biochrom, Berlin, Germany) supplemented with 10 % heat-inactivated FCS (Biochrom, Berlin, Germany) and 100 µg/ml penicillin and streptomycin (Biochrom, Berlin, Germany). Cultured cells were regularly tested for mycoplasma contamination and authenticity (cell surface markers by flow cytometry).

AZD5153 (AZD), I-BET 151 (GSK1210151A) (I-BET) and Entospletinib (GS-9973) (Ento) were obtained from Selleck Chemicals (Absource Diagnostics GmbH, Munich, Germany) and prepared according to the manufacturer's instructions to a 10 mM Stock and stored at -80 °C until ready for use.

Cell lines (3.33×10^5 cells / ml) were exposed to AZD, I-BET, Ento or DMSO (control) as mono substance (0.001 µM – 10 µM) or in combination for up to 72 h (0.01 µM AZD, 0.1 µM I-BET, 1 µM Ento)

2.2. Cell Proliferation and WST-1 Proliferation Assay

Exposed cells were harvested and washed with PBS (Biochrom, Berlin, Germany). Viable cells were determined by trypan blue staining and cell count with a hemocytometer (Sigma-Aldrich Chemie GmbH, Steinheim, Germany). Metabolic activity was determined via tetrazolium compound WST-1 (TaKaRa Bio Inc., Kusatsu, Japan) according to the manufacturer's protocol and previously described in [30].

2.3. Apoptosis assay

Early and late apoptosis was analyzed by Annexin V FITC (BD Biosciences, Heidelberg, Germany) and Propidium Iodide (PI) (Sigma Aldrich, St. Louis, USA) staining according to the manufacturer's protocol and previously described in [30]. Measurements were performed using FACS Verse™ (BD Biosciences, Heidelberg, Germany) and BD FACSSuite Software (BD Biosciences, Heidelberg, Germany, Version 4.0.2).

2.4. Cell Cycle Analysis

Protocol was previously described in [30]. Briefly, cells were fixed with 70 % ice cold Ethanol and frozen at -20 °C (≥ 24 h). Fixed cells were twice washed with PBS and then RNase treated in 500 µl Ribonuclease A (1 mg/ ml) (Carl Roth, Karlsruhe, Germany) for 45 min at 37 °C. Cells were washed, cell pellet resuspended in 400 µl PI Solution (50 µg/ml) (Sigma Aldrich Chemie GmbH, Steinheim, Germany) and analyzed by Flow Cytometry (FACS Verse™, BD Biosciences, Heidelberg, Germany). Cell cycle distribution was examined by FlowJo Software (Beckton Dickinson, Franklin Lakes, NJ, USA).

2.5. May-Gruenwald Giemsa staining

Coated cytoslides (Tharmac, Waldsolms, Germany) were prepared with 5×10^4 cells per slide (700 rpm, 10 min) in a Cytospin 3 centrifuge (Shandon, Frankfurt/Main, Germany). Slides were stained for 6 min with May-Gruenwald working solution (Merck, Darmstadt, Germany), rinsed with microscopy buffer according to WEISE (pH7.2) (Merck, Darmstadt, Germany), stained 20 min in Giemsa working solution (Merck, Darmstadt, Germany) and rinsed thoroughly with microscopy buffer again. The slides were air

dried at room temperature before analysis. Morphological changes were analyzed by EVOS® XL Core Imaging System (AMG, Washington, USA).

2.6. RNA Extraction & Isolation

Cell pellets were resuspended in QIAzol Lysis Reagent (QIAGEN, Venlo, Netherlands) and RNA Isolation was performed with miRNeasy Mini Kit (QIAGEN, Venlo, Netherlands) according to the manufacturer's instructions and previously described in [30].

2.7. RNA sequencing and Microarray analyses

Poly-A RNA was enriched from 1 µg total RNA using the NEBNext Poly (A) mRNA Magnetic Isolation Module (New England Bioabs, Ipswich, USA) and sequencing libraries were prepared using the NEBNext Ultra II RNA Library Prep Kit (New England Bioabs, Ipswich, USA). Sequencing was conducted on an Illumina NextSeq500 (Illumina, San Diego, USA) as single reads with 75 bp length with a total of 480 million reads.

Gene expression analyses were also performed by microarray, using the Human Clariom D Array (Thermo Fisher Scientific, Waltham, USA) according to manufacturer's instructions and previously described in [31]. In brief, RNA quality was assessed on a Bioanalyzer 2100 (Agilent, Santa Clara, CA, USA) and RIN ≥ 9.4 considered as applicable. 200 ng total RNA was used for synthesis of first-strand cDNA, followed by second-strand and cRNA- synthesis. A magnetic bead-based method was used for cRNA purification. Further, an amount of 15 µg cRNA was applied for 2nd -cycle sense strand single-stranded cDNA synthesis, followed by RNase H hydrolyzation, magnetic bead-based purification and quantification. Subsequently, 5.5 µg ss cDNA were fragmented, fragmentation was assessed with a Bioanalyzer 2100 (Agilent, Santa Clara, CA, USA) and end labeling by Biotin attachment was performed. Hybridization was then performed in a GeneChip Hybridization Oven 645 (Affymetrix, Santa Clara, CA, USA) at 45°C overnight and washed and stained in an Affymetrix Fluidics station 450 (Affymetrix, Santa Clara, CA, USA). Microarrays were scanned in the GeneChip Scanner 3000 7G (Affymetrix, Santa Clara, CA, USA) at 0.7 micron resolution.

2.8. RNA sequencing and Microarray analysis pipeline

Microarray data were RMA normalized using *limma* and probes were mapped to genes using *affycoretools* with probe mappings drawn from *clariomhumantranscriptcluster.db*. and a linear model was fitted of the form:

$$Y_{ij} = \beta_{0j}Treatment_i + \beta_{1j}Line_i + \beta_{2j}Batch_i + \epsilon_{ij}$$

Where Y_{ij} is the intensity for gene j in sample i , $Treatment_i$ is the treatment which sample i was subjected to, $Line_i$ is the cell line from which sample i was drawn, $Batch_i$ is the batch which sample i belongs to and ϵ_{ij} is the error term, with the coefficients β_0 , β_1 and β_2 estimated by least squares. All contrasts were tested using the eBayes method of *limma* to perform a moderated t-test for each gene and the results were corrected for multiplicity using the Benjamini-Hochberg correction.

The RNAseq data were processed as follows. The raw reads from different lanes were concatenated and then trimming and quality control were performed using CutAdapt via TrimGalore! [32]. Trimmed reads were aligned to the human genome (GRCh38.p13) and feature counts were performed using *Rsubread* [33]. *edgeR* was used to filter low read counts using the *filterByExpr()* function, normalized using the TMM method, and a differential expression analysis was performed using the GLM method to fit a generalized linear model, specifying no intercept and with treatment group and batch as covariates. All

contrasts were tested using the *glmQLFTest()* function of *edgeR*, which performs an empirical Bayes quasi-likelihood F-test for each gene [34], and the results were corrected for multiplicity using the Benjamini-Hochberg correction. For both the microarray and RNAseq data, a gene was deemed significantly differentially expressed if it had an adjusted p-value of < 0.05 and a fold-change > 2 .

Principal Component Analysis (PCA) of the microarray data (using the normalized expression values) and the RNAseq data (using logCPM values, calculated setting a prior count of 3) was performed to identify trends in the data. For the PCA plots, the cell batch effect was controlled by first using the *removeBatchEffect()* function of *limma*.

Gene Ontology (GO) enrichment analysis of biological process terms was performed using *Enrichr* [35] with a Benjamini-Hochberg adjusted p-value of < 0.05 being taken as significant. When considering the importance of GO terms, terms were ranked by *Enrichr*'s combined score. This is calculated by multiplying the log of the p-value for a given term by the z-score of the deviation of that term from its expected rank, given the size of the gene set. In this way the combined score aims to better account for biases introduced into enrichment analysis by variation in gene set size.

2.10. Platform comparison

To compare the two platforms, the overlaps between all like gene lists were obtained and can be seen in Supplementary table S3.

2.11. Statistics, reproducibility and Bliss calculation

Statistical data are presented as mean \pm standard deviation (SD) from at least three biologically independent samples. Statistical differences between multiple comparisons were analyzed using one-way ANOVA followed by Tukey's test as post-hoc analysis for normally-distributed data. The Kruskal-Wallis test was applied to non-parametric data. Differences were considered statistically significant for * $p < 0.05$, ** $p < 0.01$, *** $p < 0.001$. Synergy was evaluated by a mathematical Bliss independence model [36]. Bliss synergy is defined as $EA+EB - EA EB$. The difference (Δ) of observed and expected values indicates additive, synergistic or antagonistic effects. $\Delta=0$, $\Delta>0$ and $\Delta<0$ specifies an additive-, synergistic- and antagonistic interaction, respectively.

3. Results

3.1. Both the isoform specific bivalent- and the pan-BET inhibitor affect proliferation and metabolic activity at low dosage in DLBCL and BL cell lines

Burkitt's lymphoma (BL) cell lines DG-75 and RAJI and Diffuse large B-cell lymphoma (DLBCL) cell lines SU-DHL-4 and U-2946 were exposed to dose ranges of isoform specific bivalent BET inhibitor AZD5153 (AZD) or pan-BET inhibitor I-BET 151 (I-BET) (0.001-10 μ M) for 24 h, 48 h and 72 h (*Figure 1*). Both inhibitors were able to induce a dose- and time-dependent anti-proliferative effect in all tested cell lines with slightly lower IC50 values for AZD (supplementary figure S1). The cell proliferation was most affected after 72 h substance incubation, while metabolic activity showed strongest reduction after 48 h or 72 h. The respective IC50 values for all tested B-lymphoma cell lines were calculated based on 72 h proliferation and are shown in supplementary figure S1.

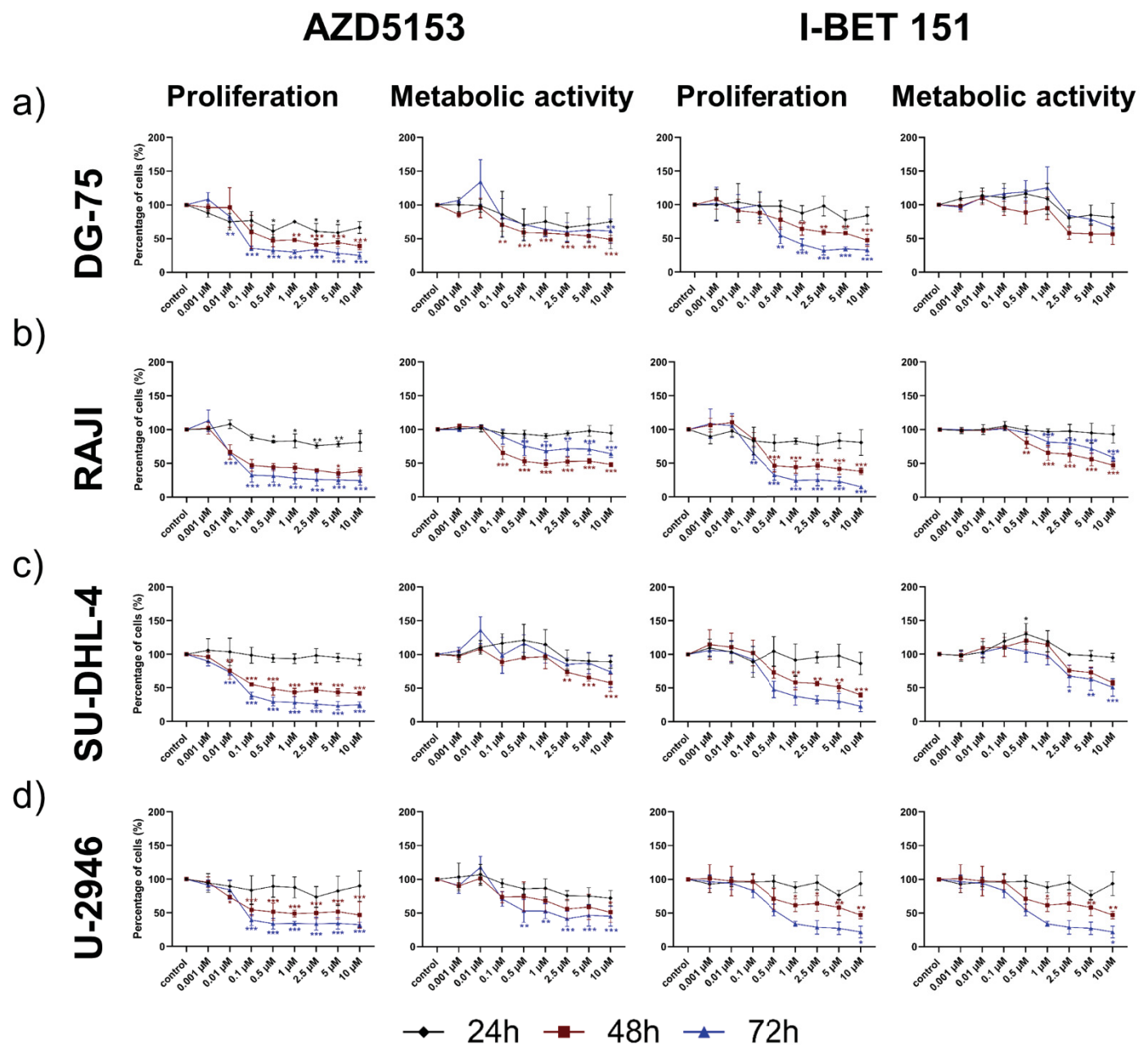


Figure 1: Evaluation of cell viability after isoform-specific- and pan-BET inhibition in Burkitt's lymphoma und Diffuse large B-cell lymphoma cell lines

Burkitt's lymphoma (BL) cell lines **a) DG-75** and **b) RAJI** and Diffuse large B-cell lymphoma (DLBCL) cell lines **c) SU-DHL-4** and **d) U-2946** were exposed to serial-diluted isoform specific inhibitor AZD5153 or pan-BET inhibitor I-BET151 (0.001 μ M – 10 μ M). Cell proliferation was determined by trypan blue staining and metabolic activity by WST-1 assay 24 h, 48 h and 72 h after exposure. Data is presented as the mean \pm SD. Statistical significance was calculated by One-way ANOVA followed by Dunnett's multiple comparison test as post hoc analysis. The Kruskal-Wallis test was applied to non-parametric data. Statistical significance is displayed as * $p < 0.033$, ** $p < 0.002$, *** $p < 0.001$ versus control group ($n \geq 3$).

3.2. Entospletinib reduced cell viability of the DLBCL cell line SU-DHL-4 selectively

The DLBCL cell line SU-DHL-4 showed a significant decrease in cell proliferation after 48h ($p < 0.05$) and 72 h ($p < 0.01$) Entospletinib (Ento) exposure. Metabolic activity

255
256
257
258
259
260
261
262
263
264
265

266
267
268

was significantly reduced within 48 h but not after 72 h of substance application (Supplementary figure S2c). IC₅₀ was calculated based on proliferation with 2.67 μ M Ento treatment (supplementary figure S2e).

In contrast, Ento was not able to reduce cell proliferation and metabolic activity significantly in DG-75, RAJI and U-2946 at the used concentration regimes (Supplementary Figure S2a,b,d respectively). Accordingly, IC₅₀ values were not reached under the tested conditions for these cell lines.

3.3. Simultaneous BET and SYK inhibition revealed a moderate synergistic effect compared to single agent response

Cell viability of combined exposure to Ento and isoform specific BET inhibitor AZD or pan BET inhibitor I-BET was carried out after 72 h of incubation with the given substances. The same single agent concentrations were used for the combined exposure for all cell lines for direct comparison (Ento: 1 μ M, AZD: 0.01 μ M and I-BET: 0.1 μ M).

Both combinations (Ento+AZD; Ento+I-BET) induced a significant reduction of cell proliferation after 72 h exposure compared to the DMSO control in DG-75, SU-DHL-4 and U-2946 (Figure 2a,b). Cell proliferation of RAJI was slightly more affected by the combinations, but without a significant decrease compared to the single agents.

However, compared to Ento single agent, the combinations induced an additional anti-proliferative effect in DG-75, RAJI and U-2946. Further, in SU-DHL-4 the combination induced a significant reduction of proliferation and metabolic activity compared to both BET inhibitors as single agents.

Furthermore, both combinations reduced metabolic activity significantly in the DLBCL cell line SU-DHL-4 compared to the DMSO control and AZD or I-BET single agents, respectively (Figure 2b). However, metabolic activity of DG-75, RAJI and U-2946 was not additionally affected by the combined exposures (Figure 2a,b).

The synergistic potential of BET and SYK inhibition in BL and DLBCL cell lines was evaluated by a Bliss independence model (Figure 2c based on 72 h proliferation). Both combinations (AZD+Ento and I-BET+Ento) revealed positive Bliss values for the BL cell lines DG-75 and RAJI as well as the DLBCL cell line U-2946 indicating a slight synergistic effect. For SU-DHL-4 an additive effect was observed for AZD+Ento with a Bliss value of 0.002. The I-BET+Ento combination showed a minor antagonistic effect with a Bliss value of -0.03. Bliss calculation based on cell cycle distribution are represented in the supplementary figure S6.

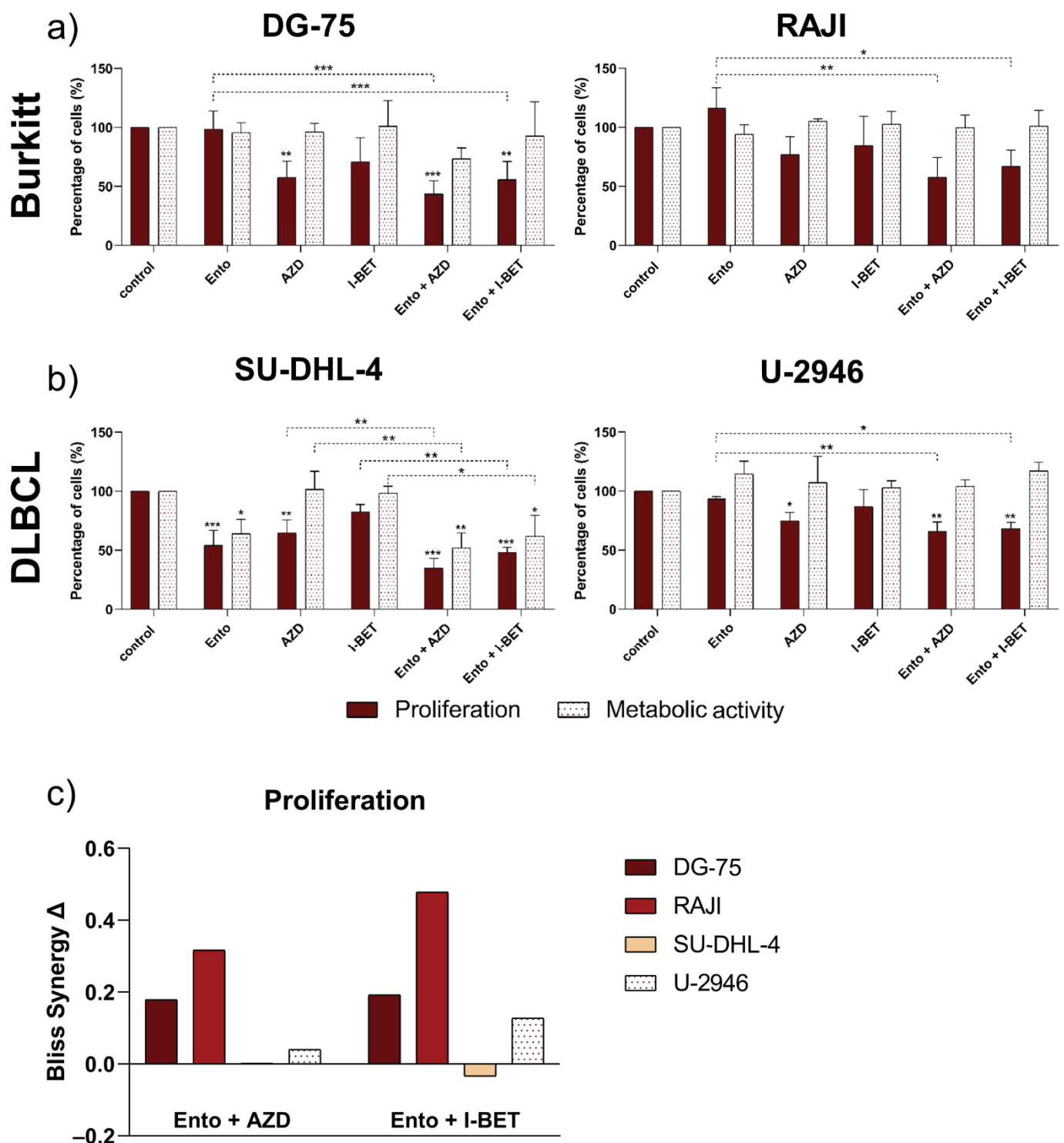


Figure 2: Simultaneous BET and SYK inhibition affected cell viability of BL and DLBCL cell lines synergistically

Cells were exposed to 1 μ M Ento, 0.01 μ M AZD or 0.1 μ M I-BET as single agent or in combination. Cell proliferation and metabolic activity were assessed in a) BL cell lines (DG-75 and RAJI) and b) DLBCL cell lines (SU-DHL-4 and U-2946) after 72 h. c) Bliss calculations were based on proliferation. Synergistic effects of both combinations were calculated with a Bliss Independence model (EA+EB-EAEB). A value $\Delta = 0, >0$ and <0 defines an additive-, synergistic- or antagonistic interaction, respectively. Data is presented as the mean \pm SD. Statistical significance of cell viability data was calculated by One-way ANOVA followed by Tukey's multiple comparison test as a post hoc

304
305
306
307
308
309
310
311
312
313

analysis and displayed as * $p < 0.033$, ** $p < 0.002$, *** $p < 0.001$ versus control group and further versus the respective single agents (dashed line) ($n \geq 3$).

3.4. Simultaneous BET and SYK inhibition modulates cell morphology moderately

Cell morphology of the BL cell line DG-75 and the DLBCL cell line SU-DHL-4 was investigated by May-Gruenwald Giemsa (Pappenheim) staining at 72 h (Figure 3a,b). The enlarged figures can be found in the supplements (supplementary figure S3 and S4). In DG-75 AZD and I-BET single agent exposure provides marginal indications for apoptosis and stress induction such as nuclear vacuolization, chromatin condensation and cellular fragmentation. Ento, in contrast, particularly induced membrane blebs. The combined exposure only moderately intensified morphological changes. Likewise, the SU-DHL-4 cell line provided evidence for slight apoptosis and stress induction after treatment, with particular changes of nuclear vacuolization and cellular fragmentation.

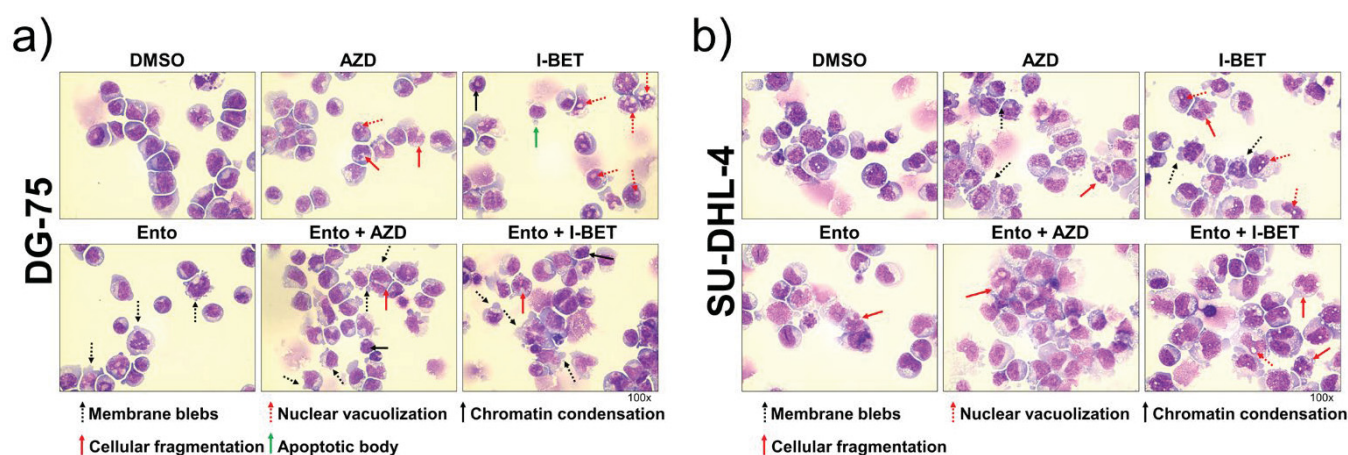


Figure 3: Morphological characterization after BET and SYK inhibition

Cells were exposed to 1 μM Ento, 0.01 μM AZD or 0.1 μM I-BET as single agent or in combination. Representative light microscopy images of exposed cells after 72 h incubation. Cytospins were stained with May-Gruenwald Giemsa stain (Pappenheim method). Light microscopy images (x100) revealed only moderate morphological changes in a) BL cell line DG-75 and b) DLBCL cell line SU-DHL-4.

3.5. Simultaneous BET and SYK inhibition induced cell cycle blockade in DLBCL and BL cell lines, but not apoptosis

Moreover, we investigated if simultaneous inhibition of BET and SYK is able to boost the effect on cell cycle blockade after 72 h exposure, compared to the single agents. AZD as a mono application significantly increased the percentage of cells in G0/G1 phase in the BL cell line DG-75 and the DLBCL cell line SU-DHL-4. The AZD+Ento combination enhanced this effect selectively in U-2946 leading to a G0/G1 cell cycle blockade compared to control.

Application of I-BET as a single agent did not induce cell cycle changes, while the I-BET+Ento combination significantly intensified the G0/G1 blockade compared to control as well as to the single agents in DG-75, SU-DHL-4.

However, the cell cycle of BL cell line RAJI was not significantly affected (Figure 4a). Representative figures of cell cycle distribution are shown in supplementary figure S5a. The sub-G1 cell population only increased significantly in SU-DHL-4 after Ento+AZD exposure and in AZD treated RAJI cells (supplement figure S5b).

To evaluate if Ento, AZD, I-BET as single agent or in combination induce apoptosis in BL or DLBCL cell lines after 72 h exposure, Annexin V/PI double staining was performed and

analyzed by flow cytometry. During the tested conditions, no significant apoptosis induction could be observed for any tested lymphoma cell lines after 72 h (Figure 4c).

351
352
353

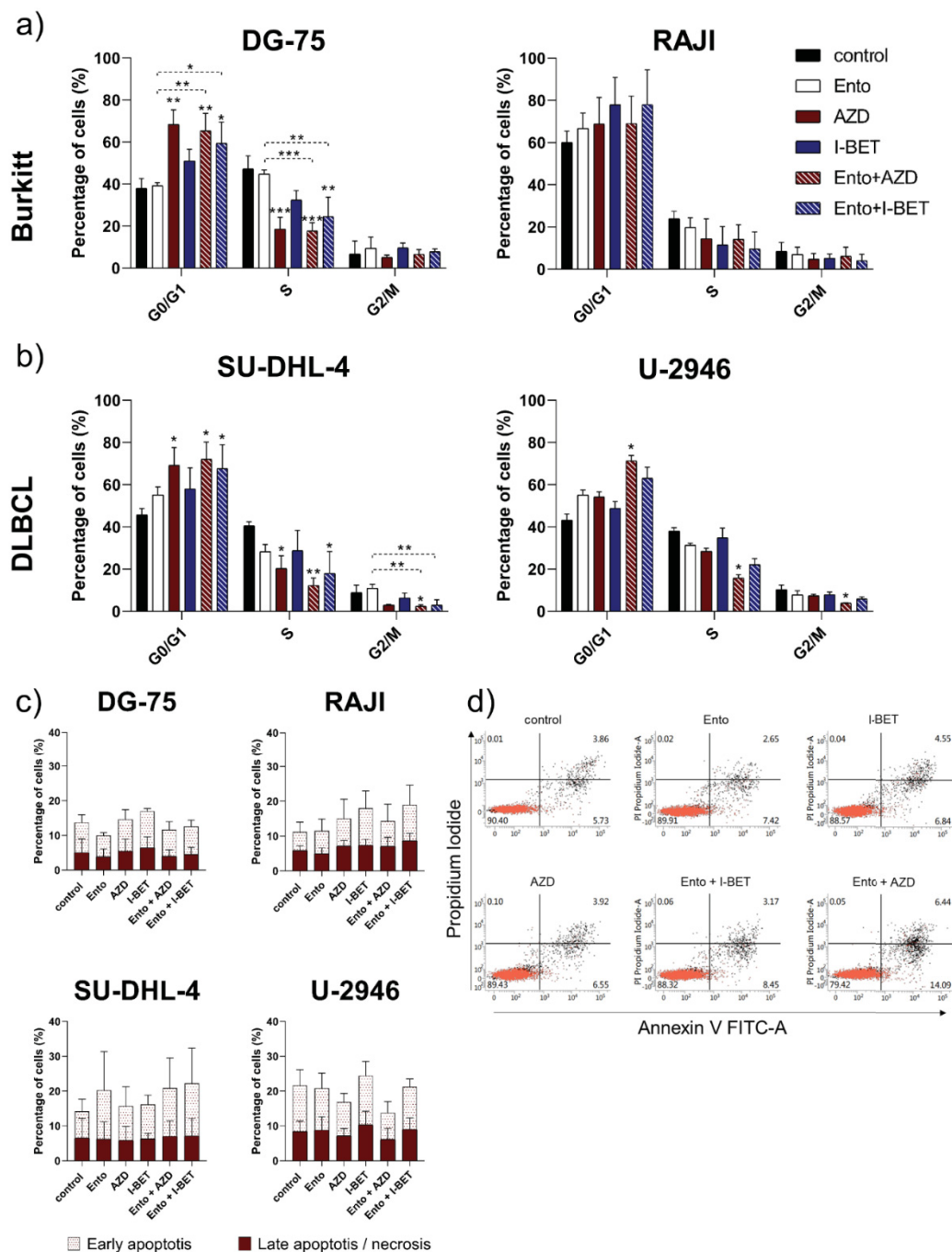


Figure 4: Cell cycle analysis and apoptosis measurement after combined BET and SYK inhibition
 Cell cycle analysis was performed 72 h after agent exposure by PI staining and DNA content was measured by flow cytometry. Percentage of cells per cell cycle phase was calculated using FlowJo Software. **a)** Mean cell cycle distribution of BL cell lines, **b)** and DLBCL cell lines **c)** Apoptosis was measured by Annexin V / PI double staining 72 h after incubation. **d)** Representative dot plots of Apoptosis induction in the SU-DHL-4 cell line. Data is presented as the mean ± SD. Statistical significance was calculated by One-way ANOVA followed by Tukey’s multiple comparison test as a post hoc analysis. Kruskal-Wallis test was applied to non-parametric data. Statistical significance is displayed as *p < 0.033, **p < 0.002, ***p < 0.001 versus control and further versus the respective single agents (dashed lines) (n ≥ 3).

354
355
356
357
358
359
360
361
362
363
364

3.6. Combined BET and SYK inhibition boost the changes in gene expression

RNA sequencing was performed in order to evaluate the underlying molecular mechanism of simultaneous BET and SYK inhibition in the DLBCL cell line SU-DHL-4. Principal Component Analysis (PCA) of exposed SU-DHL-4 cells (after batch correction) showed a distinct clustering of the treatment groups (Figure 5a).

Volcano plots of the differential gene expression analysis highlight the significant deregulated genes by each respective treatment. In particular, Ento+AZD combined exposure (Figure 5b III) demonstrated a distinct increase of significantly deregulated genes and a slightly enhanced logF_c range compared to the DMSO control. The simultaneous Ento+AZD exposure induced 1285 significantly differentially expressed genes (DEGs) in total (765 down- and 520 upregulated genes with a fold change range of -3.80 to 6.47 (supplementary tables S1e,f)).

Ento and AZD single agent exposures vs. DMSO control (Figure 5b I, II) modulated a lower number of genes. Ento exposure induced a significant deregulation of 251 genes in total (83 down- and 168 upregulated genes). The observed expression fold change ranged between -2.73 and 4.17 after Ento exposure (supplementary tables S1a,b). The comparison of AZD vs. DMSO revealed 480 significantly deregulated genes (374 down- and 106 upregulated genes with a fold change range of -2.92 to 5.75 (supplementary tables S1c,d).

Furthermore, comparing Ento+AZD combined exposure to the single agents Ento (Figure 5b IV or AZD (Figure 5b V) demonstrated a specific gene deregulation, representing the significantly and exclusively deregulated genes arising by the respective single agent. The condition Ento+AZD vs. AZD (68 down- and 190 upregulated genes) represents fewer deregulated genes compared to Ento+AZD vs. Ento (384 down- and 132 upregulated genes), indicating that most modulation was induced by AZD (supplementary tables Sg-j).

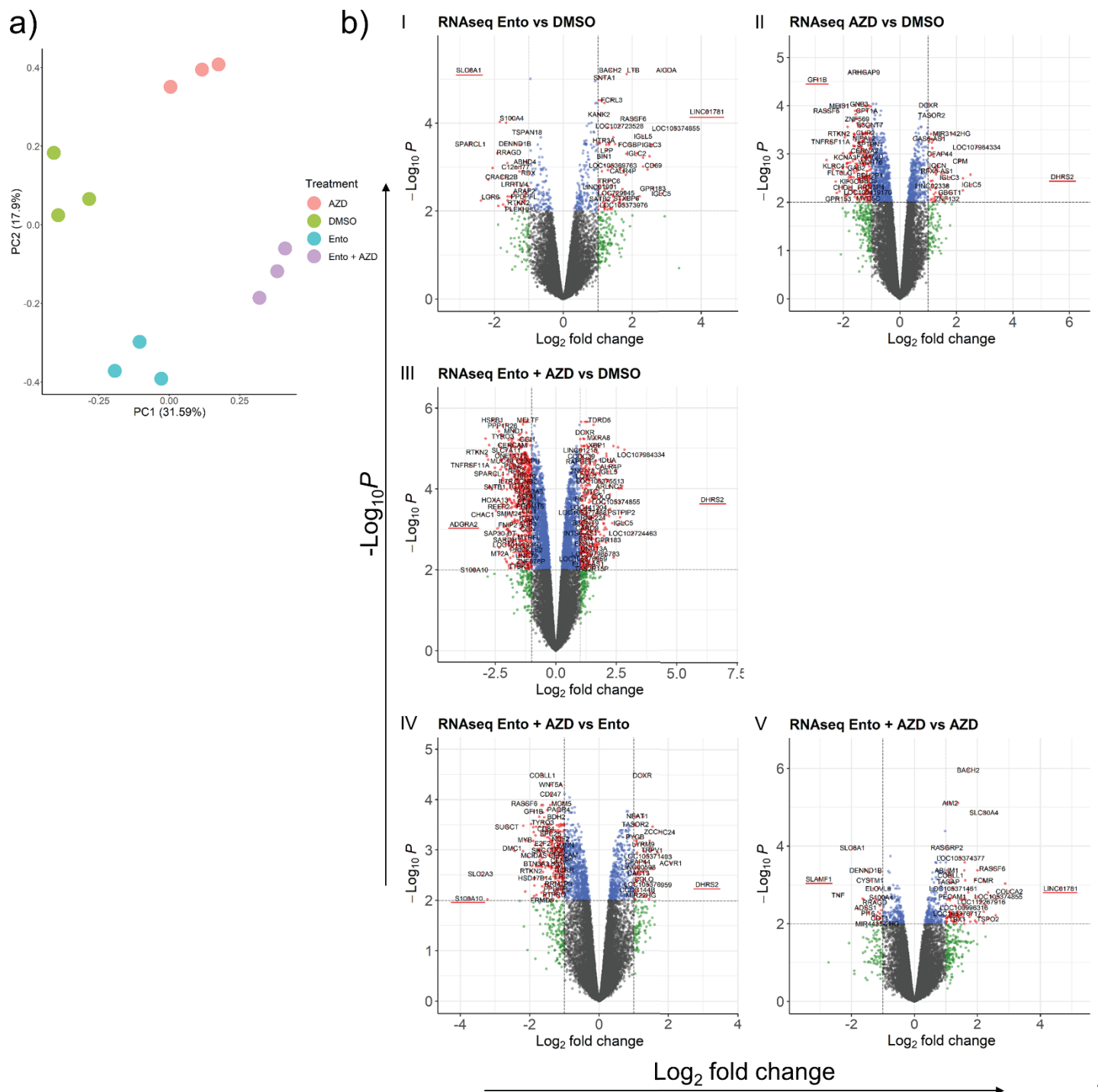


Figure 5: Gene expression modulation in SU-DHL-4 identified by RNAseq
 Intensification of gene expression modulation by combined Ento+AZD exposure a) PCA plot of the normalized RNAseq data (logCPM), showing the distinct clustering of the exposure groups in SU-DHL-4 cells b) Volcano plots of the differential expression analysis of the RNAseq dataset for I) Ento vs DMSO, II) AZD vs DMSO, III) Ento+AZD vs DMSO, IV) Ento+AZD vs Ento and V) Ento+AZD vs AZD. Highest ranked DEG (overexpressed and underexpressed) is underlined (red) (n = 3).

RNAseq data validation by Microarray analyses – platform comparison

To validate the RNAseq data, Human Clariom D Array analyses (Thermo Fisher Scientific, Waltham, USA) were carried out for the DLBCL cell line SU-DHL-4 and the BL cell line DG-75 (supplementary figure S7-S11, supplementary table S3) affirming the RNAseq data, indicating similar findings, while RNAseq seemed to be the more sensitive method.

Direct platform comparison was carried out by looking at the top10 DEGs based on microarray and exposed SU-DHL-4 cells (supplementary table S3).
Within the Ento+AZD combination, we found the genes of the long non-coding RNA (lncRNA) FOXP1 Antisense RNA 1(*FOXP1-AS1*) and Solute Carrier Family 30 Member 4 (*SLC30A4*) highly overexpressed by both procedures.
Furthermore, MYB Proto-Oncogene, Transcription Factor *MYB*, Leucine Rich Repeat Containing 2 (*LRRCC*), E2F Transcription Factor 8 (*E2F8*) and Chromatin Assembly Factor 1 Subunit B (*CHAF1B*) were identified as highly downregulated by both tools and in both cell lines.
Ento single agent exposure revealed Activation Induced Cytidine Deaminase (*AICDA*) and BTB Domain And CNC Homolog 2 (*BACH2*) genes as significantly overexpressed, affirmed by both the RNAseq and Microarray analyses. In DG-75, *AICDA* was also significantly upregulated by Ento single agent exposure. However, SPARC Like 1 (*SPARCL1*) was identified as significantly downregulated in SU-DHL-4.
AZD single agent only showed overlaps in downregulated genes. Here, Cordon-Bleu WH2 Repeat Protein Like 1 (*COBLL1*), Ras Association Domain Family Member 6 (*RASSF6*) and Rhotekin 2 (*RTKN2*) were identified as significantly downregulated, while *COBLL1* and *RTKN2* were also found to be significantly downregulated in DG-75.
Throughout, the RNAseq analyses revealed a higher number of DEGs, indicating RNAseq as the more sensitive method. Thus, all following analyses were based on the RNAseq data analyses.

3.7. Ento+AZD combination intensified the gene expression changes compared to the single agents and induced a specific gene set modulation

The Ento+AZD combination induced a distinct enhanced gene modulation compared to both the single agents, indicated by a greater number of DEGs as well as increased logFC values. The top10 genes significantly modulated by the Ento+AZD combination are highlighted in Figure 6a,b compared to the differential gene expression of the single agents (all significant DEGs are listed in supplementary tables S1e,f). Figure 6c-f illustrates the top10 DEGs of the single agents Ento and AZD including the compared differential expression of the other single agent and the combined exposure (all significant DEGs are listed in supplementary tables S1a-d).

The gene intersections of the treatment conditions revealed overlapping and uniquely significantly differentially expressed genes (Figure 6g,h). The Ento+AZD combination demonstrated the most exclusively differentially expressed genes for both the over- and underexpressed directions (Figure 6g,h and supplementary table S4). The largest overlaps (208 DEGs) were identified in the underexpressed direction between single agent AZD single agent and Ento+AZD combination (Figure 6h and supplementary tables S4c). However, the Ento+AZD combination, revealed a specific gene set modulation, since the majority of differentially expressed genes for both under- and overexpressed genes (369 and 495 genes, respectively) were unique to this treatment.

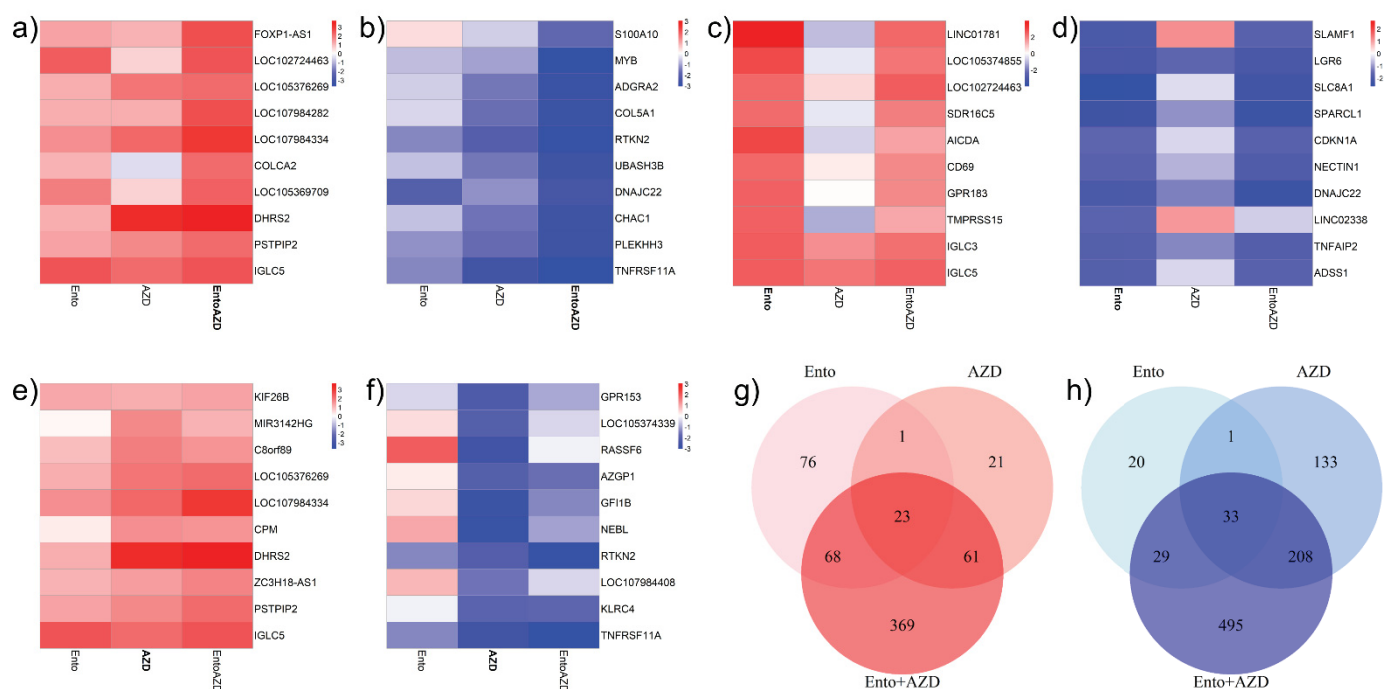


Figure 6: Top10 over- and underexpressed DEGs and gene intersections in SU-DHL-4 by RNAseq

Heatmaps indicating differential expression of the top10 DEGs by the respective condition. **a)** Top10 overexpressed genes induced by Ento+AZD combined exposure compared to the both single agents in SU-DHL-4 and **b)** Top10 underexpressed genes, respectively. **c)** Top10 overexpressed genes induced by Ento single agent compared to AZD single agent and Ento+AZD combination and **d)** Top10 underexpressed genes, respectively. **e)** Top10 overexpressed genes induced by AZD single agent compared to Ento single agent and Ento+AZD combination and **f)** Top10 underexpressed genes, respectively. Color range indicates respective $|\log_{2}FC|$ values. Bold print condition indicates the condition which is analyzed. Treatment conditions in SU-DHL-4 revealed gene intersections and uniquely deregulated genes. **g)** Gene intersections of overexpressed genes between the treatment conditions (Ento single agent, AZD single agent, Ento+AZD combination) in SU-DHL-4 cells **h)** Gene intersections of underexpressed genes between the treatment conditions (Ento single agent, AZD single agent, Ento+AZD combination) in SU-DHL-4 cells.

3.8. Gene Ontology Enrichment analyses identified DNA replication as the biological process most modulated by the Ento+AZD combined exposure

Gene Ontology (GO) enrichment analyses by Enrichr identified several GO terms for the respective condition in the DLBCL cell line SU-DHL-4. The combination of Ento and AZD induced a significant downregulation of several genes, allocated to GO terms, which are mostly related to DNA replication and cell cycle processes (**Figure 7a** and supplementary table S5e). However, the combination induced no significant enrichment of overexpressed genes (supplementary table S5f). Single agent exposures revealed no significantly enriched GO terms at the adjusted $p < 0.05$ level. The Ento+AZD combination revealed no enriched terms for the overexpressed differentially expressed genes but a total of 120 enriched terms for the underexpressed genes (supplementary tables S5b,d,f).

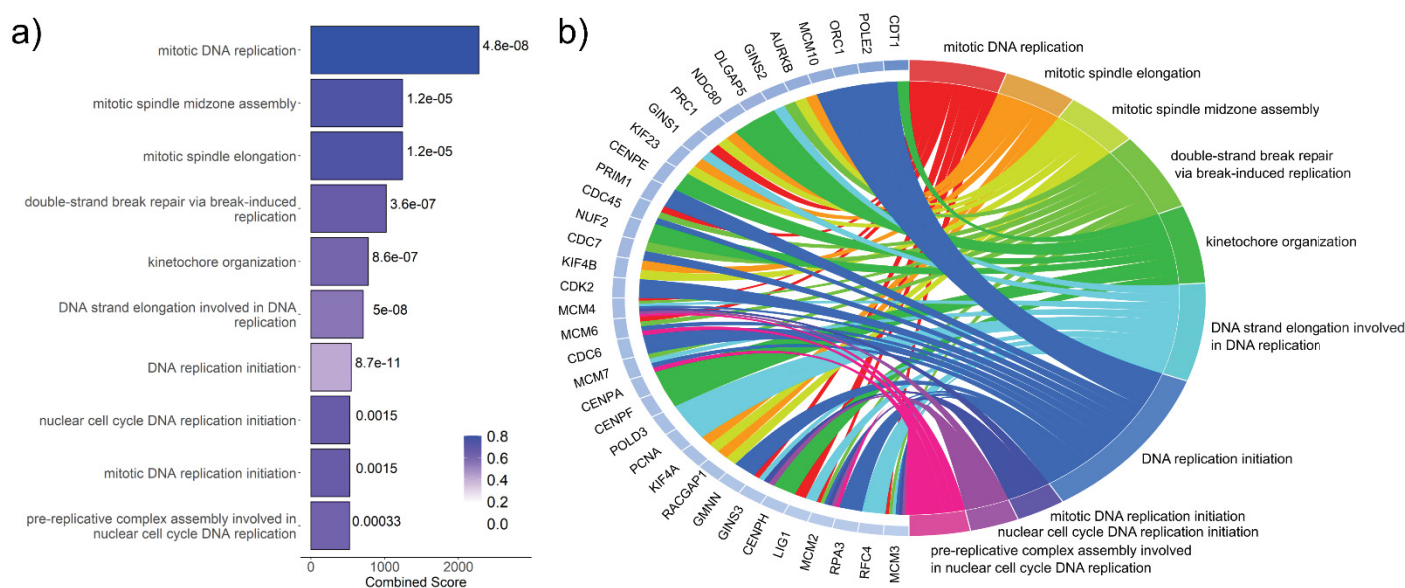


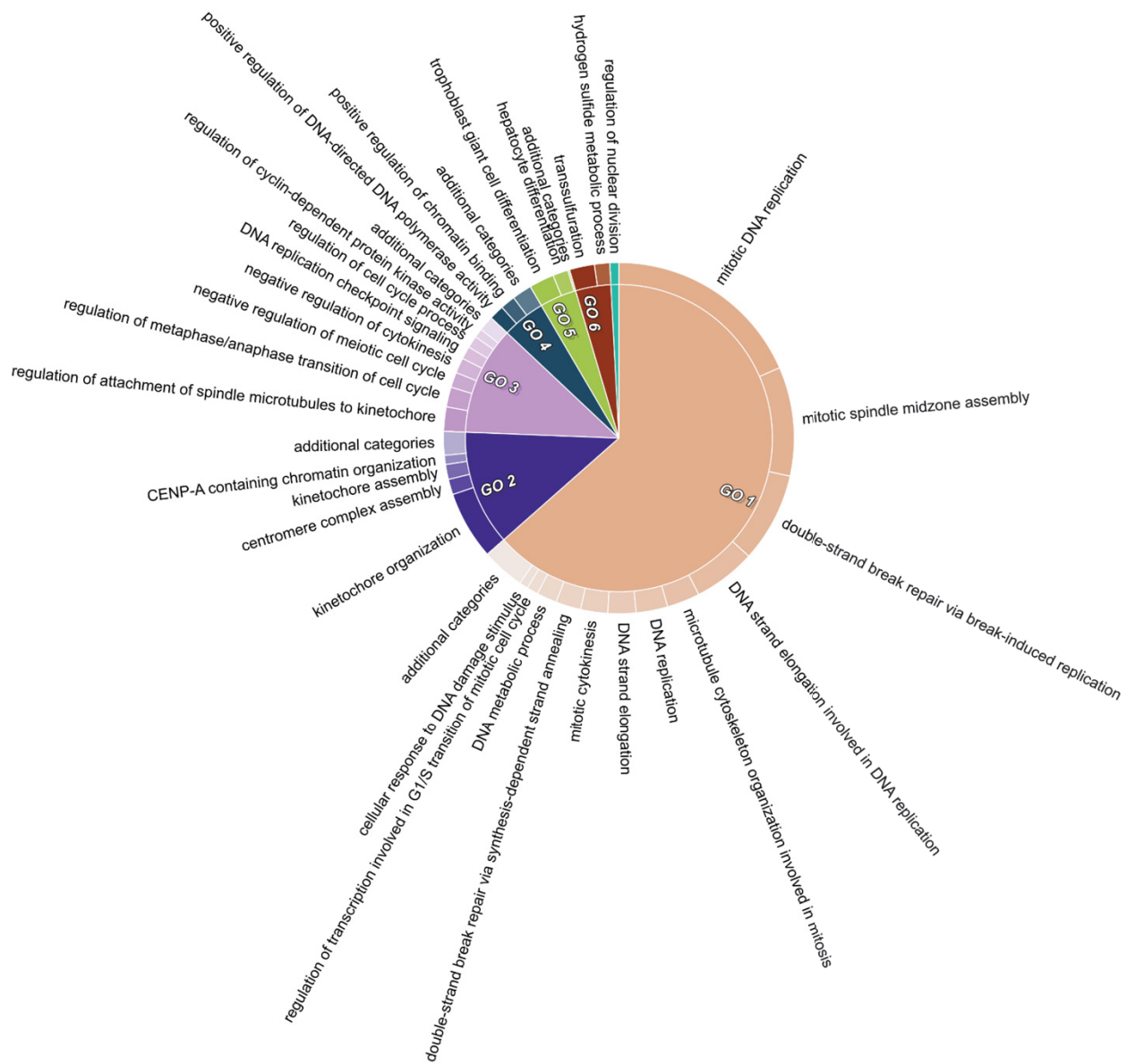
Figure 7: Significant Gene Ontology term enrichment in Ento+AZD exposed SU-DHL-4 cells by RNaseq

Significant Gene Ontology (GO) enrichment analyses by Enrichr in Ento+AZD exposed SU-DHL-4 cells. **a)** Top 10 significantly enriched GO terms of underexpressed genes after Ento+AZD exposure. GO terms were ranked by the combined score. The color gradient indicates the decreasing fraction of significant genes, while darkest color represents the highest significant fraction of genes. < 0.05 = significant. n.s. = not significant. **b)** Chordplot of top10 enriched GO terms of underexpressed genes. GO terms were ranked by combined score and top10 significantly downregulated GO terms are illustrated and linked to the significant DEGs. The genes are ranked by logFC, with the relative strength of the logFC indicated by the color adjacent to the gene name (blue indicates underexpression, and a darker color indicates a stronger logFC).

A further approach was to identify which of the most strongly downregulated DEGs were allocated to the top10 significantGO terms (Figure 7b). This analysis identified which strongly downregulated DEGs contributed to the enrichment of the top GO terms, helping to visualize and clarify the most significant transcriptomic changes. All of the top allocated genes have pivotal roles in DNA replication processes. Furthermore, different gene sets were identified such as mini chromosome maintenance (MCM), Centromer (CEN), cell division cycle (CDC), Kinesin Family (KIF), GINS complex subunit (GINS), having more than one gene allocated to the top10 GO terms.

3.9. GO term clusters revealed DNA replication and cell cycle as the most affected cell biological processes by the Ento+AZD combination

Furthermore, GO terms were condensed using REVIGO and subsequently visualized by CirGO identifying GO clusters. Figure 8 highlights the most significant GO term clusters for the Ento+AZD underexpressed condition which are allocated into 6 representative GO terms (GO clusters) and one non-clustering GO term. Three big clusters were identified revealing DNA replication, kinetochore organization and cell cycle as the most affected biological processes. Most GO terms (> 50%) were associated with representative GO cluster 1 “mitotic DNA replication”. This GO cluster mainly contains GO terms related to DNA replication, double-strand break repair and cell cycle.



Name and Proportion of the Biological Process (Inner Ring)

- GO1 mitotic DNA replication, 63.5%
- GO2 kinetochore organization, 12.1%
- GO3 regulation of attachment of spindle microtubules to kinetochore, 11.4%
- GO4 positive regulation of DNA-directed DNA polymerase activity, 4.6%
- GO5 trophoblast giant cell differentiation, 3.9%
- GO6 transsulfuration, 3.7%
- regulation of nuclear division, 0.8%

Figure 8: Identified Gene Ontology clusters after Ento+AZD combined exposure

Gene Ontology terms were clustered by CirGO tool. Legend indicates the representative GO terms (GO clusters). Underexpressed GO term cluster after Ento+AZD combined exposure

510
511
512
513

4. Discussion

Epigenetic changes and deregulated BCR signaling by molecular lesions are able to promote B-lymphomagenesis [37]–[39]. The target-specific inhibition of epigenetic readers like BET or B-Cell receptor associated kinases (BAKs) such as the spleen tyrosine kinase (SYK) enables interference of the associated pathway signal transduction. Here, we comparatively evaluated the anti-tumorigenic effect of isoform specific bivalent BET inhibitor AZD5153 and pan-BET inhibitor I-BET151 in a DLBCL and Burkitt's lymphoma *in vitro* approach and further investigated the cell- and molecular effect of simultaneous SYK inhibition by Entospletinib.

Both BET inhibitors efficiently affected cell proliferation in B-lymphoma cell lines

Both, AZD5153 and I-BET151 as single agents efficiently reduced proliferation and metabolic activity at low dosage in all tested BL and DLBCL cell lines, with slightly lower IC50 values for AZD compared to I-BET. Compared to Rhyasen et al., our evaluated IC50 values were slightly higher for AZD [18]. Further, we have recently shown, that the comparative approach of AZD and I-BET in a canine DLBCL *in vitro* model also revealed stronger anti-proliferative effects by specific bivalent BET inhibition by AZD exposure [40]. This effect was already suggested by simultaneous ligation of both BRD4 bromodomains and the associated efficient and prolonged displacement of BRD4 from chromatin [18], [41].

Simultaneous BET and SYK Inhibition additionally affected cell's response

Following, the simultaneous exposure of BET inhibitor AZD or I-BET with SYK inhibitor Entospletinib to the BL and DLBCL cell lines further affects proliferation. A pronounced effect was observed in DLBCL cell line SU-DHL-4 by Ento addition, revealing additionally reduced proliferation and metabolic activity. However, the corresponding Bliss values of both combinations showed no synergistic effect, due to the good response to Ento single agent exposure by SU-DHL-4 cells. Ento addition in all other tested cell lines improved anti-proliferative activity moderately, while respective positive Bliss values indicate slight synergy due to the low response to Ento single agent exposure. In a recent study by Kim et al. it was shown, that BET inhibition by GS-5829 in combination with Ibrutinib (BTK inhibitor) or Entospletinib synergistically increased anti-leukemia activity and induced apoptosis in primary co-cultured CLL cells [26]. Combinations with several PI3K pathway specific inhibitors also revealed additional anti-proliferative activity in a panel of B-lymphoma cell lines *in vitro* due to the upregulation of PI3K pathway components following BET inhibition [42].

Moreover, we identified a significant G0/G1 cell cycle arrest induced by both combinations in BL cell lines DG-75 and DLBCL cell line SU-DHL-4 compared to control. In DLBCL U-2946 only Ento+AZD induced a significant cell cycle arrest. However, the comparison of both combinations to the single agents only slightly increased the cell cycle blockade.

Similar findings were observed for BET inhibition as a single agent with BRD4 inhibitor JQ1, inducing a G1 cell cycle arrest in DLBCL cell lines [5]. JQ1 was also able to increase the percentage of cells in G1 in RAJI cells, which is in contrast to our findings [8]. Comparing our findings to Takimoto-Shimomura et al., BET inhibition by AZD induced a G1/S cell cycle blockade in a double hit lymphoma-derived cell line, STR-428, without significantly affecting apoptosis induction [41]. SYK inhibition by PRT060318 on sensitive DLBCL cell lines further suggested affecting cell cycle but not apoptosis induction [43]. This agrees with our results, indicating that Ento and BET inhibition as single agents did not induce significant apoptosis, while the combined exposure likewise was not able to enhance this effect under the tested conditions.

Simultaneous BET and SYK inhibition identified a combination-specific gene signature in DLBCL cell line SU-DHL-4

In order to clarify the underlying molecular mechanism, we further investigated the gene expression modulation and functional enrichment of single agents Ento and AZD and the specific gene set modulation by the Ento+AZD combination. By RNAseq analyses we identified that both single agents induced gene expression changes, while the combination was capable of highly increasing the gene expression modulation compared to control as well as to the both single agents. The fold change range of the combination likewise increased compared to the single agents. Rhyasen et al., investigated the effect of AZD5153 in xenograft leukemia and lymphoma models and also performed RNAseq on a hematologic cell line panel revealing 174 differentially expressed genes (DEGs) across this panel [18]. Compared to our study, Rhyasen et al., found lower number of DEGs presumably due to other treatment conditions and a different analysis approach.

Within the Ento+AZD combination, we identified the Adhesion G Protein-Coupled Receptor A2 (*ADGRA2*) as the most significantly underexpressed gene in SU-DHL-4 cells. *ADGRA2* or TEM5/ GPR124 (Tumor Endothelial Marker 5) was identified as an orphan G protein-coupled receptor in endothelial cells with roles in brain angiogenesis and wnt signaling [44], [45]. In pancreatic cancer it has been shown that patients with alterations in *ADGRA2* had a worse overall survival [46]. High expression of TEM5 in colorectal cancer has likewise been related to poor survival as well as suggested for use as a progression- and bio-marker [47]. Furthermore, the altered expression of *ADGRA2* in glioblastoma significantly decreased the proliferation of the cancer cells by disrupting the mitotic progression and chromosome segregation [48], while TEM5 also plays a role in VEGF-induced tumor angiogenesis [49]. Indeed, high expression of *ADGRA2* and its role in lymphoma is unknown. However, the DLBCL cell line SU-DHL-4 exhibits an *ADGRA2* missense mutation inducing a protein change p.A765T [50]. According to the Cosmic database, the protein change is unknown. Whether or not this mutation influences the *ADGRA2* expression remains to be clarified.

A further significant downregulation has been observed in the gene TNF receptor superfamily member 11a (*TNFRSF11A*). This receptor regulates various biological processes such as apoptosis, cell survival and differentiation through the activation of several signal transduction pathways such as nuclear factor κ B (NF- κ B), Jun N-terminal kinase (JNK), p38, extracellular signal-related kinase (ERK) and phosphoinositide 3-kinase (PI3K) [51], [52]. Aberrant *TNFRSF11A* (RANK) expression has been linked to several cancers. Its overexpression is correlated to breast cancer and prostate cancer with high metastatic potential and to gliomas [53]–[55]. It further correlates with metastasis and poor prognosis in colon cancer and can act as a prognostic factor [56]–[58]. Together with the stem cell marker KLF5, *TNFRSF11A* induces cancer cell proliferation, migration and invasiveness in cervical cancer [55]. However, *KLF5* was not significantly affected by any of the treatments. Finally, *TNFRSF11A* induces survival and proliferation pathways in B cells *in vitro* with progression to B-cell malignancies [59]. The significant downregulation of *TNFRSF11A* could be one reason for the effective anti-proliferative effect by the single agents and the intensification by Ento+AZD combination in SU-DHL-4 cells.

The Ento+AZD combination was exclusively able to significantly downregulate the S100 Calcium Binding Protein A10 (*S100A10*). *S100A10* is involved in various cellular processes, regulates plasminogen activation [60] and has been shown to suppress pro-apoptotic capacity of Bcl-2-associated death protein (BAD), which is suggested to have anti-apoptotic function in cancer cells (reviewed in [61]). Furthermore, *S100A10* expression is correlated with tumor development, invasion, poor prognosis and further can act as a biomarker due to its expression in various tumor cells [61]–[64].

The combined exposure additionally revealed *MYB* (MYB Proto-Oncogene, Transcription Factor) as highly underexpressed. The transcription regulator is known to be aberrantly expressed or rearranged in leukemias, lymphomas and also solid tumors [65], [66]. SU-DHL-4 exhibits aberrant overexpression of *MYB* [67], which was decreased by the Ento+AZD combined exposure. It has already been shown that *MYB* downregulation inhibits cell proliferation and invasion in solid tumors [68], [69].

Pleckstrin Homology, MyTH4 And FERM Domain Containing H3 (*PLEKHH3*) was also identified as significantly downregulated. The function of *PLEKHH3* is not yet understood, while pleckstrin homology (PH) domains are known to be part of several proteins e.g., cytoskeletal proteins, function in signal transduction, mediating protein-protein interactions and membrane association [70], [71]. Overexpression of *PLEKHH3* was identified in blood immune cells associated with obstructive sleep apnea [72], while the role of *PLEKHH3* in cancer is has not been described up to know.

However, within the Ento+AZD combination we identified that the gene Dehydrogenase/Reductase 2 (*DHRS2*) was highly and significantly upregulated. High *DHRS2* expression was observed in BET inhibitor resistant liver cancer cell lines. The specific BET inhibition in liver cancer cells induced an increase of *DHRS2* expression in sensitive (Hep3B) and resistant cells (HepG2). This could be assumed to be related to drug escape mechanisms [73]. Other studies suggest a tumor suppressor function [74], [75]. The downregulation of *DHRS2* was further related to invasion, lymph node metastasis and is associated with worse prognosis in esophageal squamous cell carcinoma. The overexpression of *DHRS2* leads to decreased tumor proliferation and tumor volume both *in vitro* and *in vivo*, while the *DHRS2* knockdown increases it [75]. In ovarian cancer, HDAC inhibition likewise increased *DHRS2* levels, which was linked to HDACi sensitivity [76]. However, the function of *DHRS2* needs to be clarified in DLBCL.

Furthermore, the Colorectal Cancer Associated 2 gene (*COLCA2*) was significantly upregulated after combined Ento+AZD exposure in SU-DHL-4 cells. Currently, detailed knowledge about the actual function of *COLCA2* is limited. However, it is assumed to have tumor suppressor function and low expression has been correlated to colorectal cancer [77], [78].

The function of both genes *DHRS2* and *COLCA2* in B-cell lymphoma is unknown. Due to its proposed function as a tumor suppressor, the high expression suggests a possible slowing effect on tumor progression.

Overlapping DEGs between RNAseq and Microarray platform in DLBCL cell line SU-DHL-4

To affirm the RNAseq data, we further analyzed the overlapping DEGs of RNAseq and microarray analyses. Genes identified by both analyses are highly likely to play pivotal roles in Entospletinib and AZD5153 exposure.

For example, *MYB* downregulation and *SLC30A4* upregulation by ENTO+AZD, *AICDA* upregulation by Ento single agent and *COBLL1* and *RTKN2* downregulation by AZD single agents can be supposed to be part of a general molecular mechanism induced by the respective substance, emerging in DLBCL SU-DHL-4 as well as BL cell line DG-75.

Compared to the RNAseq analyses, the number of identified deregulated genes are distinctly lower in SU-DHL-4 and DG-75 by microarray analyses. However, Ento exposure in DG-75 only identified *AICDA* as significantly upregulated. This small effect on gene modulation is in concordance with the investigated biological parameters in DG-75 after exposure, where Ento was not able to induce a significant anti-proliferative effect. It can be assumed, that Ento exposure as well as Ento+AZD combination is very effective in gene modulation in DLBCL cell lines but less so in BL cell lines.

Comparison of identified DEGs affected by Ento+AZD combination with external gene lists

Additional validation of the identified DEGs was carried out by comparing to external canine and human data. Potentially important DEGs were compared to published results from two different canine primary B-cell lymphoma sample cohorts [79], [80]. Canine primary B-cell lymphoma samples showed underexpression of *ADGRA2* compared to non-neoplastic controls [79]. In Glioblastoma the alteration of *ADGRA2* expression reduced cell proliferation [48]. It could be suggested, that the alteration of *ADGRA2* expression in DLBCL cell line SU-DHL-4 likewise induced anti-proliferative effects. Aberrant *MYB* expression has been identified in several tumors and leukemias [65], [66]. DLBCL cell line SU-DHL-4 also showed high *MYB* expression [67]. Likewise, *MYB* showed high expression in canine primary B-cell lymphoma samples [79]. As *MYB* down-regulation inhibits cell proliferation and invasion in solid tumors [68], [69], it could be also suggested to influence the anti-proliferative effects in SU-DHL-4. *TNFRSF11A* overexpression is linked to several cancers [53]–[55]. *TNFRSF11A* expression in the canine primary B-cell lymphoma samples also showed to be underexpressed compared to non-neoplastic primary material [79].

AICDA is underexpressed in the canine primary B-cell lymphoma samples compared to the non-neoplastic primary material, except for two outliers with high *AICDA* expression [79]. The study by Mudaliar *et al.* likewise indicates *AICDA* underexpression in canine DLBCL samples [80]. In our study, *AICDA* is upregulated by the Ento single agent exposure and slightly upregulated by the combination of Ento and AZD. Due to the fact that *AICDA* expression has been correlated to poor outcome in DLBCL patients [81], it could indicate a drug escape mechanism induced by the Ento single exposure.

Gene Ontology (GO) enrichment analyses identified combination-specific biological processes

Gene Ontology (GO) enrichment analyses identified the main biological processes which were affected after combined or single agent exposure in DLBCL cell line SU-DHL-4. For the Ento+AZD combination, GO term enrichment analysis identified combination specific GO terms compared to the single agents. Furthermore, only the underexpressed results of Ento+AZD combined exposure revealed several highly significantly modified GO terms. All other conditions showed no significance, but sometimes a high combined score.

The identified downregulation of general biological processes is related to DNA replication and cell division processes which may be caused by cell death induction due to combined BET and SYK inhibition (Figure 8a). This assumption can be affirmed by the observed significant downregulation of cell cycle related genes such as *CDK2*, *CDC45*, *CDC7*, *WEE1*, *E2F8*, *CCNA2*, *CDC6*, *CDC25A* and *CDC25C*.

Furthermore, the relation of the top10 GO terms (all underexpressed) and significant DEGs identified various gene sets with crucial roles in DNA replication processes such as mini chromosome maintenance (*MCM*), Centromer (*CEN*), cell division cycle (*CDC*), Kinesin Family (*KIF*), GINS complex subunit (*GINS*). Several top GO terms contain significantly modulated genes related to the minichromosome maintenance complex (*MCM*). *MCM* proteins are DNA Helicases regulating and initiate DNA replication processes by unwinding duplex DNA, thus playing a pivotal role in cell division [82]. Various *MCMs* have been shown to be involved in tumorigenesis. *MCM3* for example, has been identified being overexpressed in several cancers including leukemia and lymphoma [83]. High *MCM2* expression was also suggested as a negative prognostic marker in DLBCL [84]. Down-regulation of *MCM5* by JQ1 BET inhibitor was already identified in thyroid cancer cells [85]. However, AZD as single agent induced only slight downregulation of *MCM* genes in our study. Further, the cell division cycle gene *CDC7* is highly expressed in a

variety of tumors, suggesting a role as a biomarker [86], [87]. Thus, targeted CDC7 inhibition is already under preclinical and clinical investigation (reviewed in [88]). CDC7 and MCM2 have been also suggested as prognostic marker in DLBCL [89].

GINS1 and GINS2 are likewise involved in DNA replication initiation and are upregulated in a variety of tumors, indicating potential as a prognostic marker [90], [91]. CDC45, likewise downregulated by the combination, is a member of the CMG (CDC45/MCM2-7/GINS) complex. This complex has a pivotal role in DNA replication initiation by unwinding the DNA in order to initiate DNA synthesis [92], [93]. The CMG complex is overexpressed in several cancers and is thus suggested as a prognostic marker and target for anticancer therapy strategies (reviewed in [94]). The significant downregulation of CMG complex members intimates its role in the underlying mechanism induced by Ento+AZD combined exposure.

Several of the identified genes related to the top10 GO terms are involved in DNA replication processes. We further identified their functions in tumorigenesis or high expression in cancers, suggesting biomarker and prognostic marker potential.

Main GO clusters in SU-DHL-4 after combined exposure

Furthermore, GO terms were condensed using REVIGO, summarizing the GO terms based on semantic similarities and they were then visualized using CirGO, which highlighted changes in GO clusters. In particular, the arising GO clusters enriched in the underexpressed DEGs revealed that more than 50 % of identified GO terms are related to DNA replication and cell cycle processes, as with the top GO terms when simply sorted by combined score. The emerging GO clusters match with the biological data of cell cycle blockade as well as the mode of action of BET inhibition by AZD and its interference in histone recognition.

The intervention in the biological processes is suggested to be mainly caused by the BET inhibition process, due to its major effects on biological and gene expression levels. However, the Ento addition leads to the specific gene and pathway deregulation caused by the combined exposure.

The combination specific emerging GO terms as well as gene modulation are, for the most part, exclusive and therefore they provide an indication for a combination-specific gene set modulation by Entospletinib and AZD5153 combined exposure. Both, the enhanced biological response as well as the strongly enhanced gene modulation by the combination suggest an advantageous intervention for DLBCL subtypes, which requires further investigation.

5. Conclusion and future perspective

Here, we identified a moderate synergy of simultaneous BET and SYK inhibition in a BL and DLBCL *in vitro* approach affecting cell cycle modulation but not apoptosis. Expression analysis characterized a distinct gene expression modulation, while the combination strongly increased this modulation. The combination specific emerging DEGs and GO terms are mostly exclusive and therefore provide an indication for a combination specific gene set modulation. Although the changes in the main processes are mainly provoked by AZD exposure, Ento addition leads to specifically modified gene and pathway deregulation. The main affected biological processes can be related to DNA replication and cell division.

The significantly differentially expressed genes *ADGRA2*, *MYB*, *TNFRSF11A*, *S100A10*, *PLEKHH3*, *DHRS2* and *FOXP1-AS1* presumably play a pivotal role of the Ento+AZD acting mode in SU-DHL-4 cells.

Future work remains to fully understand the underlying mechanism of the Ento+AZD combination. Prospectively, it remains to clarify which modulated genes are

key regulators by including functional analyses and extend the work to other B lymphoma cell lines. Proteomic analyses as well as STRING analyses could further validate the affected biological processes investigated by RNAseq. A full understanding of the Ento+AZD combination induced effects will also need to involve 3D and *in vivo* models. This is especially important for a better transferability and investigation of a clinical value.

Supplementary Materials: The following supporting information can be downloaded at: www.mdpi.com/xxx/s1, and includes Supplementary File A (Figures), Supplementary table S1, Supplementary table S2, Supplementary table S3, Supplementary table S4, Supplementary table S5, Supplementary table S6a-f, Supplementary table S7.

Author Contributions: Conceptualization, S.S. and H.M.E.; methodology, S.S.; software, D.P., L.T.; validation, S.S., formal analysis, S.S., D.P. and L.T.; investigation, S.S., A.W.S, A.S., D.K., J.B.; resources, D.K., E.S., C.J., G.F., H.M.E; data curation, S.S.; writing—original draft preparation, S.S.; writing—review and editing, H.M.E. D.P.; visualization, S.S. and D.P.; supervision, E.S., B.B., G.F., C.J., H.M.E.; All authors have read and agreed to the published version of the manuscript.

Funding: This research received no external funding.

Data Availability Statement: Data has been uploaded to GEO (NCBI): GSE207381, GSE207382, GSE207383

Acknowledgments: We would like to thank the Department of Core Facility for Cell Sorting and Cell Analysis, Rostock University Medical Center, Germany for the possibility of Flow Cytometry device and software usage and technical support. Furthermore, we would like to thank Mr. Moosheer Al Ammar for the support concerning cyto-morphological evaluation.

Conflicts of Interest: The authors declare that they have no competing interests.

References

- [1] C. Dhalluin, J. E. Carlson, L. Zeng, C. He, A. K. Aggarwal, and M. M. Zhou, "Structure and ligand of a histone acetyltransferase bromodomain," *Nature*, vol. 399, no. 6735, pp. 491–496, Jun. 1999, doi: 10.1038/20974.
- [2] P. Filippakopoulos *et al.*, "Histone recognition and large-scale structural analysis of the human bromodomain family," *Cell*, vol. 149, no. 1, pp. 214–231, Mar. 2012, doi: 10.1016/j.cell.2012.02.013.
- [3] O. B. Cox *et al.*, "A poised fragment library enables rapid synthetic expansion yielding the first reported inhibitors of PHIP(2), an atypical bromodomain," *Chem. Sci.*, vol. 7, no. 3, pp. 2322–2330, Mar. 2016, doi: 10.1039/c5sc03115j.
- [4] D. J. Owen *et al.*, "The structural basis for the recognition of acetylated histone H4 by the bromodomain of histone acetyltransferase Gcn5p," *EMBO J.*, vol. 19, no. 22, pp. 6141–6149, 2000, doi: 10.1093/emboj/19.22.6141.
- [5] B. Chapuy *et al.*, "Discovery and Characterization of Super-Enhancer-Associated Dependencies in Diffuse Large B Cell Lymphoma," *Cancer Cell*, vol. 24, no. 6, pp. 777–790, Dec. 2013, doi: 10.1016/j.ccr.2013.11.003.
- [6] M. A. Dawson *et al.*, "Inhibition of BET recruitment to chromatin as an effective treatment for MLL-fusion leukaemia," *Nature*, vol. 478, no. 7370, pp. 529–533, Oct. 2011, doi: 10.1038/nature10509.
- [7] J. E. Delmore *et al.*, "BET bromodomain inhibition as a therapeutic strategy to target c-Myc.," *Cell*, vol. 146, no. 6, pp. 904–17, Sep. 2011, doi: 10.1016/j.cell.2011.08.017.
- [8] J. A. Mertz *et al.*, "Targeting MYC dependence in cancer by inhibiting BET bromodomains," *Proc. Natl. Acad. Sci.*

- U. S. A., vol. 108, no. 40, pp. 16669–16674, Oct. 2011, doi: 10.1073/pnas.1108190108. 816
- [9] J. Zuber *et al.*, “RNAi screen identifies Brd4 as a therapeutic target in acute myeloid leukaemia,” *Nature*, vol. 478, no. 7370, pp. 524–528, Oct. 2011, doi: 10.1038/nature10334. 817
818
- [10] P. Filippakopoulos *et al.*, “Selective inhibition of BET bromodomains,” *Nature*, vol. 468, no. 7327, pp. 1067–1073, Dec. 2010, doi: 10.1038/nature09504. 819
820
- [11] E. Nicodeme *et al.*, “Suppression of inflammation by a synthetic histone mimic,” *Nature*, vol. 468, no. 7327, pp. 1119–1123, Dec. 2010, doi: 10.1038/nature09589. 821
822
- [12] E. Bernasconi *et al.*, “Preclinical evaluation of the BET bromodomain inhibitor BAY 1238097 for the treatment of lymphoma,” *Br. J. Haematol.*, vol. 178, no. 6, pp. 936–948, Sep. 2017, doi: 10.1111/bjh.14803. 823
824
- [13] F. Spriano, A. Stathis, and F. Bertoni, “Targeting BET bromodomain proteins in cancer: The example of lymphomas,” *Pharmacol. Ther.*, p. 107631, Jul. 2020, doi: 10.1016/j.pharmthera.2020.107631. 825
826
- [14] A. Alqahtani *et al.*, “Bromodomain and extra-terminal motif inhibitors: A review of preclinical and clinical advances in cancer therapy,” *Future Science OA*, vol. 5, no. 3. Future Medicine Ltd., 2019, doi: 10.4155/fsoa-2018-0115. 827
828
829
- [15] K. F. McDaniel *et al.*, “Discovery of N-(4-(2,4-Difluorophenoxy)-3-(6-methyl-7-oxo-6,7-dihydro-1H-pyrrolo[2,3-c]pyridin-4-yl)phenyl)ethanesulfonamide (ABBV-075/Mivebresib), a Potent and Orally Available Bromodomain and Extraterminal Domain (BET) Family Bromodomain Inhibitor,” *J. Med. Chem.*, vol. 60, no. 20, pp. 8369–8384, Oct. 2017, doi: 10.1021/acs.jmedchem.7b00746. 830
831
832
833
- [16] J. K. Noel, K. Iwata, S. Ooike, K. Sugahara, H. Nakamura, and M. Daibata, “Abstract C244: Development of the BET bromodomain inhibitor OTX015.,” in *Molecular Cancer Therapeutics*, Nov. 2013, vol. 12, no. 11 Supplement, pp. C244–C244, doi: 10.1158/1535-7163.targ-13-c244. 834
835
836
- [17] B. K. Albrecht *et al.*, “Identification of a Benzoisoxazoloazepine Inhibitor (CPI-0610) of the Bromodomain and Extra-Terminal (BET) Family as a Candidate for Human Clinical Trials,” *J. Med. Chem.*, vol. 59, no. 4, pp. 1330–1339, Feb. 2016, doi: 10.1021/acs.jmedchem.5b01882. 837
838
839
- [18] G. W. Rhyasen *et al.*, “AZD5153: A novel bivalent BET bromodomain inhibitor highly active against hematologic malignancies,” *Mol. Cancer Ther.*, vol. 15, no. 11, pp. 2563–2574, Nov. 2016, doi: 10.1158/1535-7163.MCT-16-0141. 840
841
- [19] G. S. Sheppard *et al.*, “Discovery of N-Ethyl-4-[2-(4-fluoro-2,6-dimethyl-phenoxy)-5-(1-hydroxy-1-methyl-ethyl)phenyl]-6-methyl-7-oxo-1 H-pyrrolo[2,3-c]pyridine-2-carboxamide (ABBV-744), a BET Bromodomain Inhibitor with Selectivity for the Second Bromodomain,” *J. Med. Chem.*, vol. 63, no. 10, pp. 5585–5623, May 2020, doi: 10.1021/acs.jmedchem.0c00628. 842
843
844
845
- [20] S. J. Hogg *et al.*, “BET-Bromodomain Inhibitors Engage the Host Immune System and Regulate Expression of the Immune Checkpoint Ligand PD-L1,” *Cell Rep.*, vol. 18, no. 9, pp. 2162–2174, Feb. 2017, doi: 10.1016/j.celrep.2017.02.011. 846
847
848

- [21] X. Zhao *et al.*, “Disruption of the MYC-miRNA-EZH2 loop to suppress aggressive B-cell lymphoma survival and clonogenicity,” *Leukemia*, vol. 27, no. 12, pp. 2341–2350, Dec. 2013, doi: 10.1038/leu.2013.94. 849
850
- [22] S. V. Muralidharan, J. Bhadury, L. M. Nilsson, L. C. Green, K. G. McLure, and J. A. Nilsson, “BET bromodomain inhibitors synergize with ATR inhibitors to induce DNA damage, apoptosis, senescence-associated secretory pathway and ER stress in Myc-induced lymphoma cells,” *Oncogene*, vol. 35, no. 36, pp. 4689–4697, Sep. 2016, doi: 10.1038/onc.2015.521. 851
852
853
854
- [23] M. Boi *et al.*, “The BET bromodomain inhibitor OTX015 affects pathogenetic pathways in preclinical B-cell tumor models and synergizes with targeted drugs,” *Clin. Cancer Res.*, vol. 21, no. 7, pp. 1628–1638, Apr. 2015, doi: 10.1158/1078-0432.CCR-14-1561. 855
856
857
- [24] R. Küppers, *Mechanisms of B-cell lymphoma pathogenesis*, vol. 5, no. 4. 2005, pp. 251–262. 858
- [25] B. Sun *et al.*, “Synergistic activity of BET protein antagonist-based combinations in mantle cell lymphoma cells sensitive or resistant to ibrutinib,” *Blood*, vol. 126, no. 13, pp. 1565–1574, Sep. 2015, doi: 10.1182/blood-2015-04-639542. 859
860
861
- [26] E. Kim *et al.*, “The BET inhibitor GS-5829 targets chronic lymphocytic leukemia cells and their supportive microenvironment,” *Leukemia*, vol. 34, no. 6, pp. 1588–1598, Jun. 2020, doi: 10.1038/s41375-019-0682-7. 862
863
- [27] S. Tinsley, K. Meja, C. Shepherd, and A. Khwaja, “Synergistic induction of cell death in haematological malignancies by combined phosphoinositide-3-kinase and BET bromodomain inhibition,” *British Journal of Haematology*, vol. 170, no. 2. Blackwell Publishing Ltd, pp. 275–278, Jul. 01, 2015, doi: 10.1111/bjh.13283. 864
865
866
- [28] T. E. C. Cummin *et al.*, “BET inhibitors synergize with venetoclax to induce apoptosis in MYC-driven lymphomas with high BCL-2 expression,” *Blood Adv.*, vol. 4, no. 14, pp. 3316–3328, Jul. 2020, doi: 10.1182/bloodadvances.2020002231. 867
868
869
- [29] A. Mócsai, J. Ruland, and V. L. J. Tybulewicz, “The SYK tyrosine kinase: a crucial player in diverse biological functions,” *Nat. Rev. Immunol.*, vol. 10, no. 6, pp. 387–402, Jun. 2010, doi: 10.1038/nri2765. 870
871
- [30] S. Sender *et al.*, “Precursor B-ALL cell lines differentially respond to syk inhibition by entospletinib,” *Int. J. Mol. Sci.*, vol. 22, no. 2, pp. 1–22, Jan. 2021, doi: 10.3390/ijms22020592. 872
873
- [31] D. Koczan, B. Fitzner, U. K. Zettl, and M. Hecker, “Microarray data of transcriptome shifts in blood cell subsets during S1P receptor modulator therapy,” *Sci. data*, vol. 5, no. 1, Dec. 2018, doi: 10.1038/SDATA.2018.145. 874
875
- [32] M. Martin, “Cutadapt removes adapter sequences from high-throughput sequencing reads,” *EMBnet.journal*, vol. 17, no. 1, pp. 10–12, May 2011, doi: 10.14806/EJ.17.1.200. 876
877
- [33] Y. Liao, G. K. Smyth, and W. Shi, “The R package Rsubread is easier, faster, cheaper and better for alignment and quantification of RNA sequencing reads,” *Nucleic Acids Res.*, vol. 47, no. 8, pp. e47–e47, May 2019, doi: 10.1093/NAR/GKZ114. 878
879
880
- [34] M. D. Robinson, D. J. McCarthy, and G. K. Smyth, “edgeR: a Bioconductor package for differential expression 881

- analysis of digital gene expression data," *Bioinformatics*, vol. 26, no. 1, pp. 139–140, Jan. 2010, doi: 10.1093/BIOINFORMATICS/BTP616. 882
883
- [35] M. V. Kuleshov *et al.*, "Enrichr: a comprehensive gene set enrichment analysis web server 2016 update," *Nucleic Acids Res.*, vol. 44, no. W1, pp. W90–W97, Jul. 2016, doi: 10.1093/NAR/GKW377. 884
885
- [36] J. Foucquier and M. Guedj, "Analysis of drug combinations: current methodological landscape," *Pharmacol. Res. Perspect.*, vol. 3, no. 3, p. e00149, Jun. 2015, doi: 10.1002/prp2.149. 886
887
- [37] R. D. Morin *et al.*, "Frequent mutation of histone-modifying genes in non-Hodgkin lymphoma," *Nature*, vol. 476, no. 7360, pp. 298–303, Aug. 2011, doi: 10.1038/nature10351. 888
889
- [38] M. R. Hassler, A. I. Schiefer, and G. Egger, "Combating the epigenome: Epigenetic drugs against non-Hodgkin's lymphoma," *Epigenomics*, vol. 5, no. 4, pp. 397–415, Aug. 2013, doi: 10.2217/epi.13.39. 890
891
- [39] R. E. Davis *et al.*, "Chronic active B-cell-receptor signalling in diffuse large B-cell lymphoma," *Nature*, vol. 463, no. 7277, pp. 88–92, Jan. 2010, doi: 10.1038/nature08638. 892
893
- [40] W. Kong *et al.*, "Pan-and isoform-specific inhibition of the bromodomain and extra-terminal proteins and evaluation of synergistic potential with entospletinib in canine lymphoma," *Anticancer Res.*, vol. 40, no. 7, pp. 3781–3792, Jul. 2020, doi: 10.21873/ANTICANRES.14367. 894
895
896
- [41] T. Takimoto-Shimomura *et al.*, "Dual targeting of bromodomain-containing 4 by AZD5153 and BCL2 by AZD4320 against B-cell lymphomas concomitantly overexpressing c-MYC and BCL2," *Invest. New Drugs*, vol. 37, no. 2, pp. 210–222, Apr. 2019, doi: 10.1007/s10637-018-0623-8. 897
898
899
- [42] E. Derenzini *et al.*, "BET Inhibition-Induced GSK3 β Feedback Enhances Lymphoma Vulnerability to PI3K Inhibitors," *Cell Rep.*, vol. 24, no. 8, pp. 2155–2166, Aug. 2018, doi: 10.1016/j.celrep.2018.07.055. 900
901
- [43] S. Cheng *et al.*, "SYK inhibition and response prediction in diffuse large B-cell lymphoma," *Blood*, vol. 118, no. 24, pp. 6342–6352, Dec. 2011, doi: 10.1182/blood-2011-02-333773. 902
903
- [44] F. Kuhnert *et al.*, "Essential regulation of CNS angiogenesis by the orphan G protein-coupled receptor GPR124," *Science*, vol. 330, no. 6006, pp. 985–989, Nov. 2010, doi: 10.1126/SCIENCE.1196554. 904
905
- [45] Y. Zhou and J. Nathans, "Gpr124 controls CNS angiogenesis and blood-brain barrier integrity by promoting ligand-specific canonical Wnt signaling," *Dev. Cell*, vol. 31, no. 2, p. 248, Oct. 2014, doi: 10.1016/J.DEVCEL.2014.08.018. 906
907
908
- [46] J. Du *et al.*, "Molecular Landscape and Prognostic Biomarker Analysis of Advanced Pancreatic Cancer and Predictors of Treatment Efficacy of AG Chemotherapy," *Front. Oncol.*, vol. 12, p. 844527, May 2022, doi: 10.3389/FONC.2022.844527. 909
910
911
- [47] Ł. Pietrzyk and P. Wdowiak, "Serum TEM5 and TEM7 concentrations correlate with clinicopathologic features and poor prognosis of colorectal cancer patients," *Adv. Med. Sci.*, vol. 64, no. 2, pp. 402–408, Sep. 2019, doi: 10.1016/J.ADVMS.2019.07.001. 912
913
914

- [48] A. E. Cherry *et al.*, “GPR124 regulates microtubule assembly, mitotic progression, and glioblastoma cell proliferation,” *Glia*, vol. 67, no. 8, p. 1558, Aug. 2019, doi: 10.1002/GLIA.23628. 915
916
- [49] Y. Wang, S.-G. Cho, X. Wu, S. Siwko, and M. Liu, “G-protein coupled receptor 124 (GPR124) in endothelial cells regulates vascular endothelial growth factor (VEGF)-induced tumor angiogenesis,” *Curr. Mol. Med.*, vol. 14, no. 4, pp. 543–554, May 2014, doi: 10.2174/1566524014666140414205943. 917
918
919
- [50] “DepMap, Broad (2022): DepMap 22Q2 Public. figshare. Dataset.” 920
https://figshare.com/articles/dataset/DepMap_22Q2_Public/19700056/2 (accessed Jun. 08, 2022). 921
- [51] P. W. Dempsey, S. E. Doyle, J. Q. He, and G. Cheng, “The signaling adaptors and pathways activated by TNF superfamily,” *Cytokine Growth Factor Rev.*, vol. 14, no. 3–4, pp. 193–209, Jun. 2003, doi: 10.1016/S1359-6101(03)00021-2. 922
923
924
- [52] E. González-Suárez and A. Sanz-Moreno, “RANK as a therapeutic target in cancer,” *FEBS J.*, vol. 283, no. 11, pp. 2018–2033, Jun. 2016, doi: 10.1111/FEBS.13645. 925
926
- [53] A. von dem Knesebeck *et al.*, “RANK (TNFRSF11A) Is Epigenetically Inactivated and Induces Apoptosis in Gliomas,” *Neoplasia*, vol. 14, no. 6, p. 526, 2012, doi: 10.1596/NEO.12360. 927
928
- [54] N. Bonifaci *et al.*, “Evidence for a link between TNFRSF11A and risk of breast cancer,” *Breast Cancer Res. Treat.*, vol. 129, no. 3, pp. 947–954, Oct. 2011, doi: 10.1007/S10549-011-1546-7. 929
930
- [55] D. Ma *et al.*, “KLF5 promotes cervical cancer proliferation, migration and invasion in a manner partly dependent on TNFRSF11a expression,” *Sci. Reports 2017 71*, vol. 7, no. 1, pp. 1–13, Nov. 2017, doi: 10.1038/s41598-017-15979-1. 931
932
933
- [56] Q. Liang *et al.*, “RANK promotes colorectal cancer migration and invasion by activating the Ca²⁺-calcineurin/NFATC1-ACP5 axis,” *Cell Death Dis.*, vol. 12, no. 4, Apr. 2021, doi: 10.1038/S41419-021-03642-7. 934
935
- [57] J. Zhao *et al.*, “A nine-gene signature to improve prognosis prediction of colon carcinoma,” *Cell Cycle*, vol. 20, no. 10, p. 1021, 2021, doi: 10.1080/15384101.2021.1919827. 936
937
- [58] C. Ieranò *et al.*, “Original research: In PD-1+ human colon cancer cells NIVOLUMAB promotes survival and could protect tumor cells from conventional therapies,” *J. Immunother. Cancer*, vol. 10, no. 3, p. 4032, Mar. 2022, doi: 10.1136/JITC-2021-004032. 938
939
940
- [59] B. Alankus *et al.*, “Pathological RANK signaling in B cells drives autoimmunity and chronic lymphocytic leukemia,” *J. Exp. Med.*, vol. 218, no. 2, Feb. 2021, doi: 10.1084/JEM.20200517. 941
942
- [60] C. Li *et al.*, “Critical role and its underlying molecular events of the plasminogen receptor, S100A10 in malignant tumor and non-tumor diseases,” *J. Cancer*, vol. 11, no. 4, p. 826, 2020, doi: 10.7150/JCA.36203. 943
944
- [61] N. A. Tanty, A. S. Karyadi, S. Z. Rasman, M. R. G. Salim, A. Devina, and A. Sumarpo, “The prognostic value of S100A10 expression in cancer,” *Oncol. Lett.*, vol. 17, no. 2, pp. 1417–1424, Feb. 2019, doi: 10.3892/OL.2018.9751/HTML. 945
946
947

- [62] D. Huang *et al.*, "Annexin A2-S100A10 heterotetramer is upregulated by PML/RAR α fusion protein and promotes plasminogen-dependent fibrinolysis and matrix invasion in acute promyelocytic leukemia," *Front. Med.*, vol. 11, no. 3, pp. 410–422, Sep. 2017, doi: 10.1007/S11684-017-0527-6. 948
949
950
- [63] Y. Li *et al.*, "S100A10 Accelerates Aerobic Glycolysis and Malignant Growth by Activating mTOR-Signaling Pathway in Gastric Cancer," *Front. Cell Dev. Biol.*, vol. 8, p. 1430, Nov. 2020, doi: 10.3389/FCELL.2020.559486/BIBTEX. 951
952
953
- [64] K. Arai, T. Iwasaki, A. Sonoda, and A. Endo, "Membranous overexpression of S100A10 is associated with a high-grade cellular status of breast carcinoma," *Med. Mol. Morphol.*, vol. 53, no. 2, pp. 104–114, Jun. 2020, doi: 10.1007/S00795-019-00236-3/FIGURES/5. 954
955
956
- [65] D. R. Pattabiraman and T. J. Gonda, "Role and potential for therapeutic targeting of MYB in leukemia," *Leukemia*, vol. 27, no. 2, pp. 269–277, Feb. 2013, doi: 10.1038/leu.2012.225. 957
958
- [66] R. G. Ramsay and T. J. Gonda, "MYB function in normal and cancer cells," *Nature Reviews Cancer*, vol. 8, no. 7, Nature Publishing Group, pp. 523–534, Jul. 2008, doi: 10.1038/nrc2439. 959
960
- [67] R. S. Robetorye, S. D. Bohling, J. W. Morgan, G. C. Fillmore, M. S. Lim, and K. S. J. Elenitoba-Johnson, "Microarray analysis of B-cell lymphoma cell lines with the t(14;18)," *J. Mol. Diagnostics*, vol. 4, no. 3, pp. 123–136, Aug. 2002, doi: 10.1016/S1525-1578(10)60693-9. 961
962
963
- [68] B. Zhang *et al.*, "Hsa-miR-495 acts as a tumor suppressor gene in glioma via the negative regulation of MYB," *Mol. Med. Rep.*, vol. 14, no. 1, pp. 977–982, Jul. 2016, doi: 10.3892/mmr.2016.5327. 964
965
- [69] L. Yu, G. F. Ding, C. He, L. Sun, Y. F. Jiang, and L. Zhu, "MicroRNA-424 is down-regulated in hepatocellular carcinoma and suppresses cell migration and invasion through c-Myb," *PLoS One*, vol. 9, no. 3, Mar. 2014, doi: 10.1371/journal.pone.0091661. 966
967
968
- [70] M. A. Lemmon, K. M. Ferguson, and C. S. Abrams, "Pleckstrin homology domains and the cytoskeleton," *FEBS Letters*, vol. 513, no. 1, pp. 71–76, Feb. 20, 2002, doi: 10.1016/S0014-5793(01)03243-4. 969
970
- [71] E. Ingley and B. A. Hemmings, "Pleckstrin homology (PH) domains in signal transduction," *J. Cell. Biochem.*, vol. 56, no. 4, pp. 436–443, Dec. 1994, doi: 10.1002/jcb.240560403. 971
972
- [72] Y. C. Chen *et al.*, "Genome-wide gene expression array identifies novel genes related to disease severity and excessive daytime sleepiness in patients with obstructive sleep apnea," *PLoS One*, vol. 12, no. 5, May 2017, doi: 10.1371/journal.pone.0176575. 973
974
975
- [73] Y. Liu *et al.*, "Multi-omics characterization of WNT pathway reactivation to ameliorate BET inhibitor resistance in liver cancer cells," *Genomics*, vol. 113, no. 3, pp. 1057–1069, May 2021, doi: 10.1016/J.YGENO.2021.02.017. 976
977
- [74] S. S. Ekmekci *et al.*, "LEF1 Induces DHRS2 Gene Expression in Human Acute Leukemia Jurkat T-Cells," *Turkish J. Hematol.*, vol. 37, no. 4, p. 226, 2020, doi: 10.4274/TJH.GALENOS.2020.2020.0144. 978
979
- [75] Y. Zhou *et al.*, "DHRS2 inhibits cell growth and motility in esophageal squamous cell carcinoma," *Oncogene*, vol. 980

- 37, no. 8, p. 1086, Feb. 2018, doi: 10.1038/ONC.2017.383. 981
- [76] Y. Han *et al.*, “Decreased DHRS2 expression is associated with HDACi resistance and poor prognosis in ovarian cancer,” *Epigenetics*, vol. 15, no. 1–2, p. 122, Feb. 2020, doi: 10.1080/15592294.2019.1656155. 982
983
- [77] V. D. Peltekova *et al.*, “Identification of genes expressed by immune cells of the colon that are regulated by colorectal cancer-associated variants,” *Int. J. cancer*, vol. 134, no. 10, pp. 2330–2341, May 2014, doi: 10.1002/IJC.28557. 984
985
986
- [78] R. Yin, B. Song, J. Wang, C. Shao, Y. Xu, and H. Jiang, “Genome-Wide Association and Transcriptome-Wide Association Studies Identify Novel Susceptibility Genes Contributing to Colorectal Cancer,” *J. Immunol. Res.*, vol. 2022, pp. 1–14, Jul. 2022, doi: 10.1155/2022/5794055. 987
988
989
- [79] L. Taher *et al.*, “Comparative High-Resolution Transcriptome Sequencing of Lymphoma Cell Lines and de novo Lymphomas Reveals Cell-Line-Specific Pathway Dysregulation,” *Sci. Rep.*, vol. 8, no. 1, 2018, doi: 10.1038/s41598-018-23207-7. 990
991
992
- [80] doi: 10.1371/JOURNAL.P.0072591. anikhanda. A. V. Mudaliar, M[1] M. A. V. Mudaliar *et al.*, “Comparative Gene Expression Profiling Identifies Common Molecular Signatures of NF- κ B Activation in Canine and Human Diffuse Large B Cell Lymphoma (DLBCL),” *PLoS One*, vol. 8, no. 9, p. e72591, Sep. 2013 *et al.*, “Comparative Gene Expression Profiling Identifies Common Molecular Signatures of NF- κ B Activation in Canine and Human Diffuse Large B Cell Lymphoma (DLBCL),” *PLoS One*, vol. 8, no. 9, p. e72591, Sep. 2013, doi: 10.1371/JOURNAL.PONE.0072591. 993
994
995
996
997
998
- [81] M. Teater *et al.*, “AICDA drives epigenetic heterogeneity and accelerates germinal center-derived lymphomagenesis,” *Nat. Commun.*, vol. 9, no. 1, pp. 1–10, Dec. 2018, doi: 10.1038/s41467-017-02595-w. 999
1000
- [82] M. L. Bochman and A. Schwacha, “The Mcm Complex: Unwinding the Mechanism of a Replicative Helicase,” *Microbiol. Mol. Biol. Rev.*, vol. 73, no. 4, p. 652, Dec. 2009, doi: 10.1128/MMBR.00019-09. 1001
1002
- [83] S. A. Ha *et al.*, “Cancer-Associated Expression of Minichromosome Maintenance 3 Gene in Several Human Cancers and Its Involvement in Tumorigenesis,” *Clin. Cancer Res.*, vol. 10, no. 24, pp. 8386–8395, Dec. 2004, doi: 10.1158/1078-0432.CCR-04-1029. 1003
1004
1005
- [84] E. C. Obermann *et al.*, “Expression of minichromosome maintenance protein 2 as a marker for proliferation and prognosis in diffuse large B-cell lymphoma: a tissue microarray and clinico-pathological analysis,” *BMC Cancer*, vol. 5, p. 162, Dec. 2005, doi: 10.1186/1471-2407-5-162. 1006
1007
1008
- [85] C. Mio *et al.*, “MCM5 as a target of BET inhibitors in thyroid cancer cells,” *Endocr. Relat. Cancer*, vol. 23, no. 4, p. 335, Apr. 2016, doi: 10.1530/ERC-15-0322. 1009
1010
- [86] Q. Wang and W. Zheng, “Upregulation of CDC7 Associated with Cervical Cancer Incidence and Development,” *Biomed Res. Int.*, vol. 2021, 2021, doi: 10.1155/2021/6663367. 1011
1012
- [87] A. N. Cheng *et al.*, “Increased Cdc7 expression is a marker of oral squamous cell carcinoma and overexpression 1013

- of Cdc7 contributes to the resistance to DNA-damaging agents," *Cancer Lett.*, vol. 337, no. 2, pp. 218–225, Sep. 2013, doi: 10.1016/J.CANLET.2013.05.008. 1014
1015
- [88] R. Liu and Y. Huang, "CDC7 as a novel biomarker and druggable target in cancer," *Clin. Transl. Oncol.*, 2022, doi: 10.1007/S12094-022-02853-4. 1016
1017
- [89] Y. Hou *et al.*, "Expression of Cdc7 and mcm2 as a marker for proliferation and prognosis in diffuse large B cell lymphoma," *Chinese J. Oncol.*, vol. 33, no. 12, pp. 911–915, 2011, doi: 10.3760/cma.j.issn.0253-3766.2011.12.007. 1018
1019
- [90] F. Ouyang *et al.*, "GINS2 is a novel prognostic biomarker and promotes tumor progression in early-stage cervical cancer," *Oncol. Rep.*, vol. 37, no. 5, pp. 2652–2662, May 2017, doi: 10.3892/OR.2017.5573. 1020
1021
- [91] M. Ahmad *et al.*, "Up-regulation of GINS1 highlighted a good diagnostic and prognostic potential of survival in three different subtypes of human cancer," *Braz. J. Biol.*, vol. 84, 2021, doi: 10.1590/1519-6984.250575. 1022
1023
- [92] I. Ilves, T. Petojevic, J. J. Pesavento, and M. R. Botchan, "Activation of the MCM2-7 helicase by association with Cdc45 and GINS proteins," *Mol. Cell*, vol. 37, no. 2, pp. 247–258, Jan. 2010, doi: 10.1016/J.MOLCEL.2009.12.030. 1024
1025
- [93] J. Takaya, S. Kusunoki, and Y. Ishimi, "Protein interaction and cellular localization of human CDC45," *J. Biochem.*, vol. 153, no. 4, pp. 381–388, Apr. 2013, doi: 10.1093/JB/MVT004. 1026
1027
- [94] Y. S. Seo and Y. H. Kang, "The Human Replicative Helicase, the CMG Complex, as a Target for Anti-cancer Therapy," *Front. Mol. Biosci.*, vol. 5, no. MAR, p. 26, Mar. 2018, doi: 10.3389/FMOLB.2018.00026. 1028
1029

1030

12.3 Arbeit III

Pan- and isoform-specific inhibition of the bromodomain and extra-terminal proteins and evaluation of synergistic potential with entospletinib in canine lymphoma

Kong W., **Sender S.**, Perez SV., Sekora A., Ruetgen B., Junghanss C., Nolte I., Murua Escobar H.

Anticancer Res. 2020 Jul;40(7):3781-3792.
Impact Factor 2019: 1.940

Pan- and Isoform-specific Inhibition of the Bromodomain and Extra-terminal Proteins and Evaluation of Synergistic Potential With Entospletinib in Canine Lymphoma

WEIBO KONG^{1,2}, SINA SENDER¹, SIMON VILLA PEREZ¹, ANETT SEKORA¹, BARBARA RUETGEN³, CHRISTIAN JUNGHANSS¹, INGO NOLTE² and HUGO MURUA ESCOBAR^{1,2}

¹Department of Medicine, Clinic III, Hematology, Oncology and Palliative Medicine, University Medical Center Rostock, Rostock, Germany;

²Small Animal Clinic, University of Veterinary Medicine Hannover, Foundation, Hannover, Germany;

³Clinical Pathology Unit, University of Veterinary Medicine Vienna, Vienna, Austria

Abstract. *Background/Aim:* Canine B-cell lymphoma represents a useful *in vivo* model for human diffuse large B-cell lymphoma (DLBCL). Pan-Bromodomain and extra-terminal (BET) inhibition targeting BRD2/3/4 and selective inhibition of BRD4, as well as spleen tyrosine kinase (SYK) inhibition, are currently evaluated as haematologic cancer therapy. Herein, we characterized the differences in the biologic response of isoform-specific or pan-BET inhibition alone or in combination with SYK inhibition. *Materials and Methods:* I-BET151 (pan-inhibitor) and AZD5153 (BRD4 inhibitor) were combined with Entospletinib (SYK inhibitor) and comparatively analysed in the canine DLBCL cell line CLBL-1. Dose- and time-dependent cellular responses were analysed by cell number, metabolic activity, apoptosis/necrosis, and cell morphology. The synergistic potential was evaluated through the Bliss independence model. *Results:* I-BET151 and AZD5153 showed significant dose- and time-dependent inhibitory effects. Adding Entospletinib to I-BET151 or AZD5153 had no additional synergistic effects. *Conclusion:* Entospletinib did not enhance the inhibitory effects of the pan- or isoform-specific BET.

Diffuse large B-cell lymphoma (DLBCL) is one of the most common non-Hodgkin lymphomas in humans and dogs.

Correspondence to: Hugo Murua Escobar, Department of Medicine Clinic III, Hematology, Oncology and Palliative Medicine, Rostock University Medical Center, 18057 Rostock, Germany. Tel: +49 3814947519/7639, e-mail: hugo.murua.escobar@med.uni-rostock.de

Key Words: BCR, Bromodomain (BRD), BET inhibitor, SYK inhibitor, lymphoma, canine DLBCL.

Canine DLBCL shares many characteristics in terms of biology, treatment, and outcome with human DLBCL (1, 2). Further, counterparts of the common human DLBCL subtypes “germinal centre B-cell like” (GCB-DLBCL) and “activated B-cell like” can also be found in dogs but without clinical differences (3). Canine DLBCL is treated mainly with CHOP (cyclophosphamide, hydroxydaunorubicin, vincristine, prednisolone) (3, 4). Although 85–90 % of canine patients respond to treatment, almost in all cases the disease relapses and becomes resistant to therapy with a median survival time of 10-14 months (5).

In humans, the B-cell lymphoma 2 (*BCL2*) gene is located human chromosome 18 (HSA18) and the immunoglobulin (IG) locus on HSA14. Under normal conditions, *BCL2* protein is absent in most germinal centre B cells. In around 30% of human GCB-DLBCL, a translocation t(14;18) is present, bringing *BCL2* exons under the control of IG locus leading to an ectopic *BCL2* expression (6). Further, the IG locus also acts as a translocation partner of *MYC* (HSA8) resulting in a t(8;14) also causing *MYC* overexpression (7). In 5-10% of cases, human DLBCL shows chromosomal translocation affecting *MYC* and *BCL2* without causing fusion transcripts. This “double-hit” lymphoma molecular subtype can also be caused in the absence of chromosomal translocation through *BCL2* amplification, activation of NF- κ B transcription complex, and *MYC* amplification (8). In general, the “double-hit” molecular subtype shows poor outcomes with standard DLBCL chemotherapy (Rituximab +CHOP) and an aggressive course (9).

In canine DLBCL, *BCL2* and *MYC* expression can be observed showing comparable patterns to their human “double hit” lymphoma counterpart. However, immunohistochemical analyses showed that *BCL2* and *MYC* were not able to predict clinical outcome in dogs presenting an aggressive disease course (10).

In humans MYC akin to STAT, GATA, and NF- κ B (11) have been described to interact with the family of Bromodomain and extra-terminal (BET) proteins. The BET protein family including Bromodomain-containing protein 2 (BRD2), Bromodomain-containing protein 3 (BRD3), Bromodomain-containing protein 4 (BRD4), and Bromodomain testis-specific protein (BRDT) (12) act as epigenetic “readers”, identifying acetylated lysine on histones and recruiting transcriptional regulatory complexes (13). Their function is critical for adequate gene expression and cell cycle progression. The role of BET proteins in haematological malignancies has been confirmed by multiple selective inhibitors in lymphoma, leukaemia and multiple myeloma (14). To this date, there are no FDA approved BET inhibitors, but there are several ongoing clinical trials in different settings. Their ability to disrupt MYC function makes them an appealing target in DLBCL patients, both human and canine. Accordingly, pan-BET inhibitors targeting BRD2/3/4 (as I-BET151, OTX015, I-BET762, ABBV-075) and selective inhibitors targeting BRD4 (as AZD5153, CPI-0610, ABBV-744) have been tested in preclinical models and clinical trials against haematologic and solid cancers. I-BET151 (GSK1210151A) is a pan-BET inhibitor for BRD2, BRD3, BRD4 that binds BRD4 monovalently (15). AZD5153 is an isoform-specific BET inhibitor for BRD4 that markedly disrupts transcription of MYC, E2F and mTOR pathways (16). It is the first BET inhibitor to bind bivalently and ligate two bromodomains in BRD4 simultaneously (16). Transcriptome data from canine DLBCL shows overexpression of MYC (17) and it has been reported that the pan-BET inhibitor OTX015 targeting BRD4 monovalently blocks proliferation of CLBL-1 cells (18).

Tyrosine kinase inhibitors (TKIs) are therapeutic agents that target specifically a key kinase in a designated molecular pathway. In the case of lymphomas, this allows targeting specific proteins of the pathologically up-regulated pathways, as the BCR pathway (19). SYK appears to function as a prosurvival factor of pre-B cells in canine DLBCL (20). Novel agents as SYK inhibitors (Entospletinib, Fostamatinib, Cerdulatinib) show promising antineoplastic effects as new treatments of haematological malignancies (21). The selective SYK inhibitor Entospletinib has exhibited different rates of efficacy alone or in combination with other agents in clinical trials but it's not approved for clinical use yet (22, 23). There are currently no clinical trials that evaluate its use in canine DLBCL.

Due to the key roles of SYK and the available data on BET inhibition in different cancers, a combined application appears a potentially promising way to enhance the anti-tumorigenic effect. It has been described that BET and SYK inhibition separately have anti-proliferative effects through MYC regulation (24, 25). MYC, as common effector between the two pathways, classifies the combination of a BET

inhibitor with a SYK inhibitor as especially appealing. Further, a direct comparison between a pan- and specific-BET inhibitor could bear significant value in terms of latter side effect reduction. In the present study, we investigated the anti-proliferation effects of a pan-BET inhibitor (I-BET151), a selective-bivalent BRD4 BET inhibitor (AZD5153), and a SYK inhibitor (Entospletinib) in a canine DLBCL *in vitro* model (CLBL-1). Furthermore, we investigated whether the combination of Entospletinib with either I-BET151 or AZD5153 would have additional effects on proliferation inhibition and apoptosis/necrosis induction in CLBL-1.

Materials and Methods

Cell line and cell culture. The canine B-cell lymphoma cell line CLBL-1 was provided by the University of Veterinary Medicine, Vienna, Austria. CLBL-1 was derived from a male Bernese mountain dog, which was diagnosed with stage IV diffuse large cell lymphoma. Cells were maintained as suspension cultures in RPMI-1640 medium, supplemented with 20% heat-inactivated fetal bovine serum, and 100 U/ml penicillin/0.1 mg/ml streptomycin (Biochrom GmbH, Berlin, Germany) at 37°C in a humidified atmosphere containing 5% CO₂. The doubling time of CLBL-1 has been described earlier to be 31 h (26).

Inhibitors. Entospletinib (Ento), I-BET151 (IBET), and AZD5153 (AZD) were purchased from Selleck Chemicals (Absource Diagnostics GmbH, München, Germany). According to the manufacturer's information, the substances were dissolved in dimethyl sulfoxide (DMSO, Sigma Aldrich Chemie GmbH, Steinheim, Germany). The stock solutions (10 mM) were stored at -80°C and working solutions were freshly prepared.

Mono application of I-BET151, AZD5153, and Entospletinib. Cells were seeded at a density of 0.33×10⁶ cells/ml in 24 and 96-well plates for all cell biologic parameters (proliferation, metabolic activity, and apoptosis/necrosis assay). The cells were separately incubated with serial end-concentrations of I-BET151, AZD5153 (0.001, 0.01, 0.1, 0.5, 1, 2.5, 5, 10 μM) or of Entospletinib (0.001, 0.01, 0.1, 0.5, 1, 3.4, 5, 10 μM) for 24, 48 and 72 h in the mono-application setup. All experiments were performed in at least three biologically independent replicates.

Identification of IC₅₀. According to the number of the living cells for the 72-h group, IC₅₀ values of I-BET151, AZD5153, and Entospletinib were calculated through Graph Pad Prism Version 8.0.2. The concentrations and cell numbers were log-transformed and normalized. Afterwards, nonlinear regression (dose-response-inhibition, log vs. normalized response - variable slope) was used to determine the IC₅₀ values. Concerning the concentrations lower than IC₅₀ values, 0.75 μM I-BET151, 0.05 μM AZD5153, and 1 μM Entospletinib were selected for the combined application setup.

Combined application of BET inhibitors and Entospletinib. In the combined application setup, cells were seeded at a density of 0.33×10⁶ cells/ml in 24- and 96-well plates for all cell biologic parameters (proliferation, metabolic activity, and apoptosis/necrosis assay). For these experiments, the cells were separately incubated

with 1 μM Entospletinib, 0.75 μM I-BET151, 0.05 μM AZD5153, and their combinations (Ento+IBET, Ento+AZD) for 72 h. Besides that, the cells treated with the same inhibitor setups for 24, 48, and 72 h, were examined for changes in morphology. In the control groups, the DMSO-containing medium was added in the same volume as to the drug-treated cells. DMSO concentrations of control groups in single and combined applications were both 0.1% (v/v).

Cell counting analysis. CLBL-1 cells were seeded in the 24-well plate, 0.5×10^6 cells were exposed to inhibitor or vehicle in a total of 1,500 μl per well. After mono- (24, 48, and 72 h) or combined (72 h) inhibitor exposure, cells were harvested and washed by PBS. The viable cell number was assessed by counting with a hemocytometer and trypan blue live-dead staining (Sigma-Aldrich Chemie GmbH, Steinheim, Germany).

Metabolic activity assay. CLBL-1 cells seeded in the 96-well plate at a density of 0.05×10^6 cells were exposed to the respective inhibitor or vehicle in a total of 150 μl per well. After mono- (24, 48, and 72 h) or combined (72 h) inhibitor exposure, 15 μl pre-warmed WST-1 reagent (TaKaRa Bio Inc., Kusatsu, Japan) was added into 150 μl cell suspension as well as medium control. The mixture was incubated at 37°C for 2 h. The absorbance at 450 nm and a reference wavelength at 750 nm was detected by Promega GloMax[®]-Multi Microplate Multimode Reader (Promega, Madison, WI, USA). The absorbance value of the reference wavelength was subtracted from that of the corresponding sample wavelength. Then the blank value was subtracted from the difference, and the result was correlated to the metabolic activity of viable cells.

Early apoptosis and late apoptosis/necrosis measurement. After mono- (24-, 48-, and 72 h) or combined (72 h) inhibitor exposure, CLBL-1 cells were harvested, centrifuged ($180 \times g$, 10 min, 4°C) and washed with PBS twice. Then, the cell pellet was resuspended using 100 μl 1 \times Annexin binding buffer, which was diluted from 10 \times Annexin binding buffer (Becton, Dickinson and Company, Heidelberg, Germany). The cells were incubated with 5 μl Annexin V FITC (Becton, Dickinson and Company, Heidelberg, Germany) for 15 min at room temperature in the dark. The cell suspension was adjusted to a final volume of 500 μl with Annexin binding buffer. Immediately before measurement cells were stained with 20 $\mu\text{g}/\text{ml}$ Propidium iodide (PI) solution (1.0 mg/ml, Sigma Aldrich, St. Louis, MO, USA). In each experiment, unstained and single stained cells were included. Measurement was performed on a BD FACS Verse[™] flow cytometer and data analysis was carried out using BD FACSuite[™] software (Becton, Dickinson and Company). Early apoptosis (AnnexinV+/PI-) and late apoptosis/necrosis (AnnexinV+/PI+) are combined as apoptosis/necrosis.

Bliss independence model. Synergistic, additive, or antagonistic effects of the combined drugs were determined by the Bliss independence model, which uses the difference (Δ) between the observed (O) and the expected (E) inhibition of the combined treatment. E was calculated as follows: $E=(A+B) - (A*B)$, where A and B were the relative inhibition rates of the two inhibitors. $\Delta > 0$ indicating synergistic, and $\Delta < 0$ antagonistic effects (27, 28). Based on the data of viable cell number and metabolic activity in the combined application, the bliss values of the combined inhibitors (Ento+IBET, Ento+AZD) were calculated. For calculation, the mean value from three independent experiments was used.

Examination of cell morphology. CLBL-1 cells were incubated with 1 μM Entospletinib, 0.75 μM I-BET151, 0.05 μM AZD5153 and their combination (Ento+IBET, Ento+AZD) for 24, 48 and 72 h. After harvesting the cells, the standard procedure was performed to prepare cytopins, 3 glass slides for each sample. The concentration was adjusted to 5×10^4 in 200 μl PBS per slide. The slides were centrifuged in the Shandon Cytospin 3 Centrifuge (Shandon, Frankfurt/Main, Germany). The air-dried slides were stained with May-Grünwald solution (Merck, Darmstadt, Germany) for 6 min, washed with buffer (pH=7.2), then stained with Giemsa solution (1:10, Merck) for 20 min, and washed with buffer again. After Pappenheim staining, these slides were examined and visualized with Evos XL Core Imaging System (Life Technologies, Darmstadt, Germany), magnified 100 times.

Statistical analysis. Every experiment was repeated independently at least three times. Results of viable cells, metabolic activity, and apoptosis/necrosis are shown as mean value \pm standard deviation. Significance of difference between the inhibitor exposure and control group was determined using the two-tailed Student's *t*-test. *p*-Values < 0.05 were considered to be significant, **p* < 0.05 , ***p* < 0.01 , ****p* < 0.001 .

Results

Effects of I-BET151, AZD5153 or Entospletinib on CLBL-1 cell proliferation and metabolic activity. I-BET151 inhibited proliferation and metabolic activity significantly in a dose-dependent effect at all time points (Figure 1A and B). The inhibitory effects on proliferation were significant starting at 5 μM in the 24-h group, at 1 μM in the 48- and 72-h groups. The inhibitory effects on metabolic activity were significant starting at 0.5 μM in the 24- and 48-h groups, and at 0.001 μM in the 72-h group. When CLBL-1 cells were incubated with 10 μM I-BET151 for 72 h, cell proliferation and metabolic activity decreased the most, as low as $0.5 \pm 0.1\%$ and $2.6 \pm 0.7\%$, respectively. The IC₅₀ value of I-BET151 was 0.971 μM , and 0.75 μM were selected for the concentration of I-BET151 in the combined application experiment.

AZD5153 inhibited proliferation and metabolic activity with a significant dose-dependent effect at all time points (Figure 1C and D). The inhibitory effects on proliferation were significant starting at 0.5 μM in the 24-h group, at 0.1 μM in the 48- and 72-h groups. The inhibitory effects on metabolic activity were significant starting at 0.01 μM in the 24- and 48-h groups, and at 0.1 μM in the 72-h group. When CLBL-1 cells were incubated with 10 μM AZD5153 for 72 h, cell proliferation and metabolic activity decreased the most, as low as $0.1 \pm 0.1\%$ and $2.5 \pm 0.6\%$, respectively. The IC₅₀ value of AZD5153 was 0.073 μM , and 0.05 μM were selected for the concentration of AZD5153 in the combined application experiment.

In the 24-, 48-, and 72-h groups, Entospletinib inhibited neither proliferation nor metabolic activity under the tested conditions in CLBL-1 (Figure 1E and F). Since the concentrations of Entospletinib in the mono-application did

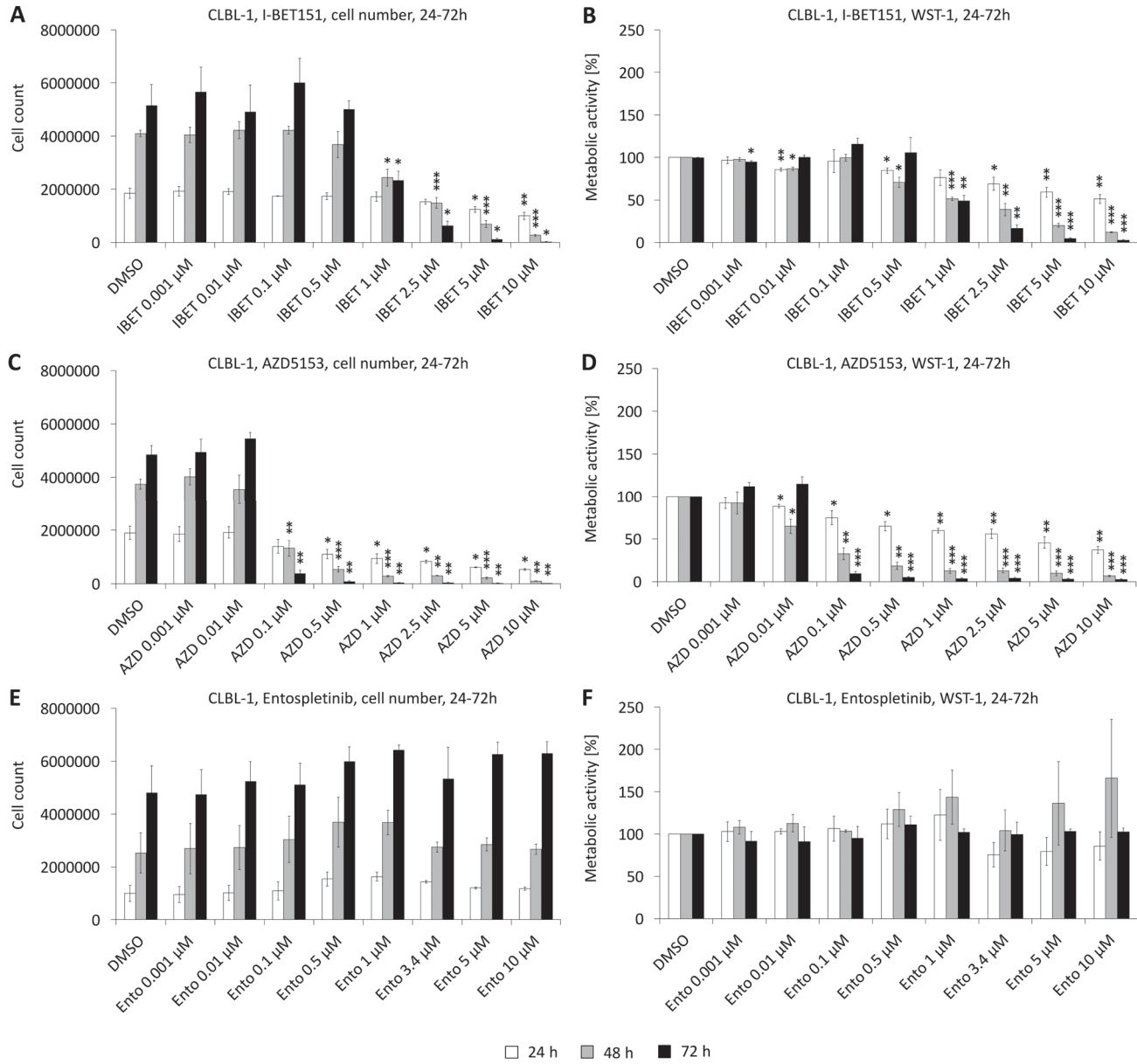


Figure 1. Bar plots for CLBL-1 cell line exposed to I-BET151, AZD5153, or Entospletinib as monotherapy at various concentrations (0.001-10 μM) for 24, 48, and 72 h measuring cell count and metabolic activity. (A), Cell count in CLBL-1 exposed to I-BET151 at different time points. (B), Metabolic activity measured by WST-1 in CLBL-1 exposed to I-BET151 at different time points. (C), Cell count in CLBL-1 exposed to AZD5153 at different time points. (D), Metabolic activity measured by WST-1 in CLBL-1 exposed to AZD5153 at different time points. (E), Cell count in CLBL-1 exposed to Entospletinib at different time points. (F), Metabolic activity measured by WST-1 in CLBL-1 exposed to Entospletinib at different time points. The results of metabolic activity were indicated as the percentage compared to the DMSO-treated cells. The figures display the average value (±SD) of three independent experiments. The significance of the treatment effect compared to the control was calculated as a p-value using the student's t-Test. *p<0.05, **p<0.01, ***p<0.001.

not show antiproliferative effect, the IC₅₀ value was not calculated. Nevertheless, 1 μM Entospletinib was selected for the combined application experiment to evaluate if Entospletinib can synergistically induce an anti-proliferative effect in combination with BET inhibition.

Both I-BET151 and AZD5153 induce early apoptosis and late apoptosis/necrosis of CLBL-1. I-BET151 concentrations above 0.5 μM significantly induced early apoptosis and late apoptosis/necrosis in a dose-dependent manner at 48- and 72-h groups (Figure 2A). Compared to

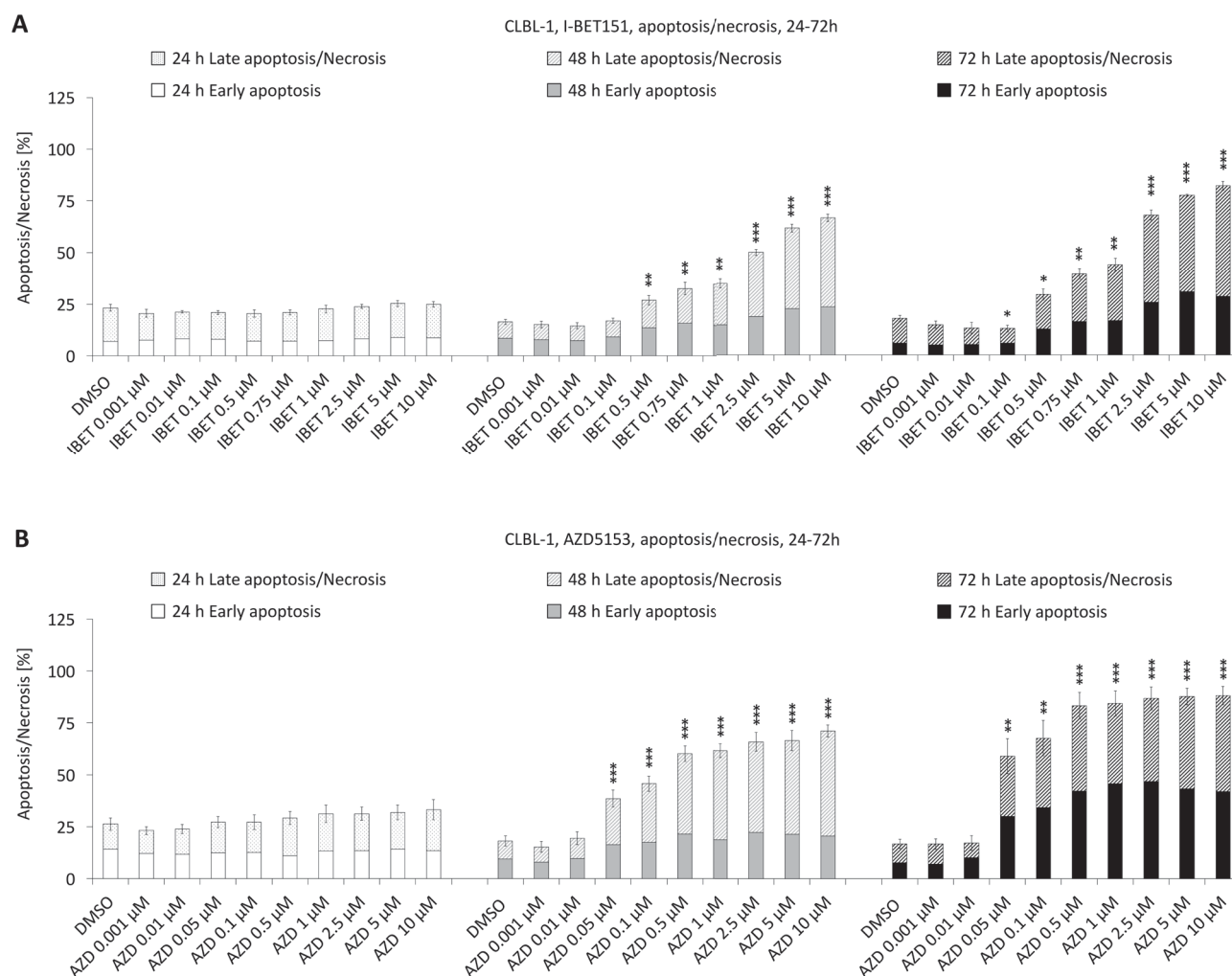


Figure 2. Apoptosis and necrosis of CLBL-1 induced by I-BET151 or AZD5153 (0.001-10 μ M) for 24, 48 and 72 h. Early apoptosis (Annexin V⁺/PI⁻) and late apoptosis/necrosis (Annexin V⁺/PI⁺), were analysed through flow cytometry stained by Annexin V and PI. Rates of cell apoptosis/necrosis (Annexin V⁺/PI) were determined and displayed as the mean \pm standard deviation of three independent measurements. (A), I-BET151 resulted in the rate of early apoptosis and late apoptosis/necrosis. (B), AZD5153 resulted in the rate of early apoptosis and late apoptosis/necrosis. The significance of difference between the control and apoptosis/necrosis was calculated as a *p*-value using the student's *t*-Test. **p*<0.05, ***p*<0.01, ****p*<0.001.

the control, I-BET151 significantly increased early apoptosis and late apoptosis/necrosis from 16.5 \pm 1.3% up to a maximum of 66.8 \pm 1.8% in the 48-h group, and from 17.8 \pm 1.5% up to a maximum of 82.3 \pm 2.2% in the 72-h group.

AZD5153 concentrations above 0.05 μ M significantly induced early apoptosis and late apoptosis/necrosis in a dose-dependent manner in 48- and 72-h groups (Figure 2B). Compared to the control, AZD5153 significantly increased early apoptosis and late apoptosis/necrosis from 18.2 \pm 2.4% up to a maximum of 71.3 \pm 2.9% in the 48-h group, and from 16.9 \pm 2.3% up to a maximum of 88.3 \pm 4.5% in the 72-h group.

I-BET151 and AZD5153 exposure induces morphological changes in CLBL-1 cells. In the DMSO control group, the CLBL-1 cells aggregated and had intact cell membranes, and, occasionally, vacuoles were apparent. After being exposed to Entospletinib and/or BET inhibitors for 24, 48, and 72 h, the integrity of most cells was disrupted. Apoptotic and necrotic phenomena were observed in the inhibitor group (Figures 5 and 6). A large number of abnormal cells and cell debris could be observed. Further, cytoplasmic blebs, condensed chromatin, cell fragmentation, rupture plasma membrane and nucleus, nuclear and cytoplasmic vacuolisation, and apoptotic bodies could be detected.

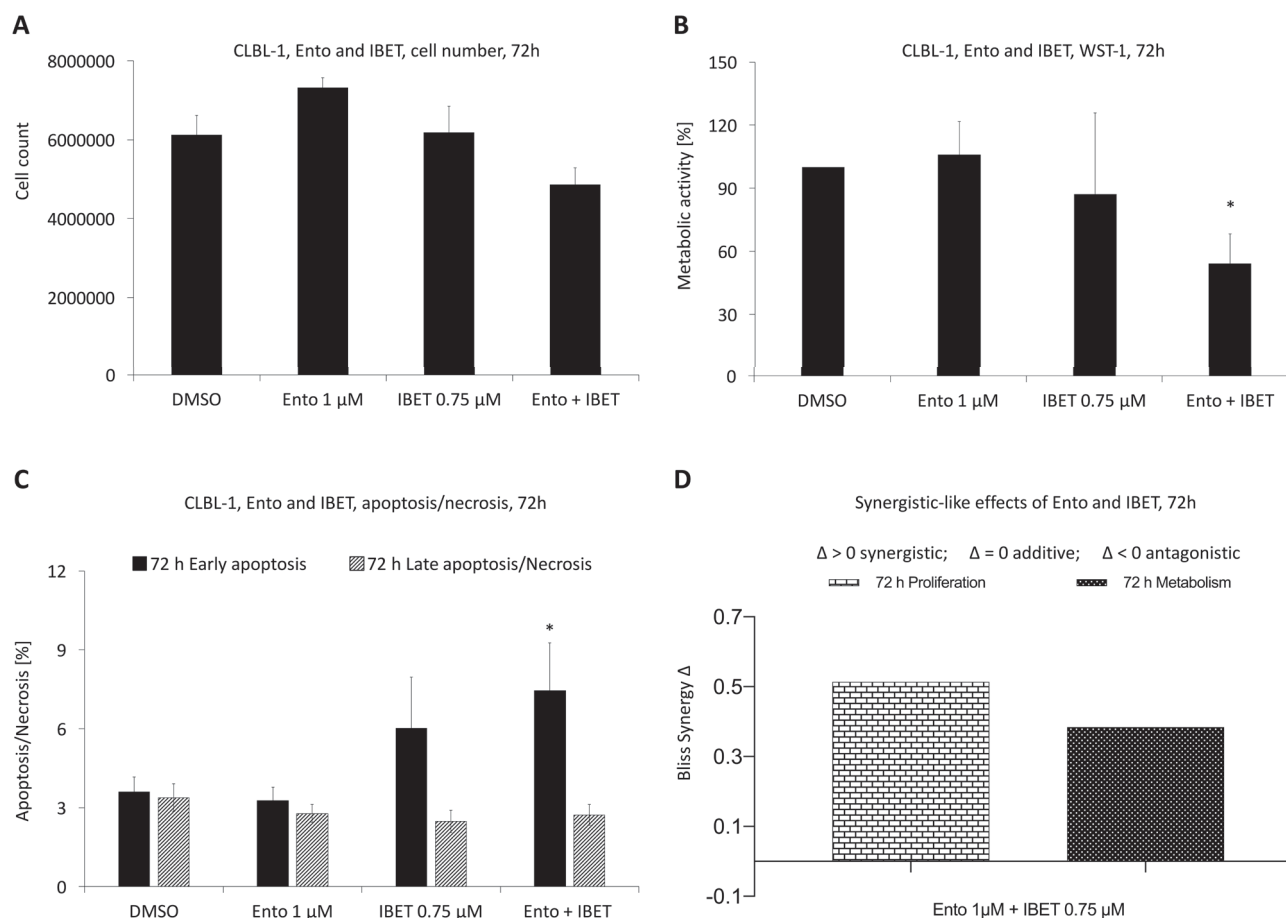


Figure 3. CLBL-1 incubated with I-BET151 (0.75 μM) or/and Entospletinib (1 μM) for 72 h. (A), The proliferation of CLBL-1 was determined by counting the number of cells. (B), The metabolic activity of CLBL-1 was decided by WST-1 assay, indicated as the percentage compared to the DMSO-treated cells. (C), The inhibitors resulted in the rate of early apoptosis and late apoptosis/necrosis. (D), The Bliss independence model was calculated based on the 72-hour proliferation and metabolic activity of the combined inhibitors. If $\Delta > 0$, then synergistic; $\Delta = 0$, additive; $\Delta < 0$, antagonistic. The results were displayed as the average value (\pm SD) of three independent experiments. The significance of difference between the control and treatment was calculated as a p-value using the student's t-Test. * $p < 0.05$, ** $p < 0.01$, *** $p < 0.001$.

Combined application of pan-BET inhibitor I-BET151 and Entospletinib does not significantly enhance inhibition of CLBL-1 proliferation and metabolic activity. Compared to the DMSO control or I-BET151, the exposure to the combination of I-BET151 and Entospletinib did not significantly enhance CLBL-1 proliferation inhibition (Figure 3A). Cell exposure to the combination of 1 μM Entospletinib and 0.75 μM I-BET151 reduced the proportion of living cells to $80.3 \pm 5.5\%$ ($p = 0.057$).

Further, compared to the control, the exposure to the combined 1 μM Entospletinib and 0.75 μM I-BET151 significantly inhibited metabolic activity in CLBL-1 cells, reducing the proportion of metabolic activity to $54.2 \pm 14.2\%$ (Figure 3B). When cells were incubated with either 1 μM Entospletinib or 0.75 μM I-BET151 for 72 h, the proportions

of metabolic activity compared to the DMSO control were $106 \pm 15.6\%$ and $87.3 \pm 38.5\%$, respectively. There was no significant difference between the effect of I-BET151 alone and combined application (IBET+Ento) on the metabolic activity ($p = 0.35$).

Combined application of isoform-specific AZD5153 and Entospletinib does not significantly enhance inhibition of CLBL-1 cell proliferation and metabolic activity. Compared to the DMSO control, the exposure to the combined AZD5153 and Entospletinib significantly inhibited proliferation and metabolic activity in CLBL-1 (Figure 4A and B). But there was no significant difference between mono and combined application with AZD5153. When cells were incubated for 72 h with either 1 μM Entospletinib or

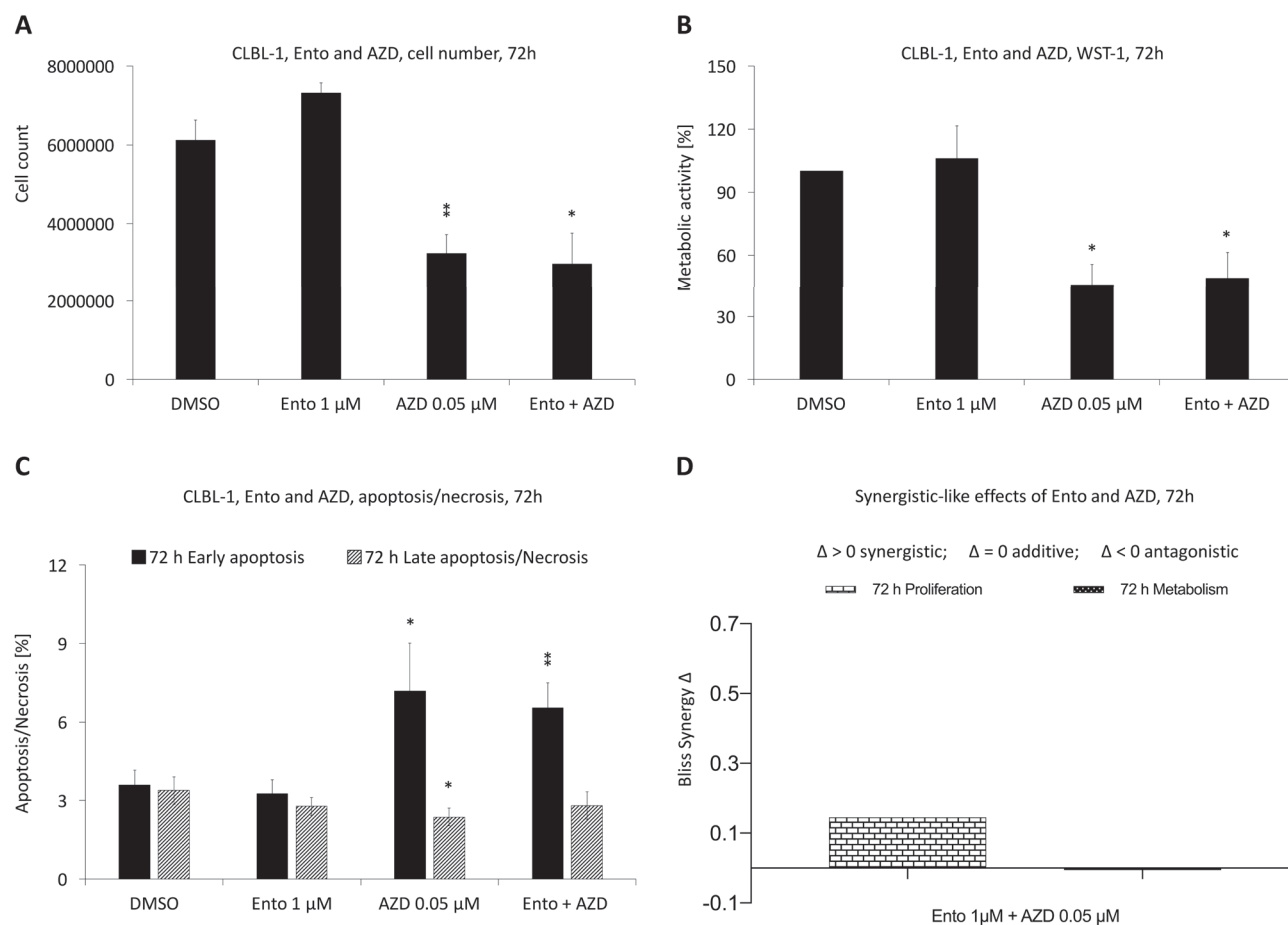


Figure 4. CLBL-1 incubated with AZD5153 (0.05 μ M) or/and Entospletinib (1 μ M) for 72 h. (A), The proliferation of CLBL-1 was determined by counting the number of cells. (B), The metabolic activity of CLBL-1 was decided by WST-1 assay, indicated as the percentage compared to the DMSO-treated cells. (C), The inhibitors resulted in the rate of early apoptosis and late apoptosis/necrosis. (D), The Bliss independence model was calculated based on the 72-h proliferation and metabolic activity of the combined inhibitors. If $\Delta > 0$, then synergistic; $\Delta = 0$, additive; $\Delta < 0$, antagonistic. The results were displayed as the average value (\pm SD) of three independent experiments. The significance of difference between the control and treatment was calculated as a *p*-value using the student's *t*-Test. **p*<0.05, ***p*<0.01, ****p*<0.001.

0.05 μ M AZD5153, the proportions of living cells compared to the DMSO control were $122.2 \pm 7.2\%$ and $52.8 \pm 6\%$, respectively. When incubated with the combination of 1 μ M Entospletinib and 0.05 μ M AZD5153, the proportion of living cells was $50 \pm 17.5\%$.

Further, when cells were incubated for 72 h with either 1 μ M Entospletinib or 0.05 μ M AZD5153, the proportions of metabolic activity compared to the DMSO control were $106 \pm 15.6\%$ and $45.7 \pm 10\%$, respectively. When incubated with the combination of 1 μ M Entospletinib and 0.05 μ M AZD5153, the proportion of metabolic activity was $49 \pm 12.5\%$.

Combined application of isoform-specific or pan-BET inhibitors and Entospletinib does not significantly enhance induction early apoptosis and late apoptosis/necrosis of

CLBL-1 cell. Compared to the DMSO control, the exposure to the combination of BET inhibitors and Entospletinib significantly increased early apoptosis of CLBL-1. But there was no significant difference between the application of BET inhibitor (I-BET151 and AZD5153) alone and the combinations (IBET+Ento, IBET+AZD) in the effect on early apoptosis and late apoptosis/necrosis (Figures 3C and 4C). When CLBL-1 cells were separately incubated with DMSO, Entospletinib (1 μ M), I-BET151 (0.75 μ M), and AZD5153 (0.05 μ M) for 72 h, the proportions of early apoptosis were $3.6 \pm 0.6\%$, $3.3 \pm 0.5\%$, $6 \pm 1.9\%$, and $7.2 \pm 1.8\%$, respectively. And the percentage of late apoptosis/necrosis were $3.4 \pm 0.5\%$, $2.8 \pm 0.3\%$, $2.5 \pm 0.4\%$, and $2.4 \pm 0.3\%$, respectively. When CLBL-1 cells were incubated with combined inhibitors (IBET+Ento, AZD+Ento), the proportions of early apoptosis

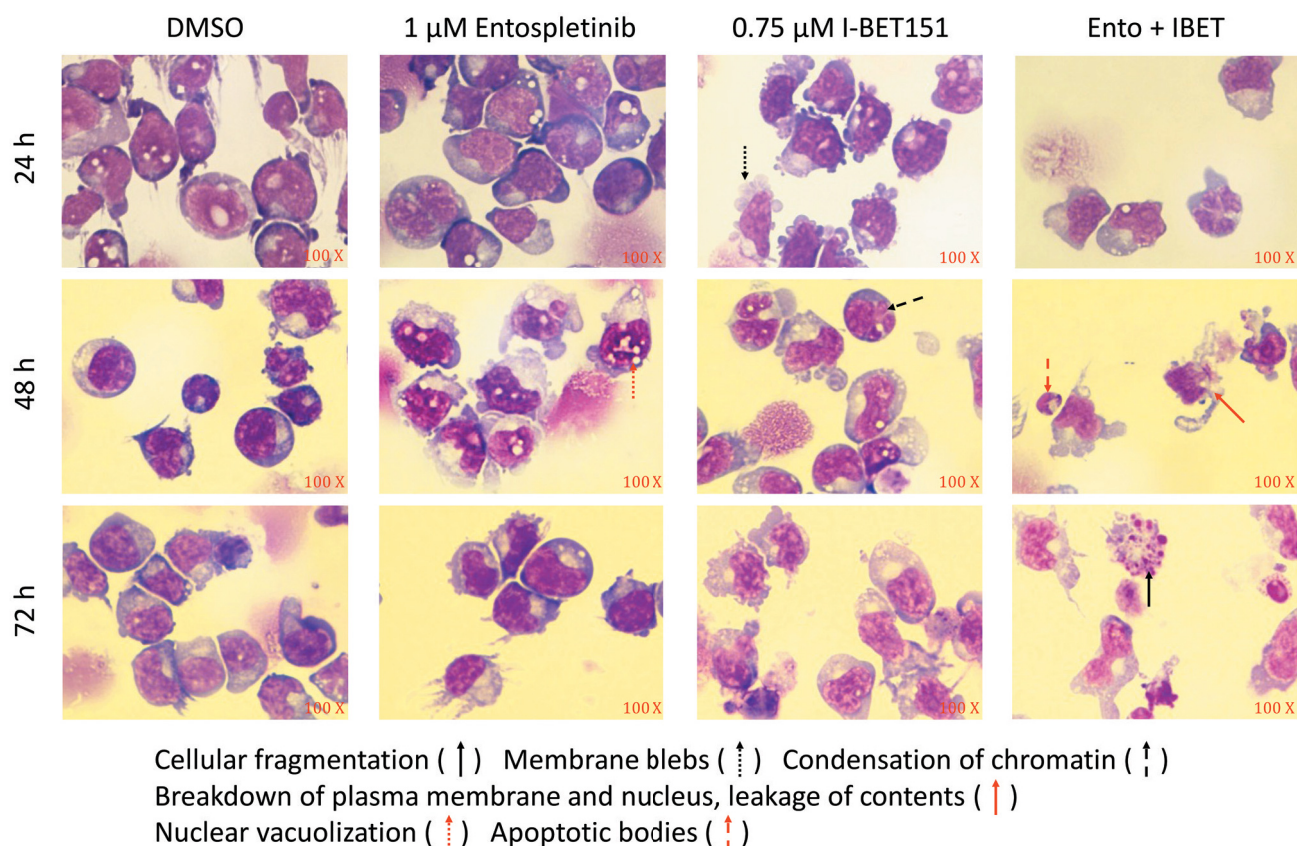


Figure 5. The CLBL-1 was incubated with DMSO, 1 μM Entospletinib, 0.75 μM I-BET151, and their combination for 24, 48, and 72 h. The stained cytopins were magnified 100 times. As exhibited by the apoptotic/necrotic phenomena in the treatment group, cellular fragmentation (black solid arrow), membrane blebs (black round-dot arrow), condensation of chromatin (black dash arrow), breakdown of plasma membrane and nucleus, leakage of contents (red solid arrow), nuclear vacuolization (red round-dot arrow) and apoptotic bodies (red dash arrow) were visualized.

were $7.4 \pm 1.8\%$ and $6.5 \pm 1\%$. And the proportions of late apoptosis/necrosis were $2.7 \pm 0.4\%$ and $2.8 \pm 0.5\%$.

Bliss value analysis. Mathematical evaluation of the synergistic potential revealed for all proliferation experiments a BLISS value above 0. The combination of I-BET151 (0.75 μM) and Entospletinib (1 μM) revealed values above 0 (Figure 3D), as well as that of AZD5153 (0.05 μM) and Entospletinib (1 μM). Concerning the corresponding analyses for metabolic activity, the combination of IBET+Ento ranged above 0 and the combination of AZD+Ento below 0 (Figure 4D). The calculated bliss values of the proliferation showed differences (Δ) between observed and expected values of 0.5141 for the combination IBET+Ento and 0.1451 for the combination AZD+Ento. Furthermore, the calculated bliss values of the metabolic activity showed that the differences (Δ) between observed and expected values were 0.3839 for the combination IBET+Ento and -0.0055 for the combination AZD+Ento.

Discussion

BET inhibition has been reported to have antineoplastic effects on lymphoma models (14, 16, 29). Different types of BET inhibition (Pan or selective) have not been assessed in combination with SYK inhibitors to evaluate respective synergistic potential. In the present study, we evaluated whether combining a SYK inhibitor (Entospletinib) with a pan-BET inhibitor (I-BET151) or a selective bivalent BRD4 BET inhibitor (AZD5153) resulted in synergistic effects. BET and SYK inhibition, especially BRD4 inhibition, have anti-proliferative effects through MYC regulation (24, 25). AZD5153 as mono-therapy has been compared with non-selective BET inhibitors in preclinical human acute myeloid leukaemia (AML), multiple myeloma (MM), and DLBCL models showing higher inhibitory effects (16). However, the combination of the SYK inhibitor Entospletinib with selective or pan-BET inhibitors has not been evaluated. Up to 10% of human DLBCL express concurrently

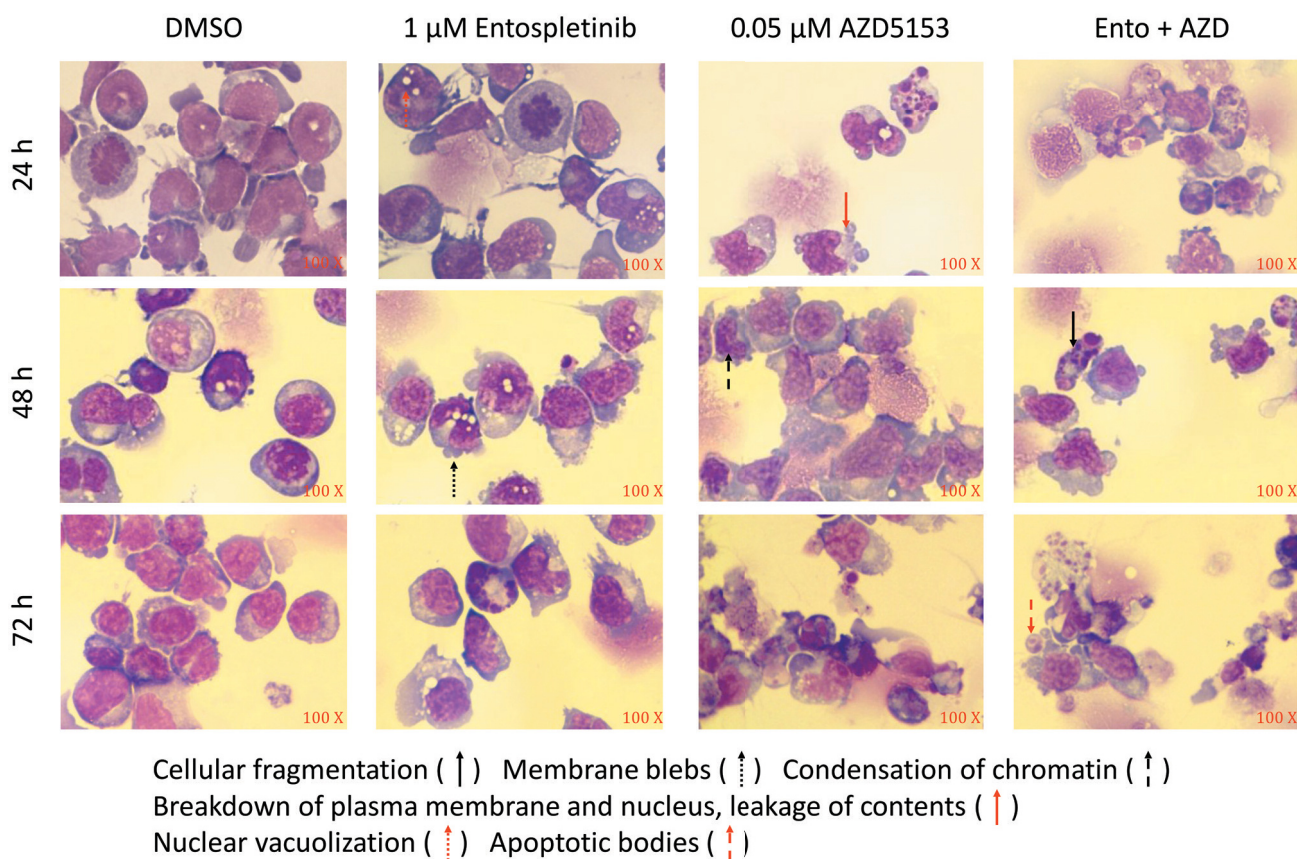


Figure 6. The CLBL-1 was incubated with DMSO, 1 μM Entospletinib, 0.05 μM AZD5153, and their combination for 24, 48, and 72 h. The stained cytopins were magnified 100 times. As exhibited by the apoptotic/necrotic phenomena in the treatment group, cellular fragmentation (black solid arrow), membrane blebs (black round-dot arrow), condensation of chromatin (black dash arrow), breakdown of plasma membrane and nucleus, leakage of contents (red solid arrow), nuclear vacuolization (red round-dot arrow) and apoptotic bodies (red dash arrow) were visualized.

rearrangements of BCL2 and MYC through coexisting translocations in the IG locus, also known as “double-hit lymphomas” (30). Data on the characterization of corresponding chromosomal rearrangements in dogs are rare due to the complicated canine karyotype. However, previous data from our group have revealed that the herein used CLBL-1 cell line shows overexpression of BCL2 and MYC DLBCL (17). The use of BET inhibitors could be of particular interest in patients with BCL2 and MYC rearrangements, as one of their main effects is lowering MYC activation (24, 31). SYK inhibition has shown promising results against lymphoma cell lines (32). Preclinical studies using Entospletinib have reported activity mainly against chronic lymphocytic leukaemia (CLL) and non-Hodgkin Lymphoma cell lines (33, 34). Patient-derived xenograft (PDX) models using DLBCL cell lines show a strong reduction in proliferation in BCR dependent cell lines (35). Our results showed that CLBL-1 cell line growth is not inhibited by Entospletinib mono- application independently

of time and concentration. The observed changes in cell morphology showed the presence of membrane blebs and nuclear vacuolization in the 48-72 h time points without compromising cell viability. But both pan- and isoform-specific BET inhibitors showed significant cell number reduction, apoptotic effects, and morphologic changes as single agents, especially AZD5153. The antiproliferative effect of AZD5153 (72 h, IC_{50} =0.054 μM) is 16 folds stronger than I-BET151 (72 h, IC_{50} =0.870 μM). In the combination setting there were no statistically significant differences after adding Entospletinib to either I-BET151 or AZD5153. The combination of I-BET151 and Entospletinib had a tendency to produce a reduction in cell number and metabolism, and higher apoptosis than I-BET151 alone at 72 h but remained not significant. Similar to I-BET151, no difference was noted with the use of AZD5153 as monotherapy or in combination with Entospletinib.

There are multiple reports of BET inhibitor assays in human haematological cell lines that show the inhibition of

cell growth (36). AZD5153, which has a bivalent binding mode to BRD4, has been compared to non-selective BET inhibitors, such as I-BET762, and was found to have 18-fold lower IC₅₀ (16). In our study, we also showed that AZD5153 is more potent than the pan I-BET151 on the CLBL-1 cell line, probably due to its dual point inhibition on BRD4.

The CLBL-1 cell line was resistant to Entospletinib mono application and Entospletinib showed no synergistic effects when added together with BET inhibitors. Preclinical studies in human AML show that hyperactivation of the RAS-MEK-ERK signalling pathway correlates with SYK inhibition resistance, especially through mutations in RAS and PTPN11 (37). Activation of RAS or PI3K pathways could also explain the resistance of CLBL-1 cells to Entospletinib.

A preclinical study has reported the modulatory effects of AZD5153 over the MYC and mTOR pathway in different haematological cell lines. The down-regulation of MYC was independent of the AZD5153 apoptotic effect (16). However, data generated in “double-hit” lymphoma *in vitro* models failed to show the down-regulation of BCL2 in cell lines overexpressing both MYC and BCL2 following exposure to AZD5153 (31). This could suggest that the effect of AZD5153 on CLBL-1 is also independent on BCL2 regulation. Previous data from our group have shown that the CLBL-1 cell line, as well as a set of primary B-cell lymphomas, overexpress MYC, INPP5D, and BCL2 compared to non-neoplastic lymph nodes (17). Further, CLBL-1 showed discrete overexpression of mTOR and strong down-regulation of PTEN in comparison to a primary lymphoma set and non-neoplastic lymph nodes (17), making this model similar in molecular characteristics with most of the canine DLBCL and “double-hit” human DLBCL. These dysregulations potentially result in activation of the BCR pathway downstream from SYK, explaining the resistance to Entospletinib but sensitivity to BET inhibitors.

In summary, data regarding the use of SYK or BET inhibitor in dogs is limited. Due to the observed expression pattern of MYC and BCL2 in canine lymphoma, it bears potential as a model for “double-hit” human lymphoma, a disease with aggressive behaviour where new therapeutic approaches are needed. To our knowledge, there are no clinical trials that evaluated BET or SYK inhibitors on canine lymphoma. The pharmacologic synergy between pan- or selective BET inhibitors and Entospletinib has not been assessed before. The present data suggests that BRD4 selective BET inhibition could be a useful approach against canine DLBCL.

In CLBL-1 cells, the BCR pathway appears to have hyperactivated effectors, such as RASGRP3, downstream from SYK (17). Therefore, the hyperactivation of downstream effectors will be independent of SYK inhibition, leading potentially to resistance to Entospletinib. Our results provide valuable data for a further evaluation of selective

BET inhibitors such as AZD5153 in an *in vivo* canine lymphoma model, potentially bearing significant value for human clinical trials in the future.

Conclusion

Pan-BET inhibitor I-BET151 and isoform-specific AZD5153 applied alone inhibit proliferation and induce apoptosis/necrosis of CLBL-1 cells at low concentrations. CLBL-1 cells are resistant to Entospletinib. The combination of Entospletinib with I-BET151 or AZD5153 does not significantly enhance inhibition of proliferation and induction of apoptosis/necrosis in CLBL-1 cells.

Conflicts of Interest

The Authors declare that they have no conflicts of interests with regard to this study.

Authors' Contributions

WK performed *in vitro* work packages, data analysis and partially drafted the manuscript. SS participated study design, supervision *in vitro* work, participated in data analysis, partial manuscript proofreading. SVP participated in data analysis and manuscript drafting. AS partial *in vitro* work and data analysis. BR provided CLBL-1, data interpretation morphology. CJ partial study design, edited and approved the manuscript. IN participated in study designing, edited and approved the final manuscript. HME principal study design, coordinated and supervised all work packages, partial manuscript drafting, and finalized the manuscript.

Acknowledgements

The Authors would like to acknowledge the financial support of the Chinese Scholarship Council (CSC) to Weibo Kong. The Authors also like to thank Dr. Carolin Gabler (Department of Medicine Clinic III, Hematology, Oncology and Palliative Medicine, Rostock University Medical Center, Germany) for assisting in proofreading and handling of the manuscript.

References

- 1 MacEwen EG: Spontaneous tumors in dogs and cats: Models for the study of cancer biology and treatment. *Cancer Metastasis Rev* 9(2): 125-136, 1990. PMID: 2253312. DOI: 10.1007/BF00046339
- 2 Zamani-Ahmadmhamudi M, Aghasharif S and Ilbeigi K: Prognostic efficacy of the human B-cell lymphoma prognostic genes in predicting disease-free survival (DFS) in the canine counterpart. *BMC Vet Res* 13(1): 17, 2017. PMID: 28069005. DOI: 10.1186/s12917-016-0919-x
- 3 Wolf-Ringwall A, Lopez L, Elmslie R, Fowler B, Lori J, Sfiligoi G, Skope A, Arnold E, Hughes KL, Thamm DH, Ehrhart EJ, Avery AC and Lana SE: Prospective evaluation of flow cytometric characteristics, histopathologic diagnosis and clinical outcome in dogs with naïve B-cell lymphoma treated with a 19-

- week CHOP protocol. *Vet Comp Oncol* 1-11, 2019. PMID: 31682319. DOI: 10.1111/vco.12553
- 4 Al-Nadaf S, Rebhun RB, Curran KM, Venable RO, Skorupski KA, Willcox JL and Burton JH: Retrospective analysis of doxorubicin and prednisone as first-line therapy for canine B-cell lymphoma. *BMC Vet Res* 14(1): 356, 2018. PMID: 30458771. DOI: 10.1186/s12917-018-1688-5
 - 5 Zandvliet M: Canine lymphoma: a review. *Vet Q* 36(2): 76-104, 2016. PMID: 26953614. DOI: 10.1080/01652176.2016.1152633
 - 6 Pasqualucci L and Dalla-Favera R: Genetics of diffuse large b-cell lymphoma. *Blood* 131(21): 2307-2319, 2018. PMID: 29666115. DOI: 10.1182/blood-2017-11-764332
 - 7 Riedell PA and Smith SM: Double hit and double expressors in lymphoma: Definition and treatment. *Cancer* 124(24): 4622-4632, 2018. PMID: 30252929. DOI: 10.1002/cncr.31646
 - 8 Burotto M, Berkovits A and Dunleavy K: Double hit lymphoma: From biology to therapeutic implications. *Expert Rev Hematol* 9(7): 669-678, 2016. PMID: 27166590. DOI: 10.1080/17474086.2016.1182858
 - 9 Horn H, Ziepert M, Becher C, Barth TFE, Bernd HW, Feller AC, Klapper W, Hummel M, Stein H, Hansmann ML, Schmelter C, Möller P, Cogliatti S, Pfreundschuh M, Schmitz N, Trümper L, Siebert R, Loeffler M, Rosenwald A and Ott G: MYC status in concert with BCL2 and BCL6 expression predicts outcome in diffuse large B-cell lymphoma. *Blood* 121(12): 2253-2263, 2013. PMID: 23335369. DOI: 10.1182/blood-2012-06-435842
 - 10 Curran KM, Schaffer PA, Frank CB, Lana SE, Hamil LE, Burton JH, Labadie J, Ehrhart EJ and Avery PR: BCL2 and MYC are expressed at high levels in canine diffuse large B-cell lymphoma but are not predictive for outcome in dogs treated with CHOP chemotherapy. *Vet Comp Oncol* 15(4): 1269-1279, 2017. PMID: 27514648. DOI: 10.1111/vco.12263
 - 11 Bechter O and Schöffski P: Make your best BET the emerging role of BET inhibitor treatment in malignant tumors. *Pharmacol Ther* 208: 107479, 2020. PMID: 31931101. DOI: 10.1016/j.pharmthera.2020.107479
 - 12 Cochran AG, Conery AR and Sims RJ: Bromodomains: a new target class for drug development. *Nat Rev Drug Discov* 18(8): 609-628, 2019. PMID: 31273347. DOI: 10.1038/s41573-019-0030-7
 - 13 Pervaiz M, Mishra P and Günther S: Bromodomain drug discovery – the past, the present, and the future. *Chem Rec* 18(12): 1808-1817, 2018. PMID: 30289209. DOI: 10.1002/tcr.201800074
 - 14 French CA: Small-molecule targeting of BET proteins in cancer. *Adv Cancer Res* 131: 21-58, 2016. PMID: 27451123. DOI: 10.1016/bs.acr.2016.04.001
 - 15 Dawson MA, Prinjha RK, Dittmann A, Giotopoulos G, Bantscheff M, Chan WI, Robson SC, Chung CW, Hopf C, Savitski MM, Huthmacher C, Gudgin E, Lugo D, Beinke S, Chapman TD, Roberts EJ, Soden PE, Auger KR, Mirguet O, Doehner K, Delwel R, Burnett AK, Jeffrey P, Drewes G, Lee K, Huntly BJP and Kouzarides T: Inhibition of BET recruitment to chromatin as an effective treatment for MLL-fusion leukaemia. *Nature* 478(7370): 529-533, 2011. PMID: 21964340. DOI: 10.1038/nature10509
 - 16 Rhyasen GW, Hattersley MM, Yao Y, Dulak A, Wang W, Petheruti P, Dale IL, Boiko S, Cheung T, Zhang J, Wen S, Castriotta L, Lawson D, Collins M, Bao L, Ahdesmaki MJ, Walker G, O'Connor G, Yeh TC, Rabow AA, Dry JR, Reimer C, Lyne P, Mills GB, Fawell SE, Waring MJ, Zinda M, Clark E and Chen H: AZD5153: A novel bivalent BET bromodomain inhibitor highly active against hematologic malignancies. *Mol Cancer Ther* 15(11): 2563-2574, 2016. PMID: 27573426. DOI: 10.1158/1535-7163.MCT-16-0141
 - 17 Taher L, Beck J, Liu W, Roof C, Soller JT, Rütgen BC, Hammer SE, Chodisetti M, Sender S, Sterenczak KA, Fuellen G, Junghanss C, Brenig B, Nolte I, Schütz E and Escobar HM: comparative high-resolution transcriptome sequencing of lymphoma cell lines and de novo lymphomas reveals cell-line-specific pathway dysregulation. *Sci Rep* 8(1): 6279, 2018. PMID: 29674676. DOI: 10.1038/s41598-018-23207-7
 - 18 Luca Aresu, Serena Ferrareso, Laura Marconato, Luciano Cascione, Sara Napoli, Eugenio Gaudio, Ivo Kwee, Chiara Tarantelli, Andrea Testa, Chiara Maniaci, Alessio Ciulli, Petra Hillmann, Thomas Bohnacker, Matthias P. Wymann, Stefano Comazzi, Massimo Milan, FB: New molecular and therapeutic insights into canine diffuse large B-cell lymphoma elucidates the role of the dog as a model for human disease. *Haematologica* 104(6): e256-e259, 2019. PMID: 30545928. DOI: 10.3324/haematol.2018.207027
 - 19 Wilson WH, Young RM, Schmitz R, Yang Y, Pittaluga S, Wright G, Lih CJ, Williams PM, Shaffer AL, Gerecitano J, de Vos S, Goy A, Kenkre VP, Barr PM, Blum KA, Shustov A, Advani R, Fowler NH, Vose JM, Elstrom RL, Habermann TM, Barrientos JC, McGreivy J, Fardis M, Chang BY, Clow F, Munneke B, Moussa D, Beaupre DM and Staudt LM: Targeting B cell receptor signaling with ibrutinib in diffuse large B cell lymphoma. *Nat Med* 21(8): 922-926, 2015. PMID: 26193343. DOI: 10.1038/nm.3884
 - 20 Wang WH, Childress MO and Geahlen RL: Syk interacts with and phosphorylates nucleolin to stabilize Bcl-xL mRNA and promote cell survival. *Mol Cell Biol* 34(20): 3788-3799, 2014. PMID: 25092868. DOI: 10.1128/MCB.00937-14
 - 21 Liu D and Mamorska-Dyga A: Syk inhibitors in clinical development for hematological malignancies. *Hematol Oncol* 10(1): 145, 2017. PMID: 28754125. DOI: 10.1186/s13045-017-0512-1
 - 22 Awan FT, Thirman MJ, Patel-Donnelly D, Assouline S, Rao AV, Ye W, Hill B and Sharman JP: Entospletinib monotherapy in patients with relapsed or refractory chronic lymphocytic leukemia previously treated with B-cell receptor inhibitors: results of a phase 2 study. *Leuk Lymphoma* 60(8): 1972-1977, 2019. PMID: 30633573. DOI: 10.1080/10428194.2018.1562180
 - 23 Andorsky DJ, Kolibaba KS, Assouline S, Forero-Torres A, Jones V, Klein LM, Patel-Donnelly D, Smith M, Ye W, Shi W, Yasenachak CA and Sharman JP: An open-label phase 2 trial of Entospletinib in indolent non-Hodgkin lymphoma and mantle cell lymphoma. *Br J Haematol* 184(2): 215-222, 2019. PMID: 30183069. DOI: 10.1111/bjh.15552
 - 24 Delmore JE, Issa GC, Lemieux ME, Rahl PB, Shi J, Jacobs HM, Kastritis E, Gilpatrick T, Paranal RM, Qi J, Chesi M, Schinzel AC, McKeown MR, Heffernan TP, Vakoc CR, Bergsagel PL, Ghobrial IM, Richardson PG, Young RA, Hahn WC, Anderson KC, Kung AL, Bradner JE and Mitsiades CS: BET bromodomain inhibition as a therapeutic strategy to target c-Myc. *Cell* 146(6): 904-917, 2011. PMID: 21889194. DOI: 10.1016/j.cell.2011.08.017
 - 25 Wang WG, Liu ZB, Jiang XN, Lee J, Zhou XY and Li XQ: MYC protein dysregulation is driven by BCR-PI3K signalling

- in diffuse large B-cell lymphoma. *Histopathology* 71(5): 778-785, 2017. PMID: 28639315. DOI: 10.1111/his.13287
- 26 Rütgen BC, Hammer SE, Gerner W, Christian M, de Arespachaga AG, Willmann M, Kleiter M, Schwendenwein I and Saalmüller A: Establishment and characterization of a novel canine B-cell line derived from a spontaneously occurring diffuse large cell lymphoma. *Leuk Res* 34(7): 932-938, 2010. PMID: 20153049. DOI: 10.1016/j.leukres.2010.01.021
- 27 Fouquier J and Guedj M: Analysis of drug combinations: current methodological landscape. *Pharmacol Res Perspect* 3(3): e00149, 2015. PMID: 26171228. DOI: 10.1002/prp2.149
- 28 Roof C, Richter A, Konkolefski C, Knuebel G, Sekora A, Krohn S, Stenzel J, Krause BJ, Vollmar B, Murua Escobar H and Junghans C: Decitabine demonstrates antileukemic activity in B cell precursor acute lymphoblastic leukemia with MLL rearrangements. *J Hematol Oncol* 11(1): 62, 2018. PMID: 29728108. DOI: 10.1186/s13045-018-0607-3
- 29 Dawson MA, Prinjha RK, Dittmann A, Giotopoulos G, Bantscheff M, Chan WI, Robson SC, Chung CW, Hopf C, Savitski MM, Huthmacher C, Gudgin E, Lugo D, Beinke S, Chapman TD, Roberts EJ, Soden PE, Auger KR, Mirguet O, Doehner K, Delwel R, Burnett AK, Jeffrey P, Drewes G, Lee K, Huntly BJP and Kouzarides T: Inhibition of BET recruitment to chromatin as an effective treatment for MLL-fusion leukaemia. *Nature* 478(7370): 529-533, 2011. PMID: 21964340. DOI: 10.1038/nature10509
- 30 Davies A: Double-hit lymphoma: So what? *Hematol Oncol* 37: 19-23, 2019. PMID: 31187528. DOI: 10.1002/hon.2581
- 31 Takimoto-Shimomura T, Tsukamoto T, Maegawa S, Fujibayashi Y, Matsumura-Kimoto Y, Mizuno Y, Chinen Y, Shimura Y, Mizutani S, Horiike S, Taniwaki M, Kobayashi T and Kuroda J: Dual targeting of bromodomain-containing 4 by AZD5153 and BCL2 by AZD4320 against B-cell lymphomas concomitantly overexpressing c-MYC and BCL2. *Invest New Drugs* 37(2): 210-222, 2019. PMID: 29931583. DOI: 10.1007/s10637-018-0623-8
- 32 Cheng S, Coffey G, Zhang XH, Shakhovich R, Song Z, Lu P, Pandey A, Melnick AM, Sinha U and Wang YL: SYK inhibition and response prediction in diffuse large B-cell lymphoma. *Blood* 118(24): 6342-6352, 2011. PMID: 22025527. DOI: 10.1182/blood-2011-02-333773
- 33 Sharman J and di Paolo J: Targeting B-cell receptor signaling kinases in chronic lymphocytic leukemia: the promise of Entospletinib. *Ther Adv Hematol* 7(3): 157-170, 2016. PMID: 27247756. DOI: 10.1177/20406207166636542
- 34 Currie KS, Kropf JE, Lee T, Blomgren P, Xu J, Zhao Z, Gallion S, Whitney JA, Maclin D, Lansdon EB, Maciejewski P, Rossi AM, Rong H, Macaluso J, Barbosa J, di Paolo JA and Mitchell SA: Discovery of GS-9973, a selective and orally efficacious inhibitor of spleen tyrosine kinase. *J Med Chem* 57(9): 3856-3873, 2014. PMID: 24779514. DOI: 10.1021/jm500228a
- 35 Chapuy B, Cheng H, Watahiki A, Ducar MD, Tan Y, Chen L, Roemer MGM, Ouyang J, Christie AL, Zhang L, Gusenleitner D, Abo RP, Farinha P, von Bonin F, Thorner AR, Sun HH, Gascoyne RD, Pinkus GS, van Hummelen P, Wulf GG, Aster JC, Weinstock DM, Monti S, Rodig SJ, Wang Y and Shipp MA: Diffuse large B-cell lymphoma patient-derived xenograft models capture the molecular and biological heterogeneity of the disease. *Blood* 127(18): 2203-2213, 2016. PMID: 26773040. DOI: 10.1182/blood-2015-09-672352
- 36 Chaidos A, Caputo V and Karadimitris A: Inhibition of bromodomain and extra-terminal proteins (BET) as a potential therapeutic approach in haematological malignancies: Emerging preclinical and clinical evidence. *Ther Adv Hematol* 6(3): 128-141, 2015. PMID: 26137204. DOI: 10.1177/2040620715576662
- 37 Cremer A, Ellegast JM, Alexe G, Frank ES, Ross L, Chu SH, Pikman Y, Robichaud A, Goodale A, Häupl B, Mohr S, Rao A v., Walker AR, Blachly JS, Piccioni F, Armstrong SA, Byrd JC, Oellerich T and Stegmaier K: Resistance mechanisms to SYK inhibition in acute myeloid leukemia. *Cancer discov* 10(2): 214-231, 2020. PMID: 31771968. DOI: 10.1158/2159-8290.CD-19-0209

Received May 5, 2020
 Revised May 25, 2020
 Accepted May 27, 2020

13. Lebenslauf

Persönliche Daten

Name: Sender, Sina
Adresse: Kurt-Tucholsky-Str. 22, 18059 Rostock
Geburtsdatum: 26.11.1988
Geburtsort: Hannover
Familienstand: ledig, ein Kind
Elternzeit: April 2021 – April 2022

Akademischer Werdegang

Seit 06/2018 **Wissenschaftliche Mitarbeiterin**
Universitätsmedizin Rostock, Zentrum für Innere Medizin,
Medizinische Klinik III, Hämatologie, Onkologie, Palliativmedizin
Arbeitsgruppe: PD Dr. rer. nat. Hugo Murua Escobar
Klinikleitung: Prof. Dr.med. Christian Junghanß

Seit 02/2016 **Promotion**
Universitätsmedizin Rostock, Zentrum für Innere Medizin,
Medizinische Klinik III, Hämatologie, Onkologie, Palliativmedizin
Arbeitsgruppe: PD Dr. rer. nat. Hugo Murua Escobar
Klinikleitung: Prof. Dr.med. Christian Junghanß

10/2013 – 10/2015 **Masterstudium** “Animal Biology and Biomedical Sciences”
Stiftung Tierärztliche Hochschule Hannover
Master of Science, Abschlussnote: 1,3
Thema der Masterarbeit: **“Laser induced cell ablation by antibody
labeled gold conjugates”**
Laser Zentrum Hannover e.V.
Arbeitsgruppe: Biophotonik, Dr.-Ing. Heiko Meyer

10/2009 – 02/2013 **Bachelorstudium** "Biologie"

Technische Universität Carolo-Wilhelmina zu Braunschweig
Bachelor of Science, Abschlussnote: 2,2

Thema der Bachelorarbeit: „**Charakterisierung der regulatorischen RNAs *GlmY* und *GlmZ* und ihre Rolle in der Virulenz-Genexpression des enteropathogenen Bakteriums *Yersinia Pseudotuberculosis***“

Helmholtz Zentrum für Infektionsforschung Braunschweig
Arbeitsgruppe: Molekulare Infektionsbiologie,
Prof. Dr.rer.nat. Petra Dersch

Schulischer Werdegang

08/2005 – 08/2009 **Allgemeine Hochschulreife** mit naturwissenschaftlicher Profilbildung
an der Integrierten Gesamtschule Garbsen

Praktika und Studienbegleitende Tätigkeiten

11/2015 – 01/2016 **Wissenschaftliche Hilfskraft**

Fraunhofer-Institut für Toxikologie und Experimentelle Medizin,
Hannover, Abteilung: Wirksamkeitsprüfung - Dr. Katherina Sewald

08/2014 – 10/2014 **Studentische Hilfskraft**

Stiftung Tierärztliche Hochschule Hannover
Institut für Physiologische Chemie, Prof. Dr. Hassan Y. Naim

10/2012 – 03/2013 **Auslandspraktikum**

Beatson Institute for Cancer Research, Glasgow, Schottland
Arbeitsgruppe: Migration, Invasion and Metastasis
Prof. Laura Machesky

Projekt: „**Investigation of the role of a *Rac*-GEF in invasive cancer cell migration and matrix degradation**“



14. Publikationsverzeichnis (anti-Chronologisch)

14.1 Veröffentlichte Originalarbeiten

1. Ma Y., Schulz, B., Trakooljul N., Al Ammar M., Sekora A., **Sender S.**, Hadlich F., Zechner D., Weiss FU., Lerch MM., Jaster R., Junghanss C., Murua Escobar H. **Inhibition of KRAS, MEK and PI3K demonstrate synergistic anti-tumor effects in pancreatic ductal adenocarcinoma cell lines** *Cancers* 2022,14(18), 4467 <https://doi.org/10.3390/cancers14184467>
2. Ma Y., **Sender S.**, Sekora A., Kong W., Bauer P., Ameziane N., Al-Ali R., Krake S., Radefeldt M., Weiss FU., Lerch MM., Parveen A., Zechner D., Junghanss C., Murua Escobar H. **The inhibitory response to PI3K/AKT pathway inhibitors MK-2206 and Buparlisib is related to genetic differences in pancreatic ductal adenocarcinoma cell lines** *Int. J. Mol. Sci.* 2022, 23(8), 4295; <https://doi.org/10.3390/ijms23084295>
3. Ma Y., **Sender S.**, Sekora A., Kong W., Bauer P., Ameziane N., Krake S., Radefeldt M., Al-Ali R., Weiss FU., Lerch MM., Parveen A., Zechner D., Junghanss C., Murua Escobar H. **Inhibitory response to CK II inhibitor silmitasertib and CDKs inhibitor Dinaciclib is related to genetic differences in pancreatic ductal adenocarcinoma cell lines** *Int. J. Mol. Sci.* 2022, 23(8), 4409; <https://doi.org/10.3390/ijms23084409>
4. Schwarz R., Seiler ERD., **Sender S.**, Pews-Davtyan A., Murua Escobar H., Zechner D., Beller M., Junghanss C., Hinz B. **A simple LC-MS/MS method for the quantification of PDA-66 in human plasma** *Molecules* 2022, 27(3), 974; <https://doi.org/10.3390/molecules27030974>
5. Alhajjar S., Nolte I., Schille JT., **Sender S.**, Trakoolju N., Villa Perez S., Zechner D., Vollmar B., Junghanss C., Murua Escobar H. **Establishment and characterization of FusionRed stable transfected canine prostate adenocarcinoma and transitional cell carcinoma cells** *In Vivo* January 2022, 36 (1) 170-179; DOI: <https://doi.org/10.21873/invivo.12688>
6. Weibo K., **Sender S.**, Taher L., Villa-Perez S., Ma Y., Sekora A., Ruetgen BC., Brenig B., Beck J., Schuetz E., Junghanss C., Nolte I., Murua Escobar H. **BTK and PI3K inhibitors reveal synergistic inhibitory anti-tumoral effects in canine diffuse large B-cell lymphoma cells** *Int. J. Mol. Sci.* 2021, 22(23), 12673; <https://doi.org/10.3390/ijms222312673>
7. Richter A., Schoenwaelder N., **Sender S.**, Junghanss C., Maletzki C. **Cyclin-dependent kinase inhibitors in hematological malignancies-current**

- understanding, (pre-)clinical application and promising approaches** *Cancers (Basel)* 2021 May 20;13(10):2497. doi: 10.3390/cancers13102497.
8. **Sender S.**, Sekora A., Villa Perez S., Chabanovska O., Becker A., Ngezahayo A., Junghanss C., Murua Escobar H. **Precursor B-ALL cell lines differentially respond to SYK inhibition by Entospletinib** *Int. J. Mol. Sci.* 2021 Jan 8;22(2):E592. doi: 10.3390/ijms22020592.
9. Grunwald L., Grosse-Thie C., **Sender S.**, Knuebel G., Krohn S., Roof C., Junghanss C., Henze L., Murua Escobar H. **Ultradeep targeted sequencing reveals low allele frequencies of somatic JAK2 and MPL variants in patients with abdominal vein thromboses: results of an ongoing prospective prevalence study in Mecklenburg-West Pomerania.** *Biomark Res.* 2020 Dec 14;8(1):73.
10. Sklarz LM., Gladbach YS., Ernst M., Hamed M., Roof C., **Sender S.**, Beck J., Schütz E., Fischer S., Struckmann S., Junghanss C., Fuellen G., Murua Escobar H. **Combination of the PI3K inhibitor Idelalisib with the conventional cytostatics cytarabine and dexamethasone leads to changes in pathway activation that induce anti-proliferative effects in B lymphoblastic leukaemia cell lines.** *Cancer Cell Int* 2020 Aug 12;20:390. doi: 10.1186/s12935-020-01431-4.
11. Möller S., Saul N., Cohen AA., Köhling R., **Sender S.**, Murua Escobar H., Junghanss C., Cirulli F., Berry A., Antal P., Adler P., Vilo J., Boiani M., Jansen L., Repsilber D., Grabe HJ., Struckmann S., Barrantes I., Hamed M., Wouters B., Schoofs L., Luyten W., Fuellen G. **Healthspan pathway maps in C. elegans and humans highlight transcription, proliferation/biosynthesis and lipids.** *Aging (Albany NY).* 2020 Jul 7;12(13):12534-12581. doi: 10.18632/aging.103514.
12. Kong W., **Sender S.**, Perez SV., Sekora A., Ruetgen B., Junghanss C., Nolte I., Murua Escobar H. **Pan- and isoform-specific inhibition of the Bromodomain and Extra-terminal proteins and evaluation of synergistic potential with Entospletinib in canine lymphoma.** *Anticancer Res.* 2020 Jul;40(7):3781-3792. doi: 10.21873/anticancer.14367.
13. Liu W.[#], **Sender S.**[#], Kong W., Beck J., Sekora A., Bornemann-Kolatzki K., Schuetz E., Junghanss C., Brenig B., Nolte I., Murua Escobar H. **Establishment and characterization of stable red, far-red (fR) and near infra-red (NIR) transfected canine prostate cancer cell lines.** *Cancer Cell Int.* 2020 Apr 29;20:139. doi: 10.1186/s12935-020-01211-0.
14. Richter A., **Sender S.**, Lenz A., Schwarz R., Hinz B., Knuebel G., Sekora A., Murua Escobar H., Junghanss C., Roof C. **Influence of Casein Kinase II inhibitor CX-4945 on BCL6-mediated apoptotic signaling in B-ALL in vitro and in vivo.** *BMC Cancer.* 2020 Mar 4;20(1):184 doi: 10.1186/s12885-020-6650-9.

15. Richter A., Roof C., Hamed M., Gladbach YS., **Sender S.**, Konkolefski C., Knuebel G., Sekora A., Fuellen G., Vollmar B., Murua Escobar H., Junghanss C. **Combined Casein Kinase II inhibition and epigenetic modulation in acute B-lymphoblastic leukemia.** *BMC Cancer.* 2019 Mar 6;19(1):202. doi: 10.1186/s12885-019-5411-0.
16. Taher L., Beck J., Liu W., Roof C., Soller JT., Rütgen BC., Hammer SE., Chodisetti M., **Sender S.**, Sterenczak KA., Fuellen G., Junghanss C., Brenig B., Nolte I., Schütz E., Murua Escobar H. **Comparative high-resolution transcriptome sequencing of lymphoma cell lines and de novo lymphomas reveals cell-line-specific pathway dysregulation.** *Sci Rep.* 2018 Apr 19;8(1):6279. doi: 10.1038/s41598-018-23207-7.
17. Ernst M., Du Y., Warsow G., Hamed M., Endlich N., Endlich K., Murua Escobar H., Sklarz LM., **Sender S.**, Junghanß C., Möller S., Fuellen G., Struckmann S. **FocusHeuristics - expression-data-driven network optimization and disease gene prediction.** *Sci Rep.* 2017 Feb 16;7:42638. doi: 10.1038/srep42638.

14.2 Veröffentlichte Originalarbeiten im Vorfeld zur Promotion

1. Kalies S., Keil S., **Sender S.**, Hammer SC., Antonopoulos GC, Schomaker M., Ripken T., Murua Escobar H., Meyer H., Heinemann D. **Characterization of the cellular response triggered by gold nanoparticle-mediated laser manipulation.** *J Biomed Opt.* 2015 Nov;20(11):115005. doi: 10.1117/1.JBO.20.11.115005.

14.3 Vorträge auf internationalen und nationalen Fachtagungen

1. **Sender S.**, Sultan W.A., Sekora A., Koczan D., Junghanss C., Murua Escobar H. **Evaluation of combined BET and SYK inhibition on cell viability and gene expression modulation in human B-lymphoma cell lines.** *Oncol Res Treat* 2020;43(suppl 4):1-288. 551 Vorgestellt auf der Jahrestagung der Deutschen Gesellschaft für Hämatologie und Medizinische Onkologie in der Session „Best gescorte Abstracts mit Diskussion – Translationale Forschung“ 2020.
2. **Sender S.**, Gladbach Y.S., Hamed M., Beck J., Schuetz E., Fuellen G., Junghanss C., Murua Escobar H. **Combined inhibition of PI3K and SYK enhances synergistically the gene expression modulation in BCR dependent and independent B-lymphoblastic leukemia cell lines.** *Oncol Res Treat* 2019;42(suppl.4)1-336 V671. Vorgestellt auf der Jahrestagung der Deutschen Gesellschaft für Hämatologie und Medizinische Onkologie 2019.
3. Richter A., Roof C., Hamed M., Gladbach YS., **Sender S.**, Sekora A., Knuebel G., Fuellen G., Murua Escobar H., Junghanss C. **Casein Kinase II inhibitor CX-4945 modulates methylation profiles of metabolism-related genes in acute B-lymphoblastic leukemia cells.** *Oncol Res Treat* 2018 41(suppl 4):25; V111. Vorgestellt auf der Jahrestagung der Deutschen Gesellschaft für Hämatologie und Medizinische Onkologie 2018.
4. **Sender S.**, Sklarz LM., Richter A., Sekora A., Roof C., Junghanss C., Murua Escobar H. **Characterization of mono and combined application induced effects of the SYK inhibitor Entospletinib on B-cell receptor dependent and independent B-lymphoblastic leukemia cell lines.** *Oncol Res Treat* 2017;40(suppl3):20-21, V95. Vorgestellt auf der Jahrestagung der Deutschen Gesellschaft für Hämatologie und Medizinische Onkologie 2017.
5. Richter A., Roof C., **Sender S.**, Sekora A., Knübel G., Vollmar B., Jeremias I., Murua Escobar H., Junghanss C. **CK2 inhibition reduces cell proliferation in acute B-lymphoblastic leukemia cells in vitro and in vivo.** *Oncol Res Treat* 2017;40(suppl 3):20, V94. Vorgestellt auf der Jahrestagung der Deutschen Gesellschaft für Hämatologie und Medizinische Onkologie 2017.
6. Sklarz LM., Ernst M., Roof C., Richter A., **Sender S.**, Gladbach YS., Struckmann S., Hamed M., Beck J., Schütz E., Fuellen G., Junghanss C., Murua Escobar H. **PI3Kdelta inhibition enhances drug sensitivity of acute B-lymphoblastic leukemia cells to Cytarabine and Dexamethasone in vitro.** *Oncol Res Treat* 2017;40(suppl3):21, V97. Vorgestellt auf der Jahrestagung der Deutschen Gesellschaft für Hämatologie und Medizinische Onkologie 2017.

14.4 Posterbeiträge auf internationalen und nationalen Fachtagungen

1. Kong W., **Sender S.**, Villa Perez S., Sekora A., Ma Y., Rütgen B., Nolte I., Junghanß C., Murua Escobar H. **Comparative analyses of pan- and isoform-specific BET inhibition and evaluation of synergistic potential by SYK inhibitor addition in a canine DLBCL in vitro model.** *Oncol Res Treat* 2020;43(suppl 4):1-288. 459 Vorge stellt auf der Jahrestagung der Deutschen Gesellschaft für Hämatologie und Medizinische Onkologie 2020.
2. Ma Y., **Sender S.**, Sekora A., Bauer P., Krake S., Radefeld M., Lerch M., Weiss F.U., Junghanß C., Murua Escobar H. **Evaluation of PI3K/AKT and CDK pathway inhibitors MK-2206, Buparlisib, Silmitasertib and Dinaciclib in eleven pancreatic cancer cell lines.** *Oncol Res Treat* 2020;43(suppl 4):1-288. 554 Vorge stellt auf der Jahrestagung der Deutschen Gesellschaft für Hämatologie und Medizinische Onkologie 2020.
3. Eichhorst A., Sekora A., **Sender S.**, Gallhof M., Brasholz M., Ehlers P., Langer P., Murua Escobar H., Junghanß C. **Evaluation of novel pyridine derivatives, indolquinones, dioxyserpine and arylated dioxyserpine as potential anti-tumor compounds.** *Oncol Res Treat* 2020;43(suppl 4):1-288. 558 Vorge stellt auf der Jahrestagung der Deutschen Gesellschaft für Hämatologie und Medizinische Onkologie 2020.
4. Kong W., **Sender S.**, Sekora A., Ma Y., Rütgen B., Nolte I., Taher L., Brenig B., Beck J., Schuetz E., Junghanss C., Murua Escobar H. **Combined inhibition of BTK and PI3K acts synergistically in a canine B-cell lymphoma in vitro model.** *Oncol Res Treat* 2019;42(suppl.4)1-336. P428. Vorge stellt auf der Jahrestagung der Deutschen Gesellschaft für Hämatologie und Medizinische Onkologie 2019.
5. **Sender S.**, Krohn S., Knübel G., Sklarz L.-M, Kong W., Richter A., Roolf C., Junghanss C., Murua Escobar H. **Evaluation of gene expression modulation by Entospletinib in mono- and combined application with PI3K pathway specific inhibitors in B-lymphoblastic leukemia cell lines.** *Oncol Res Treat* 2018 41(suppl 4):25; P194. Vorge stellt auf der Jahrestagung der Deutschen Gesellschaft für Hämatologie und Medizinische Onkologie 2018.
6. Schille J.T., Nolte I., Roolf C., Pews-Davtyan A., **Sender S.**, Beller M., Rolfs A., Beck J., Schütz E., Brenig B., Junghanss C., Murua Escobar H. **Characterization of arylindolylmaleimides mediated cell and molecular effects prostate carcinoma cell lines.** *Oncol Res Treat* 2018 41(suppl 4):25; P 974. Vorge stellt auf der

Jahrestagung der Deutschen Gesellschaft für Hämatologie und Medizinische Onkologie 2018.

7. Richter A., Roelf C., **Sender S.**, Kong W., Knübel G., Sekora A., Gladbach YS, Hamed M., Fuellen G., Vollmar B., Jeremias I., Panse JP., Murua Escobar H., Junghanss C. **Casein Kinase II inhibition by CX-4945 and epigenetic modulation by decitabine demonstrate significant antiproliferative activity as single agents as well as in combination in acute B-lymphoblastic leukemia cells.** Blood 2017 130:3887. Vorgelegt auf der Jahrestagung der American Society of Hematology 2017.
8. Struckmann S., Du Y., Warsow G., Hamed M., Endlich N., Endlich K., Murua Escobar H., Sklarz L.-M., **Sender S.**, Junghanß C., Möller S., Fuellen G., Ernst M., **FocusHeuristics - expression-data-driven network optimisation and disease gene prediction**, Poster, Session A-262, 23.07.2017, Prag, Intelligent Systems for Molecular Biology and the 16th European Conference on Computational Biology (ISMB/ECCB)
9. Gladbach Y.S., Sklarz L.-M., Ernst M., **Sender S.**, Murua Escobar H., Junghanß C., Fuellen G., Hamed M. **A data-driven computational approach to evaluate drug synergy and combinations via integrative omics analysis**, Poster, Session B-306, 25.07.2017, Prag, ISMB/ECCB

15. Eidesstattliche Erklärung

Ich versichere hiermit, dass ich die eingereichte Dissertation selbstständig und ohne fremde Hilfe verfasst, keine anderen als die angegebenen Quellen und Hilfsmittel verwendet und wörtlich oder inhaltlich entnommene Stellen der benutzen Quellen als solche kenntlich gemacht habe.

Rostock, den 19. September 2022

A handwritten signature in blue ink, appearing to read 'S. Sender', with a long horizontal flourish extending to the right.

Sina Sender

16. Danksagung

An dieser Stelle möchte ich mich ganz herzlich bei Allen bedanken, die mich während meiner Promotion begleitet und unterstützt haben.

Ein ganz besonderer Dank geht an Prof. Dr. med. Christian Junghanß für die Möglichkeit, in der Abteilung promovieren zu dürfen, für die herzliche Aufnahme, die Unterstützung und das Vertrauen in den letzten Jahren.

Mein besonderer Dank gilt Frau Prof. Dr.rer.nat. habil. Ulrike Gimsa für die Betreuung und Begutachtung meiner Dissertation an der Universität Rostock. Außerdem bedanke ich mich für die Unterstützung und Hilfestellung während der Finalisierung meiner Arbeit.

Insbesondere möchte ich mich bei meinem Betreuer und Mentor PD Dr.rer.nat. habil. Hugo Murua Escobar bedanken. Zum einem für die Bereitstellung des Themas, die Betreuung während der Doktorarbeit und auch für die kleinen Überredungskünste für die Promotion nach Rostock zu ziehen. Und zum anderen für die Unterstützung, das Vertrauen, die vielfältigen Möglichkeiten, die konstruktive Kritik und die stets positiven Worte. Außerdem für die nie endende gute Laune und die immer spaßigen Kongresstage, die stets mit einem Feierabendbier endeten.

Weiterhin möchte ich mich für die tolle Zusammenarbeit mit meinen Kooperationspartnern bedanken. Ein besonderer Dank geht an Prof. Dr.rer.nat. Georg Füllen, Dr. Daniel Palmer, Prof. Dr.rer.nat. Andreas Pich, Dr.rer.nat. Dirk Koczan, PD Dr.rer.nat. habil. Dietmar Zechner, Christin Schlie, Dr.rer.nat. Rico Schwarz, PD Dr. med. habil. Sarah Schwarzenböck, Prof. Dr.med. Schürholz, Prof. Dr.rer.nat. Brasholz, Prof. Dr.rer.nat. Ehlers, Dr. Nares Trakooljul, Dr.rer.nat. Anahit Pews-Davtyan, und auch allen anderen, die hier nicht mit aufgeführt sind.

Weiterhin bedanke ich mich bei der gesamten Arbeitsgruppe, die nicht nur immer gute Laune versprüht, sondern auch stets mit Rat und Tat zu Seite steht.

Bei Dr.rer.hum. Anna Richter bedanke ich mich für die konstruktiven, aber auch immer unterhaltsamen Gespräche in unserem Schreibraum. Für die regelmäßigen Kaffeepausen an der frischen Luft. Die regelmäßige Unterstützung, egal ob mental, im Labor oder am Schreibtisch und natürlich auch für die vielen schönen gemeinsamen Stunden außerhalb der Laborräume.

Bei Anett Sekora bedanke ich mich für die viele gute Laune, unsere lustigen Gespräche und vor allem die regelmäßigen wilden Fahrten im kleinen Riesenrad auf dem Rostocker

Weihnachtsmarkt. Außerdem für die Unterstützung im Labor, egal ob Zellkultur oder Western Blot.

Des Weiteren bedanke ich mich bei Gudrun Knübel für die immer aufbauenden und lieben Worte, die tatkräftige Unterstützung bei den Sequenzierungen und das frische Gemüse aus dem eigenen Anbau.

Auch bedanke ich mich bei Saskia Krohn für die Einarbeitung und Unterstützung bei den Sequenzierungen und die immer sehr liebevollen und unterhaltsamen Gespräche.

Weiterhin bedanke ich mich bei Lisa Madeleine Sklarz für die anfänglich liebevolle Aufnahme in die Arbeitsgruppe, die hilfreichen Tipps und die Einarbeitung. Außerdem für die Unterstützung im Labor und daraus resultierende und immer noch anhaltende liebevolle Freundschaft. Die tollen Sporteinheiten ob drinnen oder draußen, die Spielabende am Stadthafen und die immer ehrlichen Worte.

Weiterhin bedanke ich mich bei Dr.rer.nat. habil. Claudia Maletzki für die vielen lieben und hilfreichen Tipps und die schöne Zeit im gemeinsamen Büro nach der Elternzeit.

Bei der gesamten Lab-Crew, mit Weibo, Annika, Yixuan, Simon, Nina, Inken, Saskia, Sandra, Xin, Yu und Robby bedanke ich mich ebenfalls für die tolle gemeinsame Zeit, die immer spaßigen Laborausflüge und Weihnachtsfeiern und die Unterstützung.

Ein ganz besonderer Dank geht an meine gesamte Familie und Freunde, die mich während der langen Zeit immer unterstützt haben, mir immer Kraft, Mut und Liebe gegeben haben um diese Arbeit fertigzustellen. Meiner Schwester Alisha danke ich für jede wertvolle Minute, die wir während der freien Zeit miteinander verbringen konnten, egal ob in der Heimat oder mal wieder während unserer Welterkundungen. Vor allem aber für die liebevollen Worte, die tröstenden Arme und vielen wunderbaren Abende. Meinen Eltern danke ich vor allem für ihre Geduld, bis das Schriftstück dann endlich fertig geschrieben war. Vor allem aber für die Unterstützung und die immer wundervollen Stunden in der Heimat. Weiterhin bedanke ich mich bei meinen Liebsten Frauke, Sina und Karen für die wunderbare Ablenkung neben der Promotion mit tollen Spieleabenden, zauberhaften Winterurlauben in Österreich und die Möglichkeit, „Arbeit, Arbeit sein zu lassen“.

Ein ganz besonderer Dank geht an meinen Lebensgefährten Hannes, der mich während der Promotion immer unterstützt hat und mir die nötige Gelassenheit eingebläut hat. Besonders aber für die Liebe, Ruhe und Entschlossenheit, gewisse Dinge anzugehen, und nicht alles im Leben zu ernst zu nehmen, und nun auch dafür, eine eigene kleine Familie zu haben mit einer wunderbaren Tochter.

17. Anhang

17.1 Ergänzende Abbildung

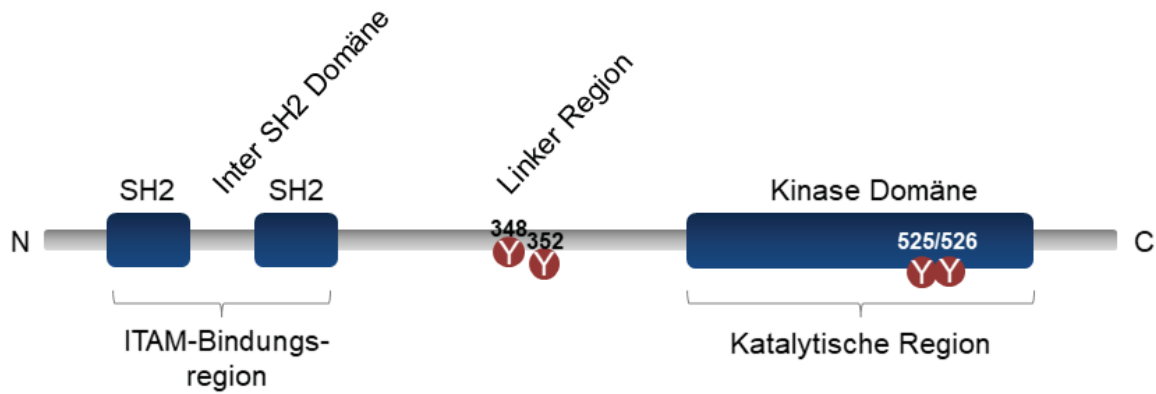


Abbildung 5: Spleen Tyrosin Kinase Struktur Schematische Darstellung der SYK Protein Struktur. Die N-terminalen SH-2 Domänen sind über eine Linker Region mit der Kinase Domäne verbunden. Die Aminosäuren Tyrosin (Y) 348, 352 und 525/526 indizieren die in dieser Arbeit evaluierten Phosphorylierungsstellen. Verändert nach Sender *et al.*, Int J Mol Sci. 2021 ¹¹⁷.

17.2 Ergänzende Tabelle

Tabelle 2: Detaillierte Auflistung der verwendeten Zelllinien inkl. Charakteristika

Zelllinie	NALM-6	SEM	RS4;11	DG-75	RAJI	SU-DHL-4	U-2946	CLBL-1
Spezies	Homo sapiens	Homo sapiens	Homo sapiens	Homo sapiens	Homo sapiens	Homo sapiens	Homo sapiens	canis lupus familiaris
Zelltyp				Burkitt Lymphom	Burkitt Lymphom	B-Zelllymphom	B-Zelllymphom	B-Zelllymphom
assoziierte Erkrankung	ALL	ALL	ALL	Burkitt	Burkitt	DLBCL	DLBCL	DLBCL
Subtyp	prä B-ALL	pro B-ALL	pro B-ALL			GCB	ABC	ABC
Oberflächenmarker/ Immunologie	CD10+, CD19+, CD20+, CD138+, sm/cyIgG-, cyIgM+, smIgM-	CD10-, CD19+, CD20-, CD138-, sm/cyIgM-	CD10-, CD19+, CD20-, CD138-, sm/cyIgM-	CD3 -, CD10 +, CD13 -, CD19 +, CD34 -, CD37 +, CD38 +, CD80 +, CD138 -, HLA-DR +, cyIgG -, cyIgM +, cykappa +, cylambda -	CD3 -, CD10 +, CD13 -, CD19 +, CD20 +, CD34 -, CD37 +, CD38 +, cyCD79a +, CD80 +, CD138 -, HLA-DR +, sm/cyIgG -, smIgM -, cyIgM +, sm/cykappa -, sm/cylambda -	CD3 -, CD10 +, CD13 -, CD19 +, CD20 +, CD34 -, CD37 +, CD38 +, cyCD79a +, CD138 -, HLA-DR +, sm/cyIgG +, sm/cyIgM -, sm/cykappa +, sm/cylambda -	CD3 -, CD5 -, CD10 +, CD13 -, CD19 +, CD20 +, CD34 -, CD37 +, CD38 +, CD138 -, HLA-DR +, sm/cyIgG -, sm/cyIgM +, sm/cykappa -, sm/cylambda +	CD79acy+, MHC II+, CD45RA+, CD11a+, CD45+, CD3-, CD4-, CD5-, CD8-, CD11d-, CD14-, CD21-, CD34-, CD56 -and TCRγδ-
Herkunft	♂, adult, 19 Jahre, Rezidiv	♀, juvenil, 5 Jahre, Rezidiv	♀, adult, 32 Jahre, Rezidiv	Pleuraerguss, ♂, juvenil, 10 Jahre, metastase, refraktär	Oberkiefer, ♂, juvenil, 12 Jahre	Peritonealerguss, ♂, adult, 38 Jahre	Pleuraerguss, ♂, adult, 52 Jahre	Berner Sennenhund, periphere Lymphknoten, ♂, 8 Jahre,
BZR Status	prä BZR +	-	-	BZR +	BZR +	BZR +	BZR +	unbekannt, evt BZR+
Ploidie	Diploid	Hypodiploid	Hyperdiploid	6% polyploidie - 46<2n	hypotetraploid	Hyperdiploid	Hyperdiploid	Hypodiploid
Zytogenetik	t(5;12)(q33.2;p13.2)	-13; t(4;11)(q21;q23), del(7)(p14)	+8, +18; t(4;11)(q21;q23), i(7q)	t(8;14)(q24;q32)	t(8;14)	t(14;18)	t(8;14)	der(13;13)
Fusionsgene	-	MLL-AF4 /KMT2A::AFF1	MLL-AF4 /KMT2A::AFF1	MYC-IGH	MYC-IGH	BCL2 (MBR)-IGH; MYC+, BCL6+	MYC-IGH	unbekannt
Hotspot-Mutationen	TP53, NRAS, KIT, MET	TP53, CDKN2A, PDGFRA, KIT, APC	TP53			EZH2		
Verdopplungszeit	~ 36 h	~ 30 h	~ 50 h	~ 40-50 h	~ 24-36 h	~ 40 h	~ 20-30 h	~ 19 h

